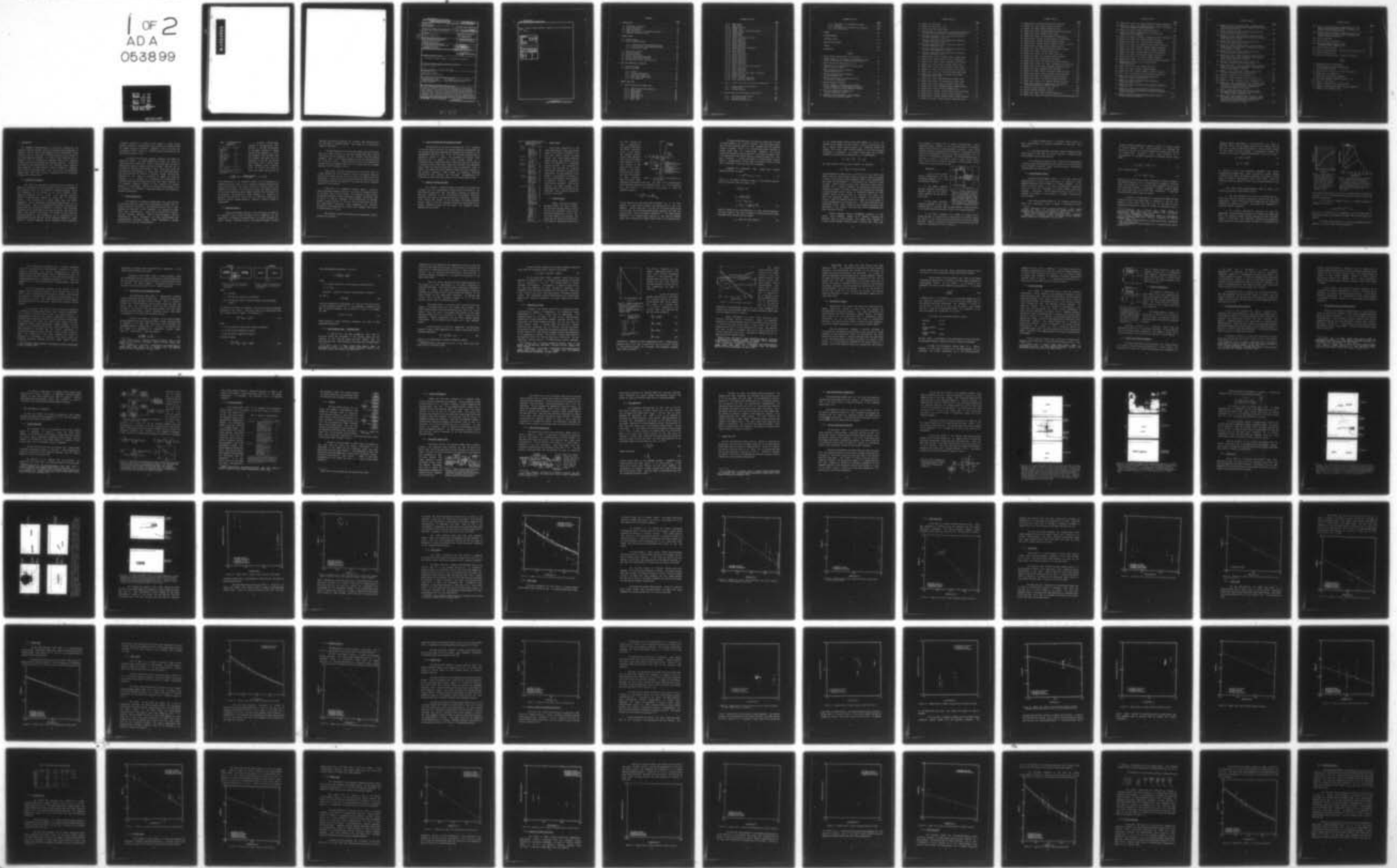
AD-A053 899
HARRY DIAMOND LABS ADELPHI MD
F/G 14/2
COMPONENT DAMAGE FROM ELECTROMAGNETIC PULSE (EMP) INDUCED TRANS--ETC(U)
OCT 77 J R MILETTA
UNCLASSIFIED
HDL-TM-77-22
NL
1 OF 2
AD A
053899

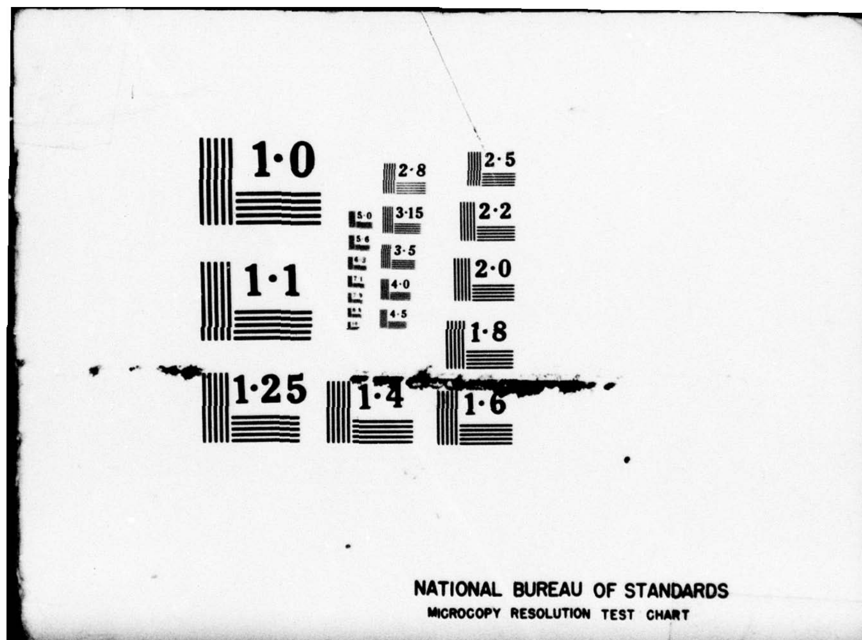
1·0
2·8
2·5
3·15
2·2
3·5
2·0
1·1
4·0
4·5
1·8
1·25
1·4
1·6
NATIONAL BUREAU OF STANDARDS
MICROCOPY RESOLUTION TEST CHART

AD A053899

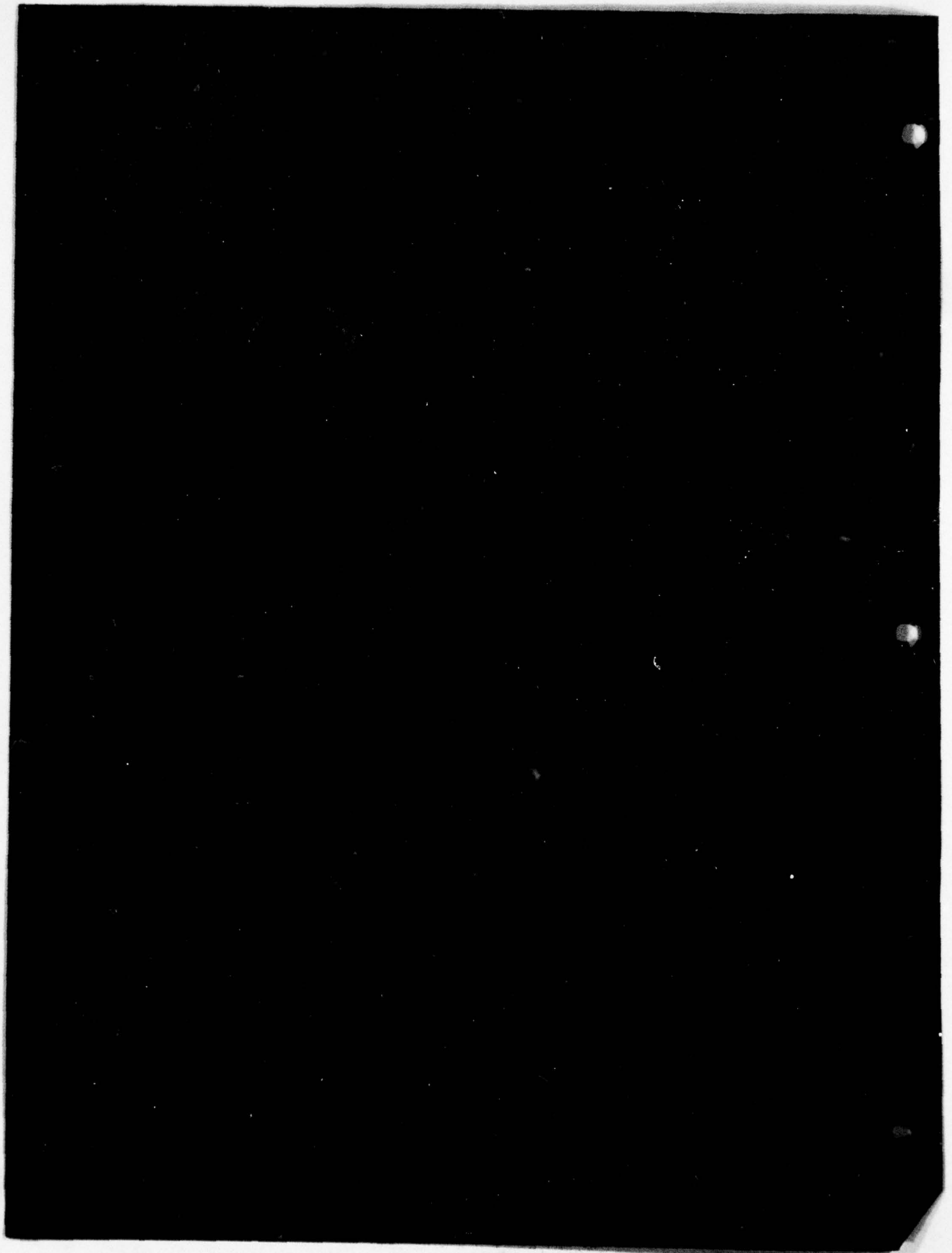

UNCLASSIFIED
SECURITY CLASSIFICATION OF THIS PAGE (When Data Entered)

REPORT DOCUMENTATION PAGE		READ INSTRUCTIONS BEFORE COMPLETING FORM
1. REPORT NUMBER HDL-TM-77-22	2. GOVT ACCESSION NO.	3. RECIPIENT'S CATALOG NUMBER
4. TITLE (and Subtitle) Component Damage from Electromagnetic Pulse (EMP) Induced Transients		5. TYPE OF REPORT & PERIOD COVERED Technical Memo
		6. PERFORMING ORG. REPORT NUMBER
7. AUTHOR(s) Joseph R. Miletta		8. CONTRACT OR GRANT NUMBER(s) DA: 1W062118AD51
9. PERFORMING ORGANIZATION NAME AND ADDRESS Harry Diamond Laboratories 2800 Powder Mill Road Adelphi, MD 20783		10. PROGRAM ELEMENT, PROJECT, TASK AREA & WORK UNIT NUMBERS Program Ele: 62118A
11. CONTROLLING OFFICE NAME AND ADDRESS US Army Materiel Development and Readiness Command Alexandria, VA 22333		12. REPORT DATE October 1977
		13. NUMBER OF PAGES 184
14. MONITORING AGENCY NAME & ADDRESS(if different from Controlling Office)		15. SECURITY CLASS. (of this report) UNCLASSIFIED
		15a. DECLASSIFICATION/DOWNGRADING SCHEDULE

16. DISTRIBUTION STATEMENT (of this Report)

Approved for public release; distribution unlimited.

17. DISTRIBUTION STATEMENT (of the abstract entered in Block 20, if different from Report)

PE 62118A
LPN- HDL_X512E1

18. SUPPLEMENTARY NOTES

HDL Project: X512E1
DRCMS Code: 502T.11.D5100

19. KEY WORDS (Continue on reverse side if necessary and identify by block number)

Electromagnetic pulse
Component EMP degradation
Second breakdown
EMP component failure mechanisms
Lance EMP component tests

20. ABSTRACT (Continue on reverse side if necessary and identify by block number)

The Lance Vulnerability and Hardening Test Program was supported by a number of in-laboratory experiments on various component types. Of prime concern was the establishment of component EMP thresholds to be used in establishing the vulnerability level of the system. Reported are pulsed transient tests on over 50 component types. Testing concentrated on sensitive semiconductor components, and about 1800 individual devices were damage tested. The tests used rectangular pulses varying in width from 5 ns to

DD FORM 1 JAN 73 1473 EDITION OF 1 NOV 65 IS OBSOLETE

UNCLASSIFIED
SECURITY CLASSIFICATION OF THIS PAGE (When Data Entered)

263 050

30 μs. Numerous nonsemiconductor components also were characterized.

ACCESSION for
NTIS White Section ☒
DDC Buff Section ☐
UNANNOUNCED ☐
JUSTIFICATION

BY
DISTRIBUTION/AVAILABILITY CODES
Dist. AVAIL. and/or SPECIAL
A

CONTENTS

Page

1. INTRODUCTION 11

1.1 System EMP Interaction 11
1.2 Device Sensitivity 12
1.3 Hardening Devices 13
1.4 Lance Vulnerability and Hardening Program 15
1.5 Component Evaluation Phase 15

2. DAMAGE MODELS 16

2.1 Device Failure 16
2.2 Second-Breakdown Models 21

2.2.1 Long-Duration Second-Breakdown Model 26
2.2.2 Short-Duration Second-Breakdown Model 28
2.2.3 Discussion of Model 30

2.3 Metalization Failure 33
2.4 Voltage Breakdown 35
2.5 General Observations 36
2.6 Failure from Complex Waveshapes 36
2.7 Bias and Multijunction Devices 37
2.8 Postdamage Electrical Characteristics 38

3. TEST AND ANALYTICAL TECHNIQUES 39

3.1 System Assessment 39
3.2 Testing Procedure 41

3.2.1 Devices 42
3.2.2 Pretest Measurements 43
3.2.3 Long-Pulse Damage Tests 43
3.2.4 Short-Pulse Damage Tests 44
3.2.5 Data Reduction 45

4. DAMAGE TEST DATA 46

4.1 Lance Semiconductor Damage Tests 47

4.1.1 1752/17 Operational Amplifier 47
4.1.2 1N69A Diode 51
4.1.3 1N270A Diode 57
4.1.4 1N457 Diode 58
4.1.5 1N539 Rectifier 62
4.1.6 1N645 Diode 63
4.1.7 1N647 Diode 65

CONTENTS (Cont'd)

		Page
4.1.8	1N816 Diode	67
4.1.9	1N914 Diode	68
4.1.10	1N956B--Varactor	70
4.1.11	1N965B Diode	71
4.1.12	1N1200, 1N1202, 1N1202A Rectifiers	72
4.1.13	1N3047B Diode	81
4.1.14	1N3064 Diode	82
4.1.15	1N3666 Diode	84
4.1.16	1N4003 and 1N4005 Rectifiers	86
4.1.17	UT254 Rectifier	90
4.1.18	2N270 Transistor	92
4.1.19	2N297A Transistor	94
4.1.20	2N328A Transistor	96
4.1.21	2N335 Transistor	98
4.1.22	2N489A Unijunction Transistor	98
4.1.23	2N526 Transistor	100
4.1.24	2N598 Transistor	102
4.1.25	2N738 Transistor	102
4.1.26	2N1132A Transistor	104
4.1.27	2N1204 Transistor	109
4.1.28	2N1308 Transistor	112
4.1.29	2N1613 Transistor	113
4.1.30	2N1711 Transistor	117
4.1.31	2N2198 Transistor	117
4.1.32	2N2297 Transistor	118
4.1.33	2N2323 Silicon Controlled Rectifier	121
4.1.34	2N2453 Transistor	123
4.1.35	2N2727 Transistor	123
4.1.36	2N2801 Transistor	126
4.1.37	2N3069 Junction Field Effect Transistor	128
4.1.38	2N3440 Transistor	131
4.1.39	2N3636 Transistor	132
4.1.40	SM692-1 (2N3801) Transistor	132
4.1.41	μA709 Operational Amplifier	134
4.2	Tests on 2N1132 Transistor from Various Manufacturers	139
4.2.1	Failure Level and Data Spread	139
4.2.2	Combined Data	154
4.2.3	Failure Analysis	155
4.3	Nonsemiconductor and Hardening Device Tests	165
4.3.1	SM-C-602932 Surge Arrestor	165
4.3.2	SM-C-602933 Filter	165
4.3.3	1N5649A TransZorb Diode	166

CONTENTS (Cont'd)

		Page
4.3.4	10164126(19) and 10158808(19) Relays	168
4.3.5	Capacitors	169
4.3.6	21-900098 and 21-900099 Filter Connectors	169
4.3.7	Erie 1200 Filter	172
5.	SUMMARY	172
	ACKNOWLEDGEMENTS	177
	LITERATURE CITED	177
	SELECTED BIBLIOGRAPHY	179
	SYMBOLS	180
	DISTRIBUTION	183

FIGURES

1	Direct-current characteristic of pn junction	17
2	Typical response of pn junction to rectangular voltage pulse of open-circuit voltage and pulse duration	20
3	Phase diagram for aluminum and silicon	24
4	Resistivity versus temperature for various boron doping levels in silicon	24
5	Model for case one of long-duration, second-breakdown model	27
6	Model for case two of long-duration, second-breakdown model	27
7	Thermal conductivity of high-purity silicon as function of temperature	31
8	Second-breakdown thresholds	32
9	Typical response of single-junction unbiased device subjected to reverse-biased rectangular transient exhibiting voltage dependent failure	36
10	Basic flow diagram for assessment of system vulnerability to EMP	40
11	Technique for determination of device damage from high-level transient pulses	40

FIGURES (Cont'd)

Page

12 Damage test flow chart 42

13 Typical long-pulse test setup 43

14 Typical short-pulse test setups 44

15 Test schematic for operational circuit checkout and pulse testing for Burr-Brown 1752/17 operational amplifier 48

16 Test data, Burr-Brown 1752/17 operational amplifier, unbiased, degradation, pulse 42 49

17 Test data, Burr-Brown 1752/17 operational amplifier, unbiased, destruction, pulse 43 50

18 Test data, Burr-Brown 1752/17 operational amplifier, biased, undamaged, pulse 5 52

19 Test data, Burr-Brown 1752/17 operational amplifier, biased, severe degradation, pulse 8 53

20 Test data, Burr-Brown 1752/17 operational amplifier, biased, destruction, pulse 10 54

21 Damage points, voltage, General Electric 1N69A diode 55

22 Damage points, power, General Electric 1N69A diode 56

23 Damage curve, power, General Instruments 1N270A diode 58

24 Damage line, power, Texas Instruments 1N457 diode 60

25 Damage points, power, Texas Instruments 1N457 diode 61

26 Damage line, power, Texas Instruments 1N539 rectifier 62

27 Damage points, voltage, Texas Instruments 1N645 diode 64

28 Damage line, power, Texas Instruments 1N645 diode, short-pulse points only 65

29 Damage line, power, TRW Semiconductors 1N647 diode 66

30 Damage curve, power, ITT Semiconductors 1N816 diode 67

31 Damage curve, power, Texas Instruments 1N914 Diode 69

32 Damage line, power, TRW Semiconductors 1N956B capacitor 70

33 Damage points, power, Motorola 1N965B diode 72

34 Damage points, voltage, General Electric 1N1200 rectifier . . . 74

35 Damage points, voltage, Motorola 1N1200 rectifier 75

36 Damage points, voltage, General Electric 1N1202 rectifier . . . 76

37 Damage line, power, General Electric 1N1202 rectifier 77

FIGURES (Cont'd)

		Page
38	Damage points, voltage, Motorola 1N1202 rectifier	78
39	Damage line, power, Motorola 1N1202 rectifier	79
40	Damage line, power, Bendix 1N1202A rectifier	80
41	Damage line, power, International Rectifier 1N3047B diode	82
42	Damage line, power, Raytheon 1N3064 diode	83
43	Damage line, power, ITT Semiconductors 1N3666 diode	85
44	Damage points, voltage, ITT Semiconductors 1N3666 diode	86
45	Damage points, voltage, Motorola 1N4003 rectifier	87
46	Damage points, voltage, TRW Semiconductors 1N4003 rectifier .	88
47	Damage points, voltage, Motorola 1N4005 rectifier	89
48	Damage line, power, TRW Semiconductors 1N4003 rectifier . . .	90
49	Damage curve, power, Unitrode UT254 diode	91
50	Damage curve, power, E-B, RCA 2N270 transistor	93
51	Damage line, power, E-B, Motorola 2N297A transistor	95
52	Damage line, power, Bendix 2N297A transistor	96
53	Damage curve, power, E-B, Crystalonics 2N328A transistor	97
54	Damage points, power, E-B, Texas Instruments 2N335 transistor .	99
55	Damage curve, power, Texas Instruments 2N489A transistor . . .	100
56	Damage line, power, Motorola 2N526 transistor	101
57	Damage line, power, General Instruments 2N598 transistor . . .	103
58	Damage curve, power, Texas Instruments 2N738 transistor	104
59	Damage line, power, E-B, Motorola 2N1132A transistor	105
60	Damage line, power, E-B, Fairchild 2N1132A transistor	106
61	Damage points, power, E-B, Raytheon 2N1132A transistor.	107
62	Damage curve, power, E-B, combined data for Motorola, Fairchild, and Raytheon 2N1132A transistors	108
63	Raytheon 2N1132A transistor (unit 12)	109
64	Raytheon 2N1132A transistor (unit 18)	110
65	Damage line, power, Motorola 2N1204 transistor	111
66	Damage curve, power, E-B, General Instruments 2N1308 transistor	113

FIGURES (Cont'd)

Page

67 Damage line, power, E-B, Texas Instruments 2N1308 transistor . . 114

68 Damage line, power, E-B, combined data for General Instruments and Texas Instruments 2N1308 transistors 115

69 Damage line, power, Motorola 2N1613 transistor 116

70 Damage line, power, combined data for Fairchild and Motorola 2N1711 transistors 118

71 Damage line, power, Electronic Transistors 2N2198 transistor. . 119

72 Damage line, power, E-B, Raytheon 2N2297 transistor 120

73 Damage line, power, E-B, Fairchild 2N2297 transistor 121

74 Damage line, power, G-C, General Electric 2N2323 rectifier . . . 122

75 Damage line, power, $E\text{-}B_1/B_2$, Motorola 2N2453 transistor 124

76 Damage line, power, $E\text{-}B_1/B_2$, Fairchild 2N2453 transistor 125

77 Damage curve, power, General Electric 2N2727 transistor 126

78 Damage line, power, E-B, Fairchild 2N2801 transistor 127

79 Damage line, power, E-B, Motorola 2N2801 transistor 128

80 Damage points, power, G-D, Solitron Devices 2N3069 transistor . . 129

81 Damage points, voltage, G-D, Solitron Devices 2N3069 transistor 130

82 Damage points, power, RCA 2N3440 transistor 131

83 Damage line, power, Motorola 2N3636 transistor 133

84 Damage line, power, Motorola SM692-1 (2N3801) transistor 134

85 Test circuit for Fairchild μA709 operational amplifier 135

86 Damage line, power, Fairchild μA709 operational amplifier input pins 2(B) and 3(C) 136

87 Damage line, power, Fairchild μA709 operational amplifier output pin 4(D) 137

88 Damage line, power, Fairchild μA709 operational amplifier output pin 6(F) 138

89 Damage line, power, Fairchild 2N1132 transistor pulse tested across collector-emitter terminals with positive pulse at collector 140

90 Spread in data points about nominal failure line for Fairchild 2N1132 transistor 141

FIGURES (Cont'd)

		Page
91	Damage line, power, Fairchild 2N1132 transistor pulse tested across collector-emitter terminals with positive pulse applied to emitter	142
92	Spread in data points about nominal failure line for Fairchild 2N1132 transistor--E+	143
93	Damage line, power, Motorola 2N1132 transistor pulse tested across collector-emitter terminals with positive pulse applied to collector	144
94	Spread in data points about nominal failure line for Motorola 2N1132 transistor--C+	145
95	Damage line, power, Motorola 2N1132 transistor pulse tested across collector-emitter terminals with positive pulse applied to emitter	146
96	Spread in data points about nominal failure line for Motorola 2N1132 transistor--E+	147
97	Damage line, power, Texas Instruments 2N1132 transistor pulse tested across collector-emitter terminals with positive pulse applied to collector	148
98	Spread in data points about nominal failure line for Texas Instruments 2N1132 transistor--C+	149
99	Damage line, power, Texas Instruments 2N1132 transistor pulse tested across collector-emitter terminals with positive pulse applied to emitter	150
100	Spread in data points about nominal failure line for Texas Instruments 2N1132 transistor--E+	151
101	Response of Motorola 2N1132 transistor--E+	152
102	Response of Texas Instruments 2N1132 transistor--E+	152
103	Response of Texas Instruments 2N1132 transistor--C+	153
104	Damage line, power, composite data of Motorola, Texas Instruments, and Fairchild 2N1132 transistors pulse tested across collector-emitter terminals with positive pulse applied to collector	155
105	Spread in data points about nominal failure line for composite data of Motorola, Texas Instruments, and Fairchild 2N1132 transistors--C+	156
106	Damage line, power, composite data of Motorola, Texas Instruments, and Fairchild 2N1132 transistors pulse tested across collector-emitter terminals with positive pulse applied to emitter	157

FIGURES (Cont'd)

		Page
107	Spread in data points about nominal failure line for composite data of Motorola, Texas Instruments, and Fairchild 2N1132 transistors--E+	158
108	Spread in data points about nominal failure line for composite data of Motorola, Texas Instruments, and Fairchild 2N1132 transistors	159
109	2N1132 transistors	160
110	Motorola 2N1132 transistor--E+	162
111	Molten metalization damage on Texas Instruments 2N1132 transistor--E+	163
112	Fairchild 2N1132 transistor--C+	164
113	Typical attenuation characteristics for SM-C-602933 filter	167
114	Relay characterizations	169
115	Pulse test of Bendix filter connector 21-900098-2	172

TABLES

I	Estimated Energy for Degradation	13
II	Devices Ordered for Lance Vulnerability and Hardening Program	16
III	Specific Heat of Silicon at Various Temperatures	31
IV	Damage Test Instrumentation	41
V	1N1200 Family Bulk Surge Impedances	81
VI	Bulk Surge Impedance, 2N1132 Transistor, C-E	153
VII	Capacitor Test Results	170
VIII	Summary of Bendix Filter Connector Tests	171
IX	Summary of Semiconductor Device Failure Parameters	174
X	Summary of Miscellaneous Tests	176

1. INTRODUCTION

The component evaluation phase of the Lance Vulnerability and Hardening (V/H) Test Program had as its objectives the determination of component failure level to electromagnetic pulse (EMP) induced system transients and the evaluation of hardening devices used to prevent or limit such damaging transients. In meeting these objectives, over 50 different types of semiconductor components (about 1800 individual devices) were tested to determine their damage thresholds. A number of semiconductors and nonsemiconductors were evaluated also to determine such parameters as their amplitude limiting capability, impedance, turn-on time, and breakdown level. The test results, the theoretical damage models with their inherent assumptions, and the measurement techniques are presented here.

1.1 System EMP Interaction

The EMP for the most part is generated by the interaction of gamma rays released by a nuclear detonation and the earth's atmosphere. The interaction results in the generation of Compton electrons. Due to such asymmetries as the presence of the earth's magnetic field, atmospheric gradients, and the ground, a net transient electrical current is produced which radiates an intense EMP. Of particular concern is the detonation of a nuclear weapon above the earth's atmosphere. Such a detonation can illuminate large portions of the earth's surface. Being an electromagnetic disturbance, the pulse will interact with any electrical conductor in its path. Thus, electrical transients will be established on all metal structures, power lines, and signal lines exposed to the field. The nature of the electrical transients induced on these conductors will be determined by the characteristics of both the EMP and the conductors themselves. Energy induced on exposed conductors can be reradiated within protective

(shielded) structures or directly cross coupled to cables within shielded structures. The magnitude of the voltages and currents induced can damage sensitive electronic components (such as diodes and transistors) if there exists an electrical path to the device for the EMP induced transient to flow.

The survival of military equipment subjected to an EMP is of particular concern. All major communication systems are linked by either hard wire or radio waves. That is, they either have long runs of communication cables or require some form of antenna. Each can act as an "effective" antenna for EMP energy, as well. Missile fire cables and umbilicals are other examples of entry ports for induced EMP energy. Since EMP energy will be induced on military systems, and since the magnitude of the energy is sufficient to damage the sensitive components, it is necessary to (1) evaluate the vulnerability of existing fielded military systems and harden them where necessary or (2) incorporate hardening concepts in those systems on the drawing boards or in development. The Lance V/H Program has encompassed both the evaluation and hardening of existing systems and the hardening of systems in development.

1.2 Device Sensitivity

The components in electronic systems which are most sensitive to high-level electrical transients are semiconductor devices, that is, diodes, transistors, rectifiers, and integrated circuits (IC's). Other components are sensitive to EMP transients, but generally at higher levels than semiconductors. (There are exceptions--for instance, thin-film low-power resistors). Table I lists the ranges of failure categorized by energy dissipation for other semiconductors and nonsemiconductors previously tested. Large differences in damage thresholds exist just among semiconductors.

TABLE I. ESTIMATED ENERGY FOR DEGRADATION

Device type	Energy (μJ)
Point contact diodes* 1N82A, 1N69A	0.7 to 12
Integrated circuit* μA709	10
Low-power transistor* 2N930, 2N1116A	20 to 1000
High-power transistor* 2N1039 (germanium)	1000
Switching diode* 1N914, 1N933J	70 to 100
Zener diode* 1N702A	1000
Rectifier* 1N537	500
Relay† (welded contacts)	$2(10)^3$ to $100(10)^3$
Resistor 1/4-W carbon	10^4

*Energy required to damage semiconductors with a 1-μs square pulse.
†EMP Handbook, Vol. 2, Defense Nuclear Agency (November 1971).

To obtain a better understanding of the destructive capabilities of the EMP, the magnitude of the energy required to damage devices can be compared to the energy available from the EMP. Typical numbers associated with the signature of the EMP are 50-kV/m peak voltage with a 100-ns pulse width. Assuming a right triangular pulse of 50 kV/m and width of 100 ns, the energy per unit area is

$$\varepsilon = \frac{1}{3}\frac{E^2T}{377}\ (J/m^2) = \frac{2500(10)^6(10)^{-7}}{3 \times 377} \simeq 0.22\ (J/m^2)$$

If the system acts as an effective antenna of 10 m^2 absorbing all available EMP energy, then 2.2 J of transient electrical energy will be induced on the system. This energy in part will eventually reach every component in the system. If the portion of energy that reaches a device in the circuit exceeds the device damage threshold, then the device will be destroyed. The objective of system hardening is, therefore, to assure that the portion of energy that the sensitive device sees is below the device's damage threshold. Generally, a margin of safety is incorporated.

1.3 Hardening Devices

Systems are hardened generally by two techniques, the addition of shielding (such as cable shielding and rf gasketing) and the installation of terminal hardening devices. This report considers the latter. Terminal hardening devices are generally designed to protect

sensitive electronics by limiting the transient EMP induced energy on the input ports to tolerable levels. The energy can be limited by a number of techniques.

Voltage limiters are one of the most common protection devices. They act as open circuits to all input voltages below their limiting level and act as low impedances for all voltages above the limiting threshold. Thus, a 75-V limiter attempts to limit all transients above 75 V to the 75-V level. Since the device has a nonzero impedance for voltages above the threshold limit, the 75-V device used as an example may limit a 200-V transient to 80 V.

Spark gaps act more in the manner of a true switch; when the voltage threshold for the initiation of an arc is reached, instead of limiting the voltage, the gap arcs and shunts the transient from the input ports. The portion of the transient which the circuit inputs see is determined solely by the impedance of the spark gap and its transient response to the excitation.

Filters act in a completely different manner. Instead of limiting transient amplitude directly, they limit the frequency content of the energy input to the circuitry. As an example, low-pass filters are generally employed in power distribution systems. The filters pass dc, 400 Hz, or 4000 Hz, depending on the requirements, but attenuate 100-kHz or greater signals to levels at which the electronics are safe from high-frequency transients. Stray impedances, poor mounting, nonlinearity, and voltage arcing are some of the problems that reduce the effectiveness of filters.

Other terminal protection techniques are circumvention, current limiting, and isolation.

1.4 Lance Vulnerability and Hardening Program

The objectives of the Lance V/H Program were (1) to determine if the Lance Missile System in its proposed production configuration and the associated battalion communications equipment were vulnerable to the exoatmospheric EMP threat and, if so, (2) to harden the system with an appropriate margin of safety. The procedure for meeting these objectives was to subject the Lance Missile System to a below-threat-level simulated EMP field, obtain the electrical transients at sensitive circuit input ports, reduce the transients to an equivalent source, model the sensitive electronics, scale the equivalent source to threat, and analyze the results based on damage test data gathered on the sensitive components. Where damage was predicted, hardening modifications were proposed and evaluated. Recommendations for hardening the system were then submitted to the Lance Project Office.

1.5 Component Evaluation Phase

The component evaluation phase of the Lance V/H Program was concerned with the establishment of damage models for devices in the Lance Missile System which were particularly sensitive to high-level electrical transients or were in particularly vulnerable electrical locations with respect to the induced high-level transients. A portion of the program was devoted to the evaluation of various hardening devices. Table II lists the components ordered for the program and the system or subsystem in which they are found. The hardening devices examined also are listed.

TABLE II. DEVICES ORDERED FOR LANCE VULNERABILITY AND HARDENING PROGRAM

System	Device	Quantity
AN/VRC-46	1N645 diode	40
	1N816 diode	40
	2N270 transistor	50
	2N297A transistor	50
	2N328A transistor	50
	2N335 transistor	40
	2N2198 transistor	50
AN/GRC-39	1N270A diode	50
	2N526 transistor	40
AN/GRC-142	SM-C-602932 surge arrestor	1
	SM-C-602933 filter	4
ME-165/G	1N69A diode	50
AN/GRC-106	2N1613 transistor	50
	1N647 diode	40
	1N3064 diode	40
	2N1132A transistor	50
MD-522/GRC	1N3047B diode	50
	1N3666 diode	50
	2N2727 transistor	50
	2N3440 transistor	50
	2N3636 transistor	50
Fire direction center	1N539 rectifier	50
	1N1202A rectifier	42
	2N489A transistor	50
	2N598 transistor	40
	2N738 transistor	50
	2N1204 transistor	50
	2N1308 transistor	85
	SM692-1 (2N3801) transistor	50
	Polar capacitor	7
Lance peculiar	1N457 diode	100
	1N965B diode	10
	1N1200 rectifier	20
	1N1202 rectifier	20
	1N4003 rectifier	20
	1N4005 rectifier	10
	2N1132 transistor	170
	2N1711 transistor	20
	2N2323 rectifier	10
	2N2453 transistor	20
	2N2801 transistor	20
	2N2297 transistor	20
	2N3069 transistor	10
	1752/17 operational amplifier	2
	10164126(19) relay	1
	10158808(19) relay	1
	µA709 (U5B770931) operational amplifier	10
	UT254 diode	50
	21-900098-1 filter connector	1
	21-900098-2 filter connector	1
	21-900098-3 filter connector	1
	21-900099-1 filter connector	1
	1200 filter	1
	1N5649A TransZorb diode	2
	1N914 diode	49
	1N956B capacitor	10

2. DAMAGE MODELS

Since it was impractical to test every semiconductor in the Lance Missile System to the variety of transient signals that could be induced, selected devices were listed, sample sizes were chosen, devices were obtained, and each device was subjected to rectangular electrical pulses. The thresholds of failure were recorded for different pulse widths, polarities, and device pin combinations. For data obtained in this manner to be applicable to analyses involving nonrectangular wave transients of different durations, appropriate models must be available. This section describes the models employed in the characterization of Lance device failure thresholds. Later sections address the accuracy of the models.

2.1 Device Failure

Before discussing the phenomenological models for device failure, the electrical characteristics of the pn junction are considered. Figure 1 presents the characteristics of a pn junction device typical of a rectifier. The figure does not show all the high-injection-level and temperature effects, but

but does include the major contributions. The equations describing the various regions are given in the figure. The important features of the diode characteristic are the low impedance exhibited in the first quadrant of the graph and the high impedance in the third. The device under reverse bias acts as an extremely large resistance until the voltage level approaches the breakdown level (V_A). The slope of the characteristic curve decreases abruptly at the breakdown level. To a first approximation, the current, I, that flows at a given voltage, V, above the breakdown voltage is

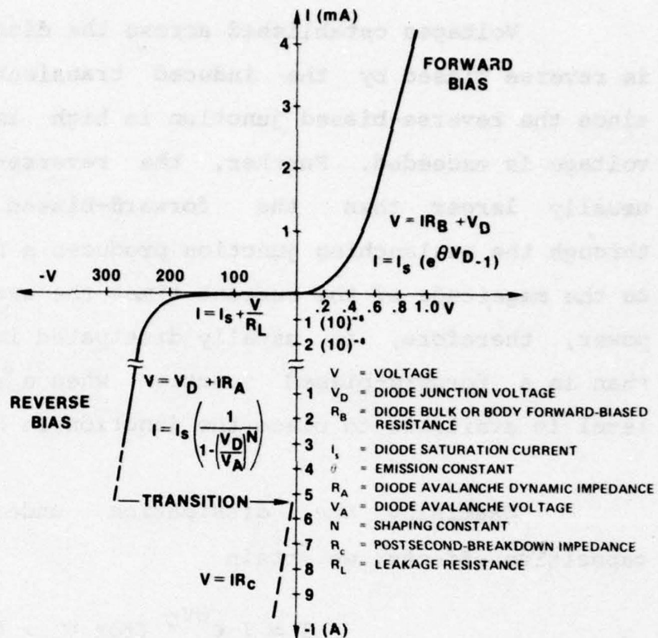

Figure 1. Direct-current characteristic of pn junction.

$$I = \frac{V - V_A}{R_A} \; ; \; R_A = \left.\frac{\Delta V}{\Delta I}\right|_{V>V_A} \tag{1}$$

For most devices, the slope after device breakdown, R_A, in the third quadrant is higher than the slope of the characteristic in the first quadrant. Typical values are 1 to 2 ohms for the forward impedance and 20 to 100 ohms for the reverse-biased dynamic impedance (R_A) under high current levels. One of the notable exceptions to the higher dynamic impedance in the reverse-biased polarity is the zener or reference diode, which is designed to conduct large current in the avalanche mode.

Voltages established across the diode are larger when the diode is reverse biased by the induced transient than when forward biased, since the reverse-biased junction is high impedance until the avalanche voltage is exceeded. Further, the reverse-biased dynamic impedance is usually larger than the forward-biased impedance. The current through the avalanching junction produces a real power dissipation equal to the magnitude of the current times the avalanche voltage level. More power, therefore, is usually dissipated in a reverse-biased junction than in a forward-biased junction when a sufficient transient voltage level is available to place the junction in breakdown.

Examining the dissipation under forward bias, ignoring capacitive effects, we obtain

$$I \simeq I_s e^{\Theta V_D} \quad (\text{for } V_D > 0.1 \text{ V}) \; , \tag{2}$$

where I_s is the diode saturation current, Θ is the emission constant, and V_D is the diode junction voltage. Then,

$$\ln\left(I/I_s\right) \simeq \Theta V_D$$

or

$$V_D \simeq \ln\left[\left(I/I_s\right)^{1/\Theta}\right] ,$$

$$P = IV = I^2 R_B + IV_D \; ,$$

$$P \simeq I^2 R_B + I \ln\left[\left(I/I_s\right)^{1/\Theta}\right] , \tag{3}$$

where P is power and R_B is the diode bulk or body forward resistance. For large currents, the $I^2 R_B$ of equation (3) dominates, and the power dissipated under forward bias, P_f, becomes

$$P_f \simeq I^2 R_B \quad (\text{for large currents}) \; . \tag{4}$$

In the reverse-biased polarity (the third quadrant of fig. 1), the response can be modeled as an ideal diode, a series resistor equal to R_A and a voltage source equal in output to V_A. Capacitive effects are ignored. The current level before avalanche is so low that the power dissipation is negligible. At voltage levels above the avalanche threshold, the reverse power dissipation, P_r, is approximately

$$P_r \simeq V_A I + I^2 R_A \quad \left(V > V_A\right) . \tag{5}$$

For large currents, the $I^2 R_A$ term of equation (5) dominates:

$$P_r \simeq I^2 R_A \text{ (for large currents)} . \tag{6}$$

The approximation of equation (6) is valid only for very short pulse widths, since the device quickly enters a transition region as depicted in figure 1 and suffers an abrupt impedance change. This transition has been termed "second breakdown." In some devices, the transition is made in steps. A device having one step in the transition is said to have a secondary and a tertiary breakdown. The states before and after the transition in figure 1 are shown as dashed lines because both the energy or power dissipated and the period of dissipation determine the level (voltage, current, or both) at which the transition will occur. The path of the transition depends on the impedance in series with the junction. After the complete transition is made, the device appears to a first approximation as a resistance, R_C. Since the transition can be exceedingly abrupt, large current can flow through the junction from capacitance in the external circuitry, and a large instantaneous $I^2 R_C$ power dissipation results.

Second breakdown receives considerable attention in this report. Second breakdown appears to be thermally initiated and generally leads to device failure. The energy level required to initiate second breakdown (reverse biased) is usually much lower than

that required to damage the pn junction forward biased. Further negligible energy (compared to the initiation energy) is required to damage a device after the second-breakdown transition. Thus, second breakdown generally establishes the threshold of the minimum energy for failure for semiconductors subjected to high-level transients of a pn junction to a rectangular voltage pulse. The second-breakdown point is indicated in figure 2. Since device failure usually occurs shortly after a device is put into second breakdown, second breakdown is often considered the point of device failure.

Summarizing:

a. The pn junction characteristic demonstrates a low forward-biased impedance and a high reverse-biased impedance.

b. The dynamic impedance R_A after breakdown (avalanche) is generally higher than the forward-biased impedance at the same current levels.

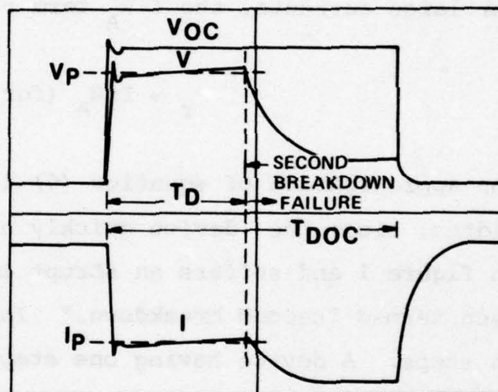

Figure 2. Typical response of pn junction to rectangular voltage pulse of open-circuit voltage (V_{OC}) and pulse duration (T_{DOC}); T_D: presecond-breakdown pulse duration (delay time); V_P: average value of presecond-breakdown voltage; V_I: average value of presecond-breakdown current.

c. For usual situations, voltages impressed on the semiconductor device are higher when the same transient biases the device in the reverse direction than when it does in the forward direction.

d. For usual situations, the transfer of energy from the induced transient to the pn device is greater when the transient biases the device in the reverse direction than when it does in the forward direction. However, the transient voltage level must be higher than the avalanche or breakdown level of the junction.

e. Second breakdown (fig. 1, 2) precedes device failure in many reverse-biased pn junctions subjected to high-level short transients.

f. The energy required to initiate second breakdown and then device failure is less than the energy required to damage the same device biased in the forward direction.

As a consequence, much work has centered on the establishment of failure levels for semiconductor devices based on the reverse-biased second breakdown mechanism leading to device failure. The generally accepted models are discussed next.

2.2 Second-Breakdown Models

Although second breakdown (fig. 1, 2) has been shown to be nondestructive in itself,[1] very little energy is required to cause permanent degradation after a device is in second breakdown. In one study,[2] the energy stored in the stray instrumentation capacitance (~10 pF at 120 V) was instrumental in causing damage after second breakdown. Consequently, second breakdown has been treated as the threshold for damage in the analysis of transient reverse-biased junction devices.

Since second breakdown appears to be thermally initiated, the energy and, consequently, power to damage a semiconductor device

---

[1]*Paul P. Budenstein, Duane H. Pontius, and Wallace B. Smith, Second Breakdown and Damage in Semiconductor Junction Devices, Auburn University Report No. RG-TR-72-15, Auburn, AL (April 1972).*

[2]*Dante M. Tasca and Joseph C. Peden, Feasibility Study of Developing a Nondestructive Screening Procedure for Thermal Second Breakdown, General Electric Co., Philadelphia, PA (July 1971).*

junction have been examined by a number of sources.[3-5] Thermal models of various complexity have been postulated. The consensus has equations (7) and (8) as the best prediction of general device failure to reverse-biased transients to date. These equations are a generalization of the models presented by the Defense Nuclear Agency (DNA).[6]

$$P_D = K_1 T_D^{-1} + K_2 T_D^{-\frac{1}{2}} + K_3 \qquad (7)$$

and, in terms of energy,

$$E_D = K_1 + K_2 T_D^{\frac{1}{2}} + K_3 T_D \,, \qquad (8)$$

where P_D and E_D are power and energy, respectively, required to damage a semiconductor junction with a reverse-biased rectangular electrical pulse. The constants K_1, K_2, and K_3 are device dependent, and T_D is the pulse time delay (seconds). K_1 represents a constant energy to damage for short pulses, and K_3 is the "dc" power dissipation. K_2 describes the relationship between these two regions.

In practice, the investigation of semiconductor damage has been divided into three time regimes based on equations (7) and (8). The regimes are short pulse, long pulse, and "dc." The term "dc" is in quotation marks because it refers to pulses of sufficient width to

---

[3] *J. B. Singletary and D. C. Wunsch, Final Summary Report on Semiconductor Damage Study Phase II, Braddock, Dunn, and McDonald BDM/A-66-70-TR, Albuquerque, NM (June 1970).*

[4] *M. E. Daniel, Development of Mathematical Models of Semiconductor Devices for Computer Aided Circuit Analysis, Proceedings of IEEE, 55 (November 1967), 1913.*

[5] *H. A. Schafft, Second Breakdown--A Comprehensive Review, Proceedings of IEEE, 55 (August 1967).*

[6] *EMP [Electromagnetic Pulse] Handbook, Vol. 2, Defense Nuclear Agency (November 1971).*

establish thermal equilibrium in the device--that is, pulses of sufficient width so that all thermal transients have subsided and the heat sink or case is effectively radiating. Since the pulses studied for this report are short compared to semiconductor thermal time constants, the K_3 term is dropped from equations (7) and (8), so that

$$P_D = K_1 T_D^{-1} + K_2 T_D^{-\frac{1}{2}} , \tag{9}$$

$$E_D = K_1 + K_2 T_D^{\frac{1}{2}} . \tag{10}$$

In practice, K_1 and K_2 are empirically determined from reverse rectangular pulse damage tests. Often, the models are further reduced to either $K_1 T_D^{-1}$ or $K_2 T_D^{-\frac{1}{2}}$ time regimes, depending on the range of pulse widths of interest. The breakpoint where $K_1 T_D^{-1} = K_2 T_D^{-\frac{1}{2}}$ varies for each device type, but appears to occur at pulse widths between 50 ns and 1 µs.

The simple thermal second-breakdown model is based on the following properties of semiconductor devices.

a. The melt temperature of an alloy of a semiconductor and a metal can be lower than the melt temperature of either of the two pure constituents. Figure 3 indicates the melt temperature and composition dependence for aluminum and silicon. The minimum melt temperature is called the eutectic temperature.

b. The intrinsic semiconductor resistivity decreases with temperature. Doped semiconductor resistivity increases with temperature until the thermally excited carriers dominate the donor or acceptor carriers. At this point, the resistivity decreases with temperature. Figure 4 shows the relationship between resistivity and temperature for

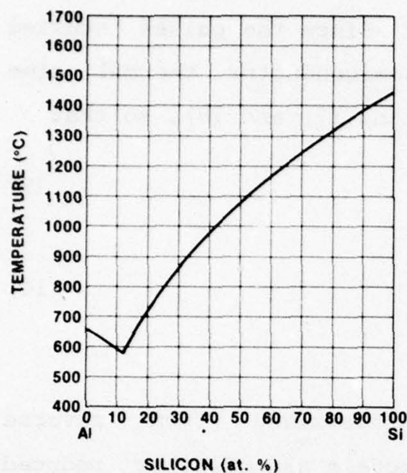

Figure 3. Phase diagram for aluminum and silicon; eutectic temperature 576°C with composition of 11% silicon and 89% aluminum (data from R. M. Warner and J. N. Fordemevalt, eds., Integrated Circuits, McGraw-Hill Book Co., New York, 1965).

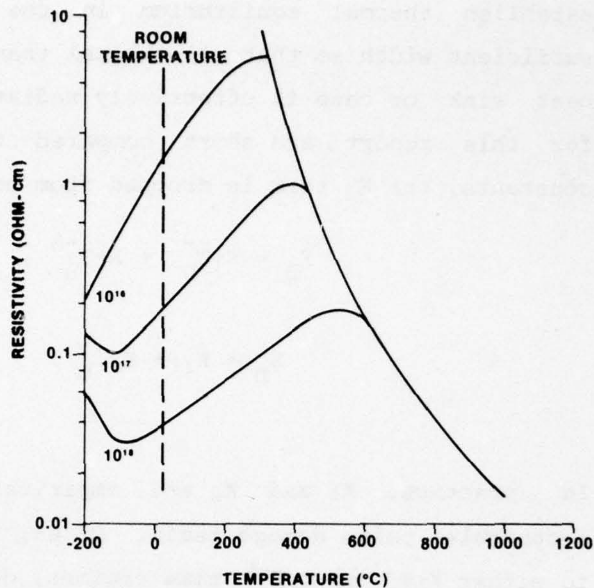

Figure 4. Resistivity versus temperature for various boron doping levels in silicon (data from D. M. Tasca and J. C. Peden, Pulsed Power Failure Modes in Semiconductor Devices, U.S. Army Mobility Equipment Research and Development Center, Fort Belvoir, VA, April 1970).

various boron doping levels in silicon. The temperature associated with each peak in the constant dopant concentration contours is called the intrinsic temperature.

c. The junction leakage current is extremely sensitive to temperature as follows:

$$I = K'T^3 e^{-E_g/kT} \left(e^{qV/kT} - 1\right) , \quad (11)$$

where K' is a constant, T is the temperature, E_g is the energy width of the forbidden band, k is Boltzmann's constant, and q is the charge on an electron.

d. Thermal "time constants" in silicon and germanium are long compared to the pulse widths under consideration.

The literature[5] has indicated that a critical temperature exists for the initiation of second breakdown. Properties a to c have a critical temperature, the eutectic temperature, the intrinsic temperature for doped semiconductors, and the temperature at which the leakage current density accounts for the total current density in a reverse-biased junction. Consequently, properties a to c have been suggested as the initiating mechanism in second-breakdown prediction models.

Since the thermal time constants of the material are long compared to the electrical transients, uneven heating occurs in the device. There is insufficient time for heat to diffuse from localized hot regions to cooler regions. Heating may be localized due to the presence of the junction, the ohmic contact regions, crystal defects, and irregularities in the passivation, metalization, junction, and bulk material.

As can be seen from figure 4, after the intrinsic temperature is reached, the resistance drops sharply with increase in temperature. If a transient electrical signal causes the unequal heating of a semiconductor device and the intrinsic temperature is reached in a localized region, additional electrical energy converted to heat lowers the resistance of the region and causes larger current flow and, consequently, larger energy dissipation (thermal runaway). If the current is not limited by external means, a melt region forms. For the metal-semiconductor interface, when the eutectic temperature is exceeded, both materials dissolve to form a large volume of eutectic alloy. The conductivity in the region increases, more energy in proportion is dissipated, the eutectic region grows larger, and eventually sufficient diffusion may mask normal device action.

---

[5] *H. A. Schafft, Second Breakdown--A Comprehensive Review, Proceedings of IEEE, 55 (August 1967).*

Considering the leakage current relationship with temperature, a local thermal runaway situation can result.

Regardless of which effect leads to second breakdown, a model can be formulated based on localized heating and a critical temperature. The model presented in this section is based on localized heating of the pn junction. The model considers a rectangular transient, and the discussion treats the $T_D^{-1/2}$ and T_D^{-1} (eq (7)) regions separately.

2.2.1 Long-Duration Second-Breakdown Model

The long-duration ($T_D^{-1/2}$) region is characterized by thermal transient diffusion from the hot-spot areas. Although the thermal time constants are large, diffusion is still a factor. Heat is allowed to diffuse into the bulk material, but the device surface and heat sink play no part. Two one-dimensional cases have been treated in the literature. The results of each case are presented. Both cases assume that the electrical energy (current × avalanche voltage × pulse width) is dissipated in a thin region at the device junction.

In case 1, the energy is dissipated at the junction between the semiconductor chip and a counterelectrode. Another counterelectrode is attached to the other side of the chip. Both electrodes were considered infinite in extent (fig. 5).[7] In case 2, the junction is at the center of a semiconductor of essentially infinite extent (fig. 6).[8] In both cases,[7,8] the heat equation

$$\frac{\partial}{\partial x}\left(k\frac{\partial T}{\partial x}\right) - \rho C_p \frac{\partial T}{\partial t} = 0 \,, \tag{12}$$

[7] *R. L. Davies and F. E. Gentry, Control of Electric Field at the Surface on PN Junctions, IEEE Trans. Electron Devices, ED-11 (July 1964), 313-323.*

[8] *D. C. Wunsch and L. Marzitelli, Semiconductor and Nonsemiconductor Damage Study, Final Report, Vol. 1, Braddock, Dunn, and McDonald BDM-376-69-F-0168, Albuquerque, NM (April 1969).*

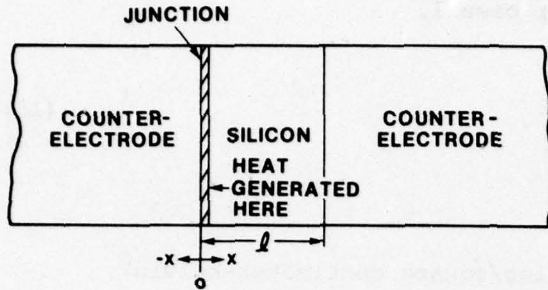

Figure 5. Model for case one of long-duration, second-breakdown model.

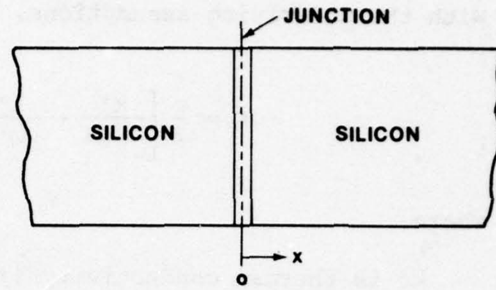

Figure 6. Model for case two of long-duration, second-breakdown model.

where

x is distance,

ρ is the density (grams/cubic centimeter),

C_p is the specific heat at constant pressure (watt-second/gram kelvin),

is solved with a number of assumptions and with the boundary conditions indicated by the figures. Both cases reduce to the same general form for a constant power to damage. The expression is

$$\frac{P_D}{A} = K\left(T_m - T_i\right)T_D^{-\frac{1}{2}} , \tag{13}$$

where

A is the effective junction area (square centimeters)

T_m is the critical temperature (kelvin)

T_i is the initial temperature (kelvin).

In terms of energy,

$$\frac{E_D}{A} = \frac{P_D}{A} T_D = K\left(T_m - T_i\right)T_D^{\frac{1}{2}} . \tag{14}$$

With the underlying assumptions, for case 1,

$$K = \frac{\pi}{2}\left[\frac{k'}{(\alpha_1)^{1/2}} + \frac{k'}{(\alpha_2)^{1/2}}\right], \tag{15}$$

where

k' is thermal conductivity (joules/square centimeter-kelvin),

α is $k'/\rho C_p$

subscript 2 indicates the model regions defined in figure 5.

For case 2,

$$K = \left(\pi k \rho C_p\right)^{1/2} \tag{16}$$

Among the assumptions for both models are that both the specific heat, C_p, and the thermal conductivity, k', are independent of temperature and that the external boundaries are at infinity. In case 1, it is assumed also that

$$k_1'(\alpha_2)^{1/2} = k_2'(\alpha_1)^{1/2} \tag{17}$$

Other researchers treated different geometries, yet found the same temperature dependency.[9]

2.2.2 Short-Duration Second-Breakdown Model

In section 2.2.1, the main assumptions were that the electrical energy was dissipated in the junction region and the thickness of this junction region was much smaller than the cross-sectional area. The thickness of this region was considered small

---

[9] *D. M. Tasca and J. C. Peden, Pulsed Power Failure Modes in Semiconductor Devices, U.S. Army Mobility Equipment Research and Development Center, Fort Belvoir, VA (April 1970).*

compared to the time required for the propagation of heat to colder bulk areas for these long-duration pulses. Local cooling to the bulk was the major factor in establishing the $T_D^{-\frac{1}{2}}$ dependency in power required for failure.* As the applied pulses become shorter, two factors come to bear which indicate an exponent of -1 or greater for pulse width in the power relationship.

The first factor has been discussed regarding equation (5). The equation is a first approximation to the power dissipated in a reverse-biased diode. At the shorter pulses, larger power dissipated is required to supply the energy for second-breakdown initiation. Therefore, at the shorter pulses, larger currents are required. At the large currents, the I^2R_A term becomes significant. At extremely high current levels, the major dissipation appears to be in the bulk material, and the region is heated more evenly.

The second factor is the width of the electrical pulses with respect to the heated regions and the thermal time constants. The heated regions expand in size with decreasing pulse width due to bulk heating, while the ratio of the thermal time constant to the pulse duration increases due to the variation in thermal conductivity with temperature. Thermal propagation from the heated regions becomes insignificant, and the problem can be treated as a local adiabatic process.

From the concept of a critical temperature, the heat energy required to reach a given temperature in a constant volume where heat is uniformly generated is

$$E_D = C_p \rho V' \left(T_m - T_i\right), \qquad (18)$$

where V' is the semiconductor volume (or effective volume).

$T_D^{-\frac{1}{2}}$ and T_D^{-1} refer to the slope ($-\frac{1}{2}$ or -1) of the power versus time delay line on a logarithmic plot.

Since the energy deposited is the power dissipated times the pulse width for rectangular pulses, equation (18) becomes

$$P_D = E_D T_D^{-1} = C_p \rho V' \left(T_m - T_i\right) T_D^{-1} \ . \qquad (19)$$

The pn junction device under transient forward bias can be expected to be dependent with a rectangular pulse duration of the same form as equations (7) and (8). The forward-biased pn junction represents a low impedance. Consequently, at moderate current levels, the I^2R_B term dominates the power dissipation expression. The uniformity of the dissipation throughout the bulk indicates a dependence of T_D^{-1} in power to fail out to much larger pulses than power-to-failure results. The relationship between forward-biased and reverse-biased power-to-fail thresholds depends on the device geometry and doping levels.

2.2.3 Discussion of Model

In figure 7, the thermal conductivity of high-purity silicon is presented as a function of temperature. The conductivity varies approximately as $T^{-3/2}$ over a broad range of temperatures. The assumptions made for the models are poor at best. Reduced thermal conductivity at higher temperatures promotes localized heating. As a region heats, the thermal conductivity drops, and the heat from the region diffuses slowly. In another study,[8] the variation in thermal conductivity was considered, and an effective value was calculated. This effective thermal conductivity was based on piecewise solutions of the heat equation for small ranges of temperature from room temperature to the temperature of interest. The effective thermal conductivity for the transition from 25° to 675°C was found to be 0.526 W/cm-K. (At this temperature, alloying occurs in a tungsten-silicon system,[7] presumably

---

[7] *R. L. Davies and F. E. Gentry, Control of Electric Field at the Surface on PN Junctions, IEEE Trans. Electron Devices, ED-11 (July 1964), 313-323.*

[8] *D. C. Wunsch and L. Marzitelli, Semiconductor and Nonsemiconductor Damage Study, Final Report, Vol. 1, Braddock, Dunn, and McDonald BDM-376-69-F-0168, Albuquerque, NM (April 1969).*

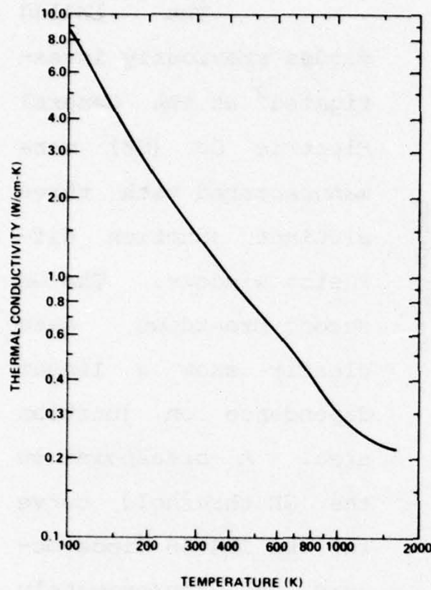

Figure 7. Thermal conductivity of high-purity silicon as function of temperature (data from M. Neuberger et al, Silicon, Hughes Aircraft Co., October 1969).

TABLE III. SPECIFIC HEAT OF SILICON AT VARIOUS TEMPERATURES

Specific heat (J/g-K)	Temperature (°C)
0.6907	0
0.7158	27
0.7702	100
0.9272	800

Source: M. Neuberger et al, Silicon, Hughes Aircraft Co. (October 1969).

the eutectic temperature of that system. Temperatures close to this value have received considerable attention in the literature.) The specific heat also varies with temperature, but much less. Values of the specific heat in silicon for various temperatures are given in table III.

By using the effective thermal conductivity of 0.526 W/cm-K and a value of 0.835 for an average of the specific heat in the temperature range of interest with $\rho = 2.33$ g/cm^3, equations (13) and (14) for case 2 and equations (18) and (19) can be written as

$$\frac{P_D}{A} = 1160 T_D^{-1/2} , \quad (20)$$

$$\frac{E_D}{A} = 1160 T_D^{1/2} , \quad (21)$$

$$\frac{P_D}{V'} = 1260 T_D , \quad (22)$$

$$\frac{E_D}{V'} = 1260 , \quad (23)$$

respectively, assuming a critical temperature of 675°C. Figure 8 plots equations (20) to (23) with a value of 10^{-4} cm^2 for A and 10^{-7} cm^3 for V'. The curves are typical of a low-power, 100-V breakdown, switching diode (1N914 and 1N4148).

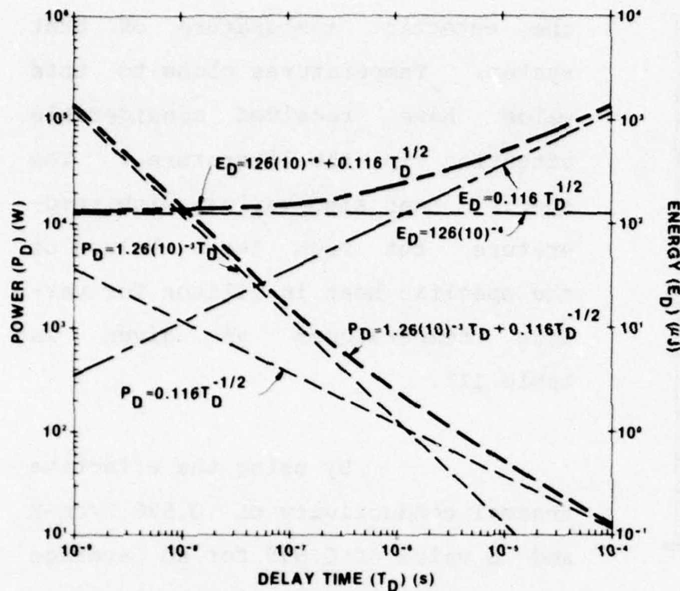

Figure 8. Second-breakdown thresholds.

The 1N4148 diodes previously investigated[2] at the General Electric Co. (GE) were manufactured with three distinct junction diffusion windows. The GE second-breakdown data clearly show a linear dependence on junction area. A breakpoint on the GE threshold curve for the 1N4148 diode occurs at approximately 1 μs. If the choice of 675°C for the critical temperature is approximately correct and all above parameters are constant over the pulse-width range, the 1N4148 diode data roughly agree with the composite curve of figure 8.

Optical measurements of devices under electrical stress indicate nonuniform junction dissipation. Wunsch and Marzitelli postulated[8] an average effective area over many device types of one-half to one-third the actual junction area. In their model, the critical temperature was 1415°C, the melt temperature of silicon. They indicated that areas as small as or smaller than 1/10 the junction area may be involved, depending on the device. Consequently, equations (20) to (23) must be used with adequate caution.

---

[2]*Dante M. Tasca and Joseph C. Peden, Feasibility Study of Developing a Nondestructive Screening Procedure for Thermal Second Breakdown, General Electric Co., Philadelphia, PA (July 1971).*

[8]*D. C. Wunsch and L. Marzitelli, Semiconductor and Nonsemiconductor Damage Study, Final Report, Vol. 1, Braddock, Dunn, and McDonald BDM-376-69-F-0168, Albuquerque, NM (April 1969).*

Summarizing, the models have been derived from rather simplistic cases. The assumptions in the derivation often contradict experiment. The nonlinearities and dynamics of the electrical and thermal system have been decoupled and linearized. As a result, the models by themselves are poor predictors of second breakdown. However, the models are useful when the constants of equations (9) and (10) are derived from test data. Large samples of the generic device type of interest are tested by subjecting the device junction to reverse-biased rectangular transients of varying duration and determining the point of second breakdown. The curves of equation (7) or (8) are then fit to the data, and values for the constants are obtained. The resultant curves are then used to predict the second-breakdown (damage) point at other pulse widths.

2.3 Metalization Failure

Experimenters have found that some devices, especially IC's, exhibit metalization failure at lower levels than expected for second-breakdown initiated failures. The prime metalization and interconnection-lead failure mechanism is thermal heating. The thermal time constants for the common metals used in semiconductor device construction are not far different from those of semiconductor materials. The electrical pulse widths of concern are small compared to the time for thermal propagation; it is a transient thermal problem.

Since the manufacturer attempts to maintain uniformity in interconnection-lead geometry and metalization runs, the heating, though transient, is more uniform than within the semiconductor chip itself (except for the skin effect). Failure invariably occurs at those points in the metalization where, by design or accident, the metallic cross section is at its minimum and, consequently, the current density is a maximum. This failure location could be at a metalization step across a

silicon dioxide layer on the chip (where metalization fracture regions can occur) or at the interconnection-lead contact-bead interface.

The skin effect could conceivably play a part in the damage of physically large devices to extremely short EMP induced transients of high-frequency content. One skin depth, δ, or the depth of wave propagation for which the wave amplitude has decayed by e^{-1}, is defined as

$$\delta = \left(\frac{2}{\omega\mu\sigma}\right)^{\frac{1}{2}} . \tag{24}$$

In equation (24), $\omega = 2\pi$ frequency, μ is the material permeability (for our situation, essentially $4\pi \times 10^{-7}$/H/m that of free space), and σ is the material conductivity (mhos/meter). For aluminum, $\sigma = 10^8/2.63$ at 0°C; for gold, $\sigma = 10^8/2.44$ at 20°C; and for both p- and n-doped silicon, σ = from 10^6 for heavy doping levels (10^{21} atoms/cm^2) to 1 for very light doping (10^{14} atoms/cm^3), all at 300 K.

At 100 MHz, the skin depths become as follows:

Aluminum	8.1 μm
Gold	7.8 μm
Silicon, heavily doped	50 μm
Silicon, lightly doped	50 mm

The skin effect is negligible in the semiconductor, but may contribute to metalization failure, though its effect is generally negligible.

A model for metalization failure based on a similar treatment to that given in section 2.2.2 for semiconductors can be formulated. The critical temperature can be the metalization melt

temperature or the eutectic temperature. The thermal conductivity of aluminum is approximately five times the effective thermal conductivity of silicon, while the density and specific heat are almost the same. The thermal time constants in aluminum are, therefore, approximately one-fifth those of silicon. A more detailed presentation of a metalization failure model is given by Tasca and Peden.[9]

2.4 Voltage Breakdown

In a number of semiconductor device types for particular manufacturers, failure depends on the magnitude of impressed voltage across the device leads. The initiating mechanism is a punch through or dielectric breakdown in the device, between metalization or across the interconnection leads. Such breakdowns occur at the points of highest field strength and, thus, are extremely geometry dependent. The dielectric strength of air and nitrogen is approximately 3 V/μm (STP); that of silicon monoxide and silicon dioxide approximates or equals 100 V/μm, depending on the doping levels. Geometric separation distances are small in semiconductors; for instance, SiO and SiO_2 layers can be as thin as 0.1 μm. Therefore, voltage-dependent failure can be expected and, indeed, is found in some semiconductors subjected to short high-voltage transients. The failure voltage level is affected by manufacturing defects, junction irregularity, and minute material irregularities. The results of such a dielectric failure are low-impedance paths across the device junction and lead or metalization damage. The extent of the damage depends on the energy dissipated after the breakdown.

Figure 9 presents a typical test series for a voltage-failure dependent device subjected to reverse-biased rectangular pulses. This

[9]*D. M. Tasca and J. C. Peden, Pulsed Power Failure Modes in Semiconductor Devices, U.S. Army Mobility Equipment Research and Development Center, Fort Belvoir, VA (April 1970).*

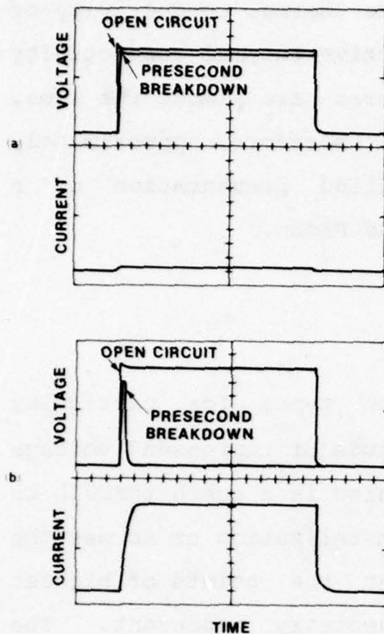

Figure 9. Typical response of single-junction unbiased device subjected to reverse-biased rectangular transient exhibiting voltage dependent (or "turn on") failure: (a) pulse 1--no device degradation; (b) pulse 2--device failure.

type of failure can occur in some high-impedance devices with a forward-biased pulse transient. The energy dissipated in pulse 2 before the drop in voltage is much smaller than the energy dissipated at the lower voltage pulse 1.

2.5 General Observations

The majority of semiconductor devices tested in the Lance component evaluation phase failed in a manner consistent with the transient thermal second-breakdown model. The overall percentage of devices which failed in such a manner ranged from 70 to 80 percent.

The voltage-breakdown failure accounted for as much as 10 to 15 percent of the device types. The remaining 5 percent exhibited metalization damage and anomalous behavior.

Generally, devices of a particular generic type and manufacturer exhibited the same failure mechanism. In the exceptions, only a few devices showed divergence. The probable causes for the multiple mechanisms were manufacturing differences or device defects.

2.6 Failure from Complex Waveshapes

The models presented for second breakdown and thermal failure are based on a constant energy dissipation for a given period. The EMP-induced transients are highly time dependent and, consequently, so

is the power that is dissipated in a device junction. Approaches[10,11] to determine the failure level of semiconductor components subjected to time-dependent excitation were based on the critical temperature concept. The device is modeled and the temperature is calculated as a function of time in a given region--generally, the junction. When the temperature reaches the critical temperature, the device is considered failed. These models have been used jointly with circuit analysis codes so that the system can be analyzed.

The validity of such an approach has not yet been verified. The model parameters such as effective volume or junction area and thermal conductivity can vary with time. The location of the effective volume or area may change, and then even the critical temperature may be some function of time.

2.7 Bias and Multijunction Devices

So far we have discussed the failure (especially that associated with second breakdown) of a single-junction unbiased device. A more typical situation is a biased multijunction device subjected to a transient. This situation has received very little attention. The subject is generally handled in the same manner as single-junction unbiased devices. Empirical data gathered from unbiased rectangular pulse testing generally are relied upon, as are the models discussed in section 2.2. However, some faiure mechanisms in multijunction devices differ from those in single-junction devices.

A transistor collector to base (C-B) (the emitter lead open) pulsed into avalanche may fail emitter to base (E-B) due to the internal

[10] *L. R. McMurray and C. T. Kleiner, Adaptation of the P-N Junction Burnout Model to Circuit Analysis Codes, IEEE Annual Conference on Nuclear and Space Radiation Effects, 19 (July 1972), 76.*

[11] *J. E. Godts, Semiconductor Avalanche Power Failure, Martin Marietta Corp. Technical Note, Orlando, FL (December 1968).*

biasing from field gradients. Portions of the E-B junction may be forward biased and portions may be reverse biased into avalanche so that failure of the E-B base junction occurs. The failure depends on current.[9,12] This failure depends strongly on device design. Multijunction devices are subjected also to failure initiated by depletion layer punch through and pnpn switching, both of which depend on voltage.

Recent studies have indicated that second breakdown can be initiated by a transient signal and can be sustained by the dc bias on the device. This action is analogous to pnpn latch up. If the current limiting is insufficient, the junction fails. If the current limiting is sufficient, the device appears to be recoverable with no apparent degradation.

2.8 Postdamage Electrical Characteristics

Failure at the threshold of damage due to an internal thermal process is indicated by a decrease in the junction breakdown voltage and device gain (where applicable). In most devices (when the transient source impedance is 50 to 100 ohms), failure is complete (that is, zero breakdown voltage and zero gain--essentially a junction short circuit). Some devices degrade to a varying degree over large ranges of energy dissipation of a given pulse width. Criteria for device failure must then be established.

---

[9] *D. M. Tasca and J. C. Peden, Pulsed Power Failure Modes in Semiconductor Devices, U.S. Army Mobility Equipment Research and Development Center, Fort Belvoir, VA (April 1970).*

[12] *R. Brown, J. D. Holder, and V. W. Ruwe, Statistical Component Damage Study, Component Damage Conference, U.S. Army Mobility Equipment Research and Development Center, Fort Belvoir, VA (April 1970).*

If a device is under bias or an extremely large transient (much larger than the failure threshold) is impressed, the device usually exhibits an open circuit between the leads in question. Usually, metalization melt has occurred. Mostly, such a failure is a result of the current surge following the second-breakdown transition.

3. TEST AND ANALYTICAL TECHNIQUES

To place the damage test program in perspective, this section discusses the complete system assessment and then briefly reviews the testing and data-reduction procedures.[13,14]

3.1 System Assessment

The procedure used in the assessment of the Lance Missile System is diagramed in figure 10. There are three basic efforts: (1) the field test of the system at an EMP simulation facility (the Harry Diamond Laboratories Woodbridge Research Facility Biconic antenna), (2) the modeling of the system circuits on computer circuit analysis codes, and (3) the damage testing of components.

The data from the field tests are reduced, and a coupling model is formed as indicated in figure 10. The model is then extrapolated to threat by a linear factor and is ready for inclusion into the circuit modeled on the circuit analysis code.

The reduction of the component test data parallels the reduction of the field data. An electrical model of the device under

[13] *LANCE Vulnerability and Hardening Program, Test Plan, Annex A, General Procedures, Harry Diamond Laboratories (3 April 1972).*

[14] *J. R. Miletta, R. E. Parsons, and M. S. Bostian, Lance Vulnerability and Hardening Test Program Interim Semiconductor Damage Report, Harry Diamond Laboratories (September 1971).*

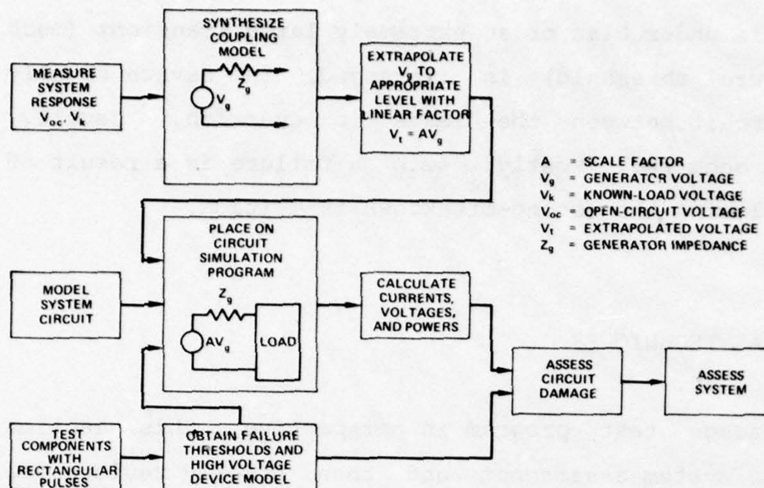

Figure 10. Basic flow diagram for assessment of system vulnerability to EMP.

high-level excitation is formed, and the failure thresholds are obtained (generally accompanied by a fit to the models presented in section 2). The high-level models are installed in the circuit analysis model. The analytic code is then run, and the voltages, currents, and power dissipations are calculated at all the critical points in the circuit. Based on the failure mode of the critical components in the circuit, the calculated variables are compared to the component thresholds. Figure 11 presents a technique for evaluating the failure of a component

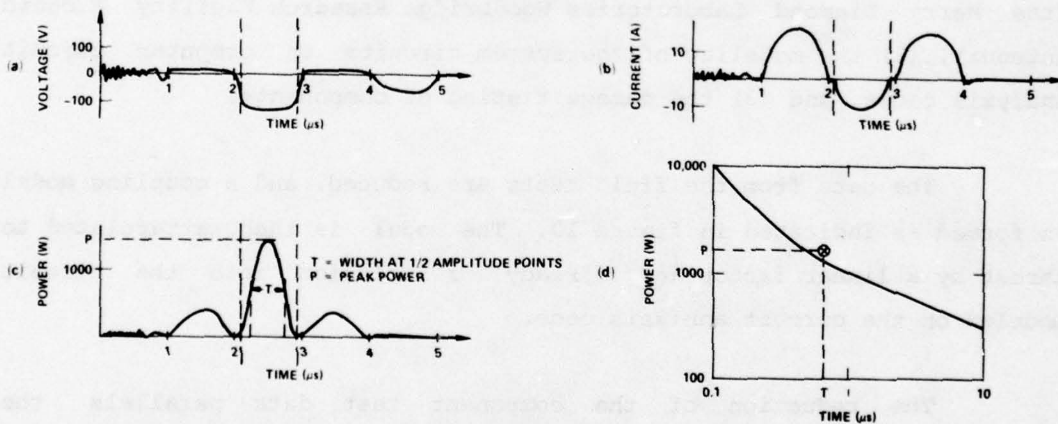

Figure 11. Technique for determination of device damage from high-level transient pulses (based on thermal-damage model): (a) calculated EMP-induced voltage across 100-V breakdown switching diode (1Nxxx); (b) calculated EMP-induced current through 1Nxxx; (c) calculated instantaneous power in 1Nxxx; (d) damage threshold for 1Nxxx (calculated dissipation indicates that device will fail).

with a thermal damage threshold. The extent and nature of damage in the circuit are evaluated. Other circuits are analyzed, and the system vulnerability is determined. The evaluation process is detailed elsewhere.[13]

3.2 Testing Procedure

The instrumentation used in the component test program is listed in table IV in three groups: (1) for short pulses (1 to 100 ns), (2) for long pulses (0.1 to 100 μs), and (3) for diagnosis (generally used in determining device degradation or damage). The semiconductor damage tests were conducted in a standard manner. The nonsemiconductor and special tests required specialized procedures, which are discussed with the test results. Figure 12 diagrams the standard procedural flow for the semiconductor damage test. The procedure is divided into short- and long-pulse tests. The long-pulse tests preceded the short-pulse tests for convenience. It is much easier to test to long pulses and reduce long-pulse data.

TABLE IV. DAMAGE TEST INSTRUMENTATION

Test	Instrumentation	Quantity
Short pulse	Tektronix T-109 pulse generator	1
	Coaxial high-voltage pulse generator*	1 set
	Dielectric-gap discharge pulse generator†	1
	Tektronix 519 oscilloscope	2
	Tektronix 454 oscilloscope	1
	Spellman ST60 power supply	1
	Sorenson 1121 power supply	1
Long pulse	Thyratron pulse generator	1
	Velonex pulse generator 350 with plug-ins	1
	Tektronix 555 oscilloscope	1
	Tektronix CT-2 current probe	1
	Pearson 411 current probe	4
	Tektronix P6006 voltage probe	1
	Tektronix P6007 voltage probe	1
	2.5-kV power supply	1
Diagnostic	Hewlett-Packard 606 pulse generator	1
	Tektronix 576 curve tracer	1
	Hewlett-Packard 8553B spectrum analyzer	1
	Nikon L-KE microscope with accessories	1
	Standard laboratory measurement equipment	
	Power supplies	
	Simpson 260 volt-ohmmeter	1

**Specifications are given in LANCE Vulnerability and Hardening Program, Test Plan, Annex A, General Procedures, Harry Diamond Laboratories (3 April 1972).*

†Specifications are given in P. H. Stadler, High Voltage Fast Pulser, Operator's Manual, Philco-Ford Corp., Newport Beach, CA (July 1971).

[13]*LANCE Vulnerability and Hardening Program, Test Plan, Annex A, General Procedures, Harry Diamond Laboratories (3 April 1972).*

The long-pulse results were used to predict the voltage levels for the short-pulse tests. All pulse data were recorded on Polaroid film.

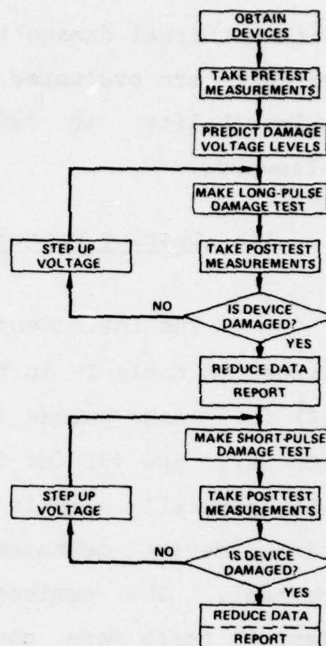

Figure 12. Damage test flow chart.

3.2.1 Devices

The Lance Missile System was analyzed, and a number of semiconductors were chosen for evaluation based on their electrical position relative to EMP induced transient sources, their relative sensitivity, or their criticality to the system mission. The literature was searched for damage threshold data on device types picked. From the data available and the types of signals expected to be impressed on each device type, the range of pulse widths for each device was established. Thus, some devices were subjected to only long-pulse tests; others, to short-pulse tests; and many, to both.

Because of the large number of device types, the quantity of each type had to be limited for testing. Arbitrarily, 10 was established as the sample size for long-pulse tests* and, since short-pulse tests were more difficult, 40 was established for them.* The devices were purchased commercially (there were no controlled sources). The choice of pin pairs for pulse testing was based on both device configuration in the system and pin-pair sensitivity to high-voltage transients.

There were two major exceptions, the 2N1132 and the 1N457.

3.2.2 Pretest Measurements

Before each device was subjected to a transient pulse, various low-signal parameters were measured. Junction breakdown voltage has been found to be a sensitive indicator of device damage and was measured before each test. It was standard practice to obtain the V-I characteristics on the Tektronix model 576 curve tracer for either polarity to the two pins to be pulse tested. For devices with multijunctions between the two pins under test, both forward and reverse breakdown levels were obtained. For transistors, both the E-B and C-B breakdown voltages were measured. Along with the breakdown voltages, a characteristic operational parameter was measured (such as beta in a transistor and intrinsic standoff ratio in a unijunction). In most devices, this parameter could be measured on the Tektronix 576 curve tracer by standard procedures. For some measurements, special circuits had to be used. They are presented in the test descriptions for the pertinent devices.

3.2.3 Long-Pulse Damage Tests

The typical setup for the long-pulse damage tests is shown in figure 13. The thyratron pulse generator was used for most of the device tests, and the Velonex model 350 pulse generator was used for the others. The text of the test description for each device type indicates which generator was used. For many devices, with either generator, a series resistance or both series and parallel resistances were used to obtain the desired pulse waveshape and effective source impedance at the device pins.

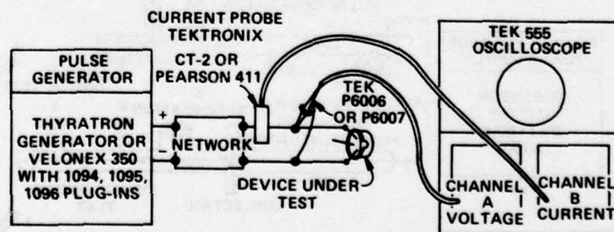

Figure 13. Typical long-pulse test setup; network block indicates that series resistance or series and parallel resistances were sometimes used to obtain desired operating characteristics.

The voltage level to fail the device under test was predicted from the failure level of similar device types or estimates based on the specified device parameters. A pulse voltage level 20 percent under the predicted level was applied. The device parameters (sect. 3.2.2) were remeasured. If any parameter was degraded by 20 percent or more, the device was considered damaged. Devices which showed no degradation within 20 percent were subjected to a pulse of higher voltage level at the same pulse width. They were then rechecked to determine the effects of the pulse. This process continued until device failure. The number of pulse tests was generally limited to three or four to avoid the possibility of accumulated effects. This step-stress technique was found to have no effect on the failure level of the devices under test.[15]

3.2.4 Short-Pulse Damage Tests

The typical test setup for the short-pulse damage tests is shown in figure 14. Either the dual-gap or the dielectric-gap pulser was used. Both pulsers are transmission-line discharge systems: the dual gap allows higher test levels; the dielectric gap, better pulse characteristics. The unit used for a test series of a device type is specified in the test description. Short-pulse damage tests were conducted as described for the long-pulse tests (sect. 3.2.2). For some devices, a Tektronix model 454 oscilloscope was used to record the

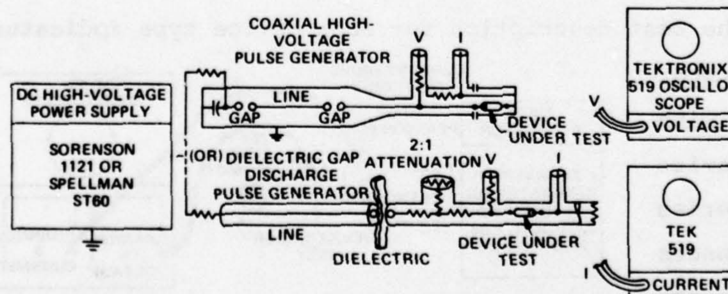

Figure 14. Typical short-pulse test setups; appropriate attenuators are used on oscilloscope input to obtain required input voltage levels.

[15] *B. Kalab, Analysis of Failure of Electronic Circuits from EMP Induced Signals--Review and Contribution, Harry Diamond Laboratories TR-1615 (August 1973).*

current pulse instead of the Tektronix model 519. This was a necessary step in measuring the current through high-impedance devices. The penalty for using the Tektronix model 454 was a reduced bandwidth.

3.2.5 Data Reduction

The parameters obtained from the data (fig. 3) are the open-circuit voltage (V_{oc}), the load voltage (V_p), the load current (I_p), the open-circuit pulse width (T_{DOC}), and the time to second breakdown (if applicable) (T_D). Both V_p and I_p are obtained by inspection as average quantities chosen so that a good approximation to the power and, consequently, the energy to the device could be calculated. Generally, if second breakdown occurred, the transition to that state was abrupt even in the nanosecond regime (under a 50-ohm source load). In some devices, the transition appears to have covered 10 to 20 ns. In such a situation, an average value of T_D was obtained based on the initial load voltage plateau and the time which the decrease in voltage level began and the final plateau and the time at which the voltage attained that level. The bulk surge impedance (Z) was calculated (based on the discussion of sect. 2.1) from

$$Z = \frac{V_p - V_z}{I_p} \tag{25}$$

reverse biased and

$$Z = \frac{V_p}{I_p} \tag{26}$$

forward biased, where V_z is the impedance voltage. Z represents a time average quantity over that portion of the pulse before T_D. In each device test section which follows, the bulk surge impedance was calculated as an average of a number of pulse tests, some of which were not at the failure level. The total number of measurements from which the average was obtained is given.

The data are input to a computer reduction program.[14] The impedance and power dissipated are calculated, and the power data are fit to the T_D^{-1} model, the $T_D^{-1/2}$ model, or the combination as given in equation (9). The program also produces plots on a Typograph terminal. The tabularized test data, the manufacturer's specifications, the computer-generated threshold plots, and the test description represent the complete test report on the device type tested. For brevity, only a description and graph of the results for each device tested appear here. The software was modified a number of times during the program, so the computer-generated plots differ slightly. The terms "reverse" and "forward" are used in some legends to describe junction polarity with respect to the damaging pulse. The most recent plots employ the pin number or description, such as A and C for anode and cathode. If the anode is pulsed positive with respect to the cathode, the legend states "anode, failure" or "anode, no failure."

4. DAMAGE TEST DATA

The data are presented in three sections. Section 4.1 describes the devices and tests and shows the damage curves for all the Lance Missile System semiconductors chosen for characterization. Section 4.2 presents the results of special tests on the 2N1132 and the observations made from the data presented in sections 4.1 and 4.2. Section 4.3 presents the results of the tests on nonsemiconductor devices and special devices proposed for system hardening applications.

---

[14] *J. R. Miletta, R. E. Parsons, and M. S. Bostian, Lance Vulnerability and Hardening Test Program Interim Semiconductor Damage Report, Harry Diamond Laboratories (September 1971).*

4.1 Lance Semiconductor Damage Tests

The semiconductor damage tests for the Lance V/H Program are presented with two exceptions in this section. The exceptions are the test of the 2N1132 (sect. 4.2) and the evaluation of the TransZorb diodes (sect. 4.3).

Each damage test series is presented in this section. First, the device is described; second, the test procedures and equipment are discussed; then the results are presented; finally, the damage curves are presented and discussed. The brief discussions generally center on the divergence from the expected device response.

4.1.1 1752/17 Operational Amplifier

The Burr-Brown 1752/17 is a hybrid field-effect-transistor input, miniature, general-purpose operational amplifier (op amp). Two op amps were tested to determine their transient response failure level. Two distinct situations were examined. The first op amp input ports were damage tested with no external bias applied. The second op amp had a bias applied, and the input was pulsed to examine any detrimental effects of the combination of bias and high-voltage transients.

Diagnostic measurements were made before and after each pulse test. The forward-biased and reverse-biased breakdown characteristics (unbiased) of the pin pair chosen for tests were taken on the Tektronix model 576 curve tracer. The circuit of figure 15 also was used as a diagnostic indicator. The output should remain at 5 V before and after each test. Damage was defined as a 20-percent degradation in the breakdown character of the junctions of the pin pairs tested, dc level of the output circuit, or both. All tests were conducted at a 2-μs pulse width on the thyratron generator.

One op amp was pulsed in the unbiased condition. Pulse testing started at the 40-V level and increased in steps of 20 V until damage was seen or 160 V was reached. The op amp was pulsed from the input pin (pin 2) to the negative terminal (-) with pin 2 positive. If failure did not occur at a level of 160 V, the tests were repeated with the polarities reversed. If no damage resulted up to 160 V, pins 1 and 2 were to be pulsed in the same manner. If no failure was seen under 160 V, pins 2 to 4 were to be pulsed next. If the op amp still survived, it was to be pulsed to destruction across pin 2 to the negative terminal.

The second op amp was biased as indicated in figure 15, and the input to ground (pin 2 to source ground) was pulse tested. Pin 2 was positive in the pulse test. The testing began at 40 V and increased at 20-V increments. Pin 2 to ground was the only pin pair tested in the biased mode.

All pin pairs tested in the unbiased mode survived a peak voltage of 160 V of both polarities. No damage could be seen from the electrical measurements before and after each pulse test. Since the device did not fail, it was pulsed again across the pin pair of pin 2 to (-), pin 2 positive. This time, the device was pulsed to destruction. Degradation was noted at 460 V; complete failure, at 550 V. The results of these two tests are presented in figures 16 and 17.

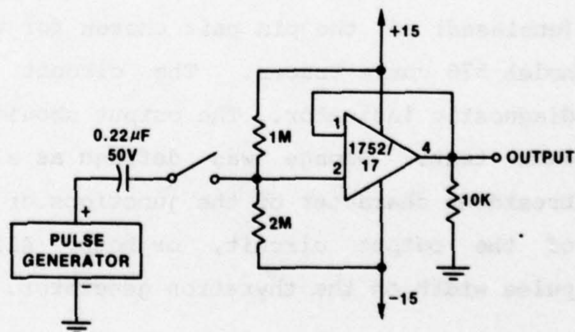

Figure 15. Test schematic for operational circuit checkout and pulse testing for Burr-Brown 1752/17 operational amplifier.

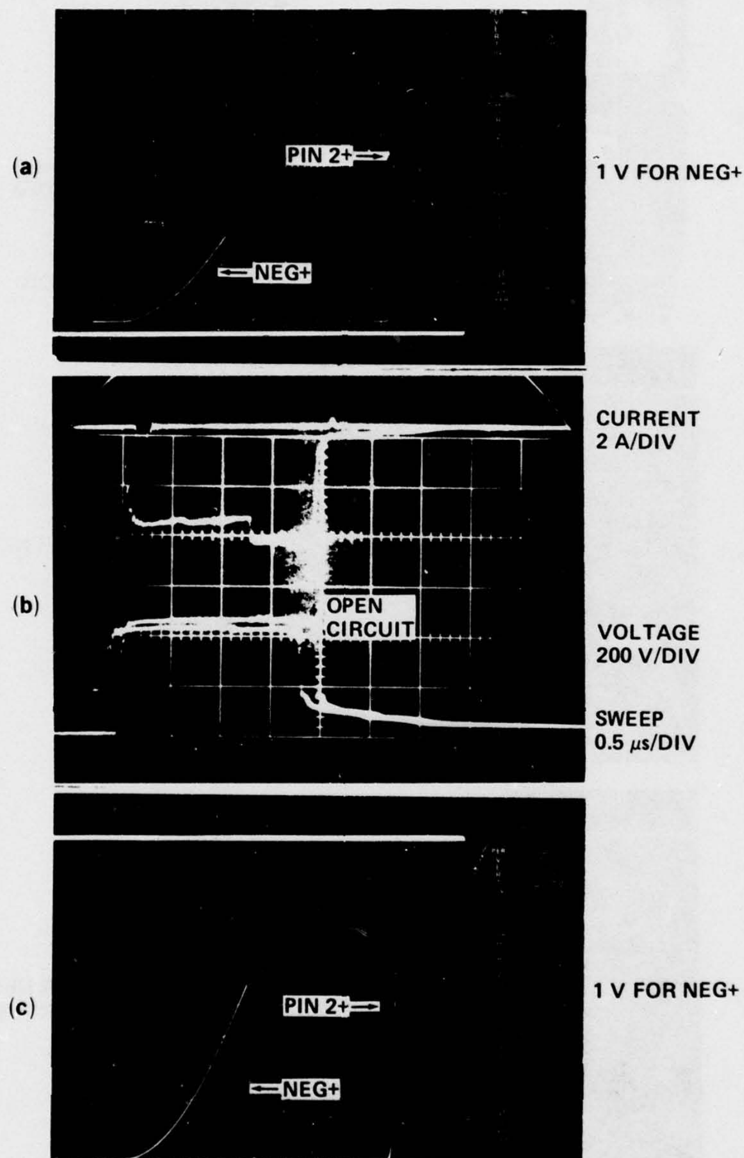

Figure 16. Test data, Burr-Brown 1752/17 operational amplifier, unbiased, degradation, pulse 42; results of 460-V test across pin 2 (input 2) and negative terminal (pin 2+): (a) before-pulse-test data; (b) pulse data showing initiation of apparent multiple second breakdowns in both voltage and current sweeps; (c) after-pulse-test electrical measurements showing slightly more conductive characteristic for "neg+." Output of voltage follower was 5.8 V before test and 5.3 V after test. Impedance of 160 ohms can be calculated from data in (b) before apparent first "second breakdown" in 330-V pulse test.

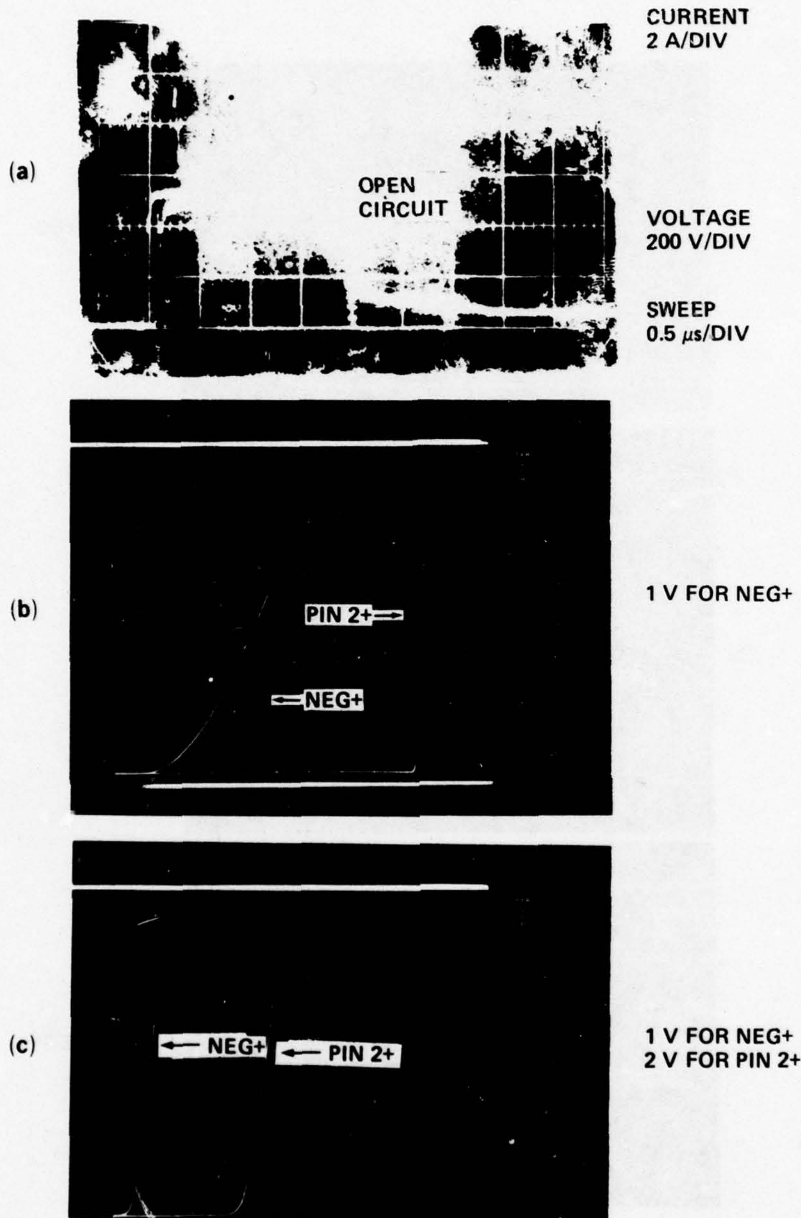

Figure 17. Test data, Burr-Brown 1752/.7 operational amplifier, unbiased, destruction, pulse 43; results of 550-V test across pin 2 (input 2) and negative terminal (pin 2+): (a) pulse data: (b) before-pulse-test electrical measurements; (c) after-pulse-test electrical measurements. Output of voltage follower was 5.3 V before test and -1.8 V after test.

Forty-three pulses were applied to device 1, including the complete failure pulse, as the following pin pairs:

Pin pair	Pulses (No.)
Pin 2 (input 2) to (-) terminal	19
Pin 1 (input 1) to pin 2 (input 2)	12
Pin 2 (input 2) to pin 4 (output)	12

The second op amp was pulsed under bias. It showed degradation at an amplitude of 230 V and complete failure at 300 V. There were three pulse test levels ranging from below the failure threshold (fig. 18, p. 52) to degradation (fig. 19, p. 53) and to failure (fig. 20, p. 54). The op amp was subjected to 10 pulses.

The actual discrete element or elements which failed in the op amps could not be determined without a complete autopsy. The autopsy was not attempted. There are multiple paths for energy flow from one pin to another for each pin pair tested. An examination of the op amp schematic (fig. 15) can give some indication of the critical low-impedance paths, but such effects as component arcing and stray leakage paths cannot be determined without extensive analysis.

From the character of the current and voltage traces, the failure of the device can be attributed to second breakdown. However, this is only an assumption, since there could be other damage mechanisms which result in similar V-I pulse traces.

4.1.2 1N69A Diode

The GE 1N69A is a germanium point-contact diode. Fifty diodes were tested. The device has a very low power rating, 80 mW, and had a corresponding low failure threshold. Long pulses (1 to 8 μs) were produced by the thyratron generator; short pulses (24 and 48 ns), by the coaxial line high-voltage pulse generator.

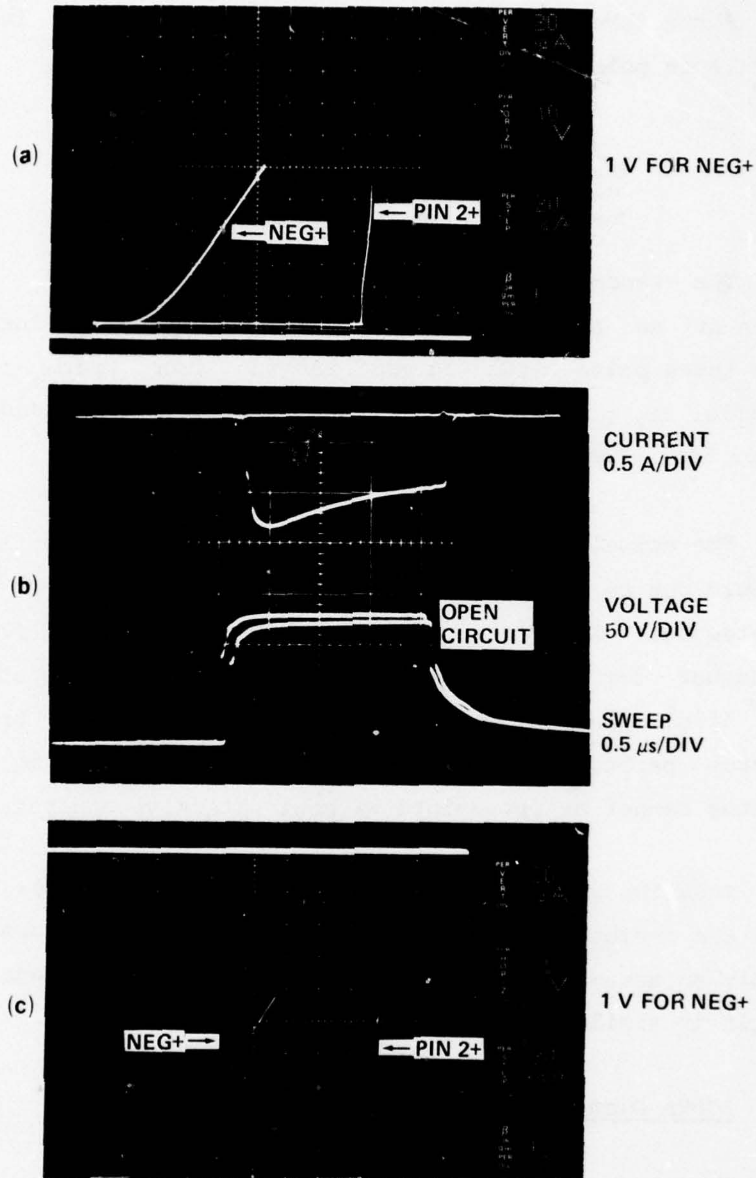

Figure 18. Test data, Burr-Brown 1752/17 operational amplifier, biased, undamaged, pulse 5; results of 160-V test on device 2 across pin 2 (input 2) and ground in active circuit: (a) before-pulse-test electrical measurements; (b) pulse data; (c) after-pulse-test electrical measurements. Active input impedance of 55 ohms can be calculated from (b). Output of voltage follower was 5.7 V before and after test.

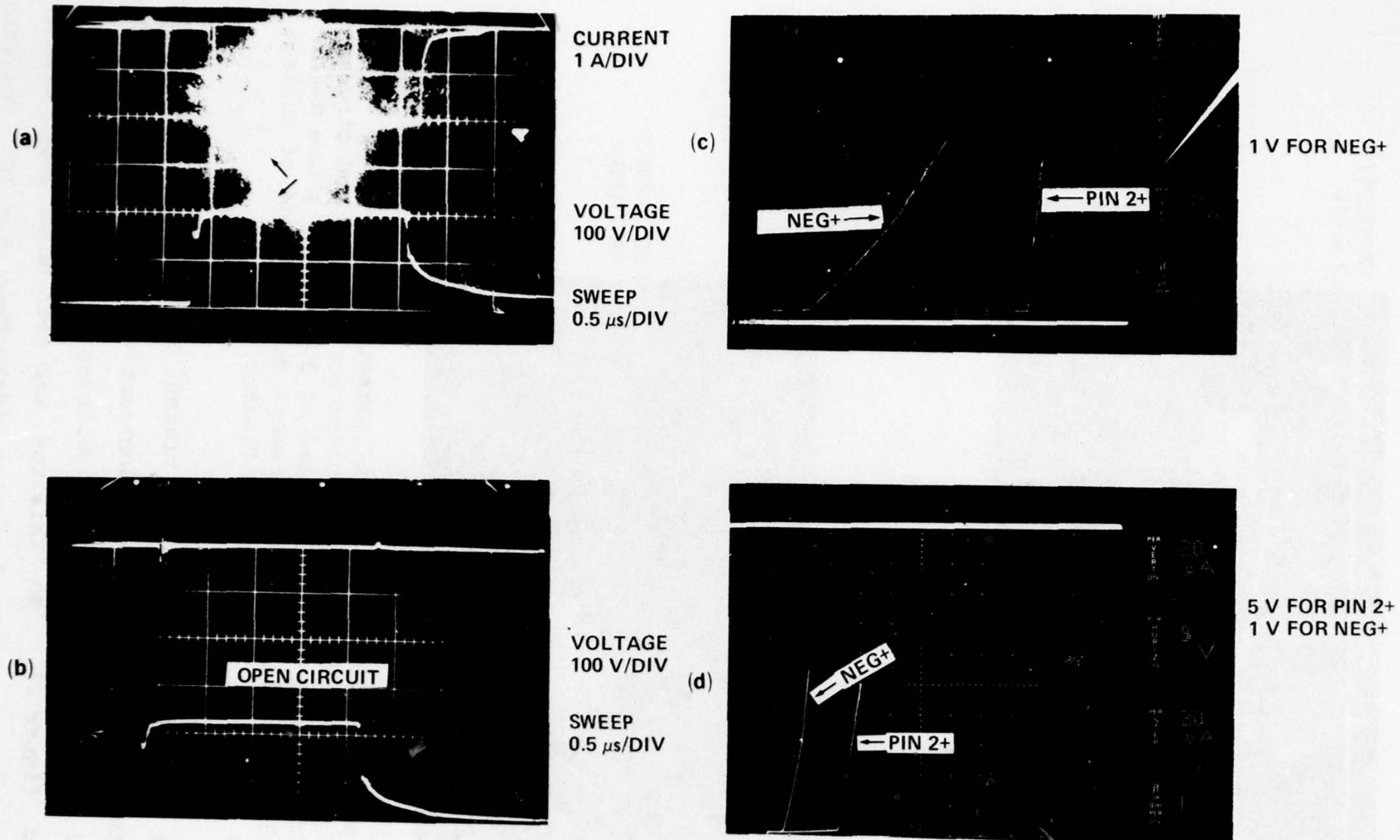

Figure 19. Test data, Burr-Brown 1752/17 operational amplifier, biased, severe degradation, pulse 8; results of 230-V test on device 2 across pin 2 (input 2) and ground in active circuit: (a) and (b) pulse data; (c) before-pulse-test data; (d) after-pulse-test data. Possible second breakdown within module is indicated in (a) (arrows). Impedance of 83 ohms can be calculated from (a) before indication of breakdown. Output of voltage follower was 5.7 V before test and 5.3 V after test.

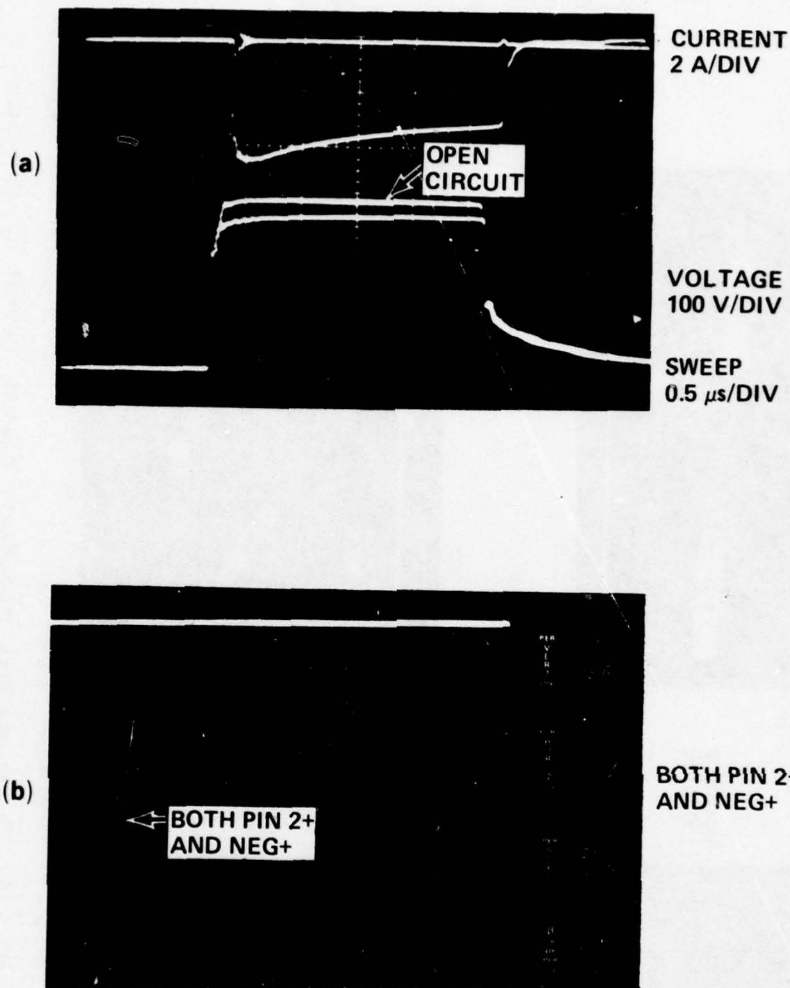

Figure 20. Test data, Burr-Brown 1752/17 operational amplifier, biased, destruction, pulse 10; device 2 was pulsed across pin 2 and circuit ground (pin 2+), with 2-μs voltage pulse of 300 V: (a) pulse data; (b) after-pulse-test electrical measurement data. Output of voltage follower was 5.2 V before test and 13 V after test.

The voltage and current traces taken during the step stressing of the diode indicated a predominant voltage threshold failure mode (fig. 9). The open-circuit voltages applied to the diode are graphed in figure 21. No failures are seen under 200 V with the 50-ohm source used. The data for pulse widths less than 10^{-7} represent

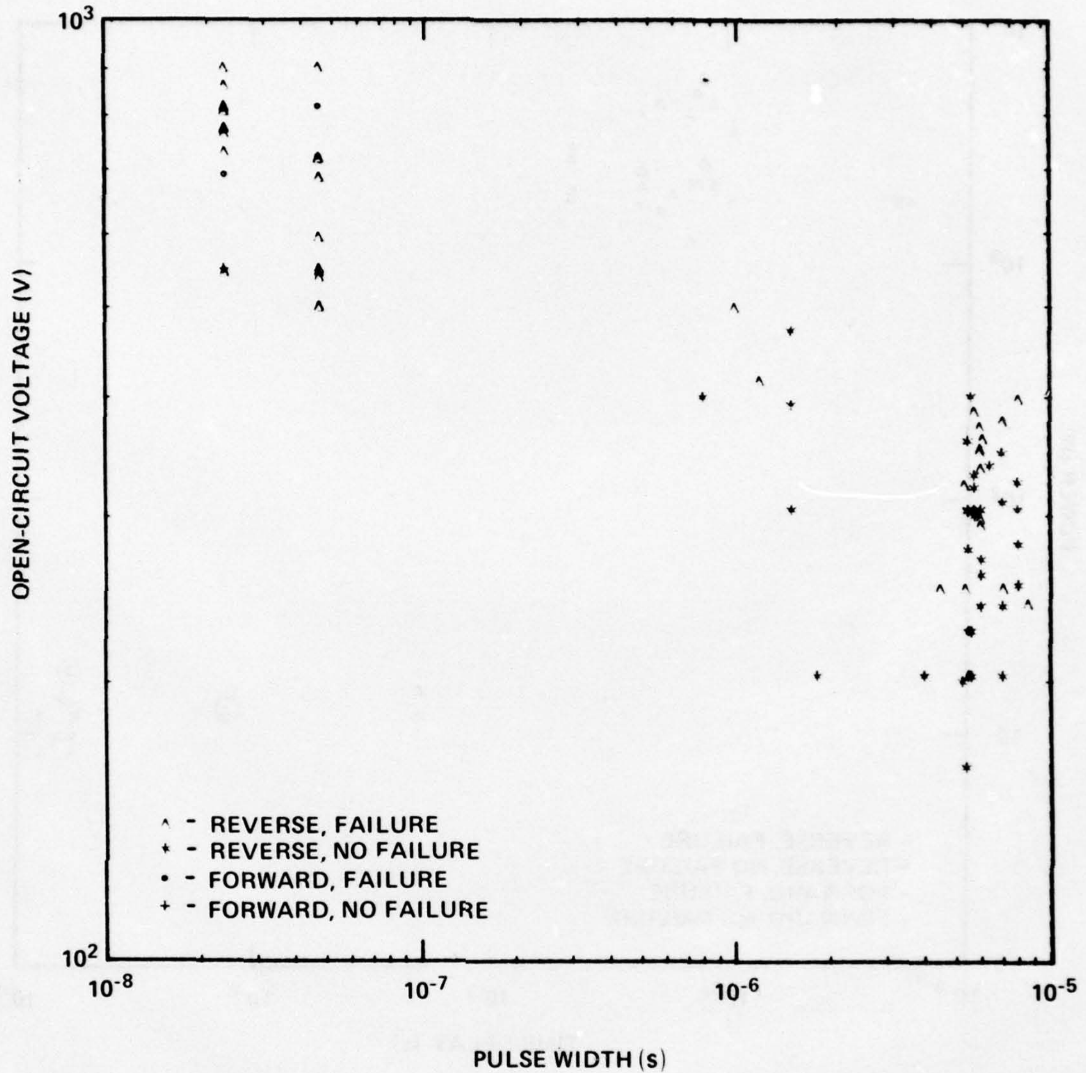

Figure 21. Damage points, voltage, General Electric 1N69A diode.

probable overtests due to instrumentation limitations and the nature of the failure mechanism.

The power dissipation points are plotted in figure 22. Two diodes did exhibit what could be termed a thermal second-breakdown failure mode. (These two points are circled in fig. 22). The time

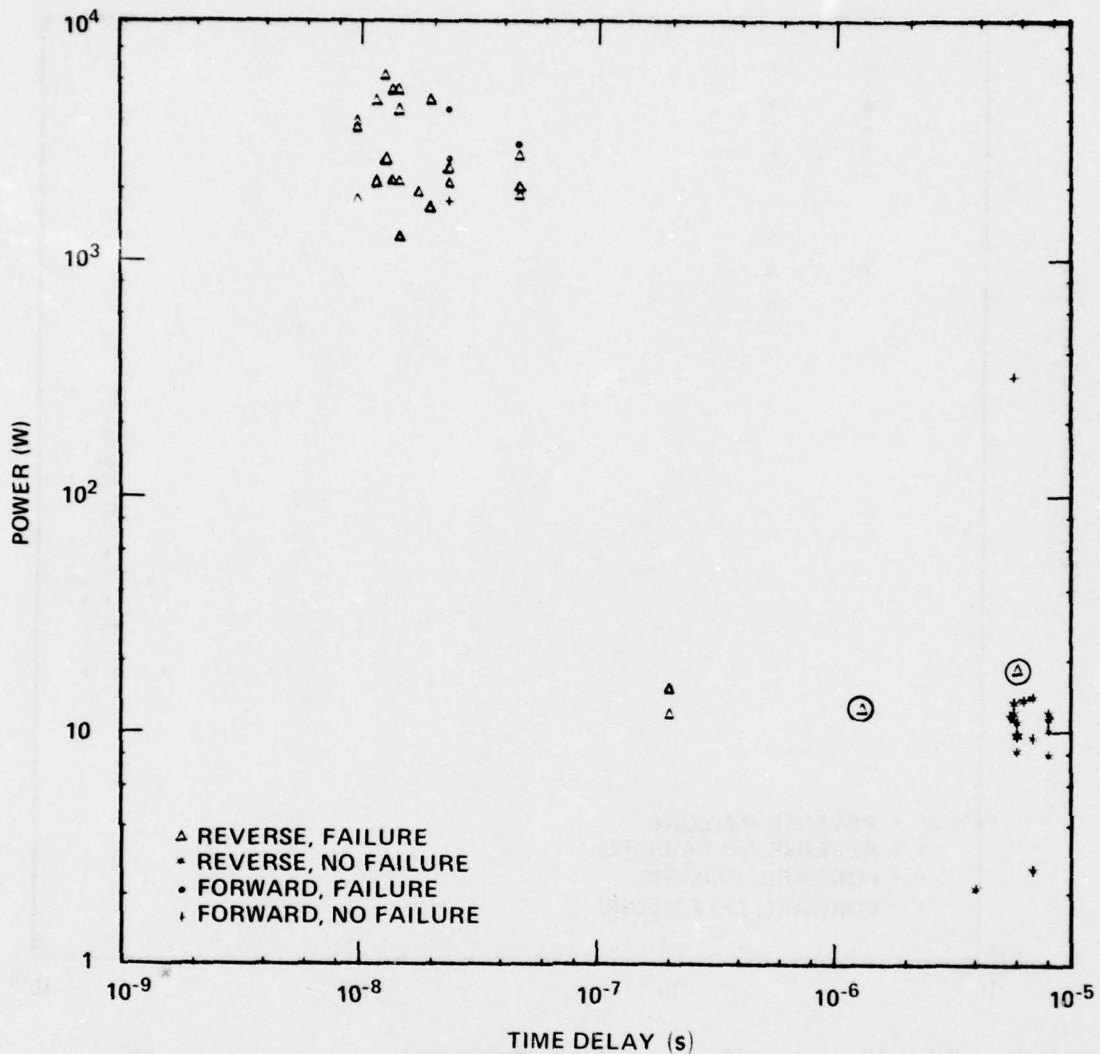

Figure 22. Damage points, power, General Electric 1N69A diode (circled symbols represent devices that exhibited thermal second breakdown).

delay reported for the two data points seen at approximately 200 ns was essentially the width of the voltage spike (fig. 9), characteristic of this type of failure. The spike was usually not discernible in the oscillograms for the microsecond regime, as can be understood by the number of failure tests depicted in figure 21 compared with the number seen in figure 22. When the spike could not be seen, the power was not

calculated. The time delay reported in figure 22 for the data in the nanosecond regime was the open-circuit pulse width. At the voltage levels in the short-pulse testing under the constraints imposed by the instrumentation, no meaningful time delay could be seen in the oscillograms. Consequently, the power points and associated delay times also represent overtests and are well above any possible thermal failure threshold. Therefore, a failure curve was not fit to the data.

The diode exhibited rather high bulk surge impedance. Reverse biased, the average bulk surge impedance was 4200 ohms from 19 points. The bulk surge impedance as reported here for each diode set represents an average overall pulse test in which sufficient information for the calculation was available.

4.1.3 1N270A Diode

The General Instruments Corp. (GIC) 1N270A is a germanium low-power diode. Fifty diodes were tested at pulses from 10 ns to 8.5 μs by using the coaxial high-voltage generator and the thyratron generator.

The diode exhibited a thermal second-breakdown failure, and the data were fit to the complete equation (9). As indicated in figure 23, there is considerable scatter about the fitted damage line. Failures were seen up to an order of magnitude below this damage line. Appropriate caution should be taken when applying these data. A larger safety margin than the nominal 1/10 line often used would be justifiable for analyses on circuits containing this diode. The forward failure points lie on or above this established line. The mean bulk surge impedance in the reverse direction is 3400 ohms for 18 long pulses (range: 75 to 9750 ohms) and 22.5 ohms for 19 short pulses (range: 2.5 to 95 ohms). The mean bulk surge impedance forward biased (15.8 ohms) was determined from only five measurements.*

**The bulk surge impedance forward biased was determined from voltage and current averages over the complete pulse.*

Figure 23. Damage curve, power, General Instruments 1N270A diode.

4.1.4 1N457 Diode

The Texas Instruments, Inc. (TI), 1N457 is a general-purpose silicon diode rated at 200 mW, 60 PIV. One hundred diodes were tested,

90 reverse biased and 10 forward biased. The coaxial high-voltage generator provided short pulses (up to 78 ns). Long pulses (1 to 8 μs) were applied from the thyratron generator.

An evaluation of the voltage and current oscillograms disclosed two types of failure with this set of diodes: typical second breakdown and voltage (or "turn-on" failure). Of 60 diodes tested to long pulses in the reverse-biased polarity, 27 exhibited voltage (or "turn-on") failure. It was hard to distinguish the voltage failure from the second-breakdown failure characteristic in the short-pulse data, though there were obvious second-breakdown data points in that time regime.

For those diodes in which typical thermal second breakdown was detected from the loaded voltage and current oscillograms, the plot shown in figure 24 was obtained. A $T_D^{-1/2}$ slope was fitted to the data because it would appear more appropriate than the complete equation (9). The mean bulk surge impedance calculated was 458 ohms for 129 points.

The observed voltage (or "turn-on") failure data were examined to detect voltage threshold for failure. The minimum voltage level seen for which the typical voltage (or "turn-on") failure resulted was 500 V. The mean bulk surge impedance for this subset averaged 913 ohms for 107 points. The higher impedance may indicate the reasons for this voltage threshold failure mode.

Ten diodes were pulsed forward biased. Figure 25 plots the power versus failure time for these samples. The mean bulk surge impedance of 32 points pulsed from 1 to 8 μs was 0.406 ohms.

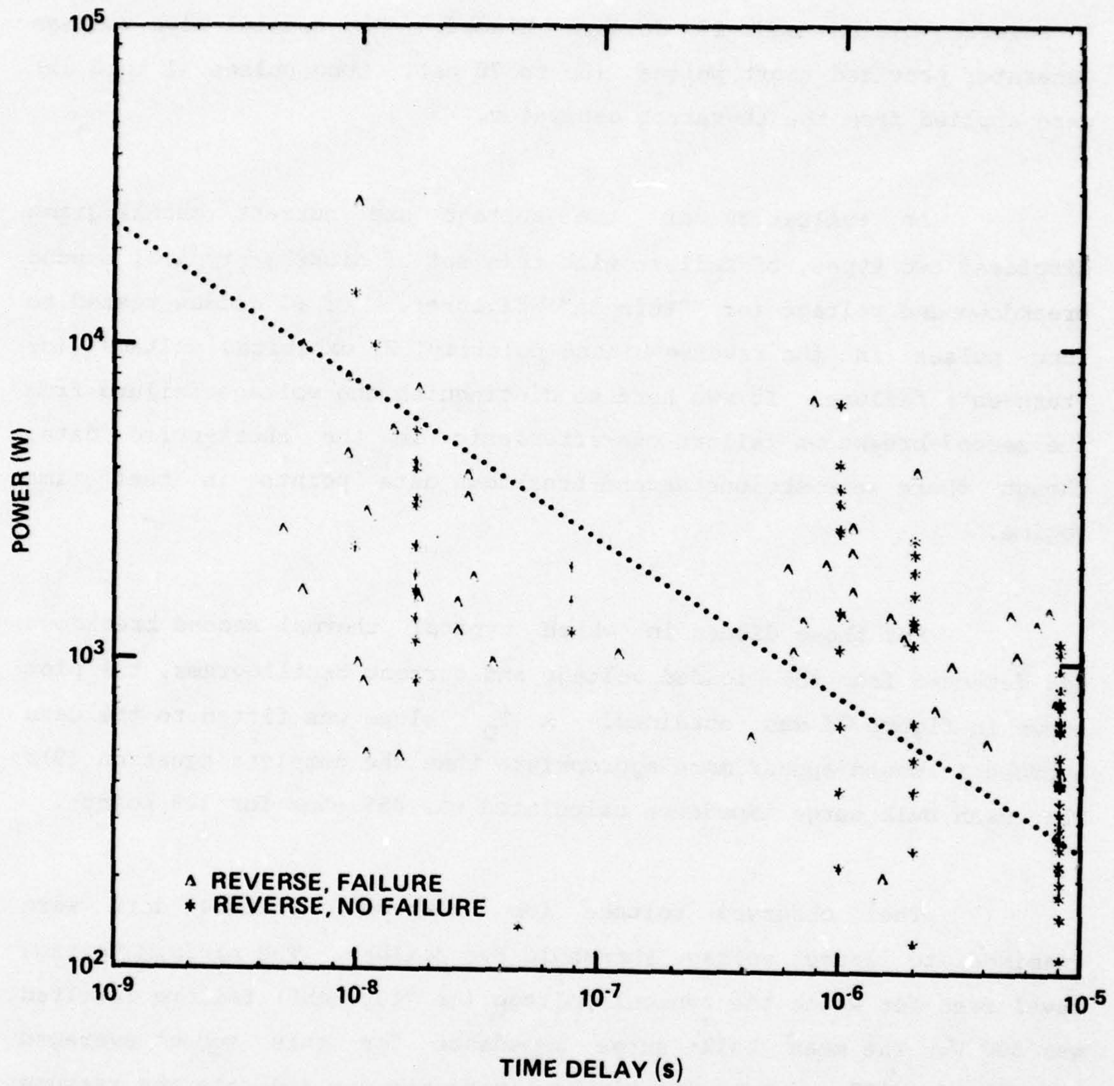

Figure 24. Damage line, power, Texas Instruments 1N457 diode (observed thermal second-breakdown points only).

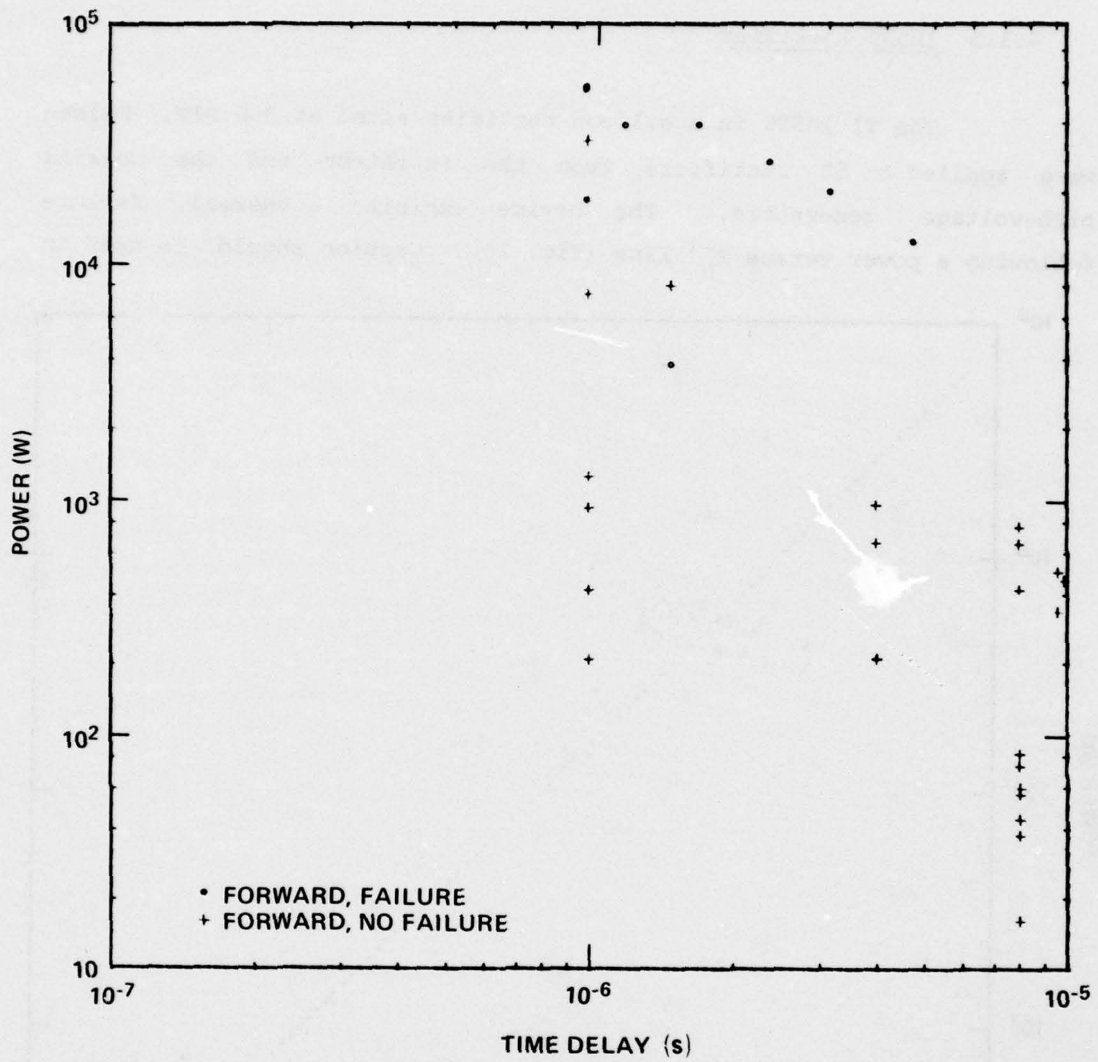

Figure 25. Damage points, power, Texas Instruments 1N457 diode (forward-biased points).

4.1.5 1N539 Rectifier

The TI 1N539 is a silicon rectifier rated at 300 PIV. Pulses were applied on 50 rectifiers from the thyratron and the coaxial high-voltage generators. The device exhibits a thermal failure following a power versus T_D^{-1} line (fig. 26). Caution should be used in

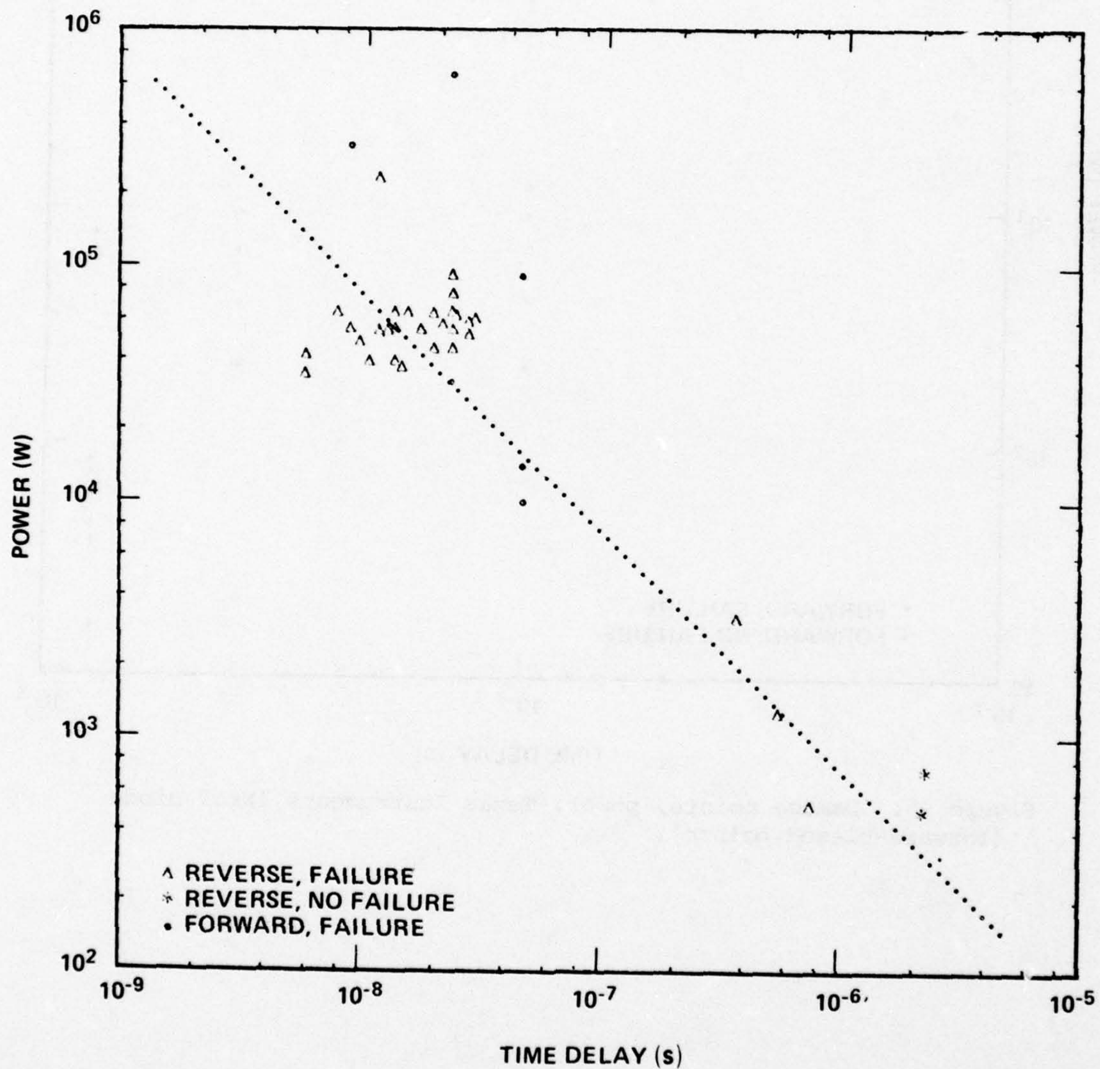

Figure 26. Damage line, power, Texas Instruments 1N539 rectifier.

applying the derived curve for pulse widths over 1 μs because the breakpoint to the $T_D^{-1/2}$ model can be expected in this range. Projection of the T_D^{-1} line could lead to extremely conservative estimates of damage, such as the two no-failure points above the line (fig. 26).

The mean bulk surge impedance for reverse-biased, short pulses averaged 8.8 ohms for 25 failure points with a range of 1.3 to 23 ohms. Reverse-biased, long pulses evidenced significantly higher bulk surge impedance levels, 288 to 1200 ohms, with a mean for three fail and two no-fail points of 811 ohms.

4.1.6 1N645 Diode

The TI 1N645 is a general-purpose silicon diode rated at 600 mW. Thirty-three were pulsed: 8 diodes at 2 to 8 μs and 25 diodes at 12 to 48 ns. The coaxial high-voltage generator was used for the short pulses; the thyratron generator, for the long pulses.

All long-pulse tests indicated voltage threshold failure. It was impossible to detect in the short-pulse tests, though the failure mechanism may be the same. Figure 27 shows the open-circuit voltage versus the open-circuit pulse for all the tests. A voltage threshold of ~1600 V is indicated. In figure 28, the short-pulse power points are shown versus the delay time. A $T_D^{-1/2}$ line is fit to the data.

The mean bulk surge impedances of reverse-biased diodes were 8.7 ohms for 21 diodes which failed at high-power short pulses and 1113 ohms for 12 no-fail diodes at long pulses. The bulk surge impedance tended to decrease under repeated pulsing at increasing power on the long pulse tests from an average of 1430 ohms for the initial pulse to 800 ohms just before failure.

OPEN-CIRCUIT VOLTAGE (V)

10^4

10^3

10^{-8} 10^{-7} 10^{-6} 10^{-5}

PULSE WIDTH (s)

Δ REVERSE, FAILURE
* REVERSE, NO FAILURE
+ FORWARD, NO FAILURE

Figure 27. Damage points, voltage, Texas Instruments 1N645 diode.

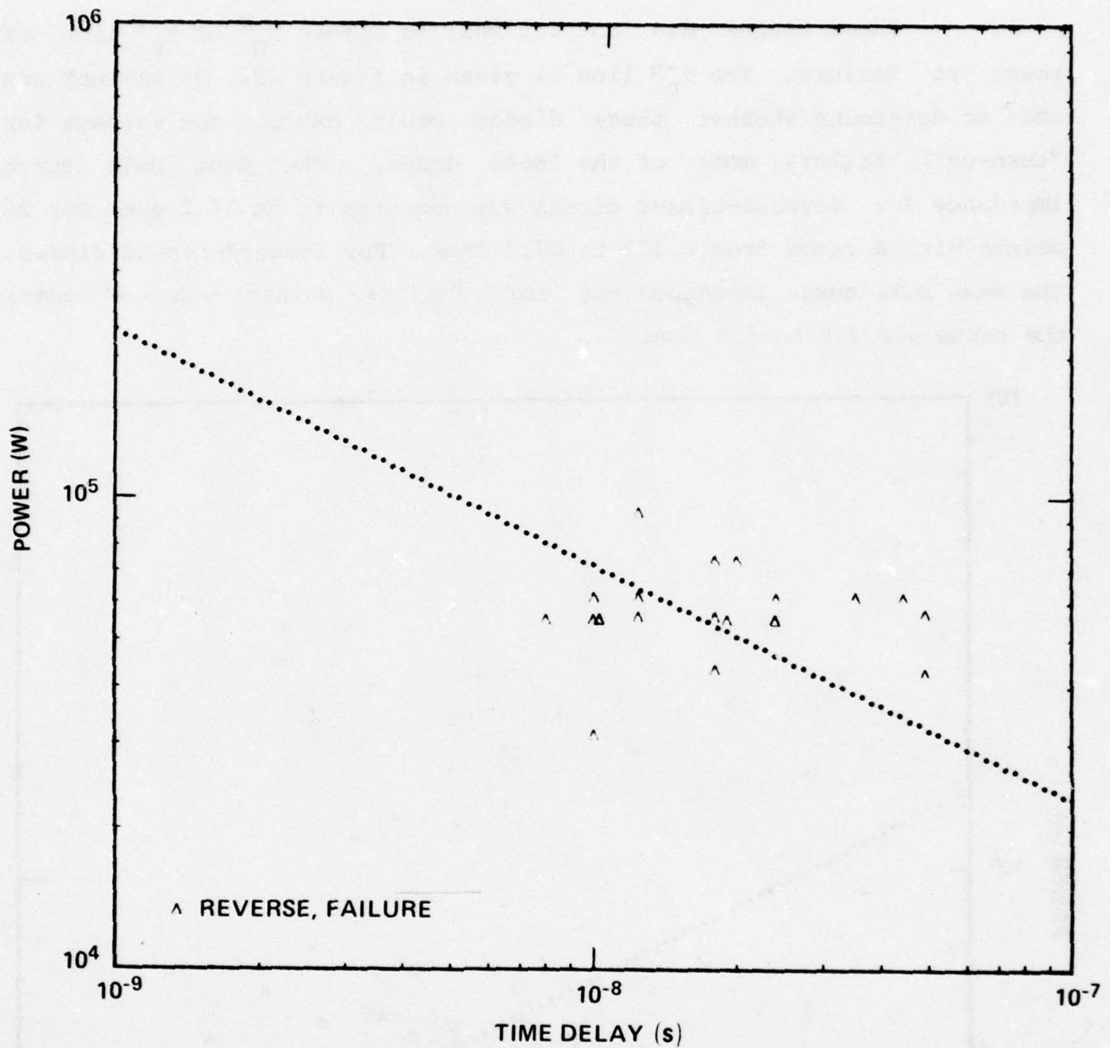

Figure 28. Damage line, power, Texas Instruments 1N645 diode, short-pulse points only.

4.1.7 1N647 Diode

The TRW Semiconductors, Inc. (TRW), JAN 1N647 is a general-purpose silicon diode rated at 600 mW, 480 PIV. Twenty-nine diodes were pulsed reverse biased and seven forward biased. The coaxial high-voltage generator with a 24-ns section and a 48-ns section was used.

These diodes did not fit well to either T_D^{-1} or $T_D^{-½}$ line of power to failure. The $T_D^{-½}$ line is given in figure 29. No attempt was made to determine whether these diodes would exhibit the voltage (or "turn-on") failure mode of the 1N645 diode. The mean bulk surge impedance for reverse-biased diodes was computed to be 17.2 ohms for 26 points with a range from 0.533 to 67.2 ohms. For forward-biased diodes, the mean bulk surge impedance for eight failure points was 5.17 ohms; the range was 2.8 to 8.8 ohms.

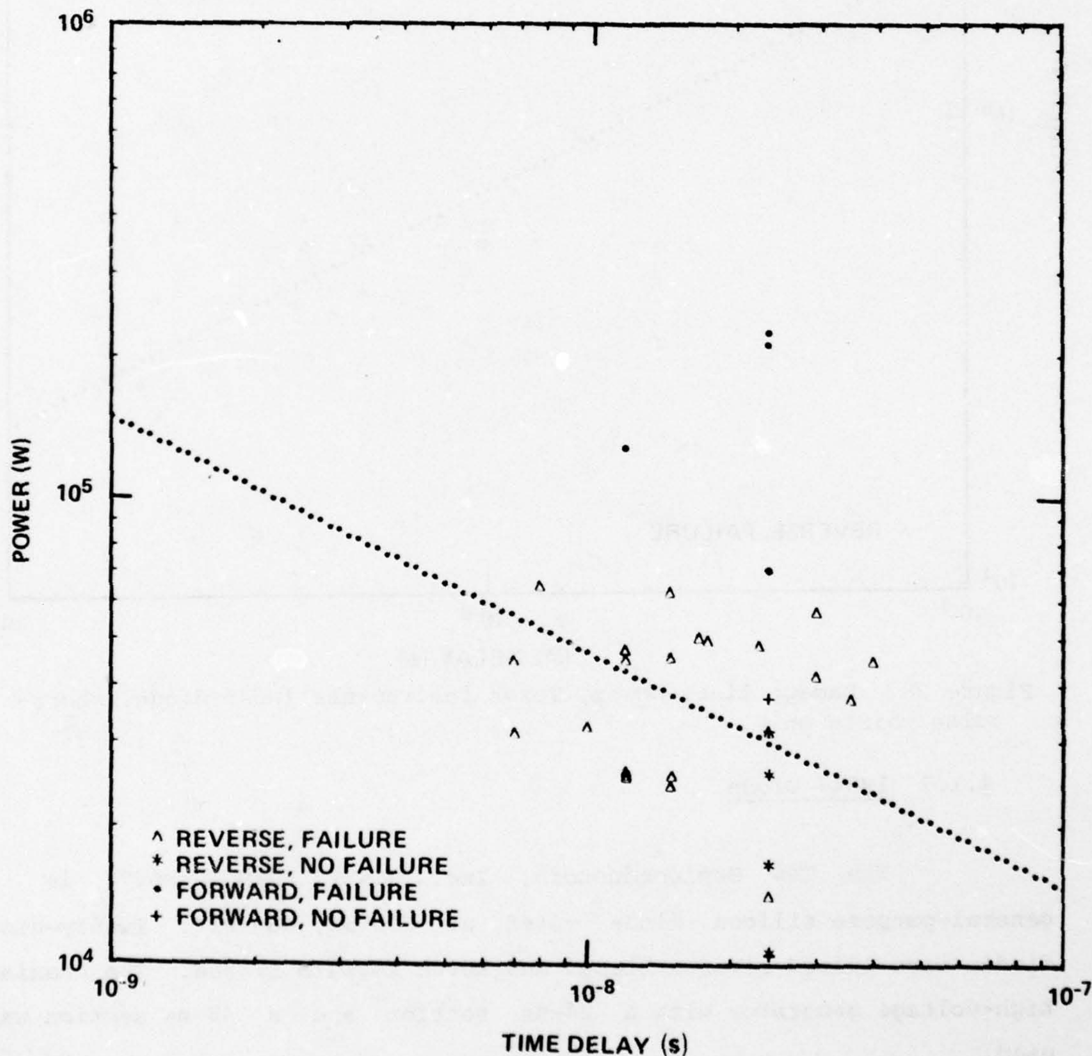

Figure 29. Damage line, power, TRW Semiconductors 1N647 diode.

4.1.8 <u>1N816 Diode</u>

The ITT Semiconductors (ITT) 1N816 is a general-purpose silicon diode. Thirty-eight diodes were tested, 34 reverse biased and 4 forward biased. Short pulses of 24 and 48 ns were applied from the coaxial high-voltage generator.

Reverse-biased failure points were fitted to the equation (9) failure model as shown in figure 30. The fit suggests a $T_D^{-\frac{1}{2}}$ dependency.

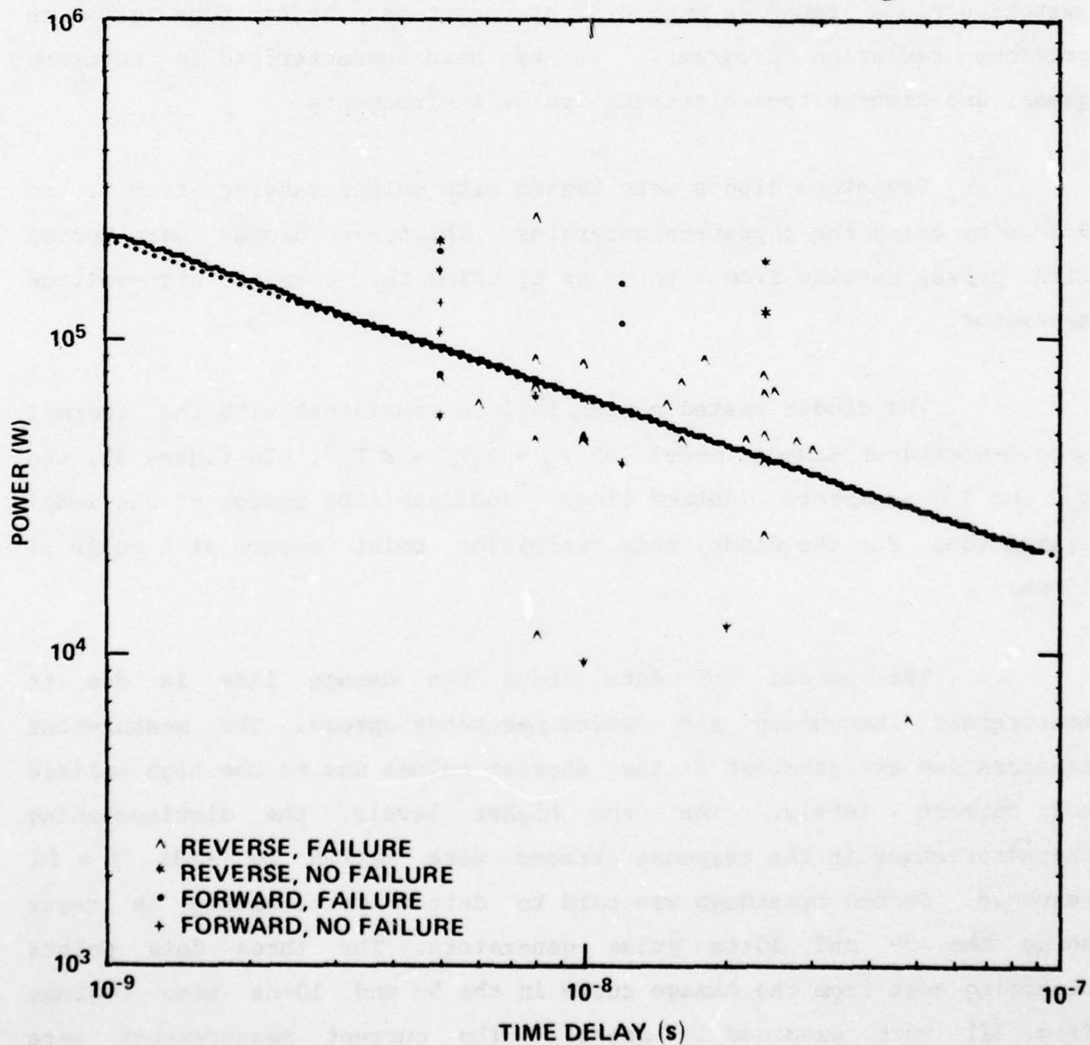

Figure 30. Damage curve, power, ITT Semiconductors 1N816 diode.

The mean bulk surge impedances for 27 diodes that failed and 11 that did not fail reverse biased averaged 20 ohms. The forward-biased bulk surge impedance for five tests including one no-failure diode averaged 10.2 ohms.

4.1.9 1N914 Diode

The TI 1N914 is a low-cost, relatively common silicon switching diode found in many U.S. Army systems. It has been tested in previous radiation programs. It has been characterized in neutron, gamma, and high-voltage electrical pulse environments.

Seventeen diodes were tested with pulses ranging from 0.5 to 9.0 μs by using the thyratron generator. Thirty-one diodes were tested with pulses ranging from 5 to 48 ns by using the coaxial high-voltage generator.

The diodes tested showed failure consistent with the thermal second-breakdown damage model of $P_T = K_1T_D^{-1} + K_2T_D^{-1/2}$. In figure 31, the T_D^{-1} and $T_D^{-1/2}$ asymptotes (dotted lines) indicate the region of the model transition. For the diode, this transition point occurs at a pulse of 15 ns.

The spread of data about the damage line is due to measurement inaccuracy and device parameter spread. The measurement inaccuracies are greatest at the shorter pulses due to the high voltage and current levels. At the higher levels, the distinguishing characteristics in the response traces were masked by bulk V = IR response. Second breakdown was hard to detect particularly in tests using the 5- and 10-ns pulse generators. The three data points diverging most from the damage curve in the 5- and 10-ns time regimes (fig. 31) were examined in detail. The current measurements were extremely poor, and second breakdown could not be detected in the current or voltage oscillograms.

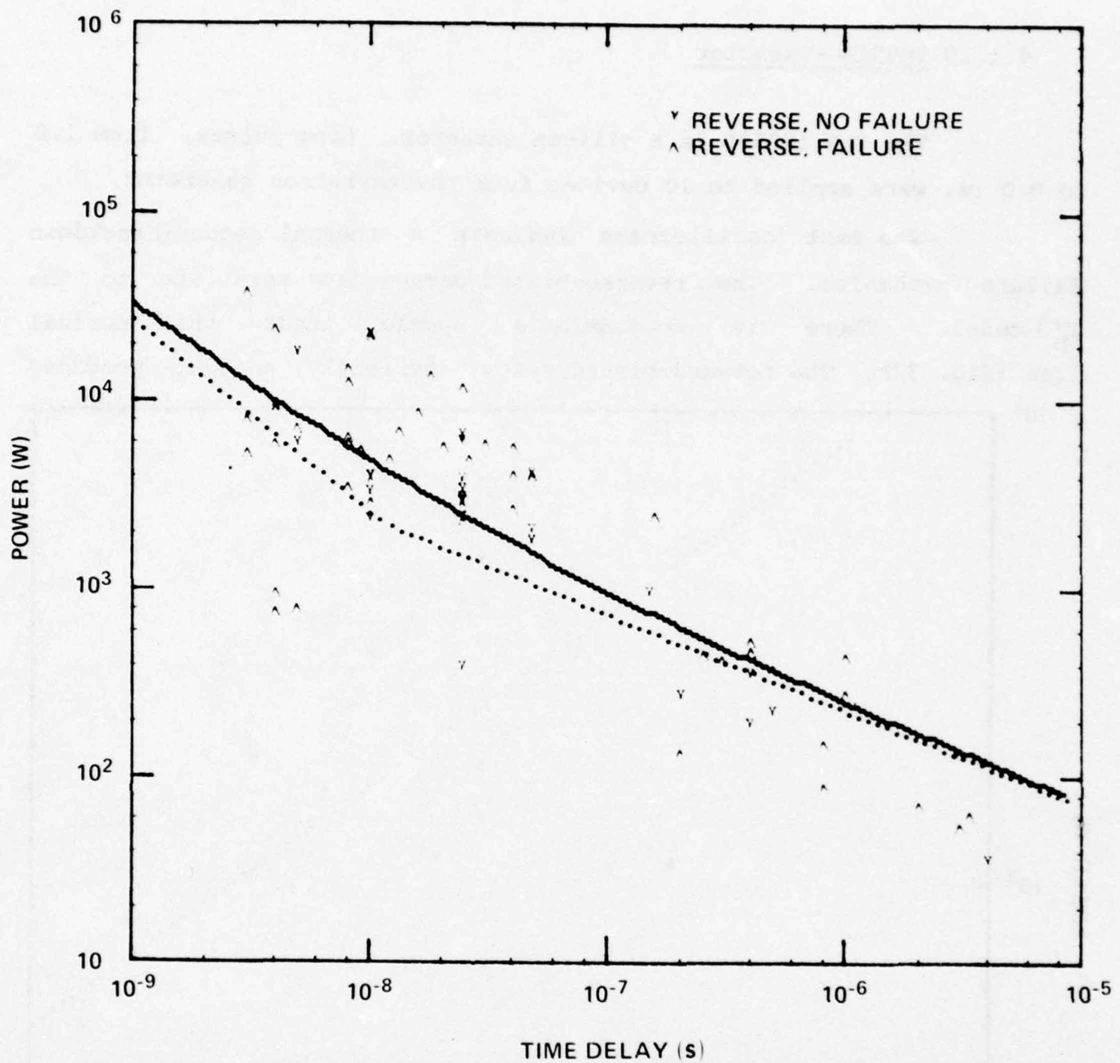

Figure 31. Damage curve, power, Texas Instruments 1N914 diode.

The bulk surge impedances calculated for ranges of open-circuit pulse widths decreased from a mean of 30.7 ohms (for 10 impedance calculations from 4 to 9 μs) to a mean of 16.7 ohms (for 11 calculations at 48 ns). The bulk surge impedance then increased to a maximum mean of 74.2 ohms for seven calculations for open-circuit pulses of 5 ns. The overall mean bulk surge impedance was calculated to be 39.9 ohms for 76 values.

4.1.10 <u>1N956B--Varactor</u>

The TRW 1N956B is a silicon varactor. Long pulses, from 1.8 to 8.0 μs, were applied to 10 devices from the thyratron generator.

The test oscillograms indicate a thermal second-breakdown failure mechanism. The reverse-biased damage data were fit to the $T_D^{-\frac{1}{2}}$ model. There is considerable spread about the nominal line (fig. 32). The forward-biased tests, curiously enough, produced

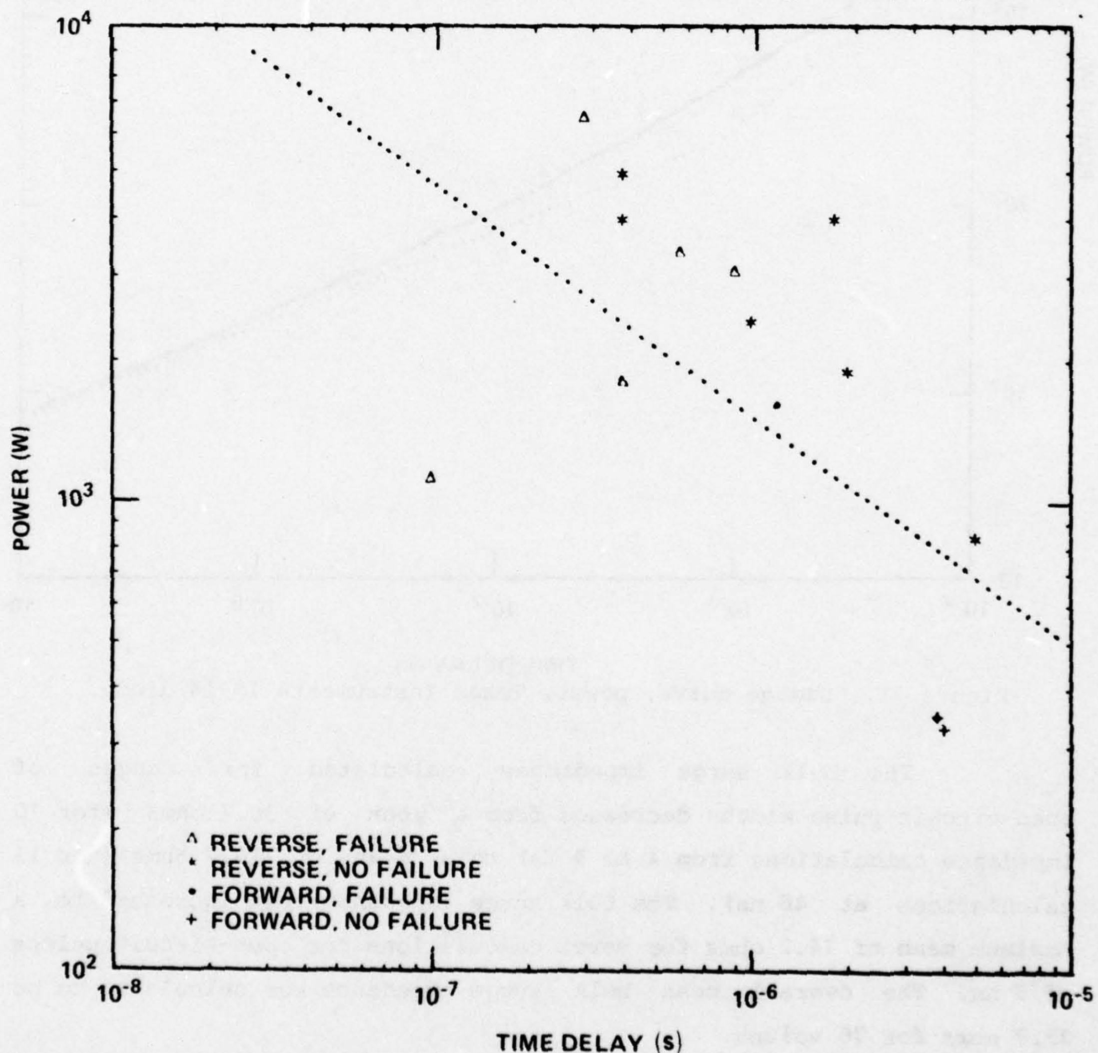

Figure 32. Damage line, power, TRW Semiconductors 1N956B capacitor.

voltage and current oscillograms similar to those of the reverse-biased tests. A phenomenon like second breakdown was apparent in the data.

The mean bulk surge impedance of seven reverse-biased tests was 2.47 ohms (from 0.313 to 10.0 ohms); three impedance calculations for forward-biased tests averaged 0.3666 ohms.

4.1.11 1N965B Diode

The Motorola (MOT) 1N965B is a silicon reference diode of a nominal reference voltage of 15 V measured at 8.5 mA. Ten diodes were tested, six reverse biased and four forward biased, by using the thyratron generator.

The diode was able to carry substantial peak currents without failure. Current measurements were biased low due to probe saturation. At the current and voltage levels applied to the diode set, both chip and lead failure were observed. These were verified by postdamage electrical tests indicating junction short circuits on some diodes and open circuits on others. One diode responded with a reverse-biased voltage failure, possibly because surface arcing or chip dielectric breakdown produced a low-impedance junction short circuit. All other reverse-biased tests indicated a thermal second-breakdown response.

The power dissipated for reverse-biased failure was not fit to the $T_D^{-1/2}$ thermal model because the spread about a line (fig. 33) would have been extreme due in part to the uncertainty in the exact current level and the combination of mechanisms to produce failure. The tests indicated that failure occurred at open-circuit voltages of ~1000 V. The source impedance, which includes an external 50-ohm series resistor, was approximately 100 ohms. The diode could not be damaged by forward-biased pulses. The device impedance averaged 0.154 ohms for 13 reverse-biased tests and 6.778 ohms for 8 forward-biased tests.

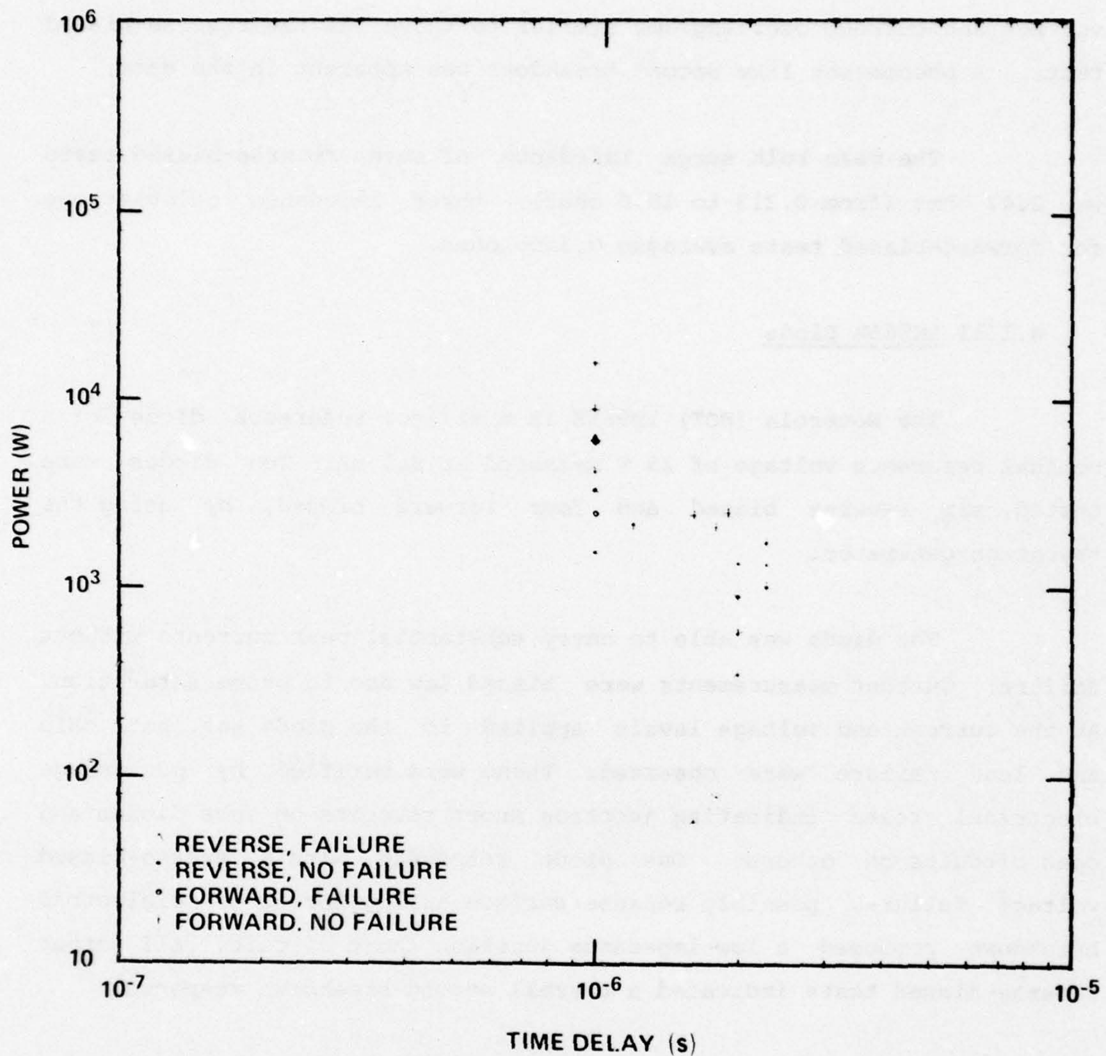

Figure 33. Damage points, power, Motorola 1N965B diode.

4.1.12 1N1200, 1N1202, and 1N1202A Rectifiers

The GE and MOT 1N1200 and 1N1202 and The Bendix Corp. (BDX) 1N1202A are diffused-junction, silicon rectifiers intended for medium current applications. Designed to carry a maximum of 21 A dc, the reverse-biased voltage rating (PIV) for the 1N1200 is 100 V; for the 1N1202 and 1N1202A, 200 V.

Long pulses (1 to 8 μs) were applied to 20 GE rectifiers (10 1N1200's and 10 1N1202's) and 16 Motorola rectifiers (8 1N1200's and 8 1N1202's) from the thyratron generator. The coaxial high-voltage generator was used for short-pulse tests (5 to 48 ns) on 32 BDX rectifiers.

The failure mode is difficult to categorize. High voltage and current levels were required to produce failure. (These rectifiers are rated to carry 240-A peak one-cycle surge current). Several of the rectifiers tested survived 2600 V--the limit of the long-pulse test equipment.

The data for the open-circuit voltage versus the pulse width for the GE and MOT 1N1200's are presented in figures 34 and 35. Reverse-biased failures were seen as low as 2100 V for the GE rectifiers and as low as 620 V for the MOT rectifiers. A number of GE rectifiers survived the 2600-V level. None of the failure characteristics common to thermal second breakdown were seen for these rectifiers, even though they were subjected to 60 kW for up to 4 μs.

The data for open-circuit voltage for the GE 1N1202 are given in figure 36. The minimum voltage for which reverse-biased failure resulted was 1700 V. In contrast to the 1N1200, the 1N1202 exhibited three reverse-biased failures characteristic of thermal second breakdown. The points are displayed in figure 37 where, rather optimistically, a $T_D^{-1/2}$ fit is shown. Analysis of this rectifier should consider both possible mechanisms for failure. Correspondingly, the data for the MOT 1N1202 are presented in figures 38 and 39. The minimum voltage for which failure resulted was 700 V.

Figure 40 presents the data for the power versus the delay time for the short-pulse tests conducted on the BDX 1N1202A. The

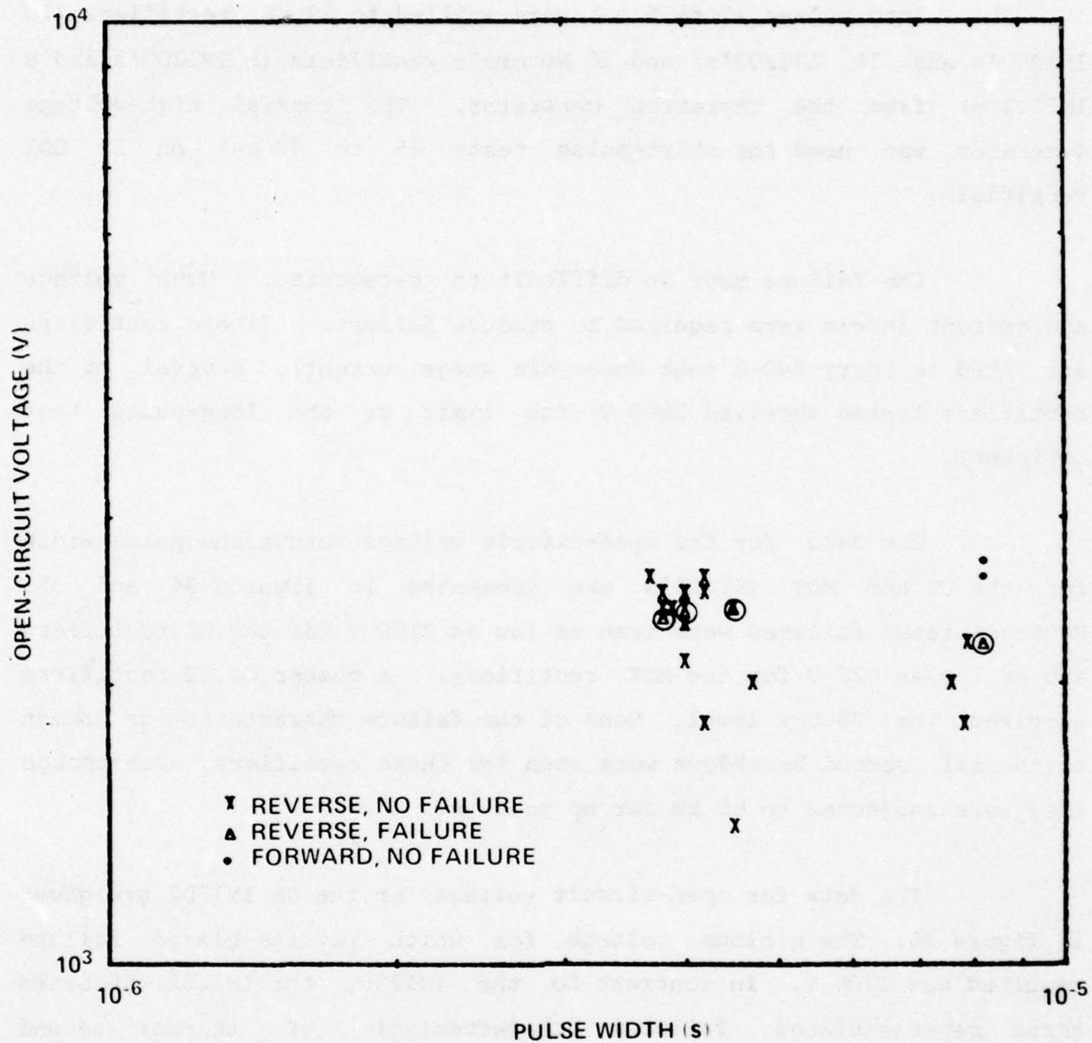

Figure 34. Damage points, voltage, General Electric 1N1200 rectifier (reverse failure data are circled).

failure characteristics were typical of second breakdown. But from the apparent failure mechanisms of the 1N1200 and 1N1202, the delay time may in fact be related to a statistical delay time for arc initiation,

Figure 35. Damage points, voltage, Motorola 1N1200 rectifier.

rather than to thermal heating. The reverse-biased failures occurred at voltage levels in excess of 2500 V. In all tests, thermal failure was assumed for the plot, and a $T_D^{-1/2}$ line was fit to the data. (It appears

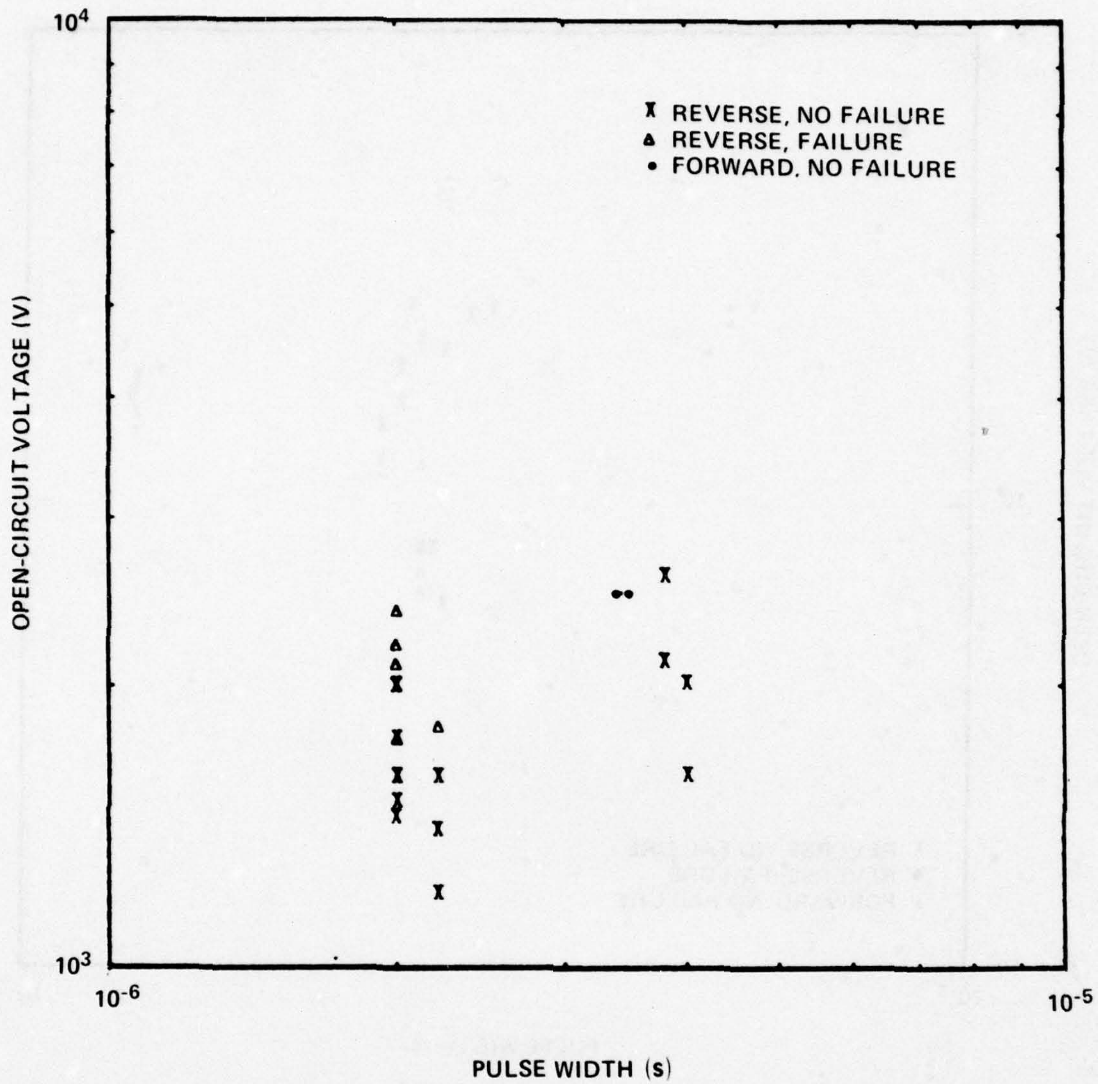

Figure 36. Damage points, voltage, General Electric 1N1202 rectifier.

to fit better than a T_D^{-1} line, even though the spread in data is extreme.)

In no test was it possible to damage any of the 1N1200 series rectifiers forward biased with the generators available. All

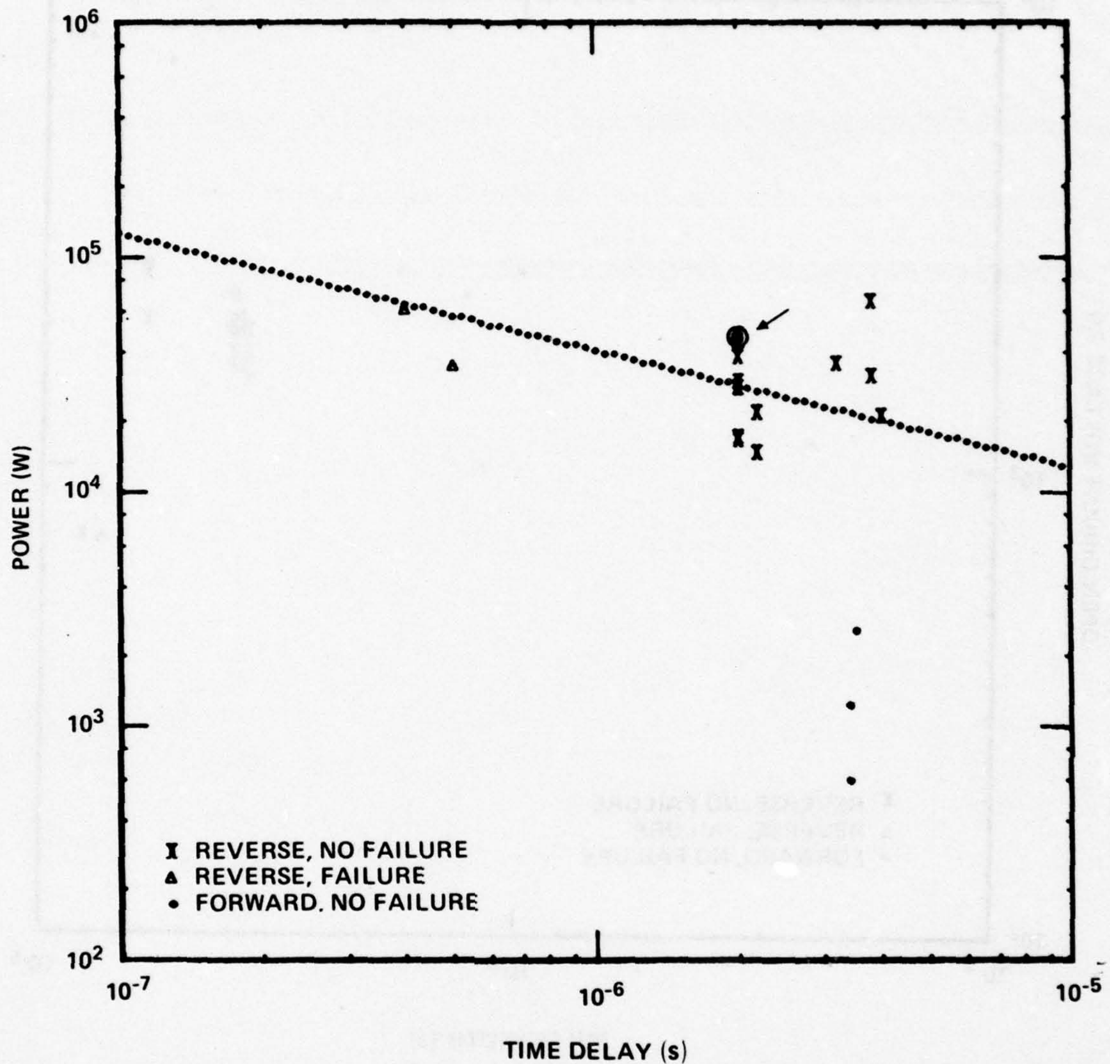

Figure 37. Damage line, power, General Electric 1N1202 rectifier (embedded reverse failure point at 2 μs is identified by arrow).

reverse-biased failures resulted in junction short circuits. In many of the reverse-biased failure tests, a series 47-ohm resistor was used to limit the pre- and postsecond-breakdown or voltage-breakdown current

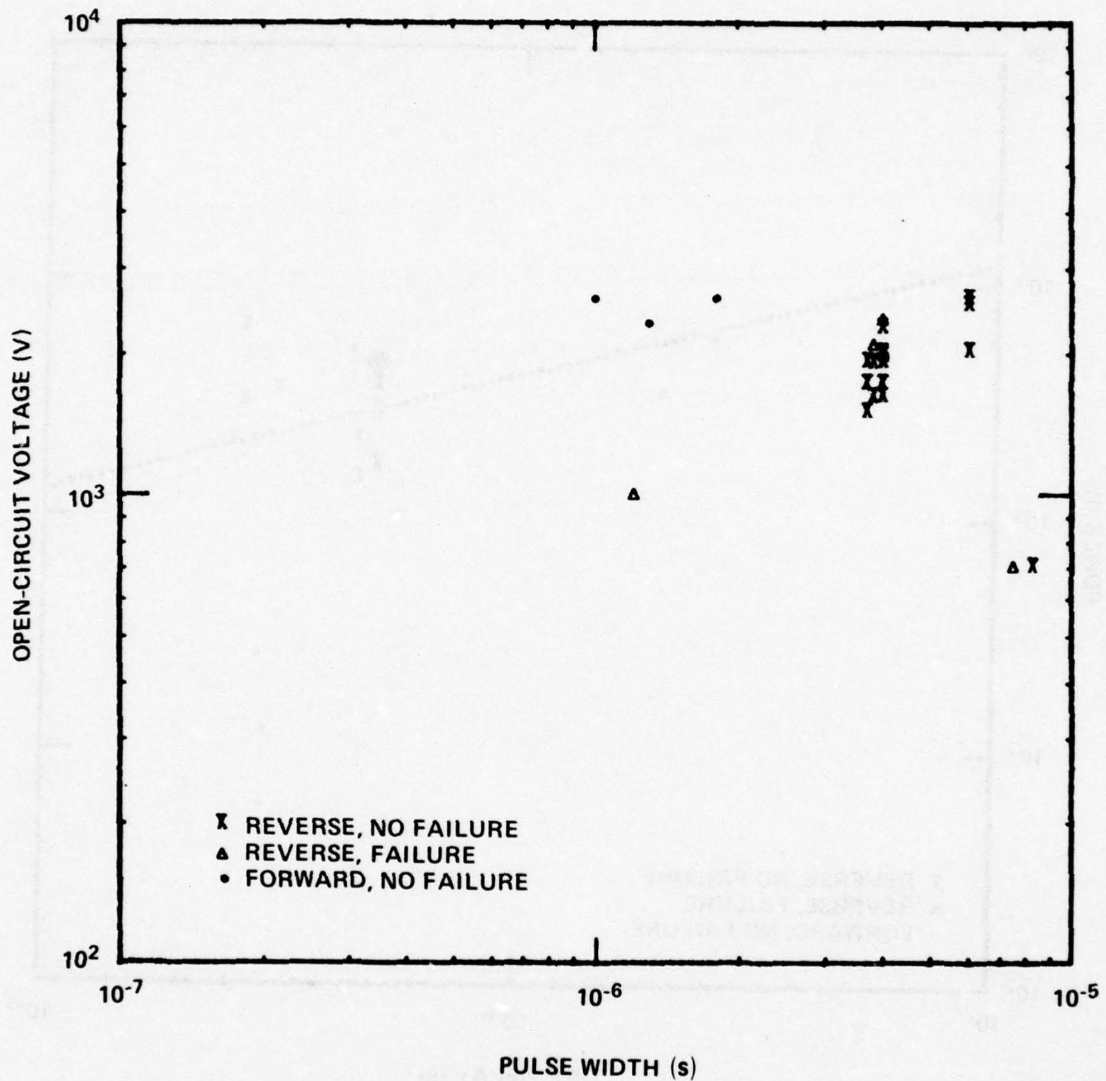

Figure 38. Damage points, voltage, Motorola 1N1202 rectifier.

levels. Table V presents the forward-biased and reverse-biased bulk surge impedance data as obtained from the voltage and current oscillograms.

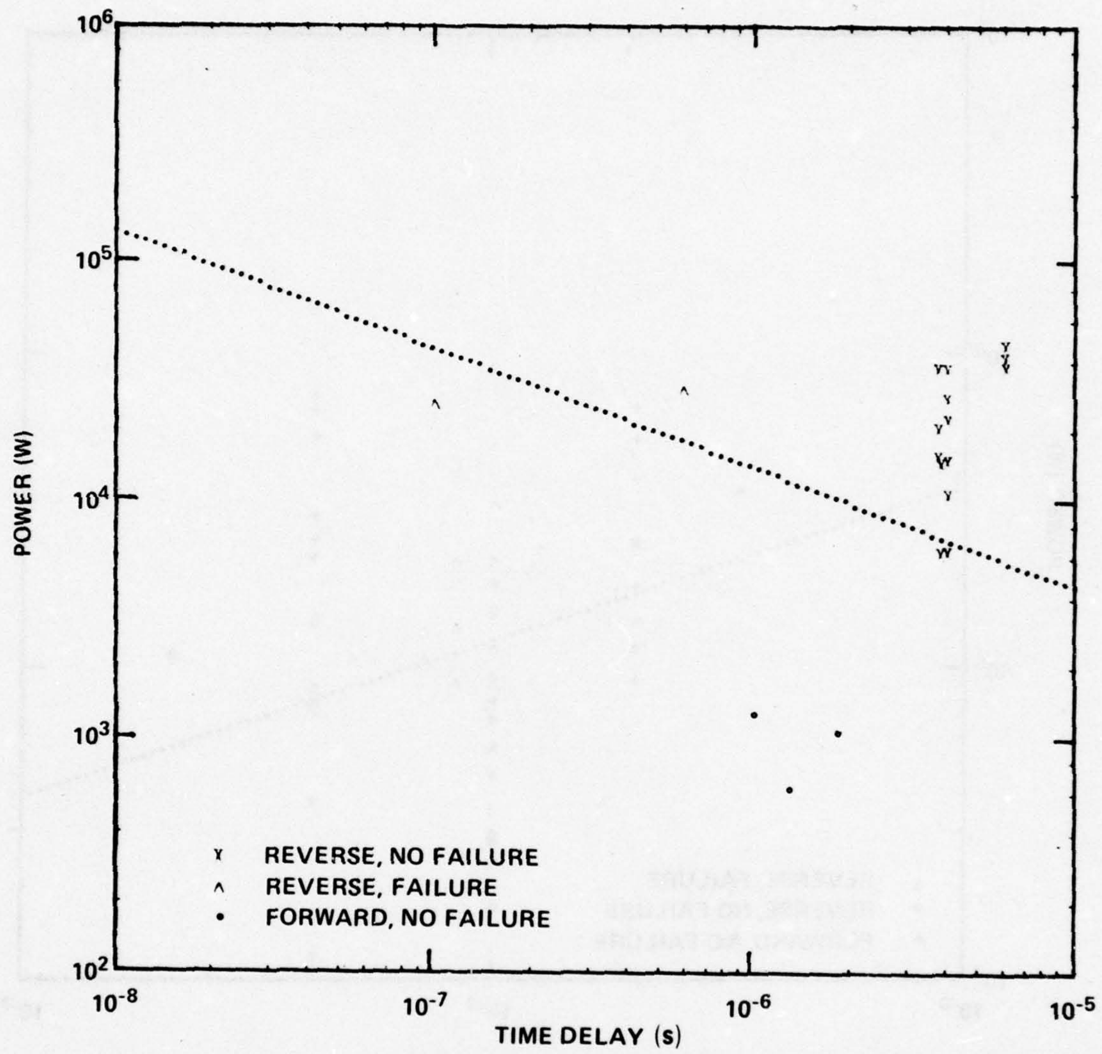

Figure 39. Damage line, power, Motorola 1N1202 rectifier.

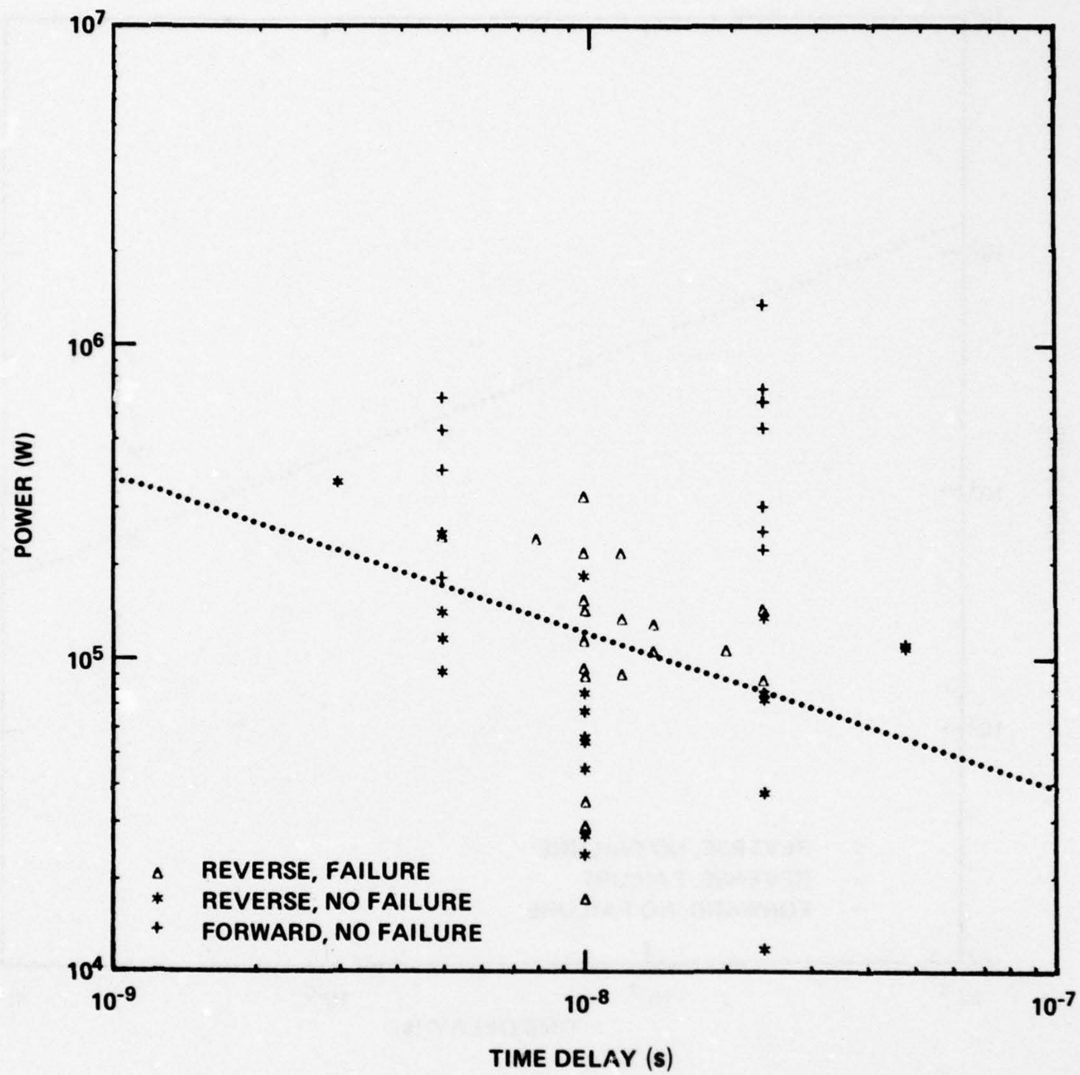

Figure 40. Damage line, power, Bendix 1N1202A rectifier.

TABLE V. 1N1200 FAMILY BULK SURGE IMPEDANCES

Device	Points (No.)	Pulse bias	Range (ohms)	Mean (ohms)	Median (ohms)	Remarks
1N1200 (General Electric)	17 3	Reverse Forward	64 to 3000 --	900 0.05	300 --	47 ohms in series
1N1200 (Motorola)	16 --	Reverse Forward	9.2 to 340 --	110 --	68 --	47 ohms in series
1N1202 (General Electric)	18 3	Reverse Forward	28 to 360 --	64 0.09	44 --	
1N1202 (Motorola)	16 3	Reverse Forward	6.4 to 175 --	65 0.10	46 --	
1N1202A (Bendix)	33 13	Reverse Forward	2.1 to 35 0.012 to 39	11.6 12.0	9.2 5	

--Insufficient data for calculation.

4.1.13 1N3047B Diode

The International Rectifier Corp. 1N3047B is a silicon reference diode with a nominal reference level of 130 V at 1.9 mA. Thirty diodes were tested: 26 reverse biased and 4 forward biased. Six reverse-biased and the four forward-biased diodes were tested with long pulses (2 to 8 μs) produced by the thyratron generator. The remaining diodes were pulsed at 24 and 48 ns from the coaxial high-voltage generator.

The diode failed in a thermal second-breakdown manner as indicated by the oscillograms. The reverse-biased failure points were fitted to the $T_D^{-1/2}$ line and to the T_D^{-1} line; the best fit was obtained from the T_D^{-1} line (fig. 41).

The bulk surge impedance of the diode decreased as pulse width increased: 28 points at the 24- and 48-ns pulses averaged 7.06 ohms from a range of 3.64 to 17.1 ohms; 23 points at times greater than 1.0 μs averaged 1.17 ohms from a range of 0.36 to 3.0 ohms. The forward-biased bulk surge impedance averaged 4.17 ohms (for three points at 2 μs).

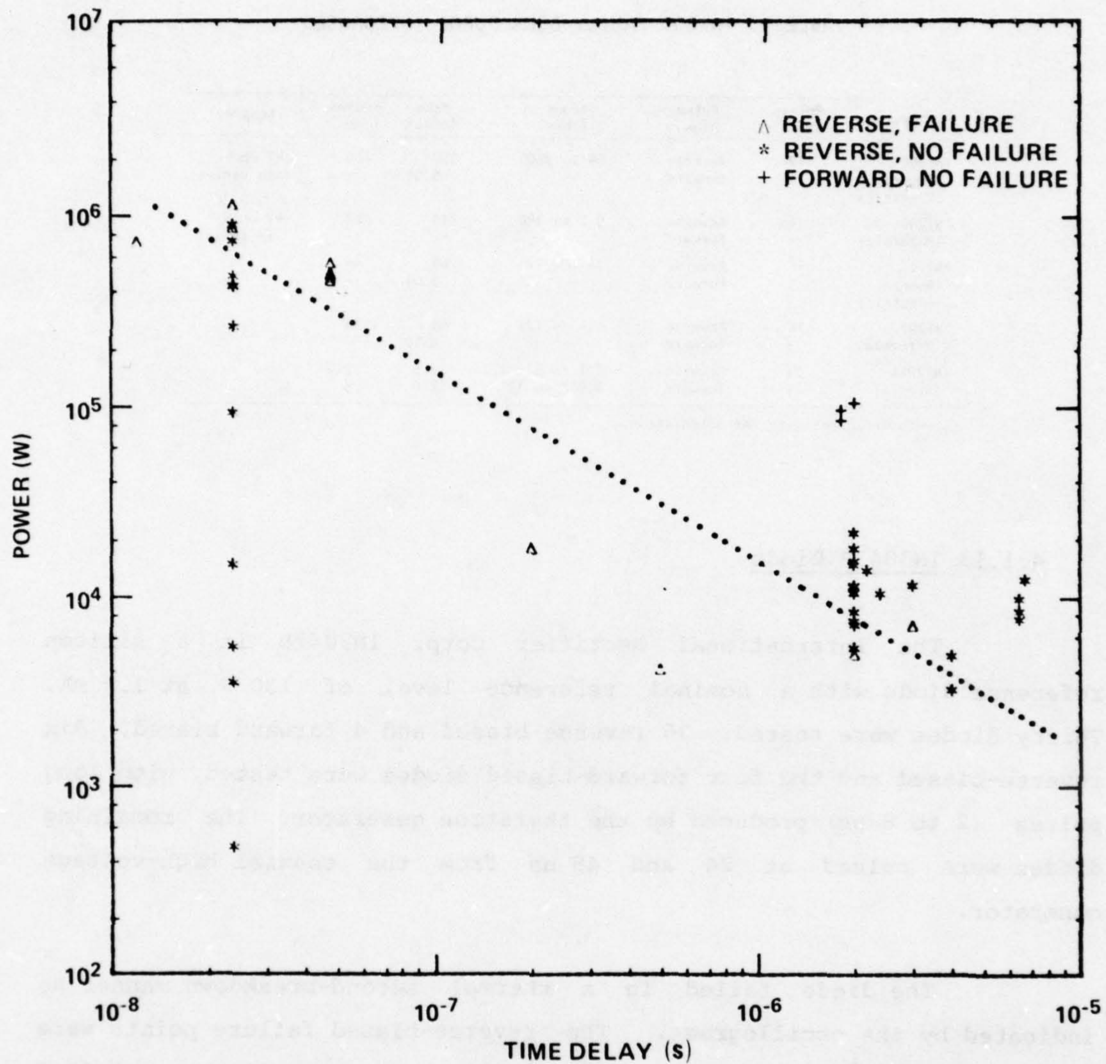

Figure 41. Damage line, power, International Rectifier 1N3047B diode.

4.1.14 1N3064 Diode

The Raytheon Co. (RAY) 1N3064 is a silicon diode designed for high-speed, low-power switching applications. Forty-two diodes were tested at 24 and 48 ns by using the coaxial high-voltage generator.

The failure mode for all diodes appears to follow the thermal model. Figure 42 shows the $T_D^{-\frac{1}{2}}$ line fitted to the reverse-biased failure points. The slope of -1/2 appears to fit the data better than a slope of -1; but, with the limited range in the data, the choice is arbitrary. The bulk surge impedance decreased at longer pulses: from a mean of 6.46 ohms for 19 reverse-biased points at 24 ns to 3.61 ohms for 15 reverse-biased points at 48 ns. Overall, the bulk surge impedance

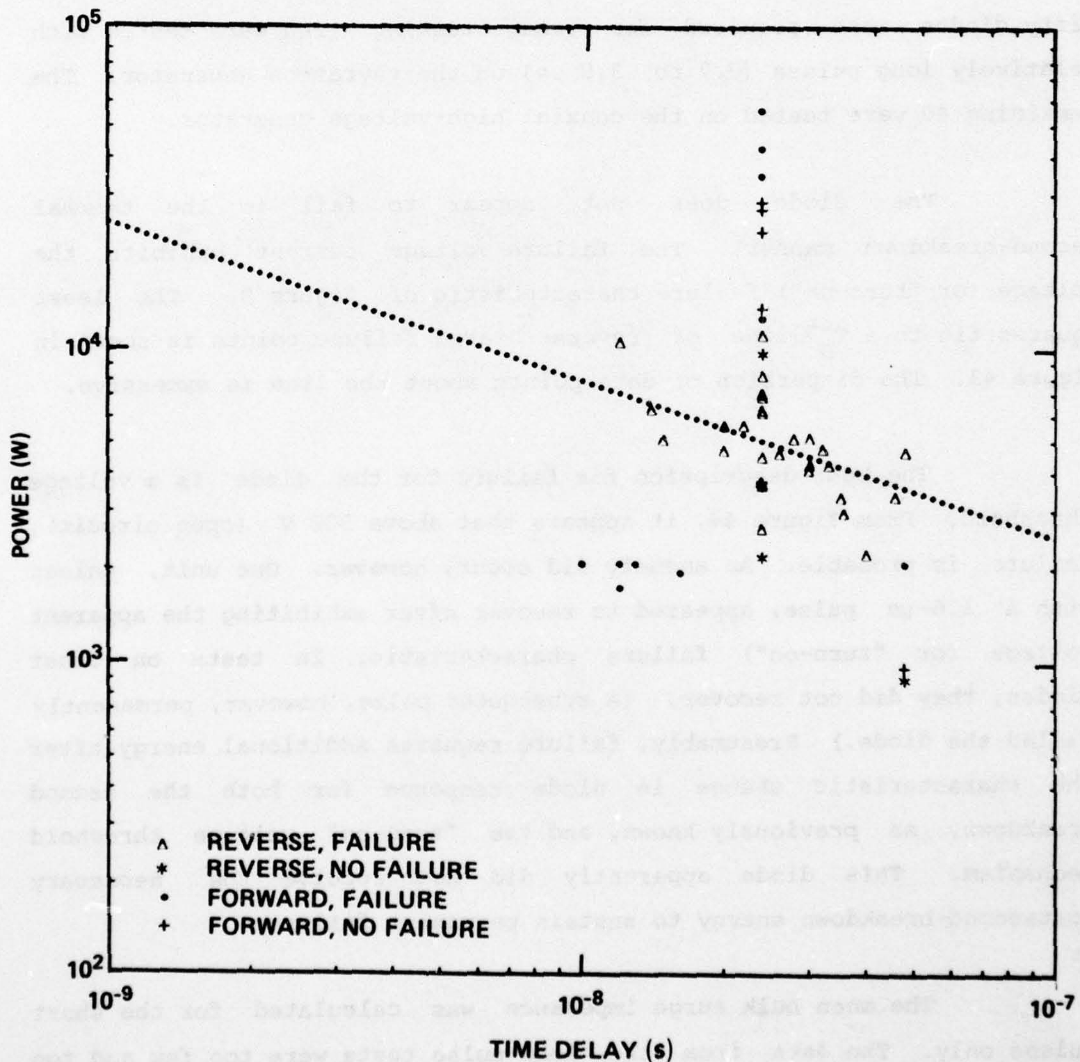

Figure 42. Damage line, power, Raytheon 1N3064 diode.

ranged from 1.24 to 11.03 ohms with a mean of 5.2 ohms. In the forward-biased direction, nine sample points from the 24-ns tests yielded a mean of 4.93 ohms bulk surge impedance.

4.1.15 1N3666 Diode

The ITT 1N3666 is a gold-bonded, germanium switching diode. Fifty diodes were acquired for damage testing. Ten were tested with relatively long pulses (0.7 to 3.8 μs) on the thyratron generator. The remaining 40 were tested on the coaxial high-voltage generator.

The diode does not appear to fail in the thermal second-breakdown manner. The failure voltage current exhibits the voltage (or "turn-on") failure characteristic of figure 9. The least squares fit to a $T_D^{-1/2}$ line of reverse-biased failure points is shown in figure 43. The dispersion of data points about the line is excessive.

The best description for failure for the diode is a voltage threshold. From figure 44, it appears that above 300 V (open circuit), failure is probable. An anomaly did occur, however. One unit, pulsed with a 1.6-μs pulse, appeared to recover after exhibiting the apparent voltage (or "turn-on") failure characteristic. In tests on other diodes, they did not recover. (A subsequent pulse, however, permanently failed the diode.) Presumably, failure requires additional energy after the characteristic change in diode response for both the second breakdown, as previously known, and the "turn-on" voltage threshold mechanism. This diode apparently did not receive the necessary postsecond-breakdown energy to sustain permanent failure.

The mean bulk surge impedance was calculated for the short pulses only. The data from the long-pulse tests were too few and too

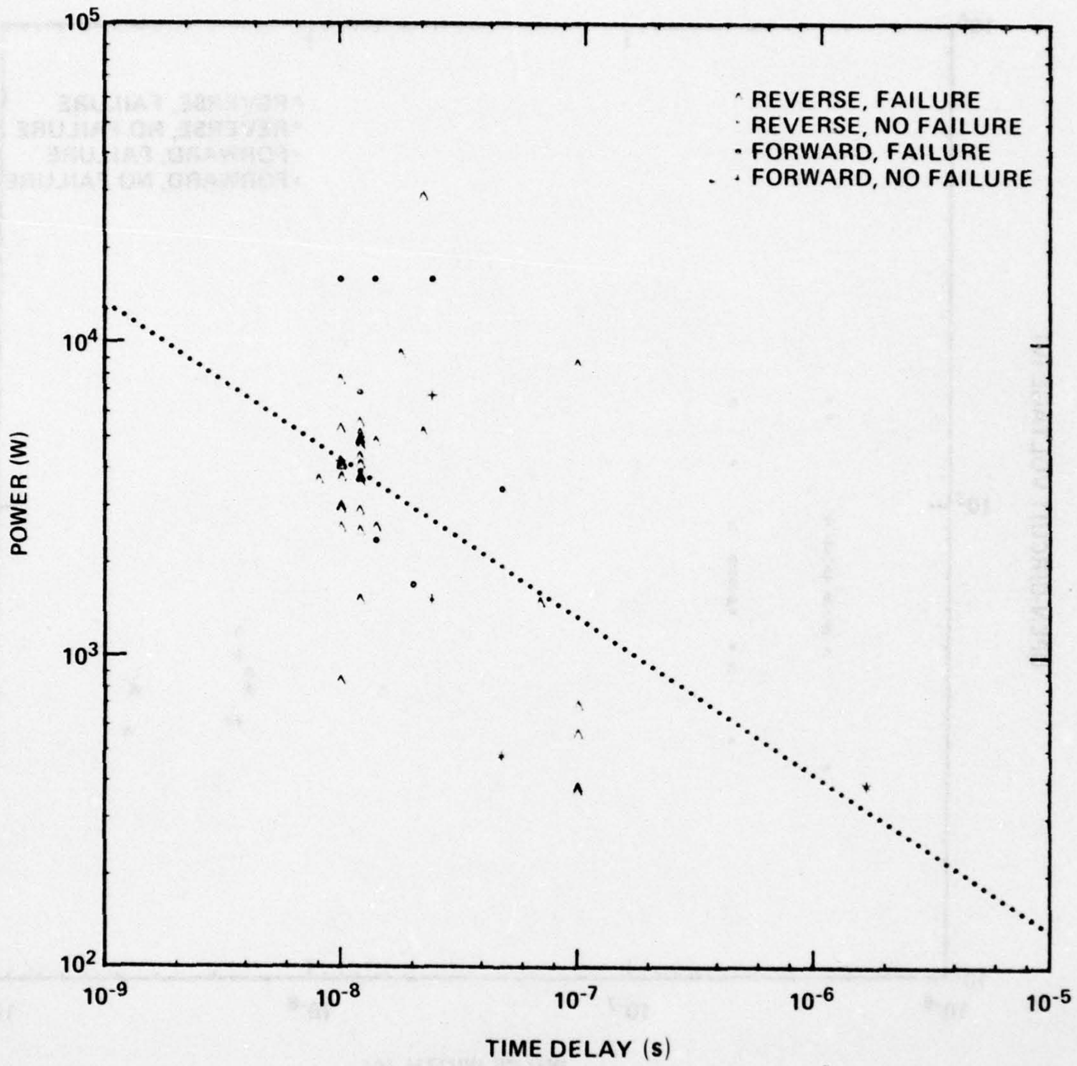

Figure 43. Damage line, power, ITT Semiconductors 1N3666 diode.

disparate to provide any useful information. Computed impedances from combined 24- and 48-ns pulses ranged from 2.0 to 17.0 ohms with a mean of 7.11 ohms for reverse-biased tests and from 1.40 to 6.23 ohms with a mean of 1.84 ohms for forward-biased tests.

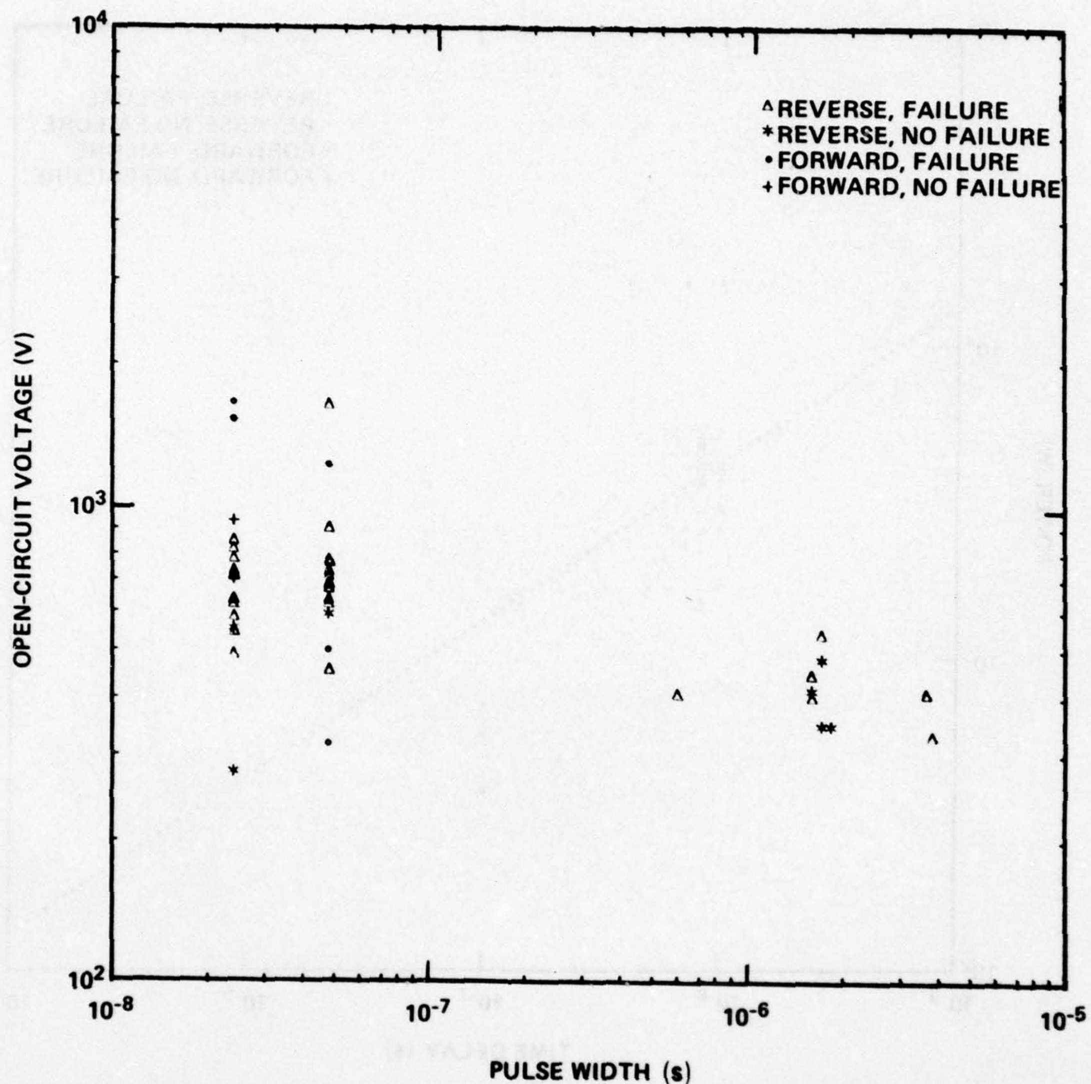

Figure 44. Damage points, voltage, ITT Semiconductors 1N3666 diode.

4.1.16 1N4003 and 1N4005 Rectifiers

The 1N4001 to 1N4007 series of devices are subminiature, lead-mounted, silicon rectifiers used for low-power circuit applications. The MOT and TRW 1N4003 is rated at 200 PIV; the MOT 1N4005, at 600 PIV. The thyratron generator stressed these rectifiers: 10 MOT and 10 TRW 1N4003's and 7 MOT 1N4005's.

Voltage (or "turn-on") failure was evident in each rectifier set tested. The MOT rectifier failure was predominantly of this type. The TRW rectifier also exhibited what appeared to be a thermal second-breakdown mechanism. Figures 45 to 47 plot the open-circuit pulse width versus the time delay for the rectifiers. The data for the power versus the delay time for the TRW rectifier are plotted in figure 48.

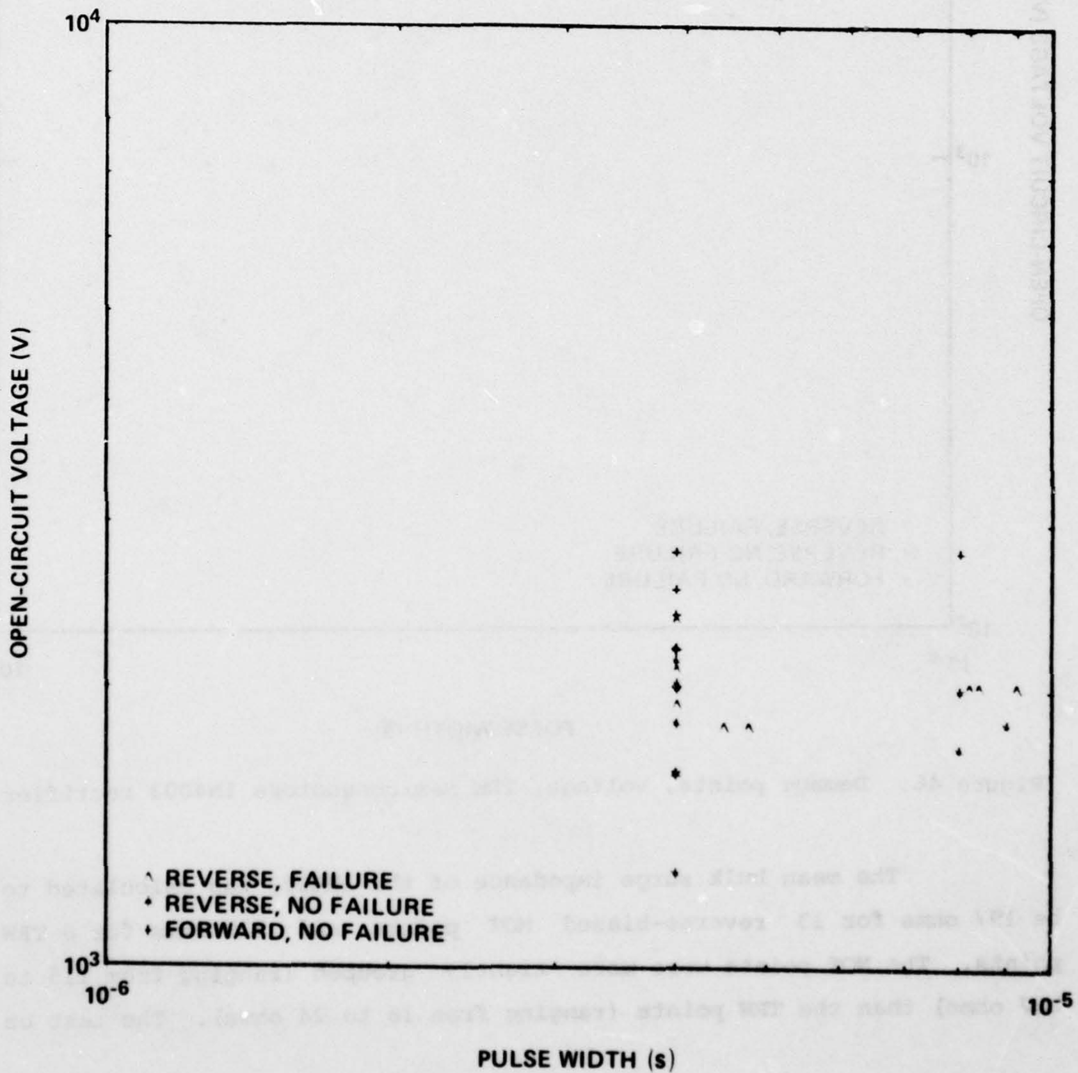

Figure 45. Damage points, voltage, Motorola 1N4003 rectifier.

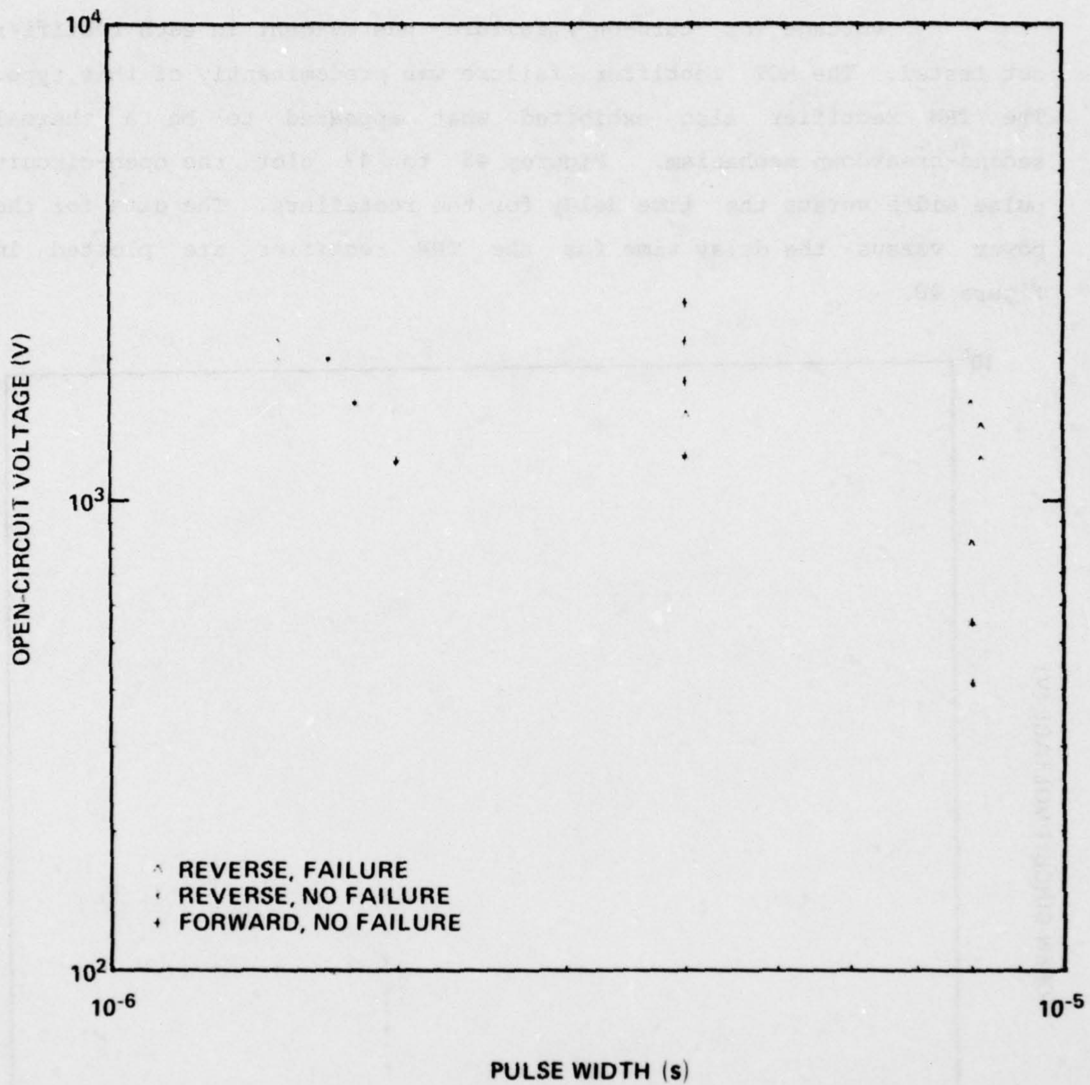

Figure 46. Damage points, voltage, TRW Semiconductors 1N4003 rectifier.

The mean bulk surge impedance of the 1N4003 was calculated to be 197 ohms for 13 reverse-biased MOT points and 129 ohms for 8 TRW points. The MOT points were more tightly grouped (ranging from 115 to 287 ohms) than the TRW points (ranging from 16 to 24 ohms). The test on

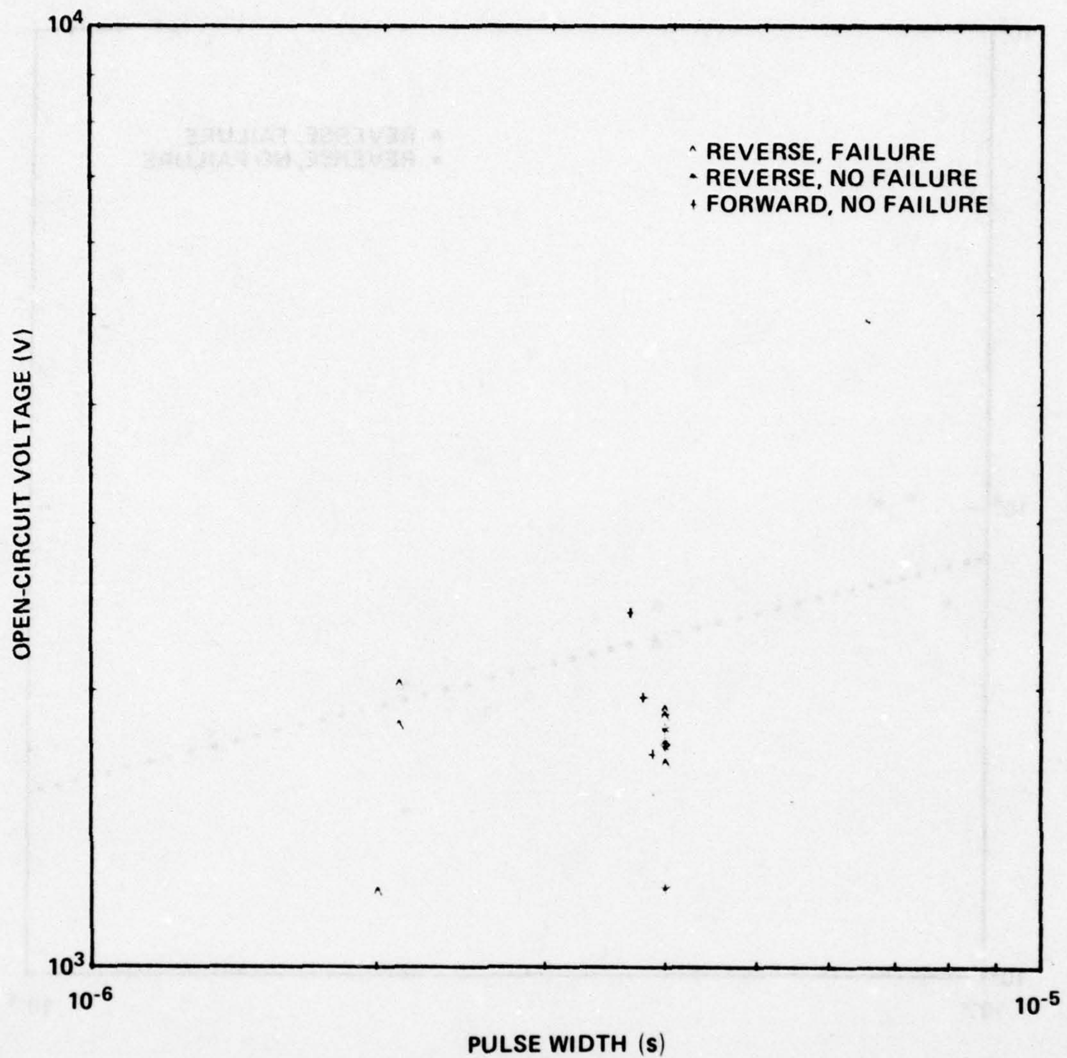

Figure 47. Damage points, voltage, Motorola 1N4005 rectifier.

the 1N4005 gave a reverse-biased mean bulk surge impedance for five points of 116 ohms. None of the 1N4000 series rectifiers could be damaged by forward-biased pulses with the instrumentation.

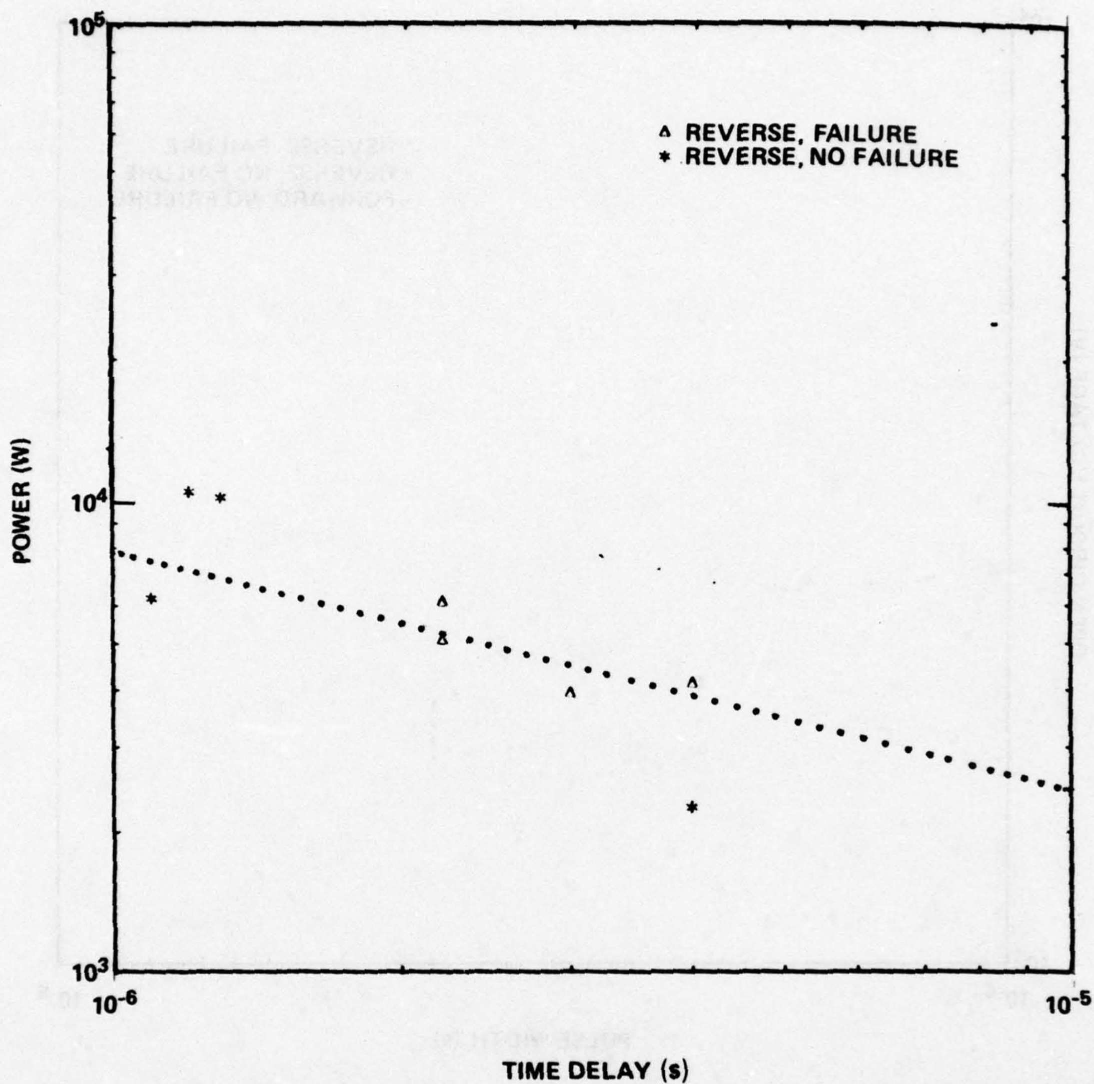

Figure 48. Damage line, power, TRW Semiconductors 1N4003 rectifier.

4.1.17 UT254 Rectifier

The Unitrode diodes are controlled-avalanche silicon rectifiers designed to provide higher power and surge capacity in a small package. The Unitrode UT254 is rated at 400 PIV, 1.5 A at 25°C, to withstand an 8.3-ms sinusoid up to 25 A without damage. Fifty rectifiers were tested: 25 reverse biased and 5 forward biased with

1.0- to 8.0-μs pulses on the thyratron generator and 20 reverse biased with 30- and 80-ns pulses on the coaxial high-voltage generator.

The rectifiers appeared to fail from the thermal second-breakdown mechanism. Figure 49 plots the power versus the time

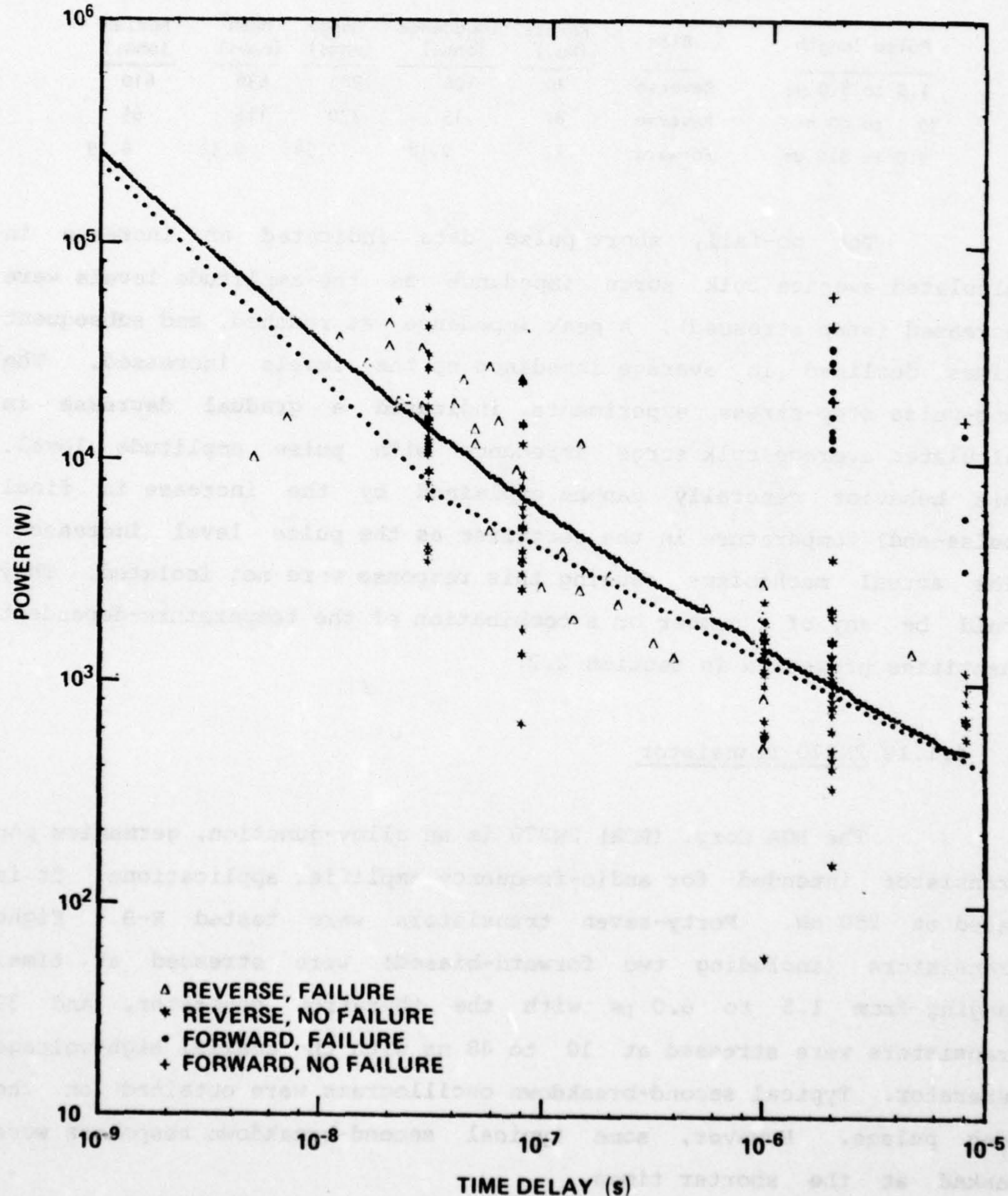

Figure 49. Damage curve, power, Unitrode UT254 diode.

to failure. The data are fit to the complete model. The breakpoint between the T_D^{-1} and $T_D^{-1/2}$ lines occurs at approximately 7000 W at 30 ns.

The behavior of the bulk surge impedance is summarized below.

Pulse length	Bias	Points (No.)	Impedance (ohms)	Range (ohms)	Mean (ohms)	Median (ohms)
1.0 to 8.0 μs	Reverse	70	106	1980	639	610
30 to 80 ns	Reverse	81	15	370	115	65
2.0 to 8.0 μs	Forward	21	0.18	0.54	0.32	0.29

The no-fail, short-pulse data indicated an increase in calculated average bulk surge impedance as the amplitude levels were increased (step stressed). A peak impedance was reached, and subsequent pulses declined in average impedance as the levels increased. The long-pulse step-stress experiments indicated a gradual decrease in calculated average bulk surge impedance with pulse amplitude level. This behavior generally can be explained by the increase in final (pulse-end) temperature in the rectifier as the pulse level increased. The actual mechanisms causing this response were not isolated. They could be any of a number or a combination of the temperature-dependent quantities presented in section 2.2.

4.1.18 2N270 Transistor

The RCA Corp. (RCA) 2N270 is an alloy-junction, germanium pnp transistor intended for audio-frequency amplifier applications. It is rated at 250 mW. Forty-seven transistors were tested E-B. Eight transistors (including two forward-biased) were stressed at times ranging from 1.5 to 6.0 μs with the thyratron generator, and 39 transistors were stressed at 10 to 48 ns with the coaxial high-voltage generator. Typical second-breakdown oscillograms were obtained on the long pulses. However, some typical second-breakdown responses were masked at the shorter times.

The power versus the time to failure is shown in figure 50. The intersection of the T_D^{-1} and $T_D^{-\frac{1}{2}}$ asymptotes is approximately 1.5 kW at 120 ns. The mean bulk surge impedance for the reverse-biased E-B junction was calculated to be 18.1 ohms for short pulses and 107 ohms for long pulses.

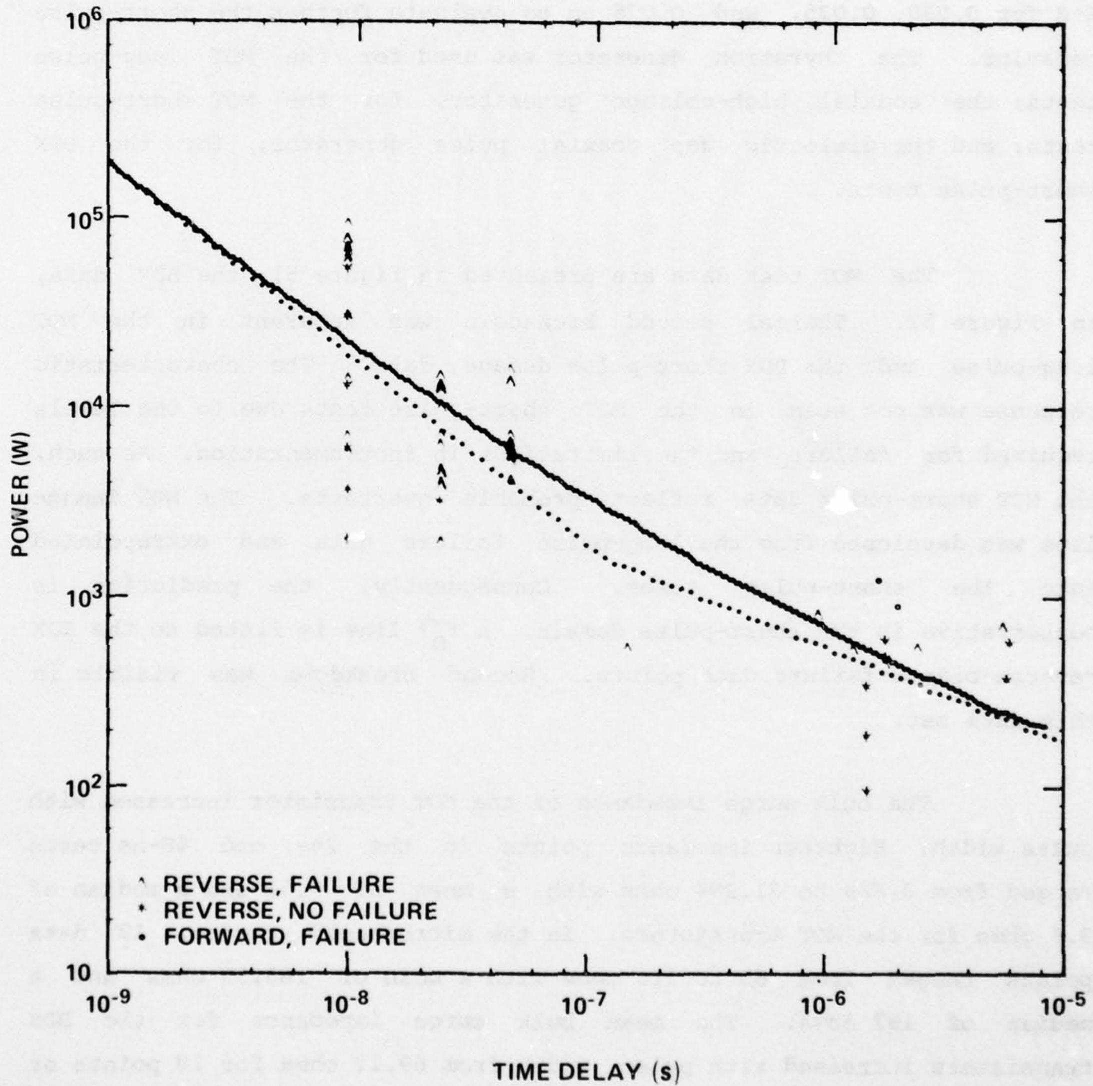

Figure 50. Damage curve, power, E-B, RCA 2N270 transistor.

4.1.19 2N297A Transistor

The MOT and BDX 2N297A's are germanium pnp power transistors rated at 90 W. Tests were run first E-B on 25 MOT transistors at 0.024, 0.048, and 0.5 to 8.0 μs. Twenty-one BDX transistors also were pulsed E-B for 0.030, 0.035, and 0.075 μs to evaluate further the short-pulse behavior. The thyratron generator was used for the MOT long-pulse tests; the coaxial high-voltage generator, for the MOT short-pulse tests; and the dielectic gap coaxial pulse generator, for the BDX short-pulse tests.

The MOT test data are presented in figure 51; the BDX data, in figure 52. Thermal second breakdown was apparent in the MOT long-pulse and the BDX short-pulse damage data. The characteristic response was not seen in the MOT short-pulse tests due to the levels required for failure and the limitations in instrumentation. As such, the MOT short-pulse data reflect probable overtests. The MOT damage line was developed from the long-pulse failure data and extrapolated into the short-pulse times. Consequently, the prediction is conservative in the short-pulse domain. A $T_D^{-\frac{1}{2}}$ line is fitted to the BDX reverse-biased failure data points. Second breakdown was visible in this data set.

The bulk surge impedance of the MOT transistor increased with pulse width. Eighteen impedance points in the 24- and 48-ns tests ranged from 3.889 to 21.294 ohms with a mean of 9.51 and a median of 9.6 ohms for the MOT transistors. In the microsecond regime, 19 data points ranged from 60 to 310 ohms with a mean of 188.39 ohms and a median of 197 ohms. The mean bulk surge impedance for the BDX transistors increased with pulse width from 69.17 ohms for 18 points at

AD-A053 899 HARRY DIAMOND LABS ADELPHI MD F/G 14/2
COMPONENT DAMAGE FROM ELECTROMAGNETIC PULSE (EMP) INDUCED TRANS--ETC(U)
OCT 77 J R MILETTA
UNCLASSIFIED HDL-TM-77-22 NL

2 OF 2
AD A
053899

END
DATE
FILMED
6-78
DDC

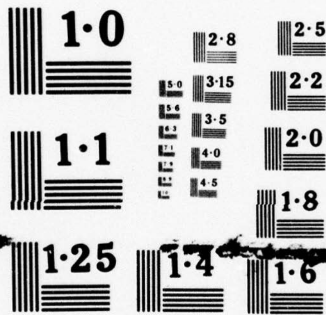

NATIONAL BUREAU OF STANDARDS
MICROCOPY RESOLUTION TEST CHART

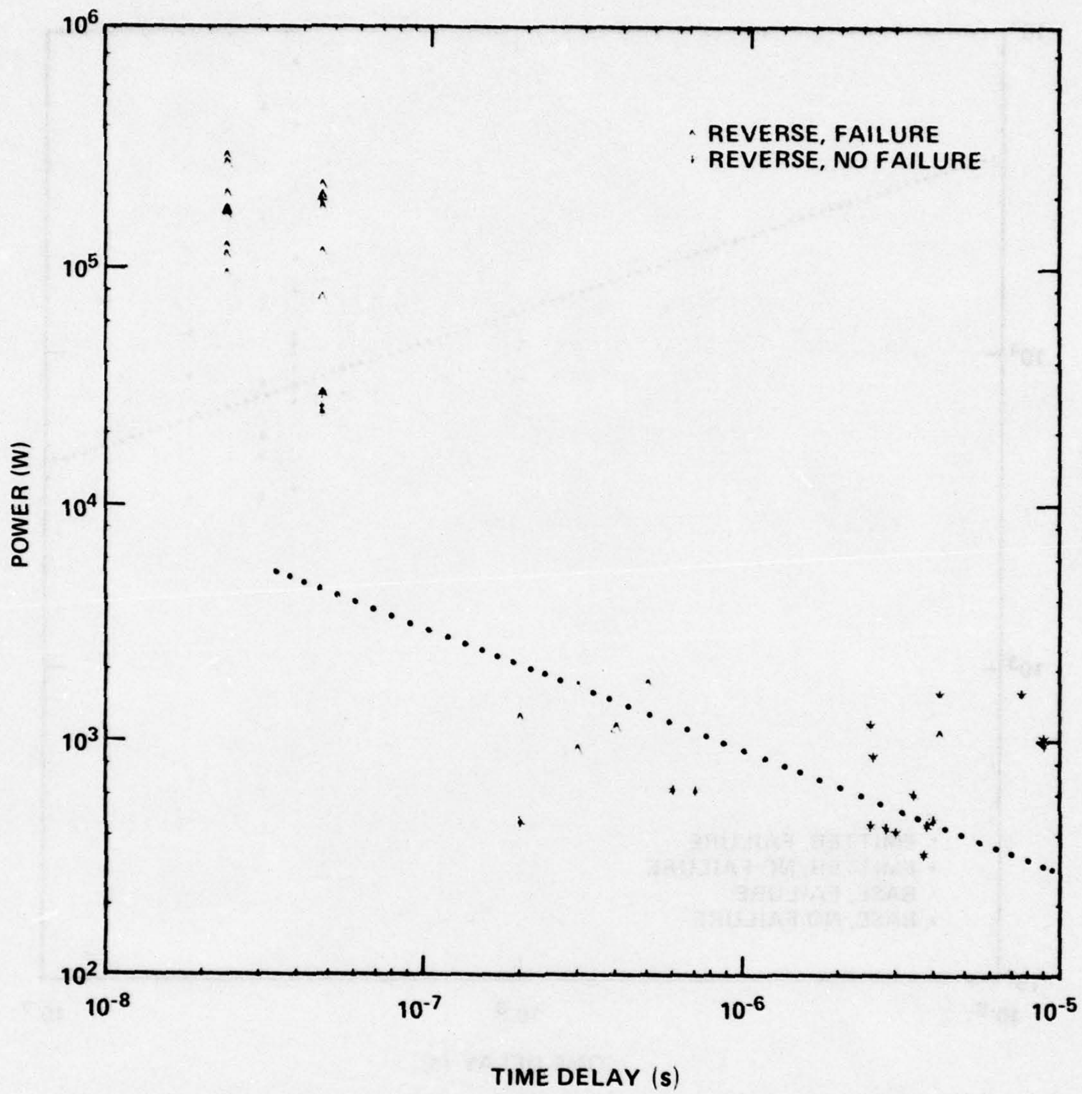

Figure 51. Damage line, power, E-B, Motorola 2N297A transistor.

30 and 35 ns to 87.3 ohms for 11 points at 75 ns. The bulk surge impedance for all data points ranged from 6.86 to 195 ohms with a mean of 73.2 ohms and a median of 57.3 ohms. The forward-biased impedance averaged 12 ohms.

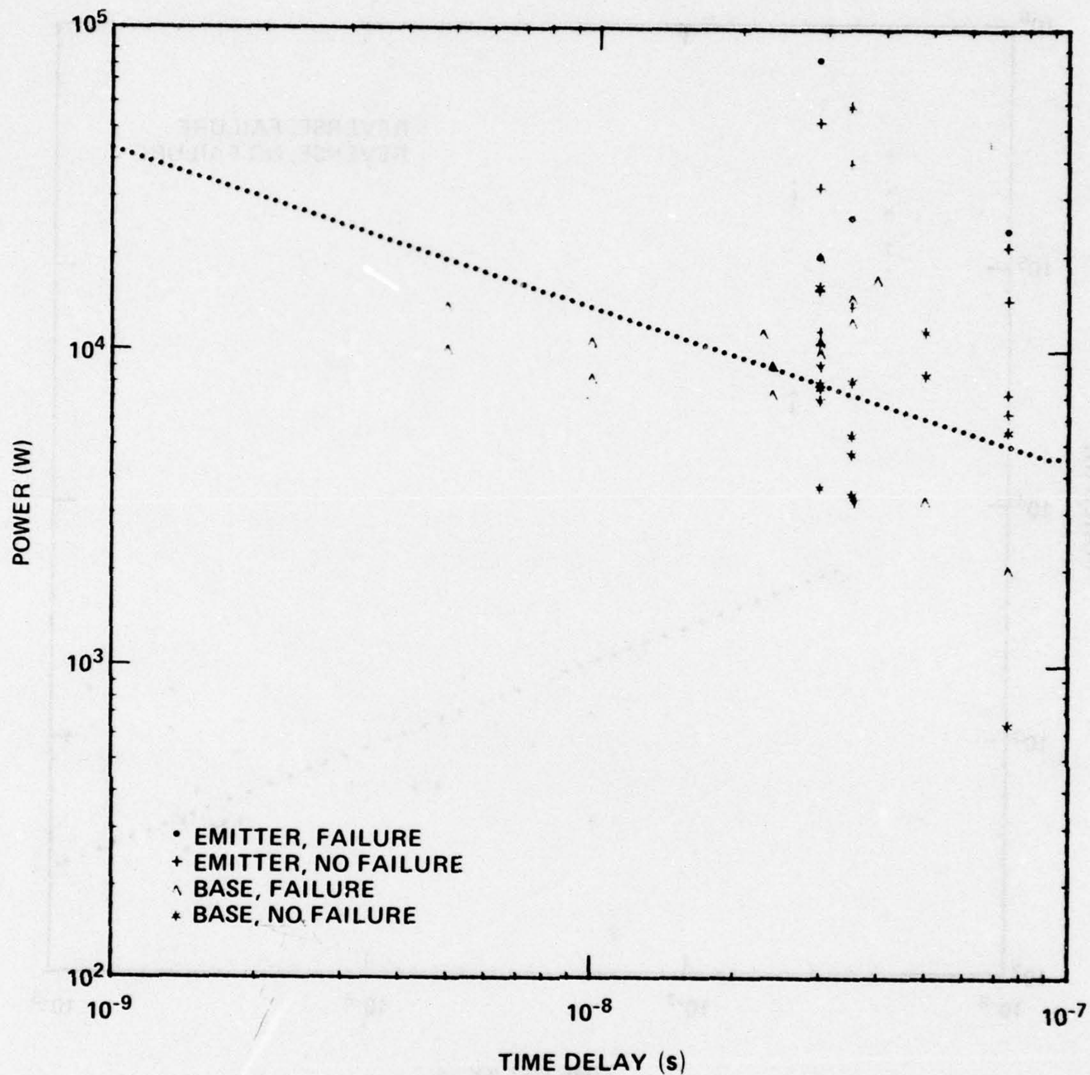

Figure 52. Damage line, power, Bendix 2N297A transistor.

4.1.20 2N328A Transistor

The Crystalonics Division, Teledyne, Inc., 2N328A is a general-purpose, epitaxial-junction, silicon pnp transistor rated at 250 mW. Fifty transistors were tested E-B, 10 with pulses ranging from 0.9 to 7.0 μs by using the thyratron generator and 40 with pulses at 24 and 48 ns by using the coaxial high-voltage generator.

The data are plotted in figure 53. A thermal second-breakdown characteristic was apparent in the oscillograms; however, the transition into second breakdown was gradual, as seen in the short-pulse data. The voltage levels during the short-pulse tests ranged from ~700 to 800 V, while the breakdown voltage of the E-B junction ranged from ~40 to 100 V. Both of these characteristics of the data made difficult an accurate determination of the time delay. The

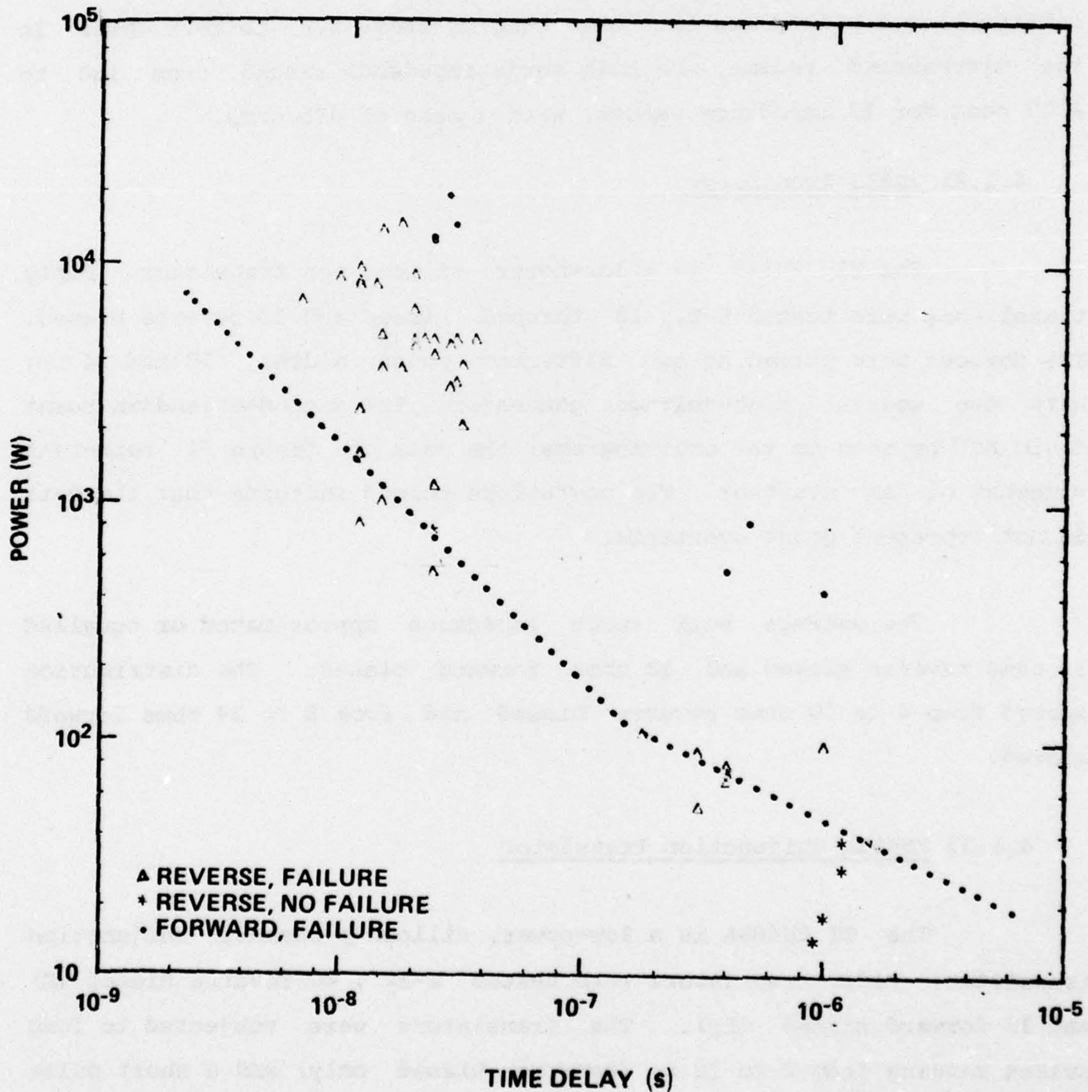

Figure 53. Damage curve, power, E-B, Crystalonics 2N328A transistor.

short-pulse data, therefore, must be viewed as slight overtests. The curve drawn in figure 53 represents an estimate based on the least squares fit of the long-pulse data and a conservative consideration of the short-pulse data.

The bulk surge impedance increased with pulse width. At 24 and 48 ns, the mean bulk surge impedance calculated from 32 reverse-biased points was 16.5 ohms ranging from 3.6 to 36.8 ohms. In the microsecond regime, the bulk surge impedance ranged from 188 to 1050 ohms for 12 impedance values, with a mean of 475 ohms.

4.1.21 2N335 Transistor

The TI 2N335 is a low-power, silicon npn transistor. Forty transistors were tested E-B, 10 forward biased and 30 reverse biased. The devices were pulsed at two different pulse widths, 50 and 24 ns, with the coaxial high-voltage generator. The second-breakdown point could not be seen on the oscillograms; the data of figure 54 represent somewhat of an overtest. The no-failure points indicate that the data do not represent gross overtests.

The average bulk surge impedance approximated or equalled 11 ohms reverse biased and 13 ohms forward biased. The distribution spread from 4 to 20 ohms reverse biased and from 8 to 24 ohms forward biased.

4.1.22 2N489A Unijunction Transistor

The TI 2N489A is a low-power, silicon p-channel unijunction transistor. Fifty transistors were tested E-B_2, 40 reverse biased (E) and 10 forward biased (B_2). The transistors were subjected to long pulses ranging from 2 to 10 μs (reverse biased only) and a short pulse of 75 ns. The thyratron generator and dielectric-gap generator were used.

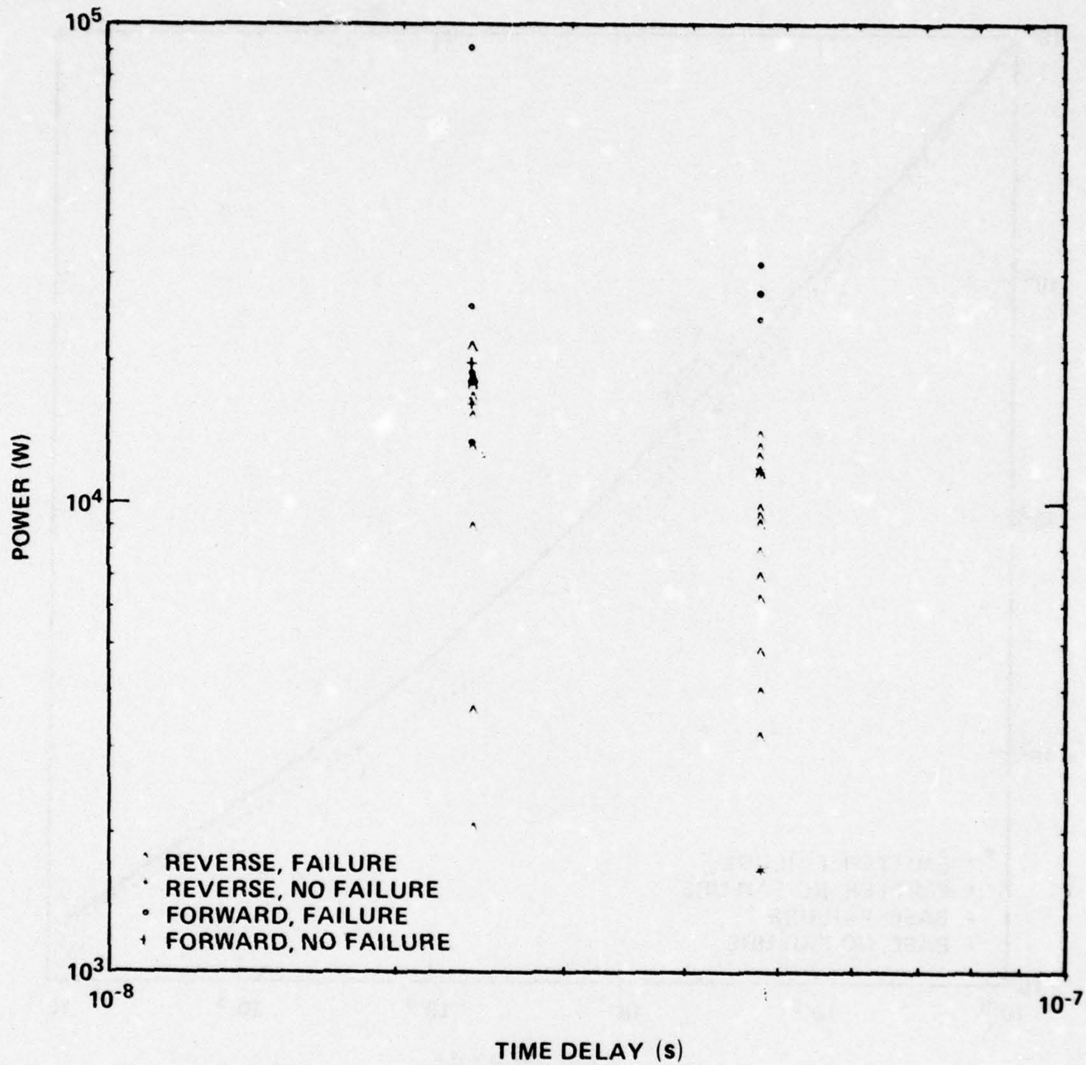

Figure 54. Damage points, power, E-B, Texas Instruments 2N335 transistor.

The failures appeared to follow the thermal second-breakdown damage model throughout the entire model range, T_D^{-1} and $T_D^{-\frac{1}{2}}$. The point where the asymptotes of the T_D^{-1} and $T_D^{-\frac{1}{2}}$ curves intersect appears at a pulse width of 230 ns and peak power of 210 W (fig. 55).

The average bulk surge impedance was ~160 ohms reverse biased and 190 ohms forward biased. The distribution spread from 59 to

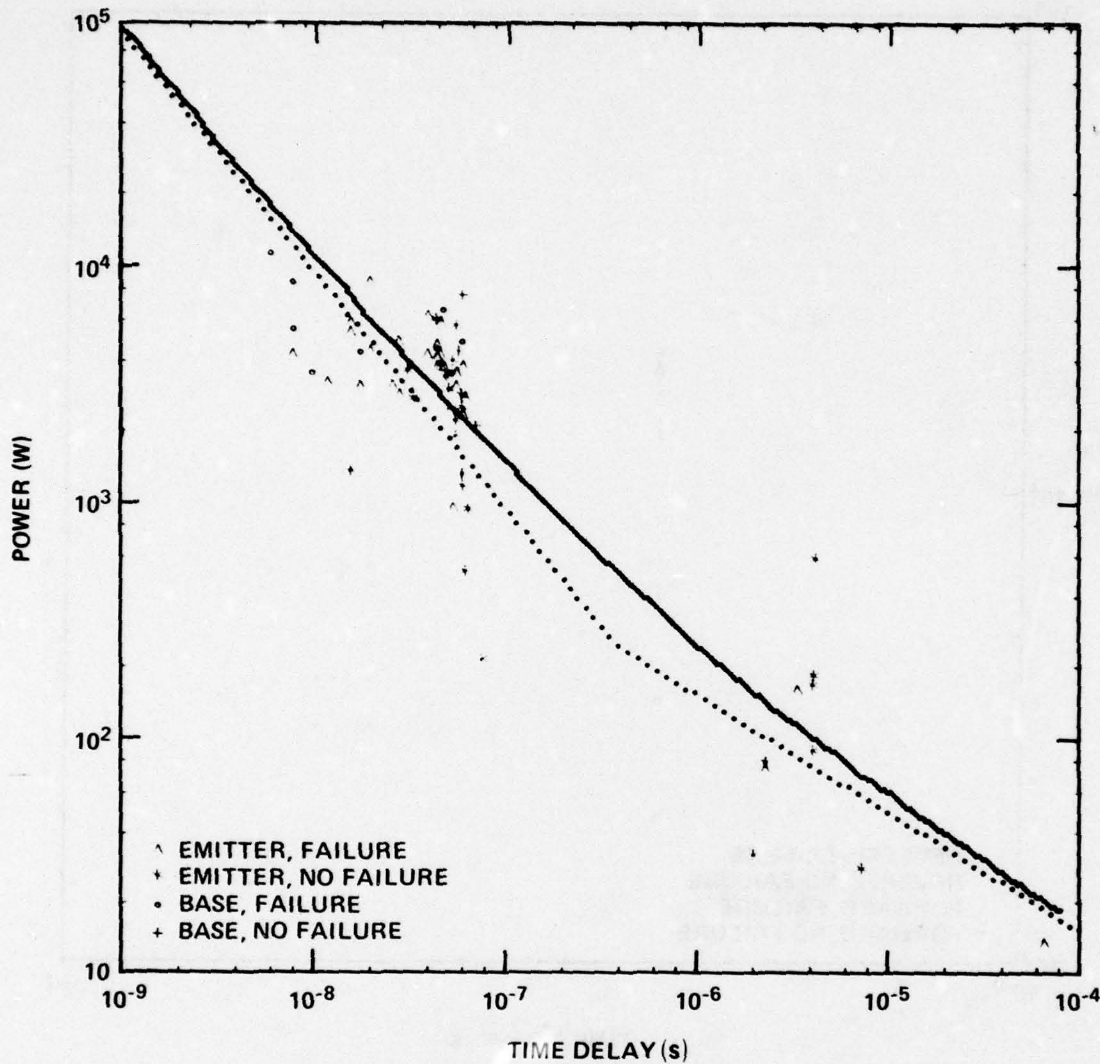

Figure 55. Damage curve, power, Texas Instruments 2N489A transistor.

430 ohms reverse biased and 100 to 300 ohms forward biased. The sample size forward biased was only 13 and may account for this value of resistance being ~12 percent larger than reverse-biased impedance.

4.1.23 2N526 Transistor

The MOT 2N526 is a low-power, germanium-alloy pnp transistor. Forty transistors were tested E-B, 10 forward biased (E) and 30 reverse

biased (B). In testing with the coaxial high-voltage generator, open-circuit pulses of 50 and 24 ns were used.

The data exhibited a thermal second-breakdown response, though the transition region was gradual (in the tens of nanoseconds). An average value was chosen for the determination of the time delay. The data are fit to the $T_D^{-1/2}$ line (fig. 56) of equation (9) for reverse-biased tests. A T_D^{-1} dependence is not apparent for this limited test range.

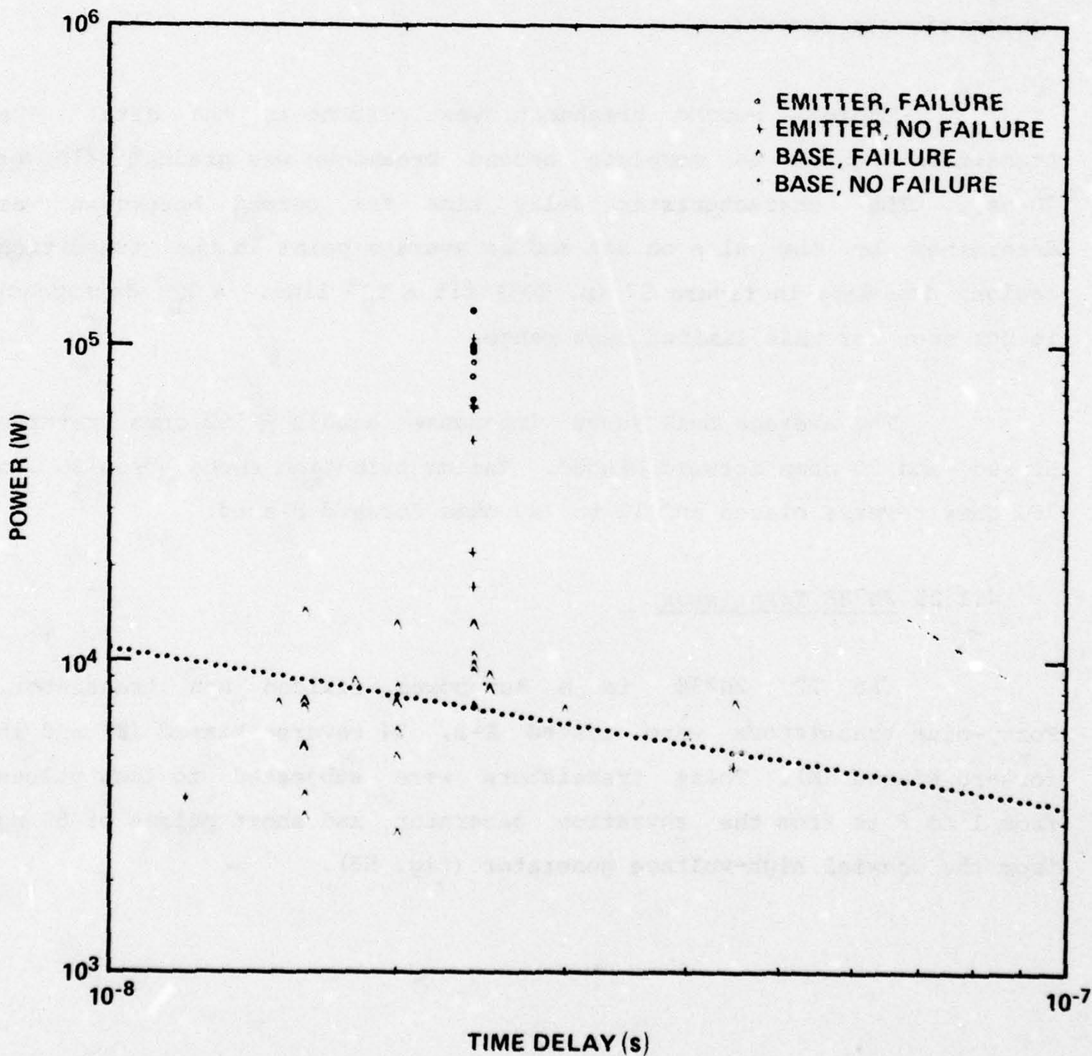

Figure 56. Damage line, power, Motorola 2N526 transistor.

The average bulk surge impedance was ~15 ohms reverse biased and 5.7 ohms forward biased. The distribution spread from 7 to 29 ohms reverse biased and 4 to 9 ohms forward biased.

4.1.24 2N598 Transistor

The GIC 2N598 is a low-power, germanium pnp transistor. Forty transistors were tested E-B, 12 forward biased (E) and 28 reverse biased (B). These transistors were pulsed at 75 ns on the dielectric-gap generator.

Thermal second breakdown was evident in the data. The transition region to complete second breakdown was gradual (10 to 20 ns). The characteristic delay time for second breakdown was determined by the pulse on set and an average point in the transition region. The data in figure 57 (p. 103) fit a $T_D^{-1/2}$ line. A T_D^{-1} dependency is not seen for this limited test range.

The average bulk surge impedance equals ~160 ohms reverse biased and 30 ohms forward biased. The distribution spread from 30 to 750 ohms reverse biased and 12 to 220 ohms forward biased.

4.1.25 2N738 Transistor

The TI 2N738 is a low-power, silicon npn transistor. Forty-nine transistors were tested E-B, 34 reverse biased (E) and 15 forward biased (B). These transistors were subjected to long pulses from 1 to 8 μs from the thyratron generator and short pulses of 50 ns from the coaxial high-voltage generator (fig. 58).

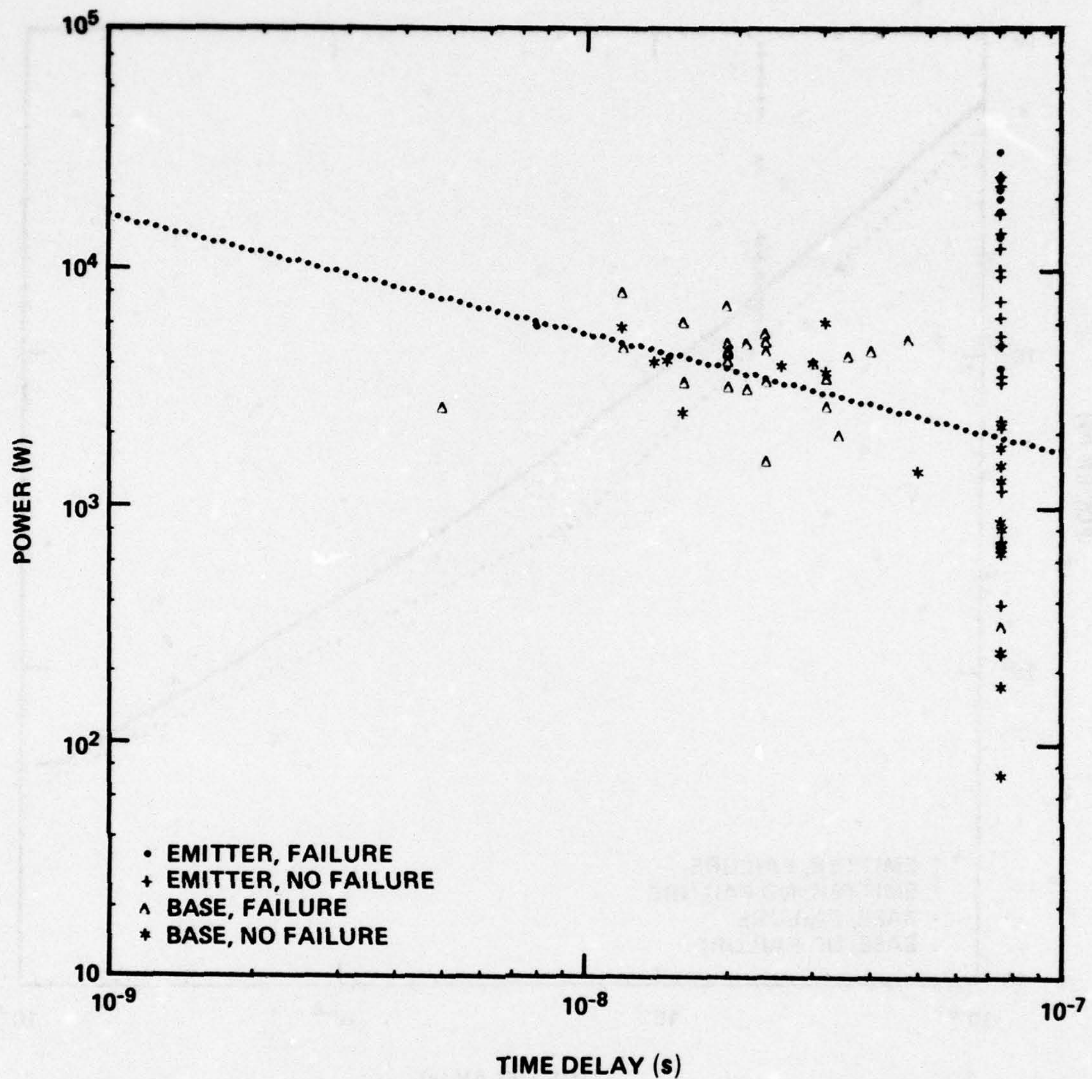

Figure 57. Damage line, power, General Instruments 2N598 transistor.

The average bulk surge impedance for the long pulses was ~18 ohms reverse biased and 1.0 ohm forward biased. The distribution spread from 9.0 to 49 ohms reverse biased and 0.7 to 1.4 ohms forward biased. For the short pulse, the corresponding impedances were 5.4 ohms reverse biased and 3.6 ohms forward biased.

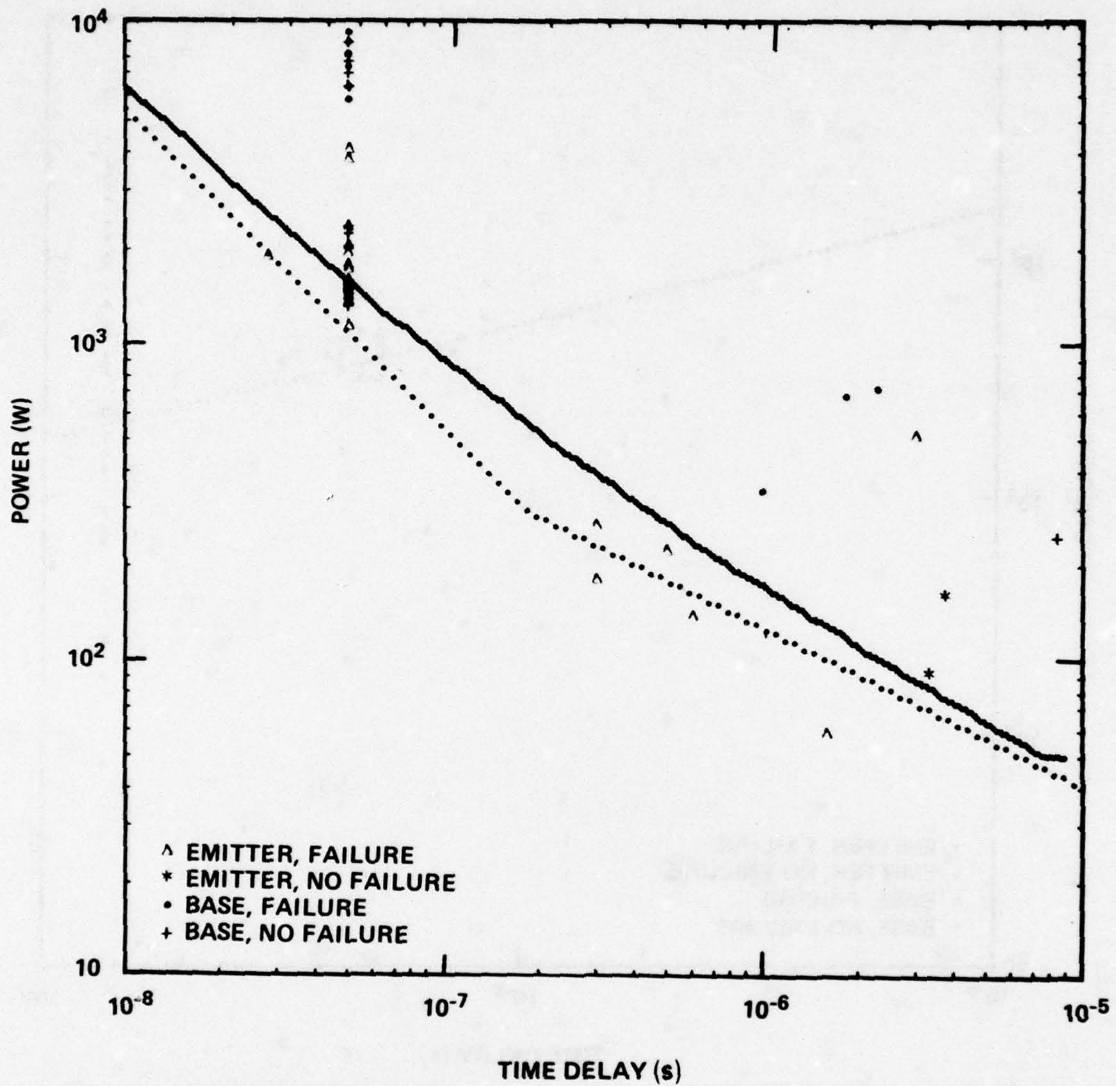

Figure 58. Damage curve, power, Texas Instruments 2N738 transistor.

4.1.26 2N1132A Transistor

The MOT, Fairchild Semiconductor Division (FSC), and RAY 2N1132A's are silicon pnp transistors for medium-current switching and amplifier circuits. The tests* were conducted on the E-B junction.

**Additional tests on the 2N1132 transistor are reported in section 4.2.*

Both the MOT and FSC transistors were characterized to long pulses on the thyratron generator, while the RAY devices were characterized to short pulses on the coaxial high-voltage generator. Of the 10 transistors each for MOT and FSC, 6 were pulsed reverse biased (B+) and 4 were pulsed forward biased (E+). All 24 RAY transistors were tested reverse biased (B+). The MOT and FSC data were fit to the $T_D^{-1/2}$ thermal second-breakdown model. Computer-fitted curves to failure points are presented in figures 59 to 61. Figure 62 displays the combined data for the three manufacturers fit to the complete expression of equation (9).

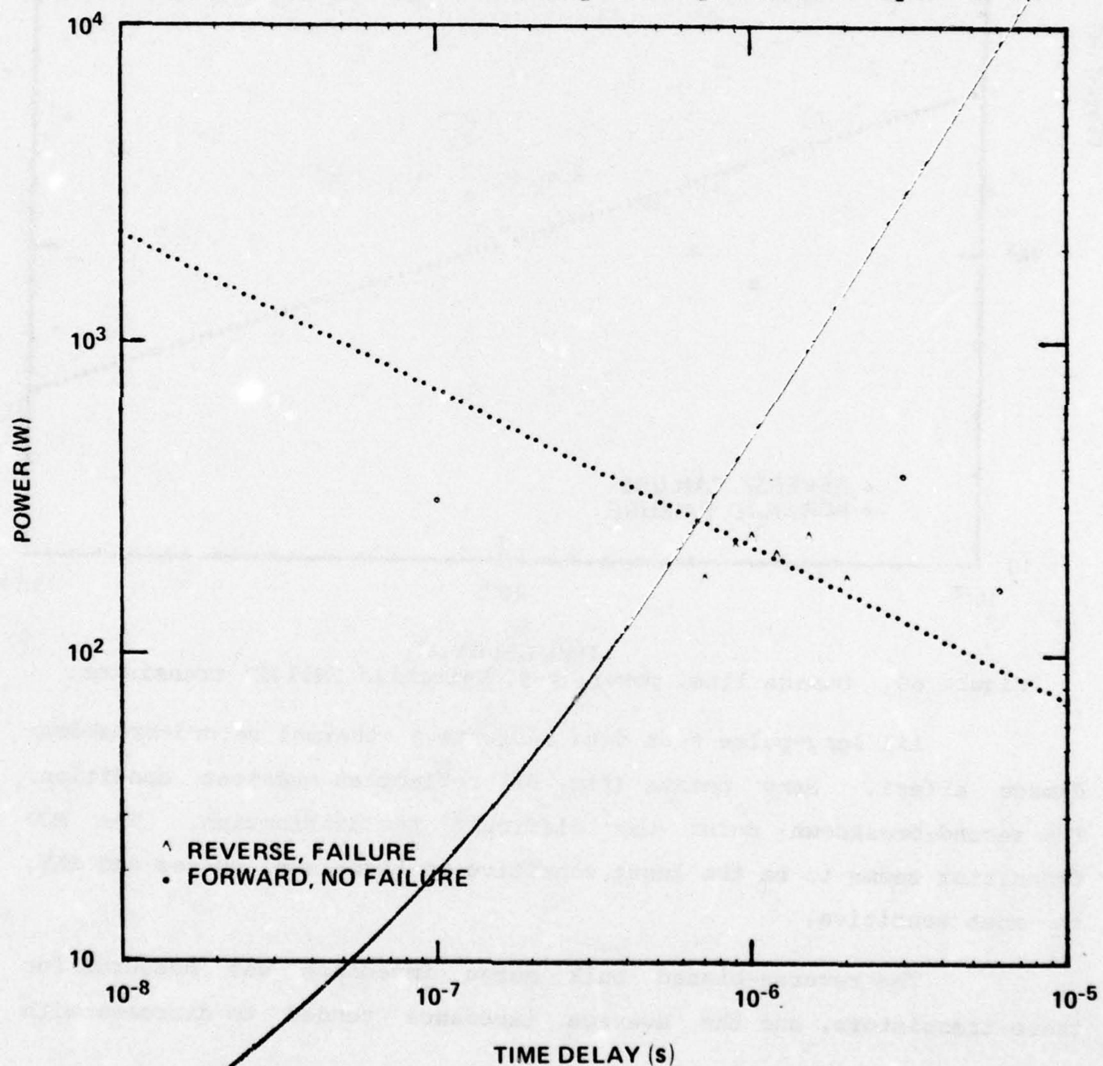

Figure 59. Damage line, power, E-B, Motorola 2N1132A transistor.

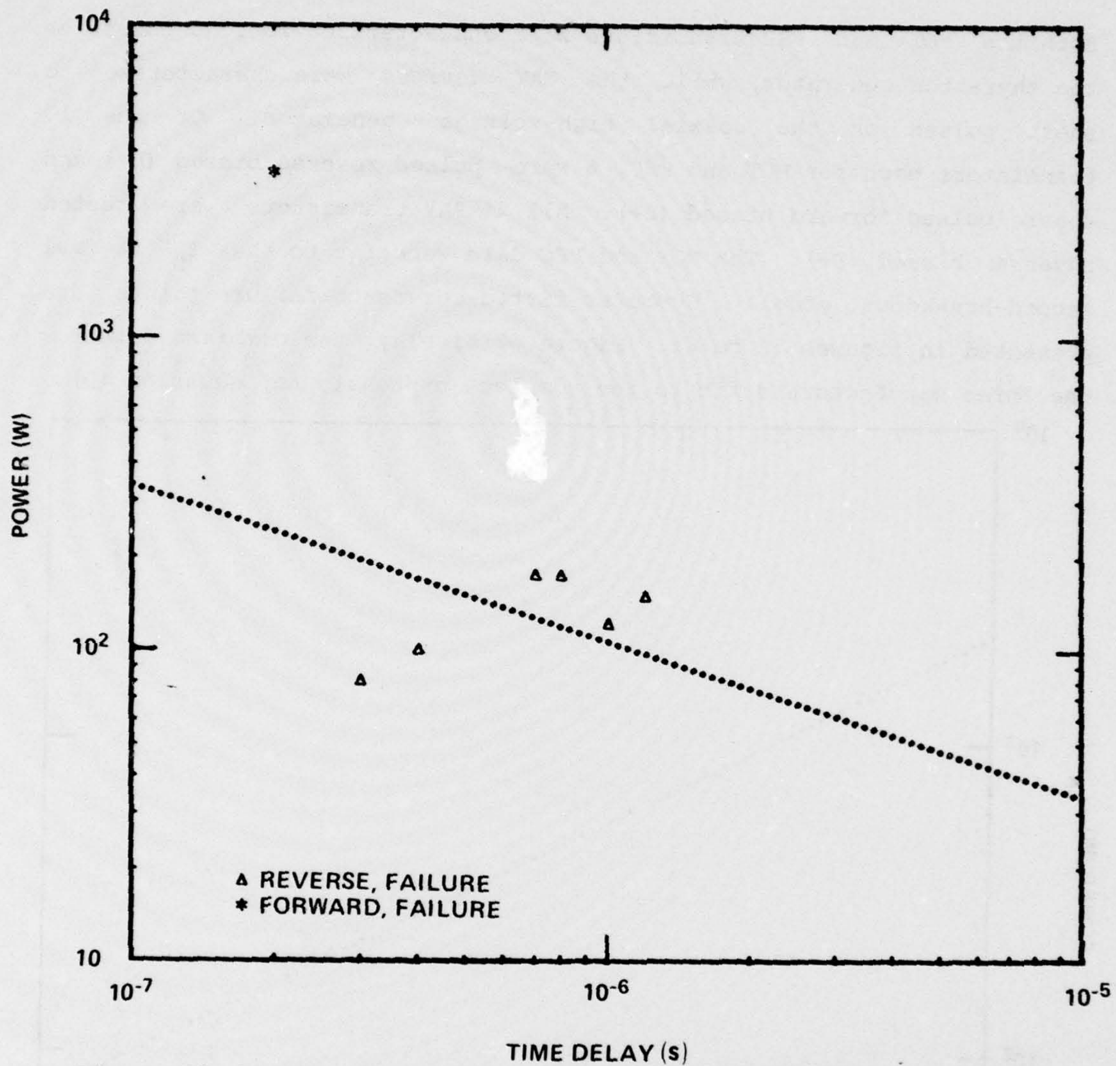

Figure 60. Damage line, power, E-B, Fairchild 2N1132A transistor.

All long-pulse test data indicate a thermal second-breakdown damage effect. Many points (fig. 61) reflect an overtest condition. The second-breakdown point was difficult to distinguish. The MOT transistor seems to be the least sensitive to high-level pulses and RAY, the most sensitive.

The reverse-biased bulk surge impedance was measured for these transistors, and the average impedance tended to decrease with

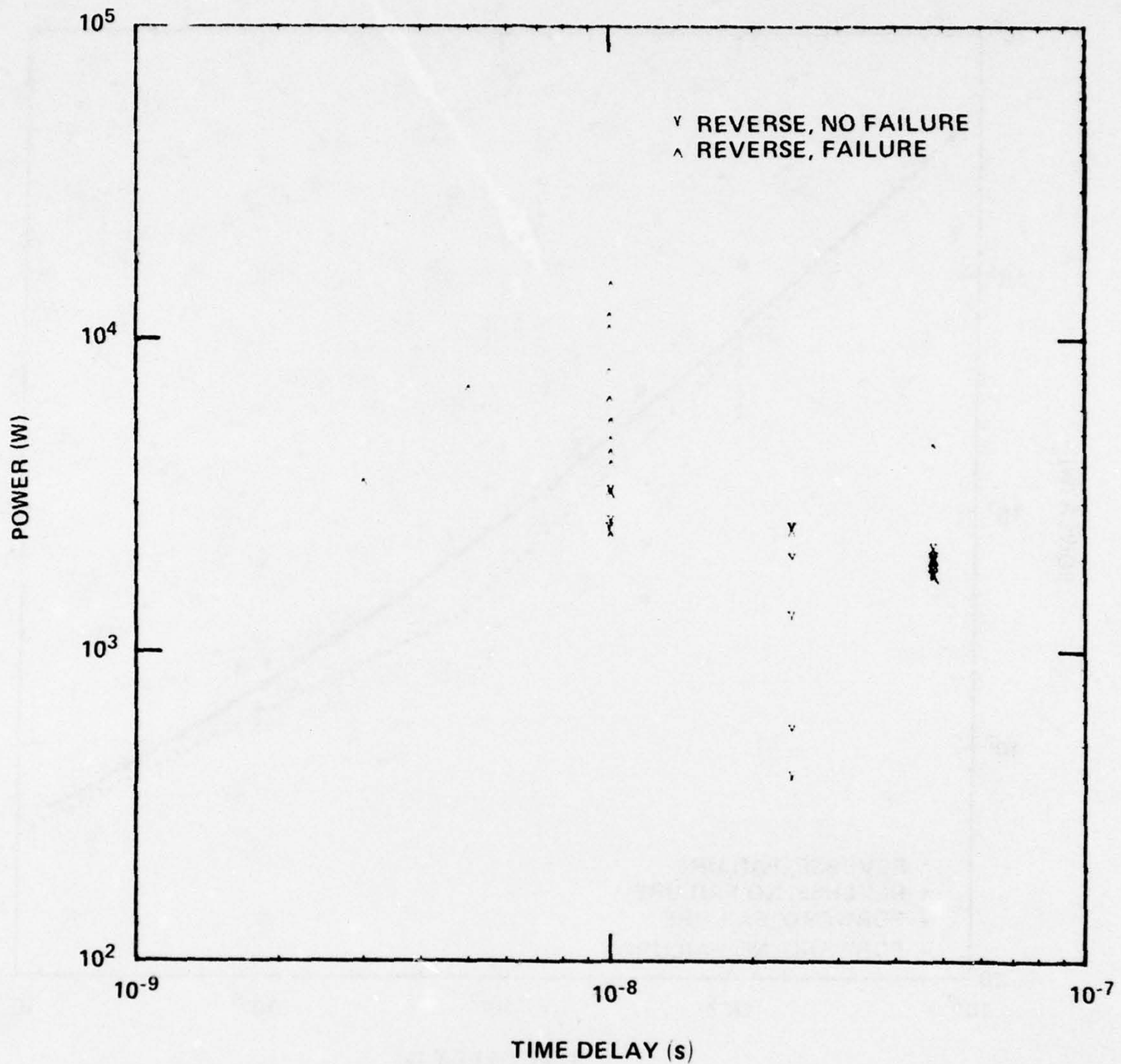

Figure 61. Damage points, power, E-B, Raytheon 2N1132A transistor.

increasing pulse width. This decrease was interesting because impedance has been observed to increase with increasing pulse width near the failure point. The reverse-biased impedance of the combined sample for the various pulse widths was 2.7 ohms for the long pulses, 9.0 ohms for 48 ns, 21 ohms for the 24-ns open-circuit pulses, and 28 ohms for 10 ns. The sample sizes were small, but the spreads were all within a factor of two. The average impedance for the forward-biased transistors for the

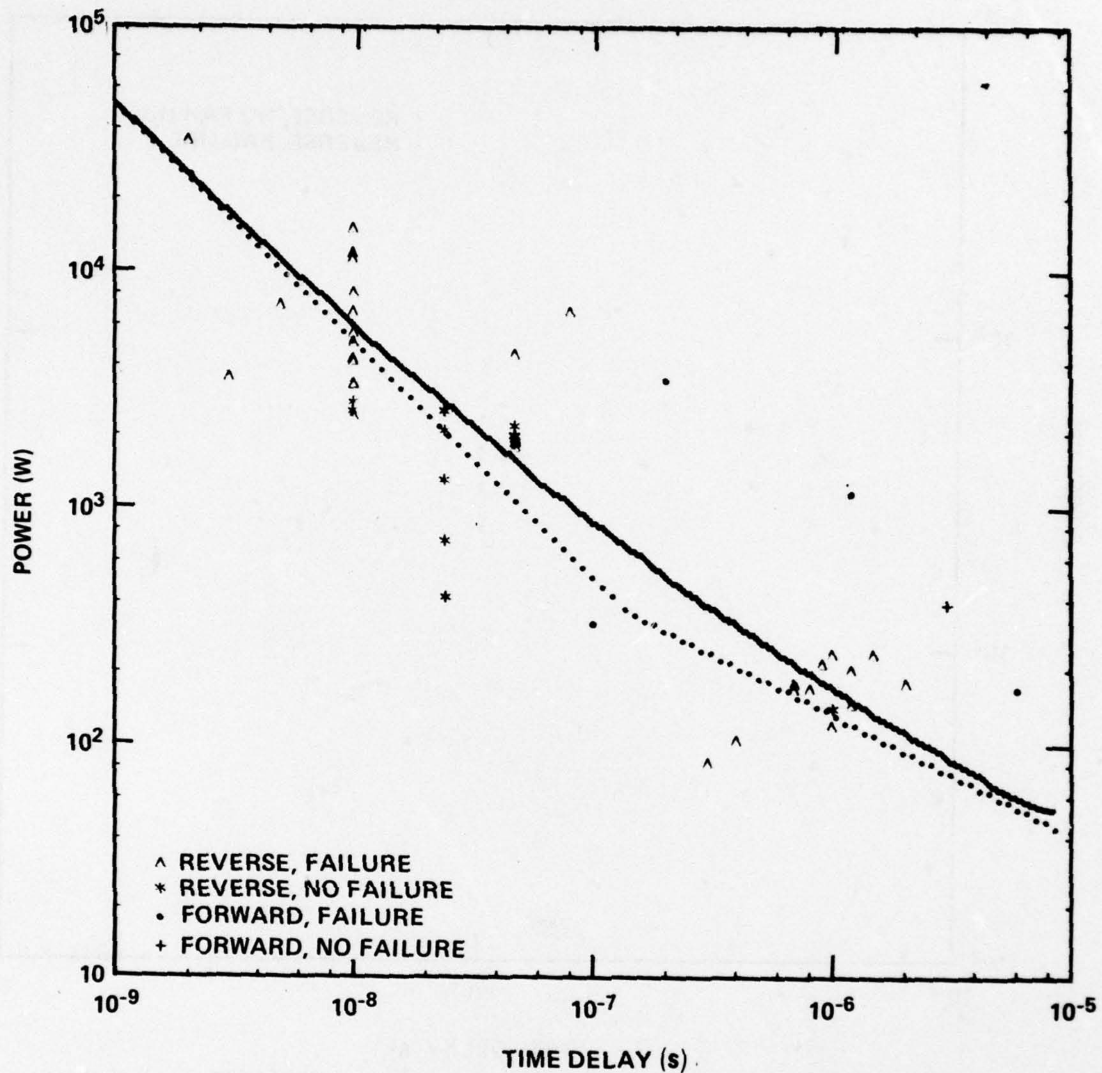

Figure 62. Damage curve, power, E-B, combined data for Motorola, Fairchild, and Raytheon 2N1132A transistors.

long pulses was 1.4 ohms. No transistors were pulsed forward biased for the short pulses.

Five RAY transistors were decanned after failure tests and examined under a microscope. Figures 63 and 64 are typical. Generally, all observed failures indicated a bulk thermal failure mechanism. No appreciable metalization disruption was seen, and no lead failures were

observed. There were no extreme surface irregularities that might have been caused by a surface arc or extreme surface phenomena. In one transistor, it was impossible to identify any apparent failure on the surface, so failure must have occurred deep within the chip, well under the metalization regions. Of particular interest in the RAY sample were the observed geometries (two were discovered) and poor lead contact button placements (as evidenced in fig. 64a, p. 110). With such variations, it is quite easy to see why large spreads can exist about derived damage lines.

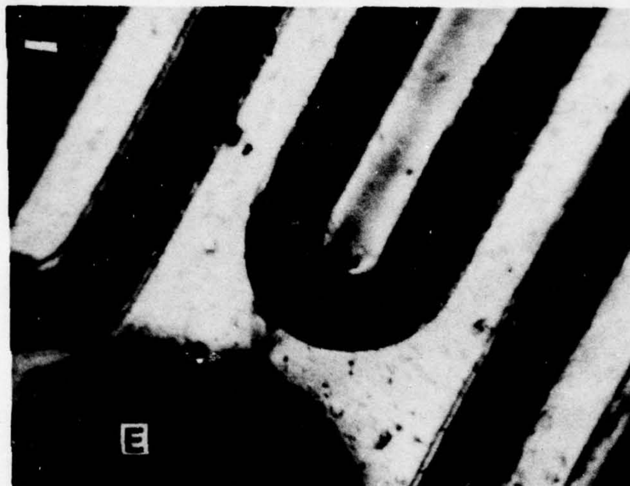

Figure 63. Raytheon 2N1132A transistor (unit 12) (500X) showing failure caused by melt path from base finger, across and under SiO_2 passivation layer, and under emitter metalization to emitter lead.

4.1.27 <u>2N1204 Transistor</u>

The MOT 2N1204 is a low-power germanium pnp, alloy-diffused structure transistor. Sixty were tested E-B, 40 reverse biased (B) and 20 forward biased (E). The transistors were all subjected to long pulses, 1 to 7 μs, and short 75-ns open-circuit pulses by using the thyratron and dielectric-gap generators.

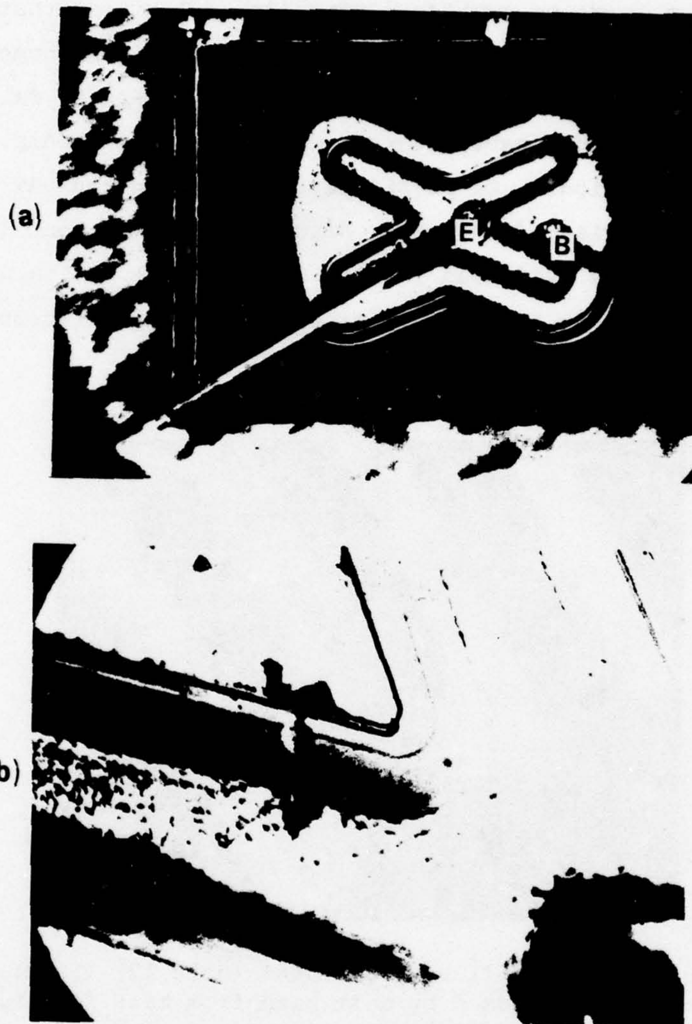

Figure 64. Raytheon 2N1132A transistor (unit 18) showing melt failure: (a) 80X and (b) 500X.

There appears to be a fair correlation between the failure data and the thermal second-breakdown model. A $T_D^{-1/2}$ curve is fitted to the data (fig. 65). No T_D^{-1} dependency is seen for the shorter pulses. The forward failure data appear to follow the reverse-biased failure data, but at a higher (~1 decade) power level.

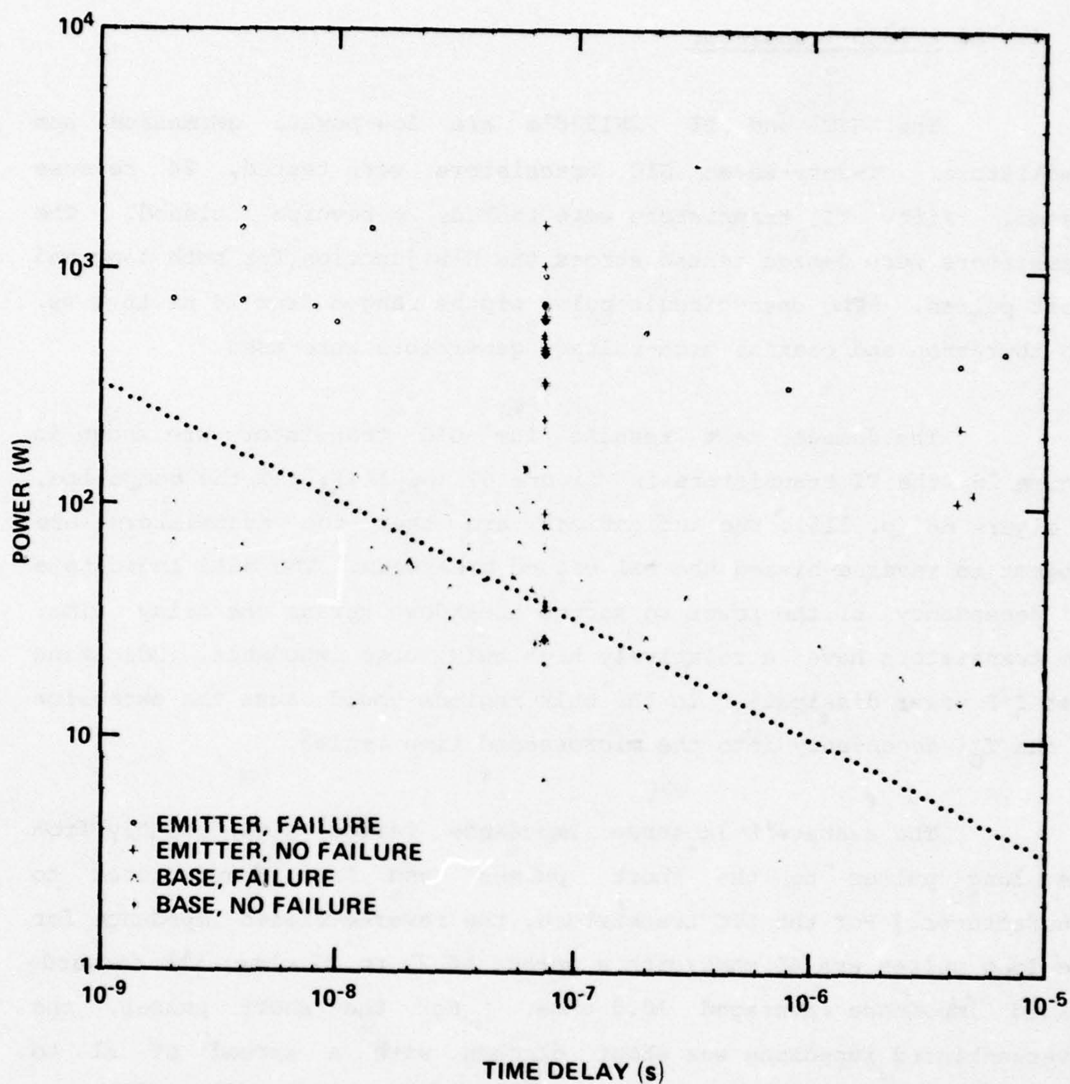

Figure 65. Damage line, power, Motorola 2N1204 transistor.

The average bulk surge impedance for the long pulses equalled ~96 ohms reverse biased and ~0.45 ohms forward biased. The distribution spread from 58 to 190 ohms reverse biased and 9.07 to 1.2 ohms forward biased. For the 75-ns pulse, the corresponding impedances were 50 ohms reverse biased and 3.8 ohms forward biased with a spread of 11 to 182 ohms reverse biased and 1.6 to 7.2 ohms forward biased.

4.1.28 2N1308 Transistor

The GIC and TI 2N1308's are low-power, germanium npn transistors. Twenty-seven GIC transistors were tested, 24 reverse biased. Fifty TI transistors were tested, 26 reverse biased. The transistors were damage tested across the E-B junction for both long and short pulses. The open-circuit pulse widths ranged from 24 ns to 8 μs. The thyratron and coaxial high-voltage generators were used.

The damage test results for GIC transistors are shown in figure 66; the TI transistors in figure 67 (p. 114); and the composite, in figure 68 (p. 115). The indications are that the transistors are subject to reverse-biased thermal second breakdown. The data indicate a T_D^{-1} dependency of the power to second breakdown versus the delay time. The transistors have a relatively high bulk surge impedance, indicating that I^2R power dissipation in the bulk regions could cause the extension of the T_D^{-1} dependency into the microsecond time regime.

The average bulk surge impedance varied significantly from the long pulses to the short pulses and from manufacturer to manufacturer. For the GIC transistors, the reverse-biased impedance for the long pulses was 46 ohms with a spread of 22 to 92 ohms; the forward-biased impedance averaged 10.5 ohms. For the short pulses, the reverse-biased impedance was about 62 ohms with a spread of 31 to 89 ohms. For the TI transistors, the reverse-biased impedance for long pulses was ~551 ohms with a spread of 160 to 1200 ohms. For the short pulses, the reverse-biased impedance was ~68 ohms within a spread of 19 to 145 ohms; and the forward-biased impedance averaged 35 ohms with a spread of 14 to 65 ohms.

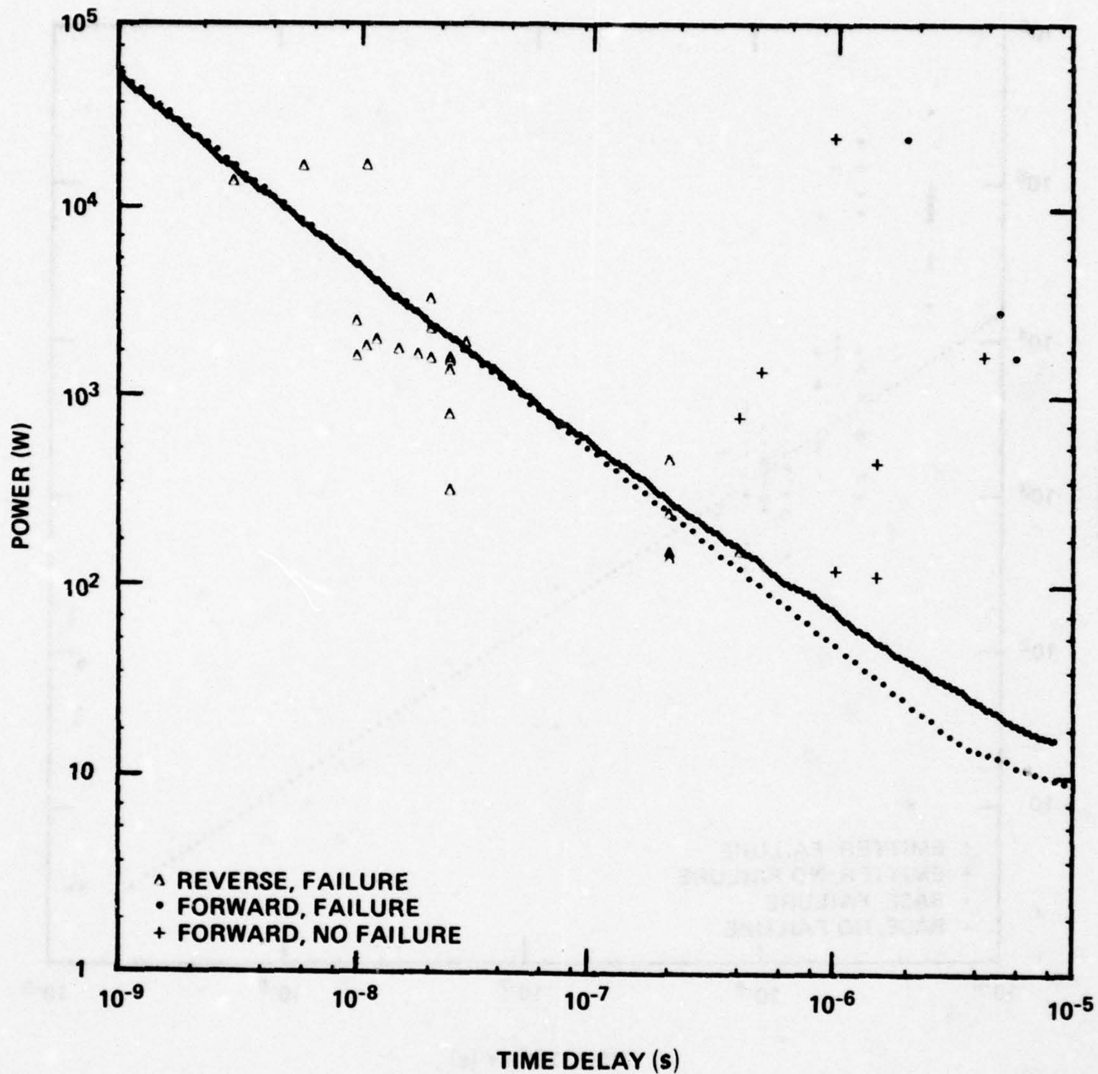

Figure 66. Damage curve, power, E-B, General Instruments 2N1308 transistor.

4.1.29 2N1613 Transistor

The MOT 2N1613 is a low-power, silicon npn, planar structure transistor. Fifty-four MOT transistors were tested E-B, 37 reverse

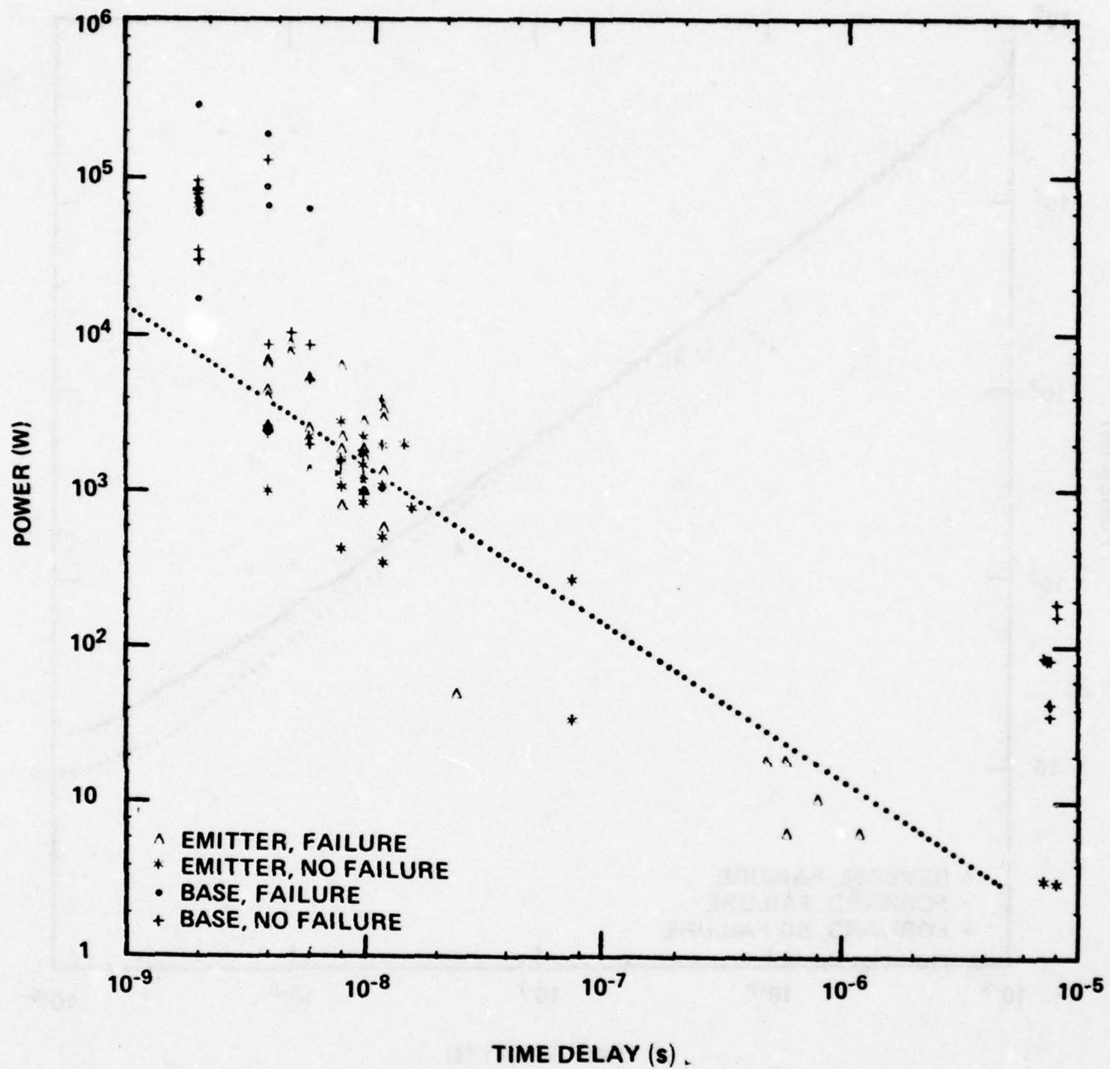

Figure 67. Damage line, power, E-B, Texas Instruments 2N1308 transistor.

biased (E) and 17 forward biased (B). The transistors were subjected to long and short pulses, open-circuit pulse widths from 1.8 to 2.8 μs for the long pulses and 75 ns for the short pulses, by using the thyratron and dielectric-gap generators.

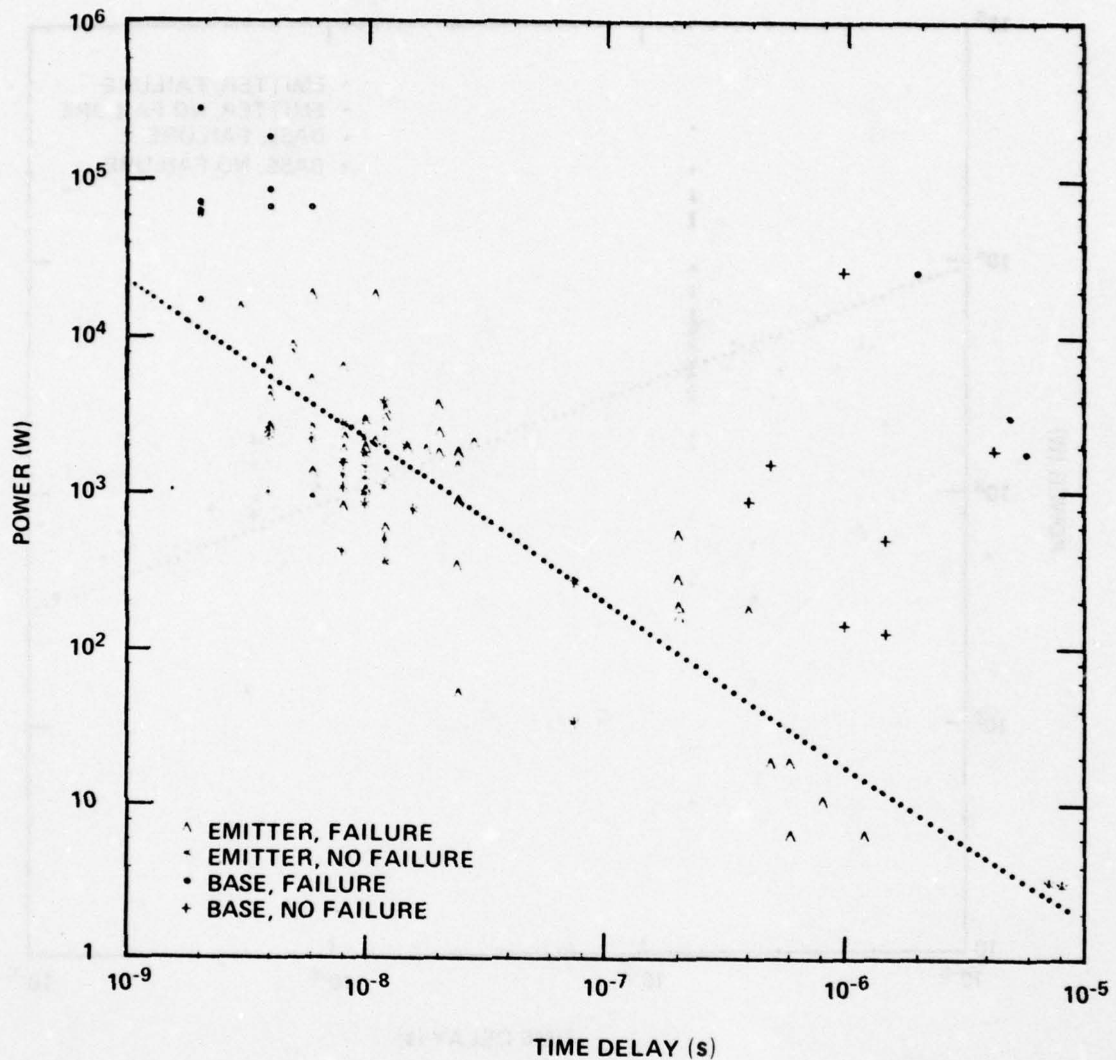

Figure 68. Damage line, power, E-B, combined data for General Instruments and Texas Instruments 2N1308 transistors.

The damage data indicate a reverse thermal second-breakdown failure mechanism. The data points are plotted in figure 69. They are fitted to the $T_D^{-1/2}$ model.

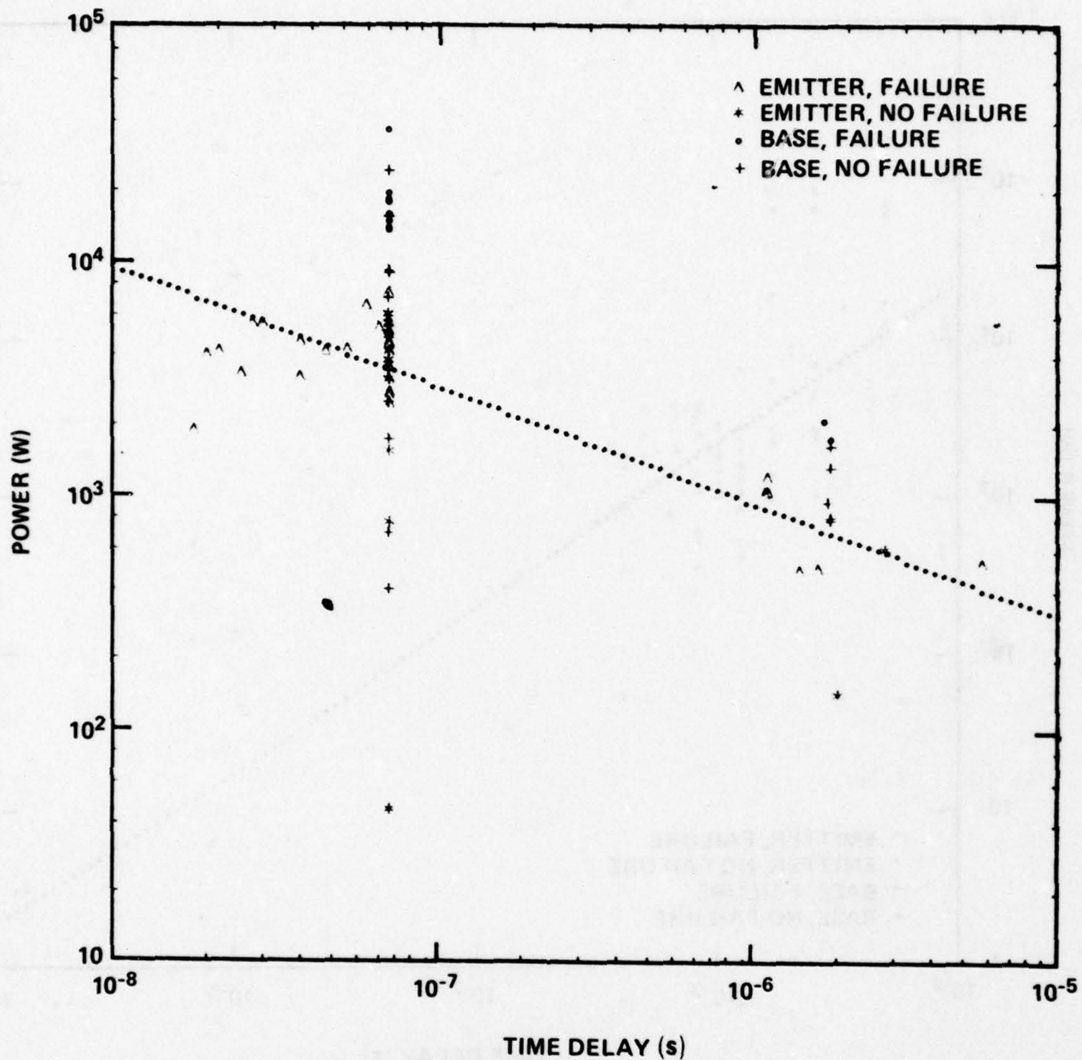

Figure 69. Damage line, power, Motorola 2N1613 transistor.

The average bulk surge impedance for the long pulses equalled ~1.4 ohms reverse biased and ~0.10 ohms forward biased. The distribution spread from 0.5 to 2 ohms reverse biased and 0.04 to 0.17 ohm forward biased. For the short pulses, the corresponding impedances equalled ~3.7 ohms reverse biased and ~3.0 ohms forward biased.

4.1.30 2N1711 Transistor

The FSC and MOT 2N1711's are low-power, silicon npn transistors. Ten transistors from each manufacturer were tested E-B, six reverse biased and four forward biased. The transistors were subjected to 0.6- to 7.8-μs pulses from the thyratron generator. There was no significant difference in the test results from either manufacturer. Transistors from both manufacturers showed second-breakdown failure characteristics. The composite data are presented in figure 70 (p. 118).

The average bulk surge impedance equalled ~4.3 ohms reverse biased and ~1.8 ohms forward biased. The distribution spread from 1.5 to 6.5 ohms reverse biased and 0.50 to 3.1 ohms forward biased.

4.1.31 2N2198 Transistor

The Electronic Transistor Corp. 2N2198 is a low-power, silicon npn transistor. Fifty transistors were tested E-B, 38 reverse biased (E) and 12 forward biased (B). The transistors were subjected to long pulses, 1.7 to 8.8 μs open circuit, and short pulses, 75 ns, from the thyratron and dielectric-gap generators.

The data indicate that reverse-biased failure was due to thermal second breakdown. A $T_D^{-1/2}$ line has been fitted to the reverse-biased failure data (fig. 71, p. 118).

The average bulk surge impedance equalled ~5.0 ohms reverse biased and ~2.9 ohms forward biased. The distribution spread from 1.1 to 45 ohms reverse biased and 1.8 to 4.5 ohms forward biased.

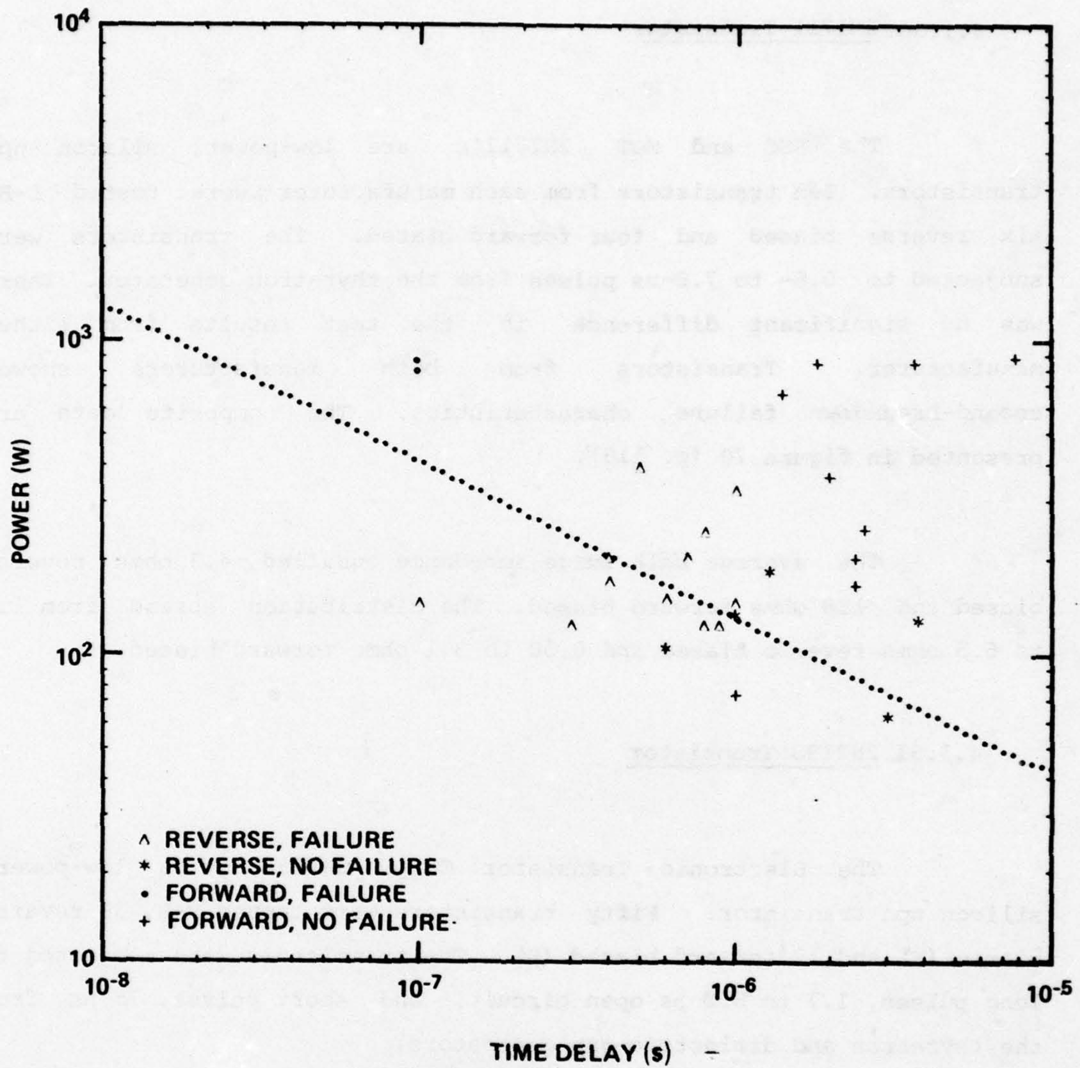

Figure 70. Damage line, power, combined data for Fairchild and Motorola 2N1711 transistors.

4.1.32 2N2297 Transistor

The RAY and FSC 2N2297's are npn planar epitaxial transistors designed for high-efficiency amplifier, logic, and oscillator applications. The transistor has a low saturation resistance, a

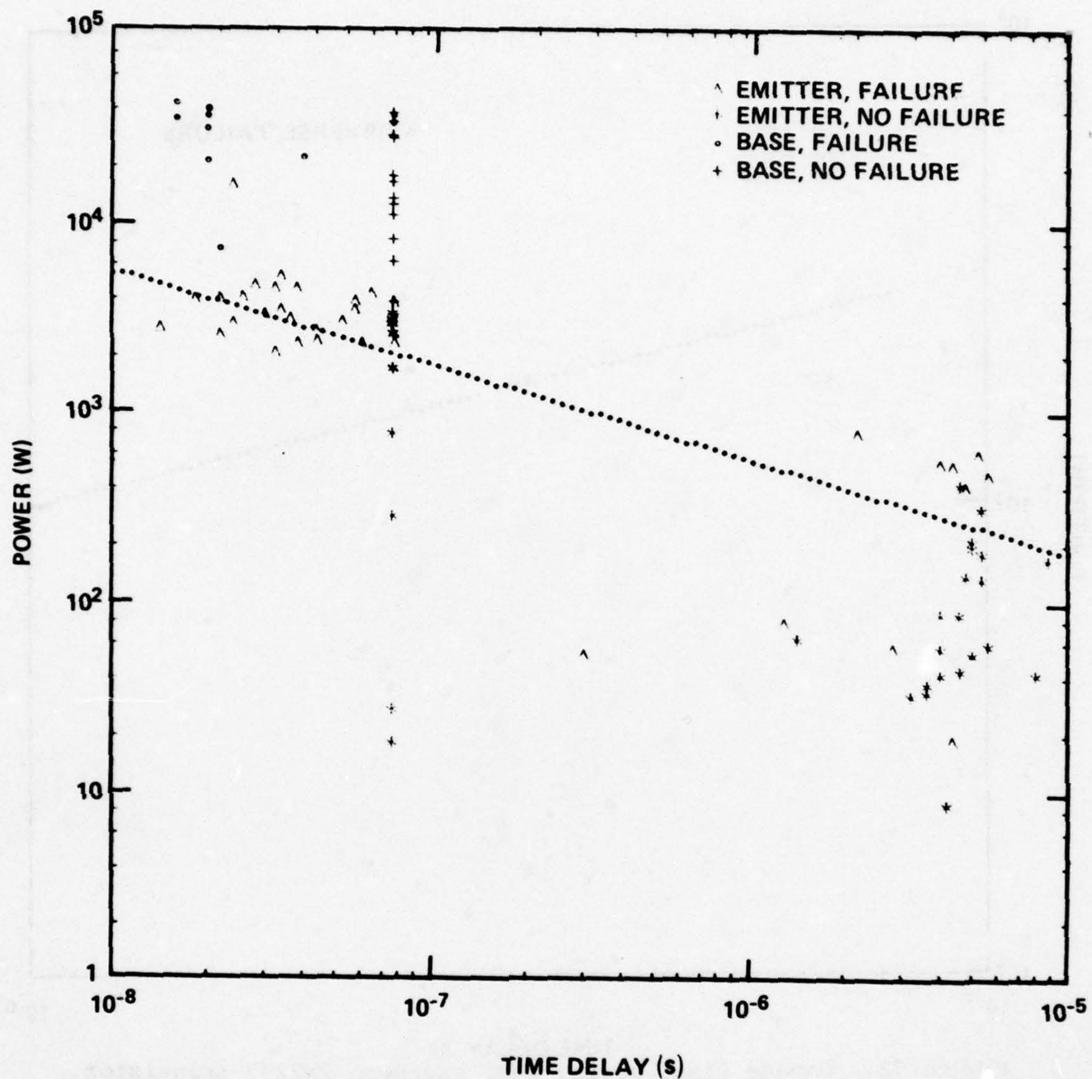

Figure 71. Damage line, power, Electronic Transistors 2N2198 transistor.

relatively high bandwidth, and high current capabilities. Eight RAY and eight FSC transistors were tested E-B. All were subjected to long pulses, 1- to 6-μs open-circuit widths, on the thyratron generator. All were pulsed reverse biased.

The test data for the RAY transistor are presented in figure 72; those for the FSC transistor, in figure 73. Both RAY and FSC

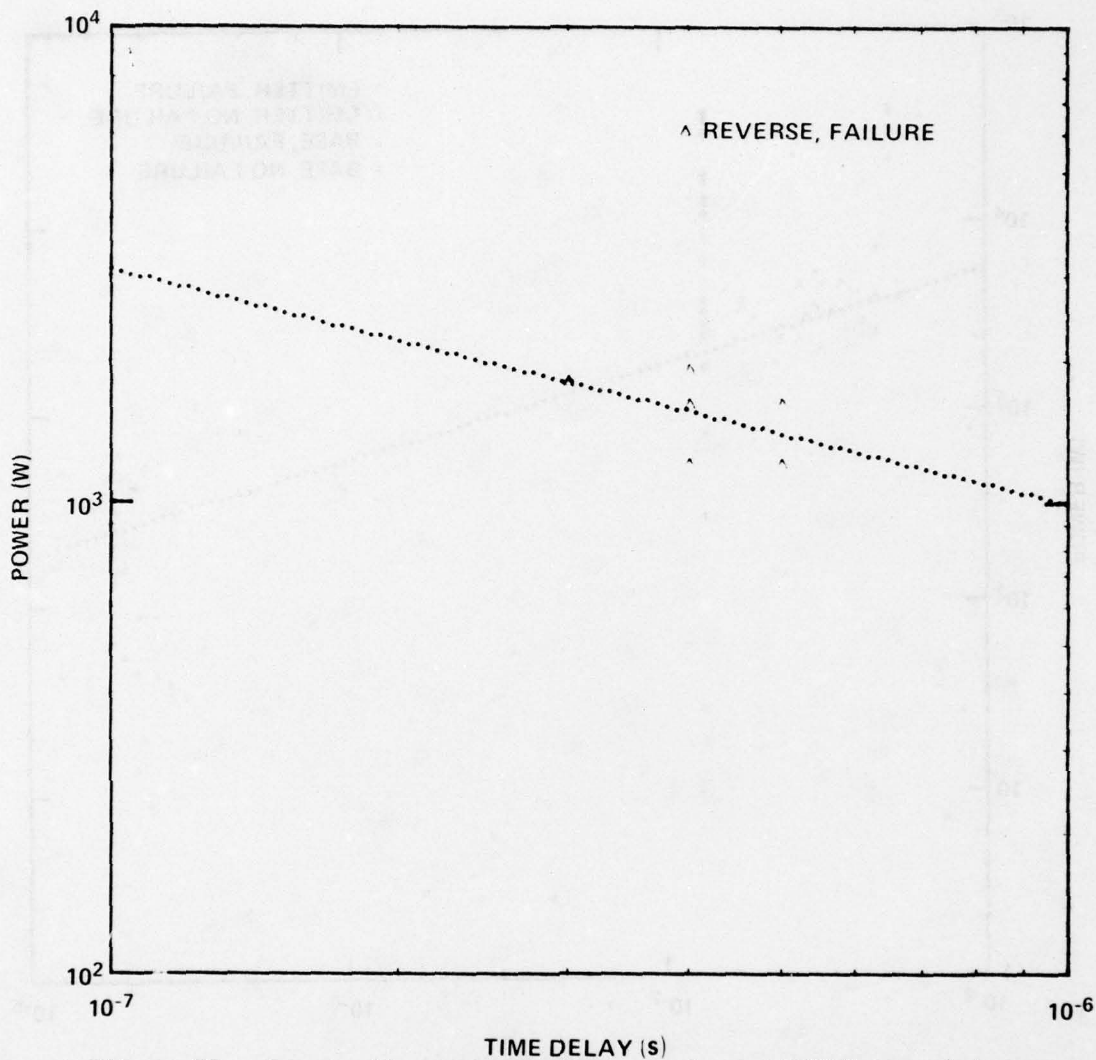

Figure 72. Damage line, power, E-B, Raytheon 2N2297 transistor.

transistors experienced apparent thermal second-breakdown induced failure as ascertained by the voltage and current oscillograms. As the data indicate, there was a considerable spread about the least-squares-fit damage line for the FSC transistor, while the RAY transistor data closely adhered to the model. There is no explanation for the spread on the FSC data. The least-squares-fit damage lines for both RAY and FSC data appear to be about a factor of two different in threshold level, the RAY transistor being the "harder."

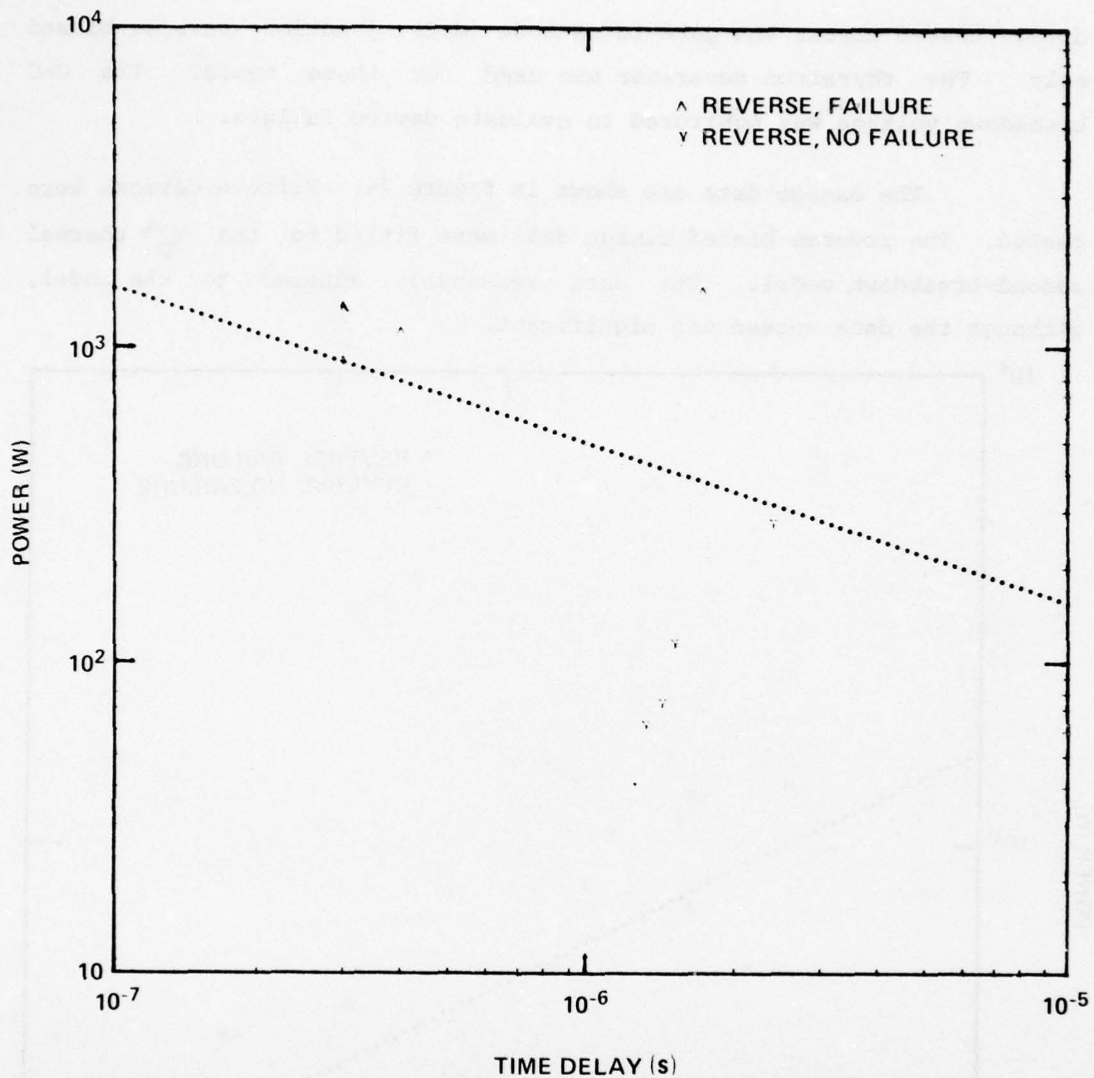

Figure 73. Damage line, power, E-B, Fairchild 2N2297 transistor.

The average bulk surge impedance reverse biased was ~9.2 ohms. The distribution spread from 1.33 to 45 ohms reverse biased.

4.1.33 2N2323 Silicon Controlled Rectifier

The GE 2N2323 is a silicon controlled rectifier, used in low-power switching and control applications. The rectifier was pulse

damage tested across the gate-to-cathode (G-C) junction, reverse biased only. The thyratron generator was used for these tests. The G-C breakdown voltage was monitored to evaluate device failure.

The damage data are shown in figure 74. Fifteen devices were tested. The reverse-biased damage data were fitted to the $T_D^{-\frac{1}{2}}$ thermal second-breakdown model. The data reasonably adhered to the model, although the data spread was significant.

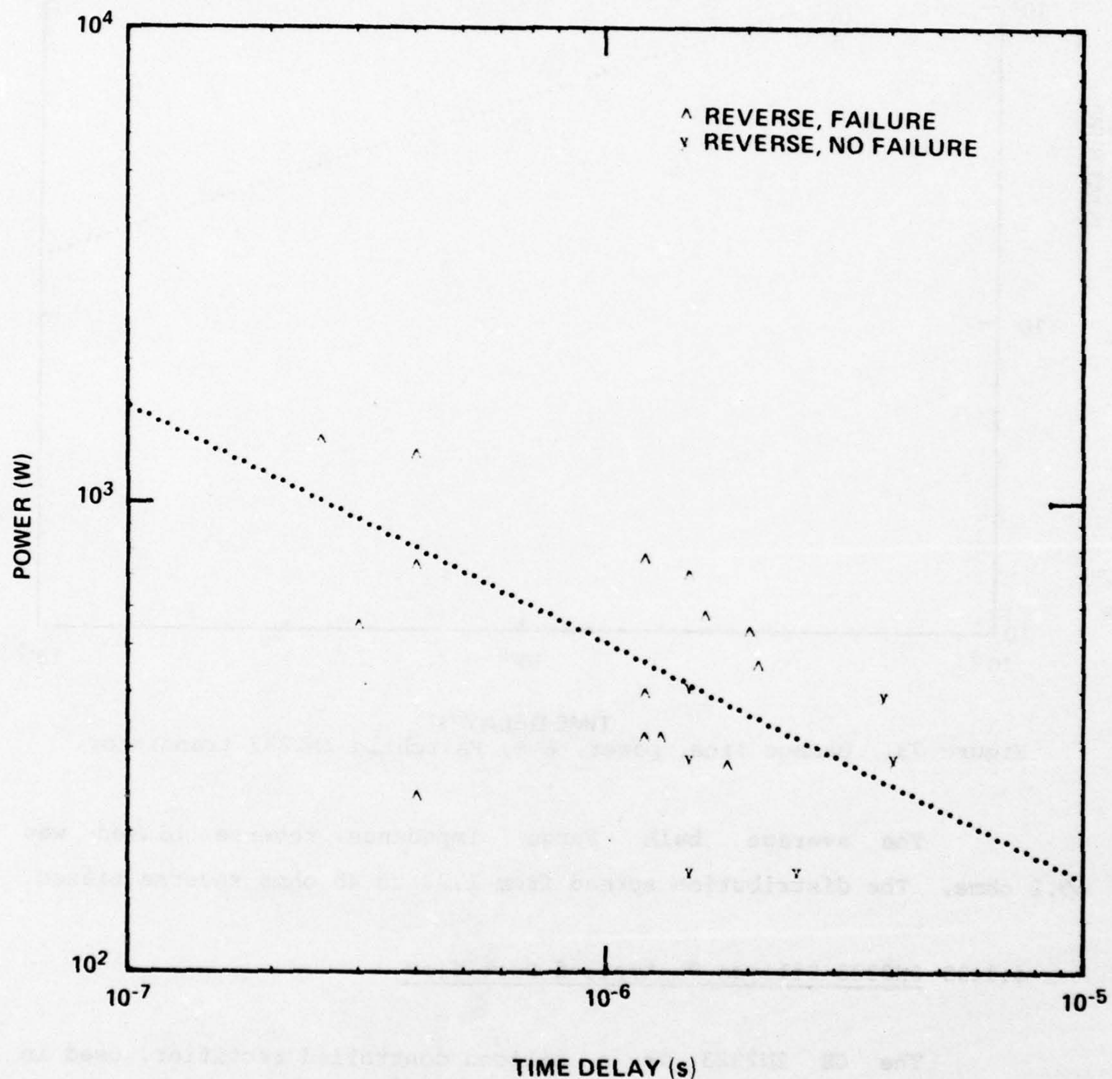

Figure 74. Damage line, power, G-C, General Electric 2N2323 rectifier.

The average bulk surge impedance reverse biased equalled ~3.2 ohms. The distribution spread from 0.21 to 6.8 ohms.

4.1.34 2N2453 Transistor

The MOT and FSC 2N2453's are dual silicon npn transistors designed for differential amplifier applications. Ten MOT and 10 FSC transistors were pulsed across each E-B junction. Thus, there were two data points for each transistor. Eight transistors (16 junctions) of each manufacturer were tested reverse biased E-B. The remainder were tested forward biased. All were subjected to long pulses, 0.8- to 6.3-μs open-circuit widths, by using the thyratron generator.

Since both MOT and FSC dual transistors are the same type and since tests on one transistor do not affect the other in the dual package, both junction damage points were plotted on the same graph (MOT, fig. 75, p. 124; FSC, fig. 76, p. 125). Both MOT and FSC transistors showed thermal second-breakdown failure. The reverse-biased failure points were fit to the $T_D^{-\frac{1}{2}}$ model. The failure levels and bulk surge impedance ranges for both MOT and FSC were essentially the same.

The average bulk surge impedance was ~7.5 ohms reverse biased and 1.05 ohms forward biased. The distribution spread from 3.9 to 11.8 ohms reverse biased and 0.74 to 1.67 ohms forward biased.

4.1.35 2N2727 Transistor

The GE 2N2727 is a high-power, silicon npn transistor. Forty-eight transistors were tested E-B, 34 reverse biased (E). These transistors were subjected to pulse widths of 1.7 to 8.2 μs, 48 ns, and 24 ns in the thyratron and coaxial high-voltage generators.

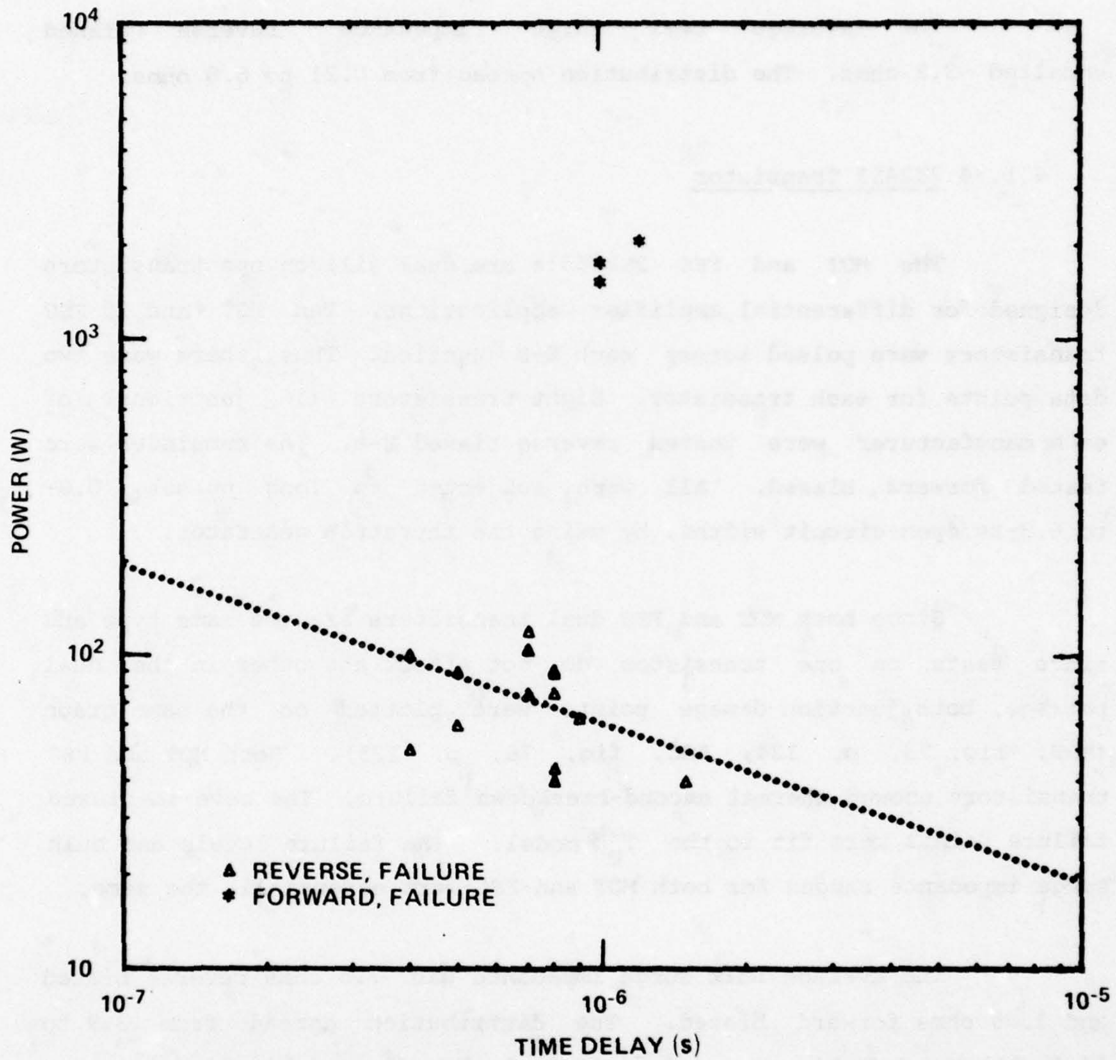

Figure 75. Damage line, power, E-B_1/B_2, Motorola 2N2453 transistor.

The damage data are shown in figure 77. The voltage and current oscillograms indicated a thermal second-breakdown failure for the junction reverse biased. The junction was pulsed forward biased, and the required voltage for failure forward biased was more than twice that reverse biased. The current levels through the transistor forward biased exceeded 100 A. At these current levels, the available current probes saturated, so it was useless to carry some of the tests to the damage point.

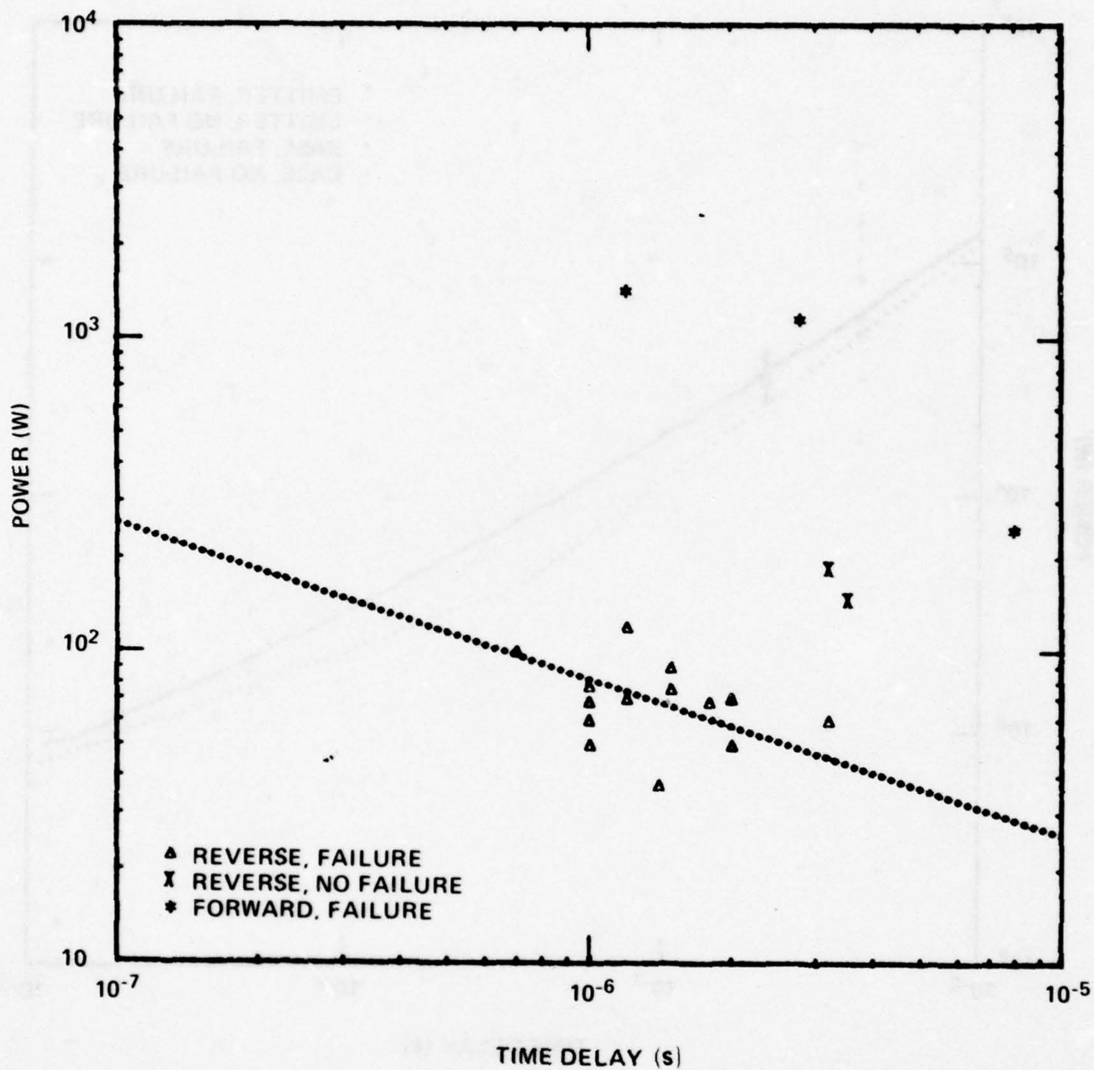

Figure 76. Damage line, power, E-B_1/B_2, Fairchild 2N2453 transistor.

The average bulk surge impedance equalled ~1.2 ohms reverse biased and ~1.0 ohm forward biased. The distribution spread from 0.8 to 1.8 ohms reverse biased and 0.3 to 2.4 ohms forward biased. For the 24-ns pulse, the reverse-biased bulk surge impedance was 4.2 ohms with an associated spread of 2.3 to 6.1 ohms. The sample size was 19.

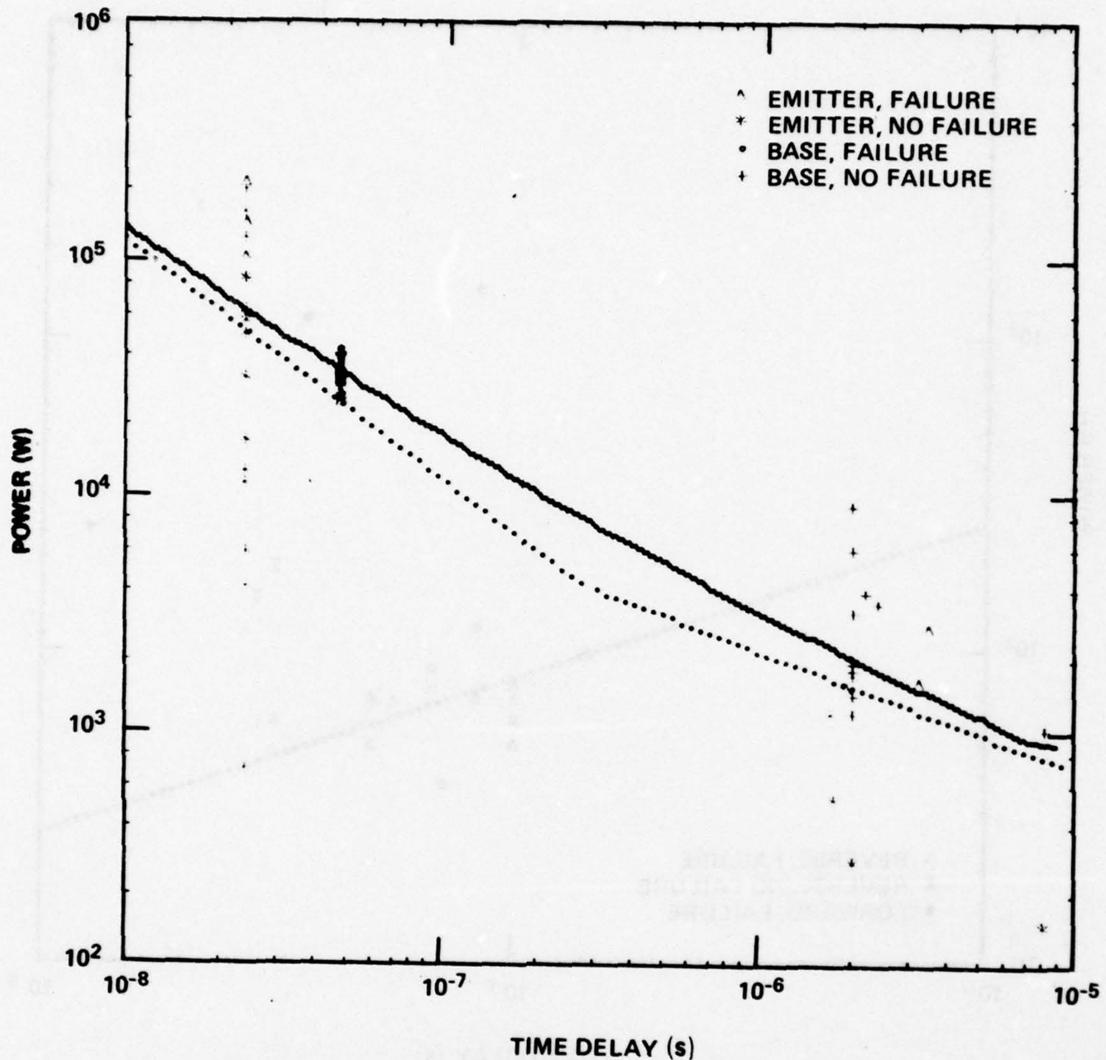

Figure 77. Damage curve, power, General Electric 2N2727 transistor.

4.1.36 2N2801 Transistor

The FSC and MOT 2N2801's are pnp switching transistors. Twenty devices were tested, 10 FSC and 10 MOT. They were subjected to long open-circuit pulses from 0.7 to 8 μs, by using the thyratron generator. Only the E-B junction was damage tested on this transistor. The FSC data are plotted in figure 78; the MOT data, in figure 79.

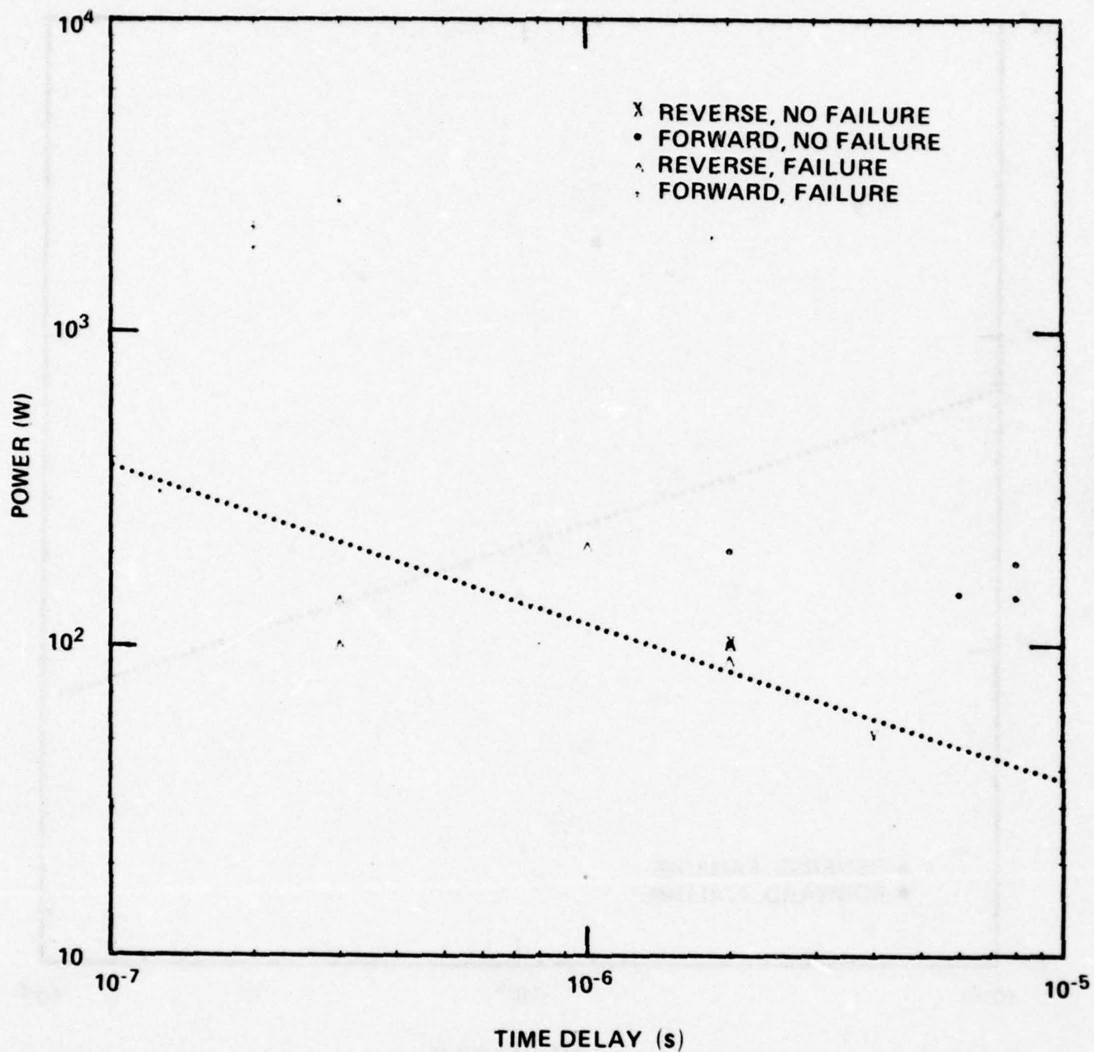

Figure 78. Damage line, power, E-B, Fairchild 2N2801 transistor.

The transistor shows a thermal second-breakdown failure mechanism in the voltage and current oscillograms. The data of both FSC and MOT transistors show fair correlation to the $T_D^{-\frac{1}{2}}$ thermal model. The least-squares-fit damage lines are within a factor of two of each other. The MOT transistor appears slightly "harder." However, the sample sizes are too small and the data are spread too much for a conclusion.

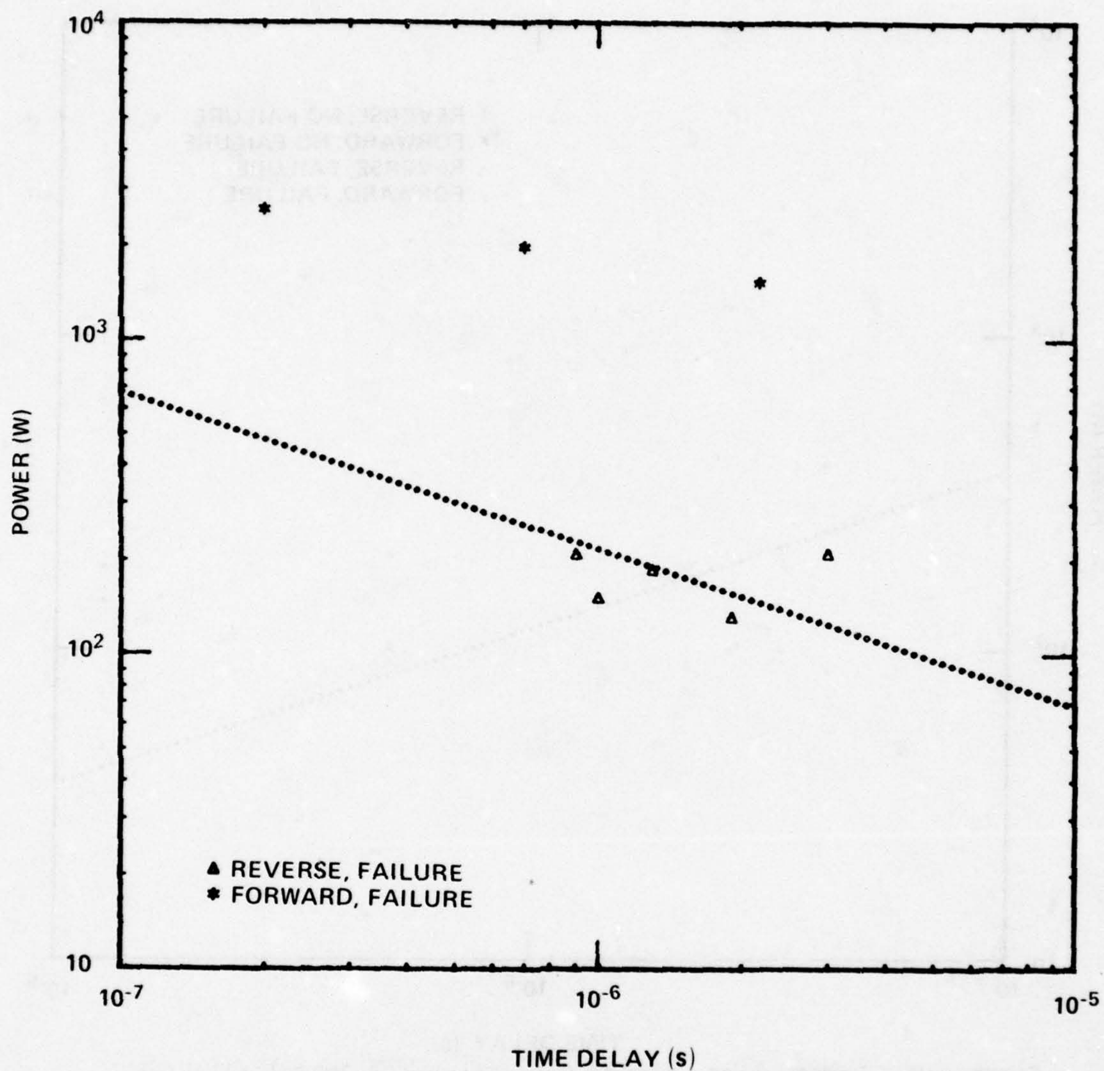

Figure 79. Damage line, power, E-B, Motorola 2N2801 transistor.

The average bulk surge impedance equalled ~2.9 ohms reverse biased and ~1.5 ohms forward biased. The distribution spread from 1.7 to 3.4 ohms reverse biased and from 1.0 to 2.8 ohms forward biased.

4.1.37 2N3069 Junction Field Effect Transistor

The Solitron Devices 2N3069 is a silicon, n-channel junction FET. It was damage tested across the gate to drain (G-D) junction.

Both the G-D breakdown voltage and the transconductance were measured before and after testing to determine failure or degradation. Eight transistors were tested in long pulses, 0.6 to 8 μs, by using the thyratron generator.

Postdamage electrical tests indicated lead or metalization failure resulting in apparent junction open circuits. The measurements did not indicate a thermal second-breakdown response. Two transistors were pulsed forward biased; one degraded as a short circuit and the other failed open. Figure 80 presents the power dissipation for

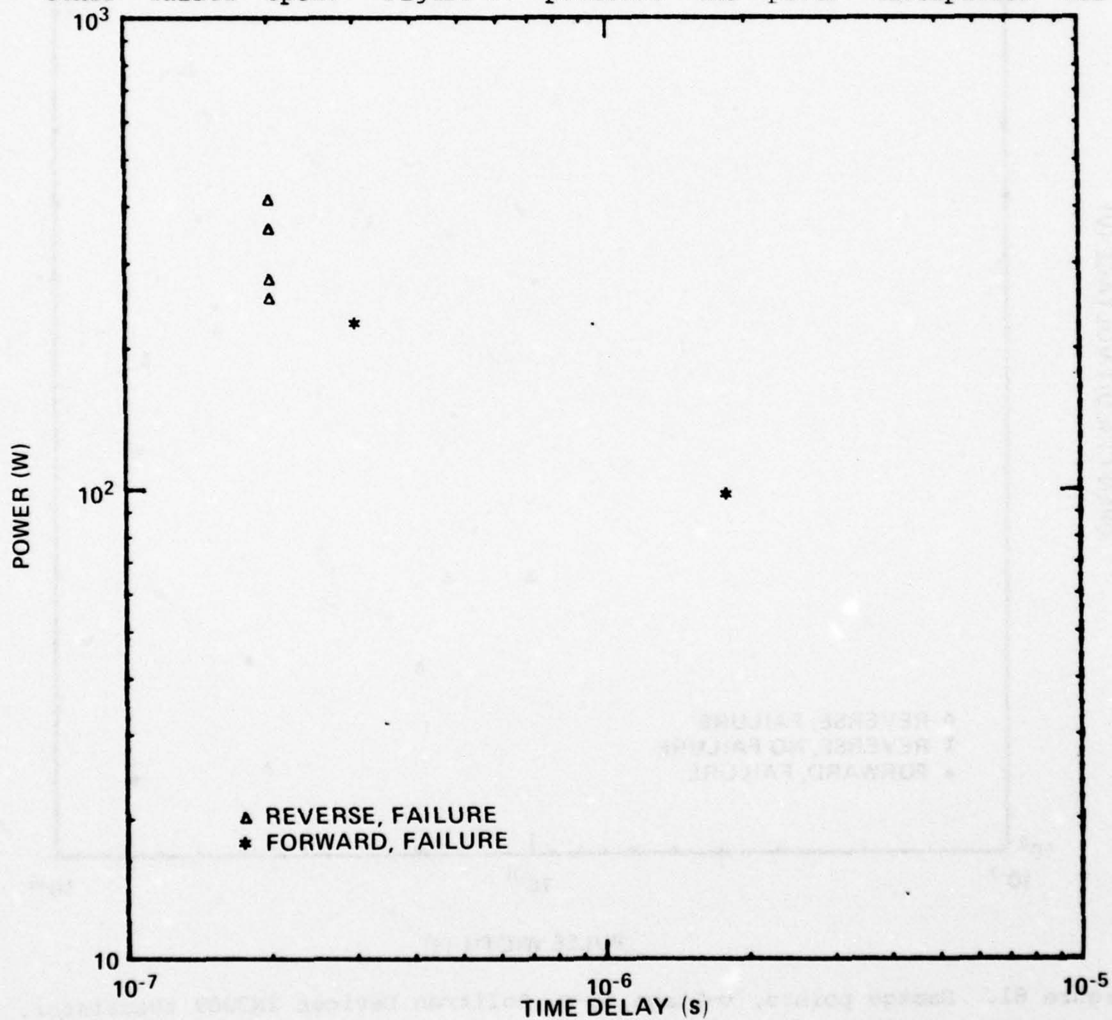

Figure 80. Damage points, power, G-D, Solitron Devices 2N3069 transistor.

failure. The data have not been fitted to the thermal models. The results of figure 81 indicate that a voltage threshold of ~100 V might be a better criterion for failure. The bulk surge impedance was impossible to calculate, the values being extremely high.

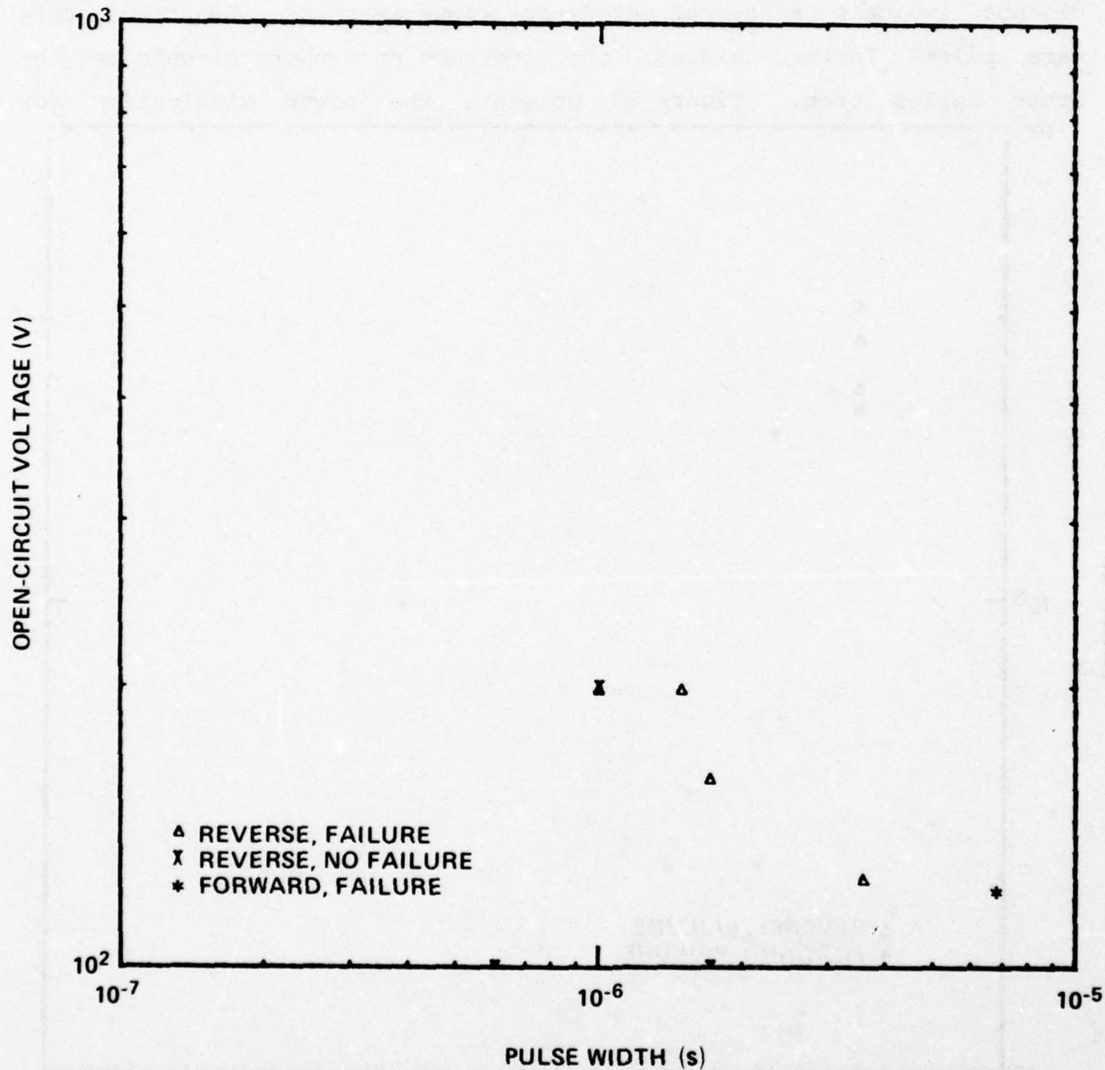

Figure 81. Damage points, voltage, G-D, Solitron Devices 2N3069 transistor.

4.1.38 2N3440 Transistor

The RCA 2N3440 is a high-power, 1-W, silicon npn transistor. Eleven transistors were tested E-B with a 50-ns pulse, 39 reverse biased (E) and 10 forward biased. The data appear in figure 82. The second-breakdown transition could not be distinguished on the traces. The data show that the fail and no-fail levels are intermeshed and

Figure 82. Damage points, power, RCA 2N3440 transistor.

that the average failure level lies somewhere in the data spread.

The average bulk surge impedance equalled ~1.7 ohms reverse biased and ~1.3 ohms forward biased. The distribution spread from 1.1 to 3.6 ohms reverse biased and 0.9 to 1.8 ohms forward biased.

4.1.39 2N3636 Transistor

The MOT 2N3636 is a high-power, silicon pnp transistor rated at 1 W. Ten transistors were stressed E-B by using the thyratron generator to apply pulses ranging from 2.3 to 9.2 μs. Nine transistors were reverse biased (B+); one was forward biased. Failures appear to have been caused by thermal second breakdown. A $T_D^{-\frac{1}{2}}$ line has been fitted to the failure points in figure 83(p. 133).

The mean bulk surge impedance (from 18 data points) was calculated to be 1.055 ohms ranging from 0.535 to 1.657 ohms. The forward-biased bulk surge impedance was 0.667 ohm.

4.1.40 SM692-1 (2N3801) Transistor

The MOT SM692-1 (2N3801) is a low-power, silicon pnp transistor. Sixty transistors were tested at long pulses, 1.2 to 7.3 μs, and short pulses, 75 ns open circuit. The thyratron and dielectric-gap generators were used.

The damage data indicate reverse-biased failure to have been due to thermal second breakdown. A $T_D^{-\frac{1}{2}}$ curve has been fitted to the data in figure 84.

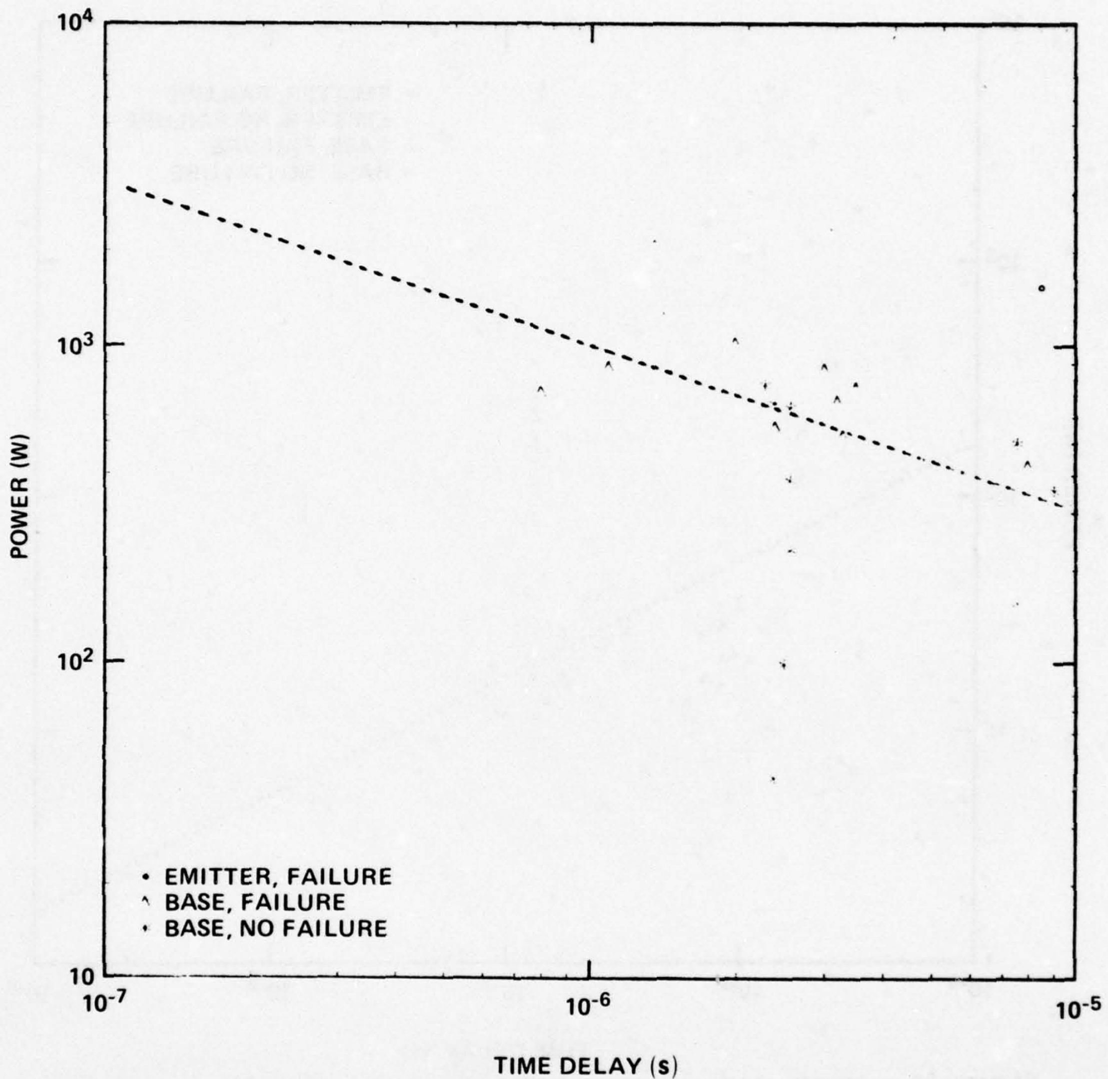

Figure 83. Damage line, power, Motorola 2N3636 transistor.

The average bulk surge impedance for the long pulse widths equalled ~450 ohms reverse biased and ~2.5 ohms forward biased. The distribution spread from 110 to 1200 ohms reverse biased and 1.2 to 4 ohms forward biased. For the 75-ns pulses, the bulk surge impedance was 72 ohms reverse biased and 3.2 ohms forward biased. For the 48-ns pulses, the sample size was only three and the average impedance was

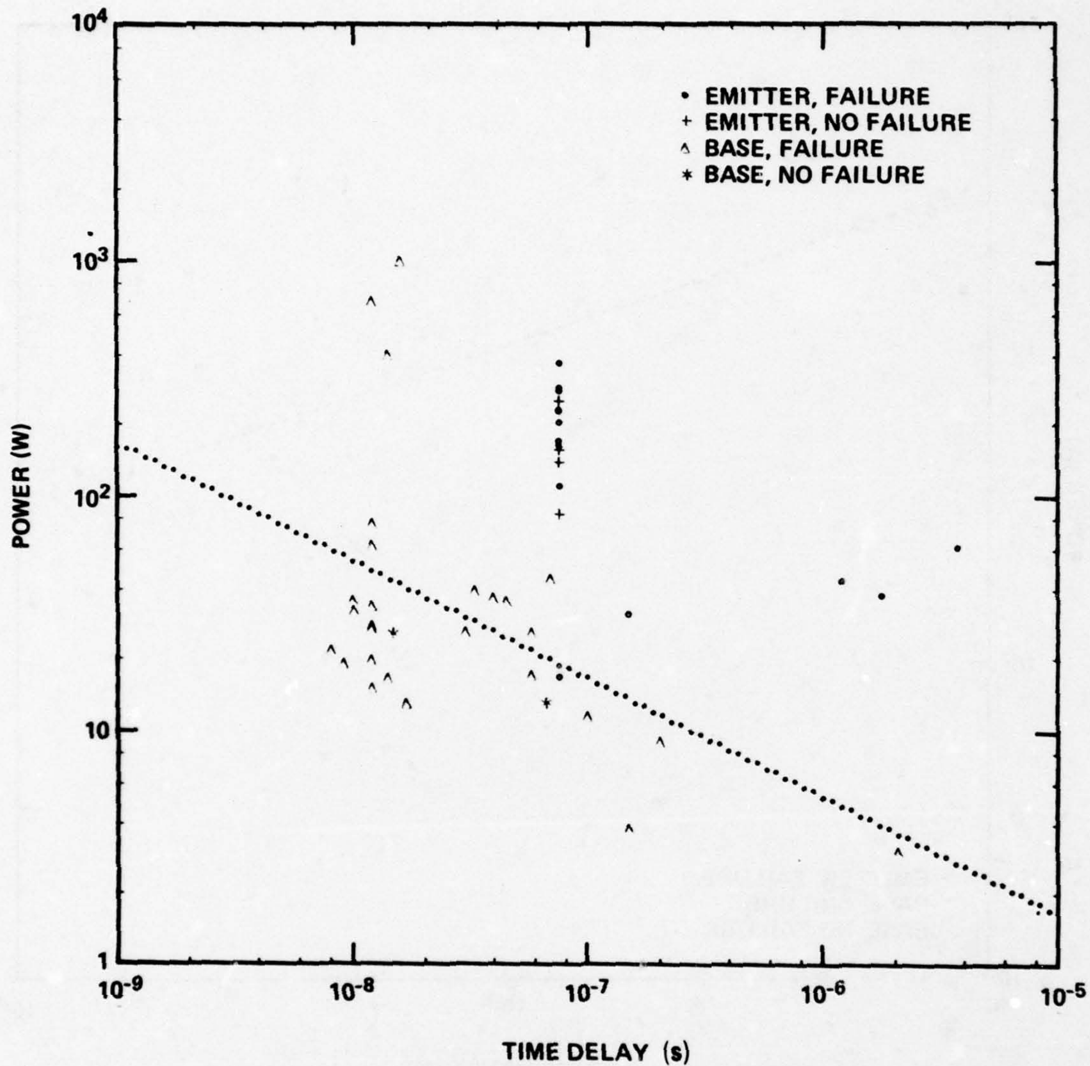

Figure 84. Damage line, power, Motorola SM692-1 (2N3801) transistor.

7.4 ohms reverse biased. None of the devices were pulsed forward biased with the 48-ns open-circuit pulses.

4.1.41 μA709 Operational Amplifier

The FSC μA709 (U5B770931) is a high-gain op amp. It is constructed on a single silicon chip by the FSC planar epitaxial

process. Ten op amps were first tested across the inverting and noninverting input leads, pins 2(B) and 3(C). The op amps were then damaged tested across the output and (V-) pins, 6(F) and 4(D), after no damage was detected from the previous pulse tests to the input pins on the same device. (The U.S. Army Missile Command Guidance and Control Directorate in support of the Lance Test Program has conducted damage tests on this op amp to characterize the damage threshold levels from pin 3(C) to pin 4(D).)

The object of testing across pins 2(B) and 3(C) was to isolate and test the smallest area E-B junction and thus to establish the minimum damage level for the op amp. The test circuit shown in figure 85 was breadboarded and used to measure the gain of the op amp before and after pulsing.

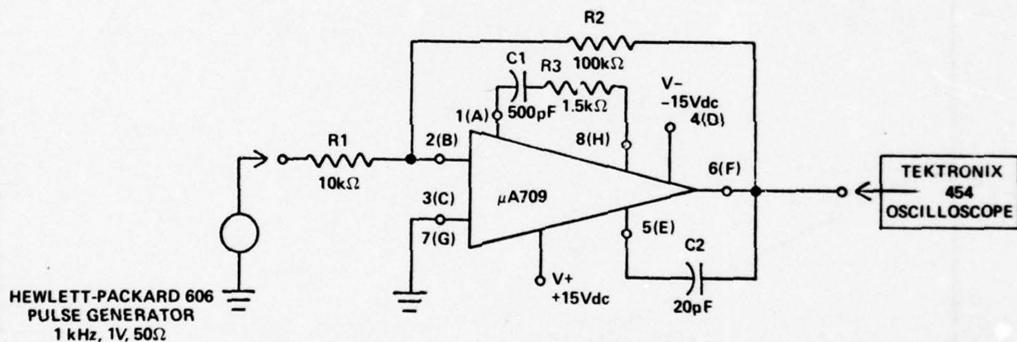

Figure 85. Test circuit for Fairchild μA709 operational amplifier.

The results of the tests are presented in figures 86 to 88. All reverse-biased data are fitted to the $T_D^{-1/2}$ damage model. The device has an electrically and topologically symmetrical input circuit which permitted the plotting of both the pin 2(B) positive and pin 3(C) positive polarities on the same curve as the reverse-biased data (fig. 86). Figures 87 and 88 document the results of the output tests. There was no bipolar symmetry on the output circuitry; consequently, two damage curves are shown.

The tests on input pins 2(B) and 3(C) indicated a thermal second-breakdown failure. All op amps failed at the open-circuit voltage of 100 V or less. The output tests between pins 4(D) and 6(F) also indicate some thermal second-breakdown failure. Due to the complexity of the electrical circuit between these pins (not even considering the possible physical complexity), there were numerous steps in the voltage and current response. The data were characterized to

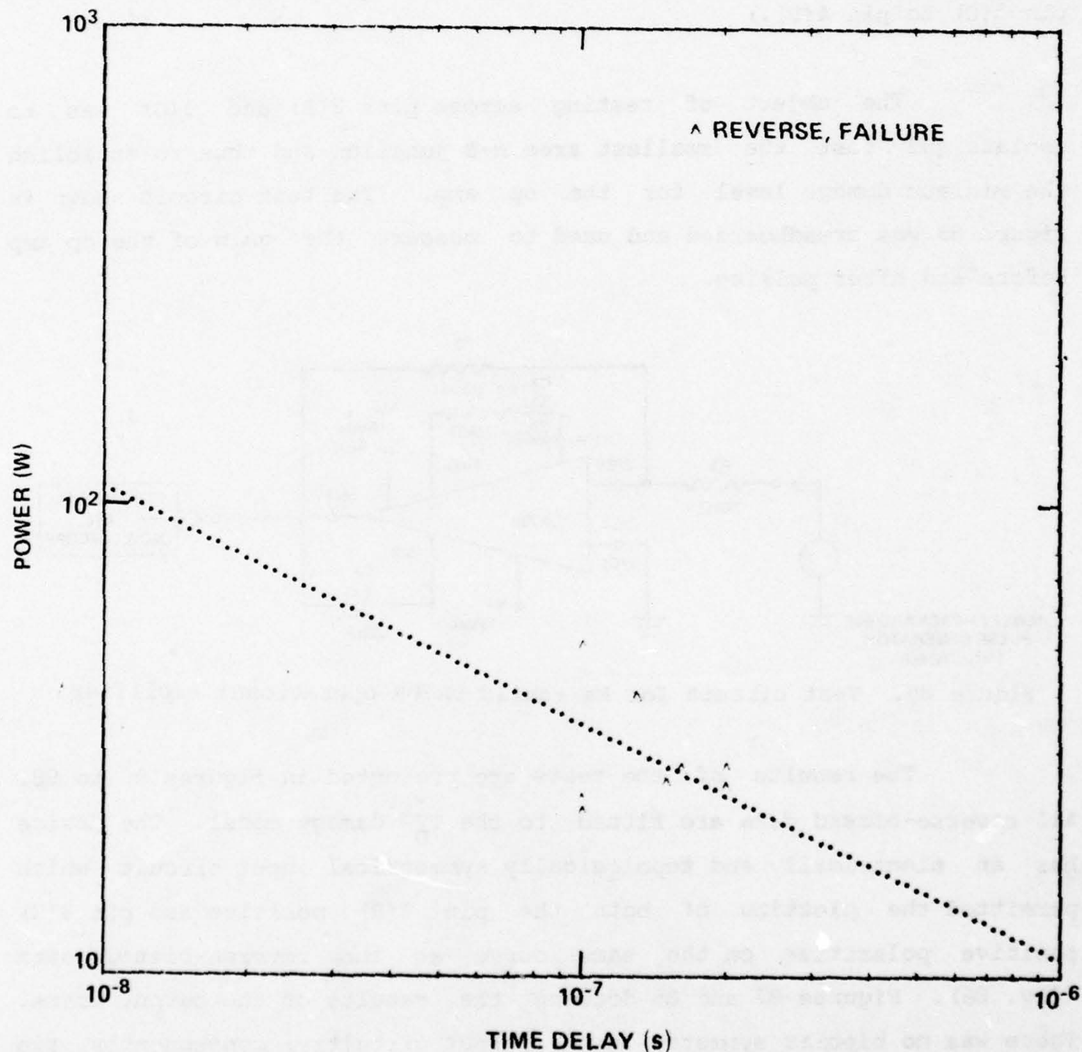

Figure 86. Damage line, power, Fairchild μA709 operational amplifier input pins 2(B) and 3(C).

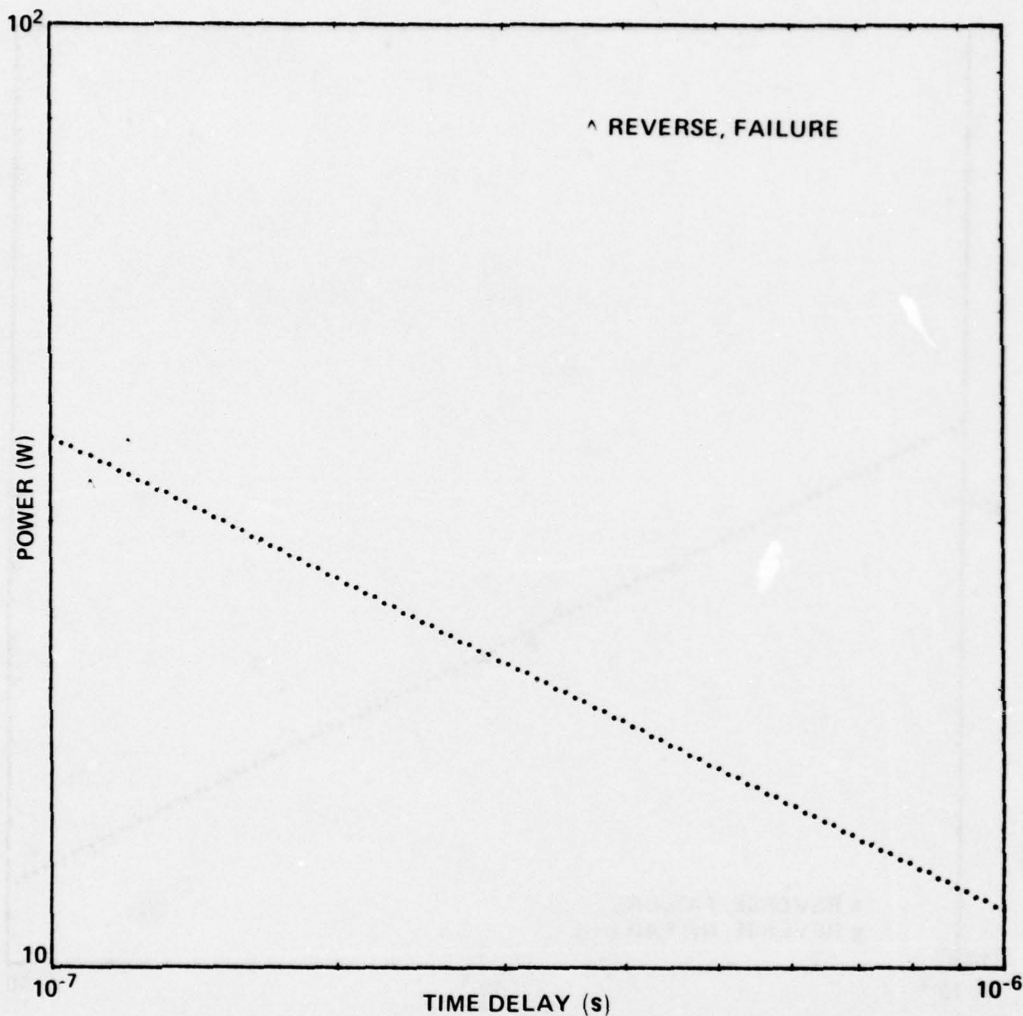

Figure 87. Damage line, power, Fairchild μA709 operational amplifier output pin 4(D).

their first appreciable step. All devices failed at levels at or under 100 V.

The bulk surge impedance was calculated from the test data for each pin pair examined. The average impedance calculated for pins 2(B) to 3(C) was 35 ohms with a spread from 20 to 51 ohms. The

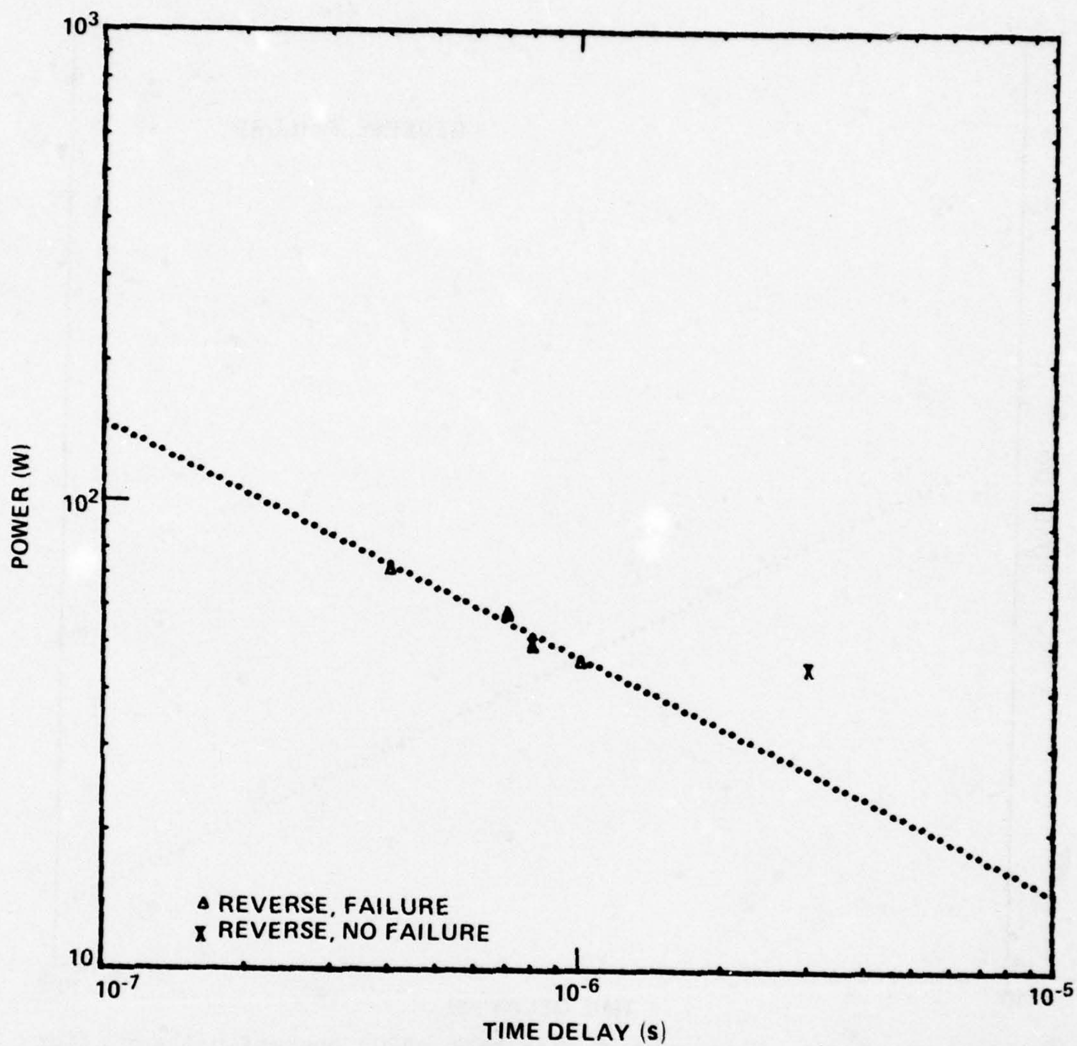

Figure 88. Damage line, power, Fairchild μA709 operational amplifier output pin 6(F).

average bulk surge impedances as measured across pins 6(F) to 4(D) were these:

+ Pin	Bulk surge impedance (ohms)	Spread (ohms)
4(D)	21.4	18.5 to 24
6(F)	102.5	88.4 to 121

4.2 Tests on 2N1132 Transistor from Various Manufacturers

One hundred fifty 2N1132 transistors were purchased commercially: 50 MOT, 50 FSC, and 50 TI. The only control imposed was that both MOT and TI transistors were designated Joint Army-Navy (JAN) devices. The FSC transistors could not be conveniently purchased to the JAN specifications at that time. All transistors were tested under controlled conditions, pulsed to destruction with a rectangular pulse of 2 μs across the E-C terminals. The instrumentation setup remained constant throughout the test. The thyratron generator was used with a series 50-ohm resistor in the basic measurement setup of figure 13. The objectives of the investigation were these:

a. To establish the failure level of the transistor in the 1- to 2-μs pulse-width regime

b. To examine the spread in the failure data, especially as it related to the predicted failure curve

c. To examine the effects of manufacturing differences

4.2.1 Failure Level and Data Spread

The transistor is a diffused, low-power, silicon pnp transistor generally used in switching circuits. The transistor is extensively used in the Lance Missile System. Damage testing on the samples was conducted across the unbiased E-C terminals. The base lead was left unconnected during the pulse tests. A rectangular pulse of 2 μs was applied across the appropriate terminals. The pulse amplitude was set at a level near the suspected point of second-breakdown initiation as established by previous tests. The voltage was then increased until second breakdown and eventual failure.

Failure has arbitrarily been defined here as a 20-percent degradation in junction breakdown voltage or device gain. Twenty-five transistors from each manufacturer were pulse tested with the polarity of the pulse generator to bias E+ with respect to C. The remaining transistors were tested with the opposite polarity. In the following graphs, the polarity is indicated by designating the device terminal connected to the positive terminal of the pulse generator. For example, in figure 89, the pin C failure and no-failure test data points are plotted for the FSC transistors.

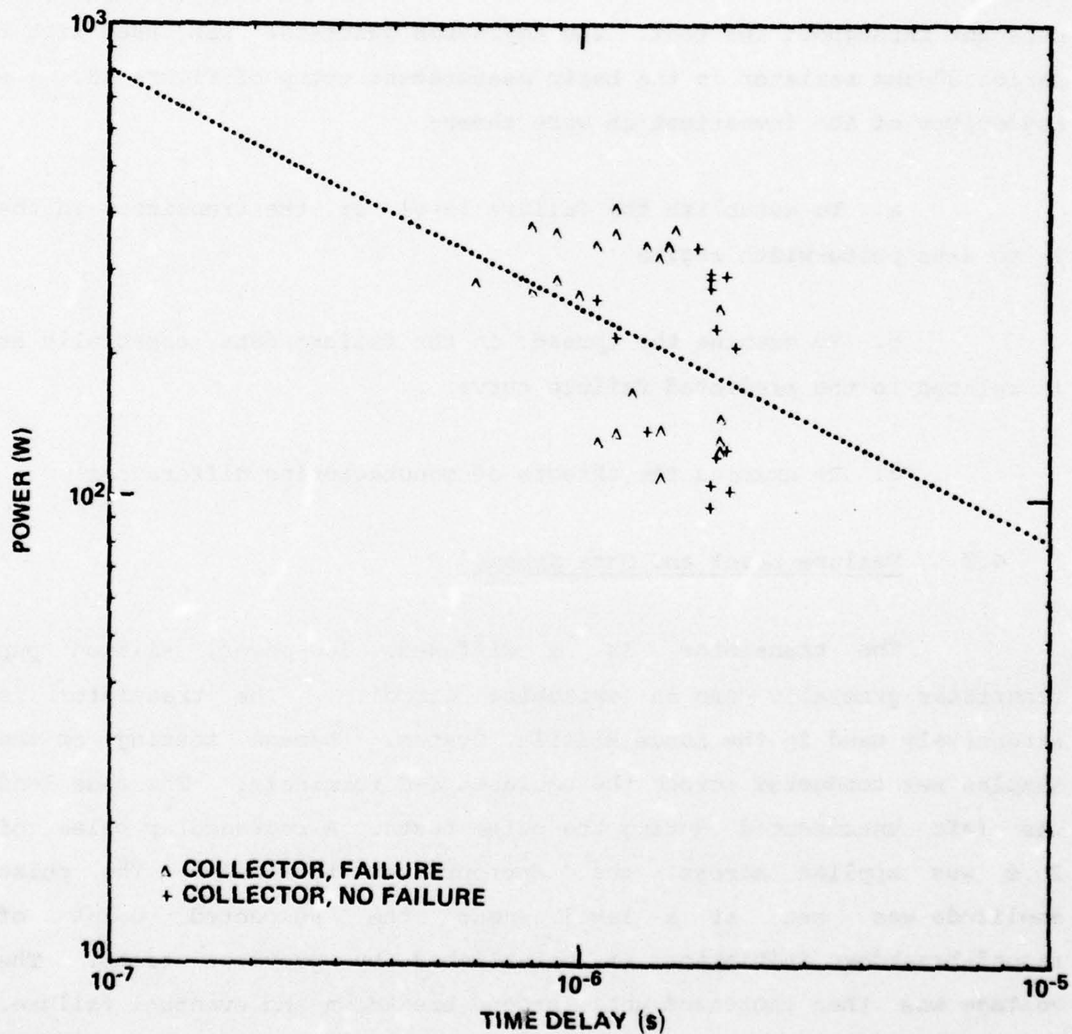

Figure 89. Damage line, power, Fairchild 2N1132 transistor pulse tested across collector-emitter terminals with positive pulse at collector.

The test data for each transistor condition and manufacturer are given in figures 89 to 100. Figure 89 plots the power dissipated in the transistor prior to second breakdown; figure 90 is a histogram indicating the spread in second-breakdown level for the failed transistors. The power points are plotted versus the time duration to the second-breakdown point or, if no second breakdown is seen, to the

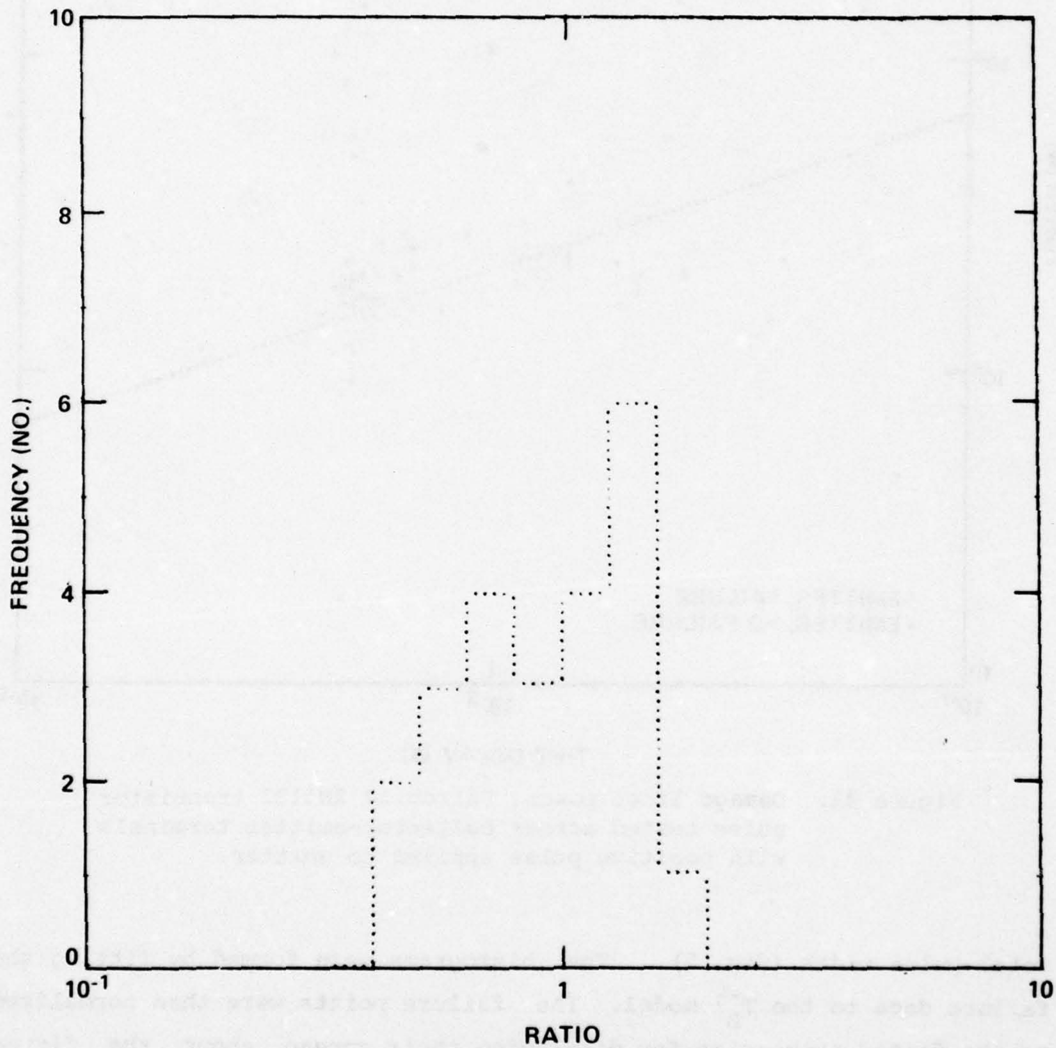

Figure 90. Spread in data points about nominal failure line for Fairchild 2N1132 transistor; pulse polarity biased collector positive with respect to emitter.

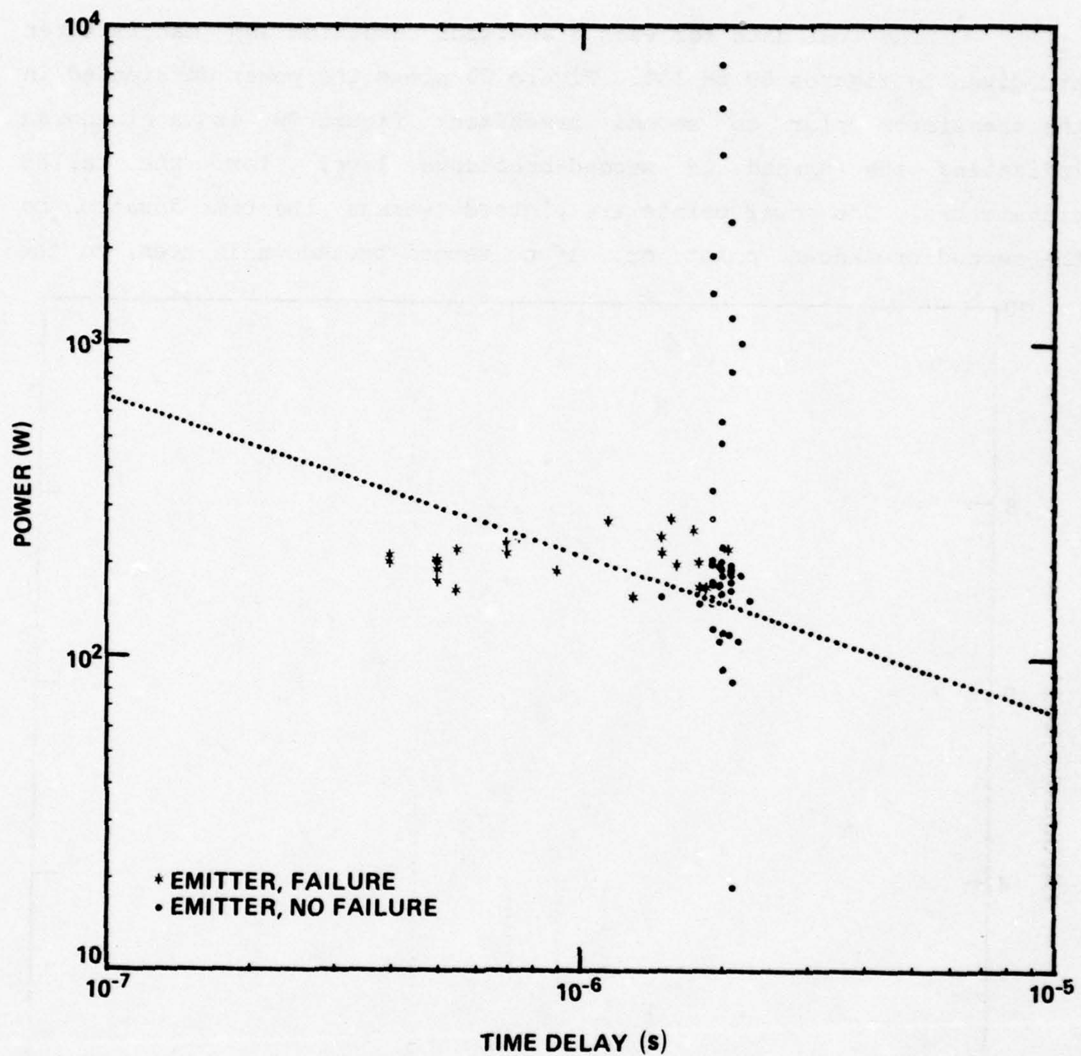

Figure 91. Damage line, power, Fairchild 2N1132 transistor pulse tested across collector-emitter terminals with positive pulse applied to emitter.

total pulse width (fig. 2). The histograms were formed by fitting the failure data to the $T_D^{-\frac{1}{2}}$ model. The failure points were then normalized to the fitted expression for displaying their spread about the fitted line. This spread is seen in the histogram, where the frequency of occurrence is plotted against the ratio of experimental over predicted

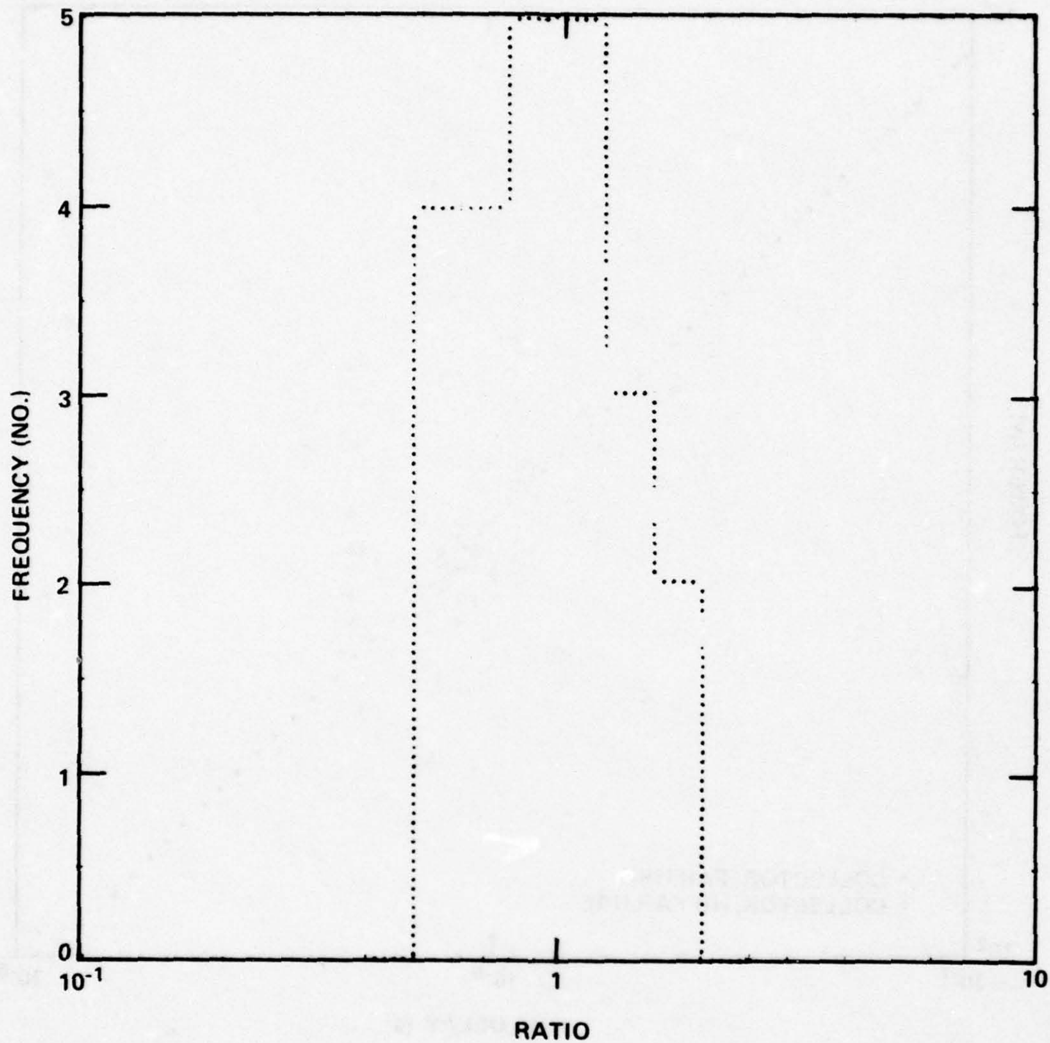

Figure 92. Spread in data points about nominal failure line for Fairchild 2N1132 transistor; pulse polarity biased emitter positive with respect to collector.

(from the fit) power for second-breakdown initiation for each transistor. The bin size for figures 92, 94, 96, 98, and 100 was a linear 1/10 decade.

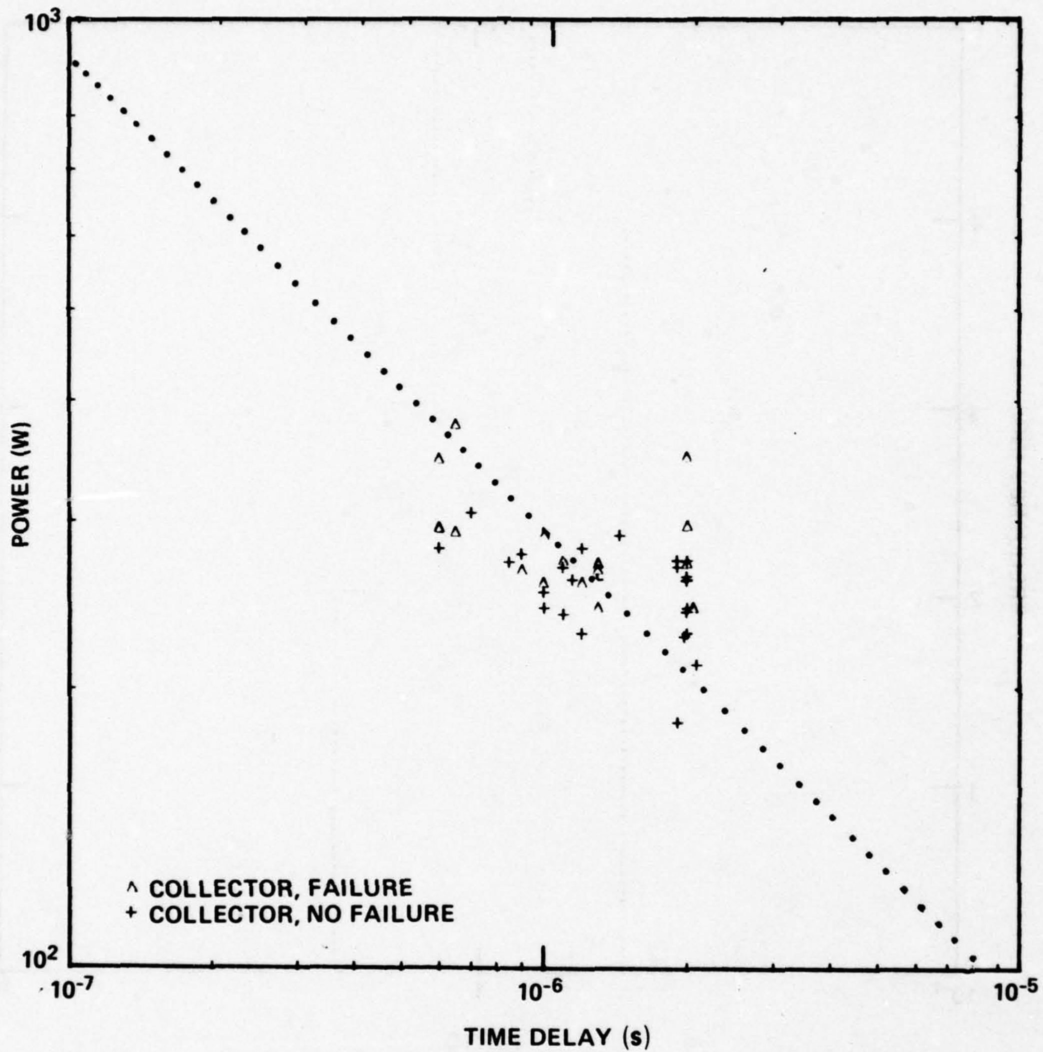

Figure 93. Damage line, power, Motorola 2N1132 transistor pulse tested across collector-emitter terminals with positive pulse applied to collector.

The failure response for the same pin polarity was similar for each manufacturer, but there were specific differences. Figure 101 presents the typical response of the MOT transistors pulsed E(+)-C. A

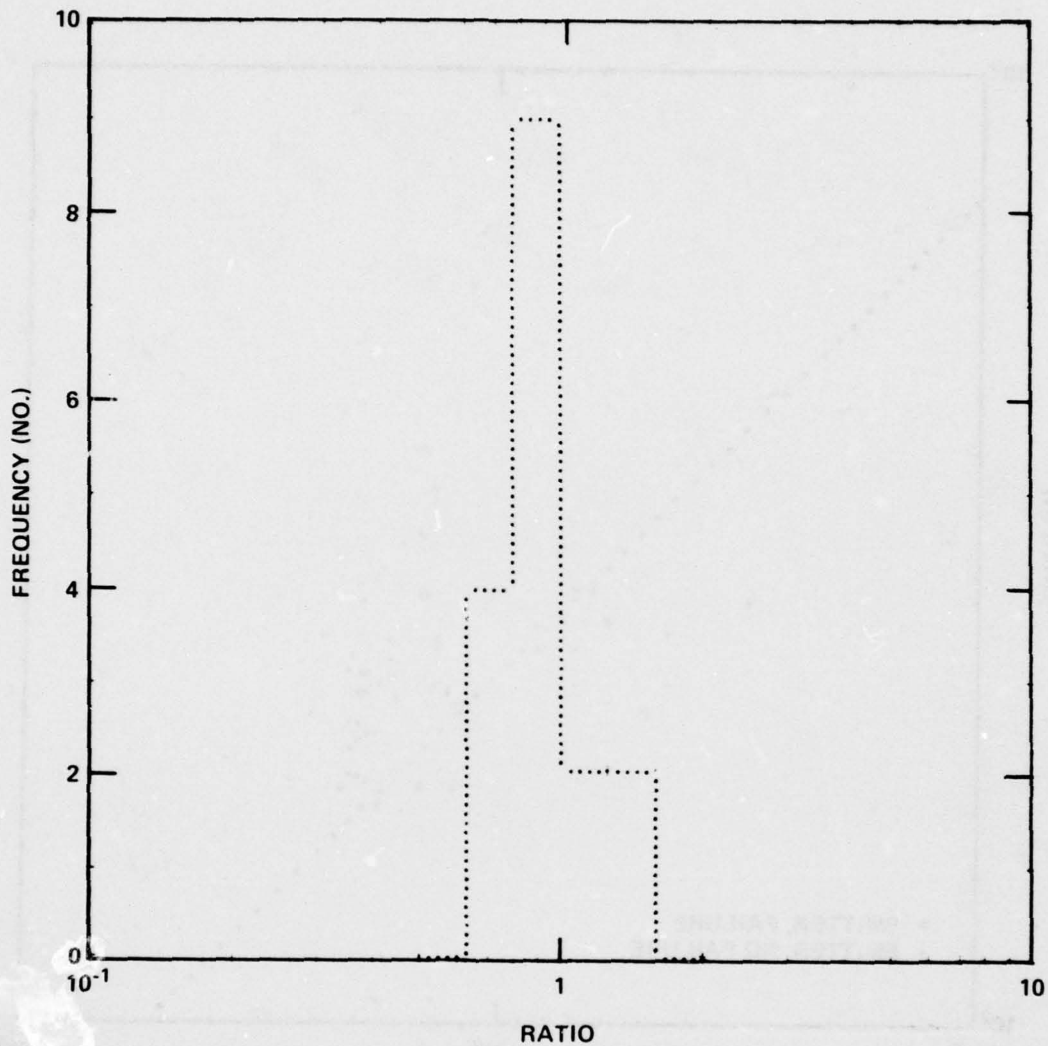

Figure 94. Spread in data points about nominal failure line for Motorola 2N1132 transistor; pulse polarity biased collector positive with respect to emitter.

two-stage second breakdown is noted. The TI transistor's typical response showed (fig. 102) a longer delay time between the two stages of second breakdown. The FSC data (fig. 89 to 92) had examples of both

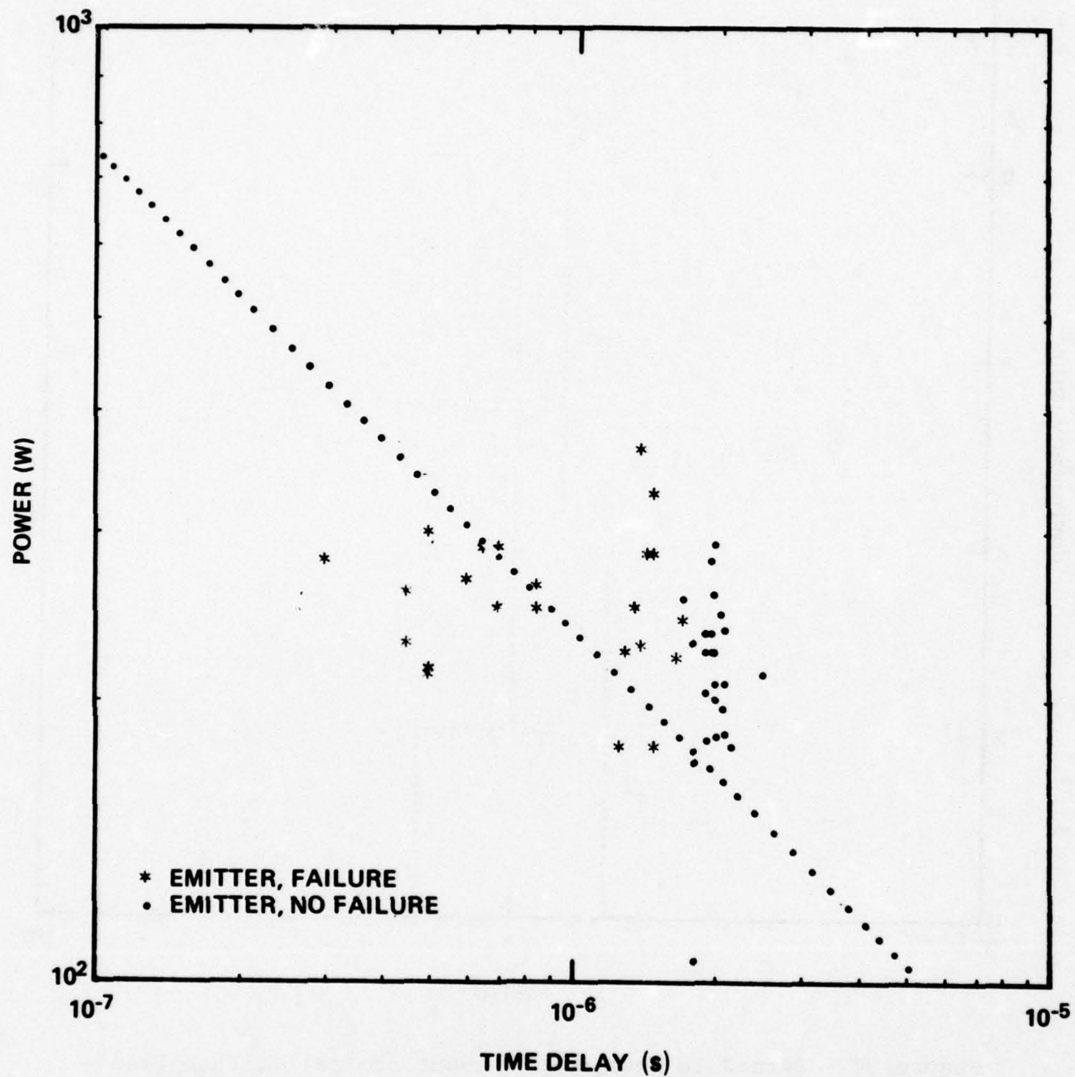

Figure 95. Damage line, power, Motorola 2N1132 transistor pulse tested across collector-emitter terminals with positive pulse applied to emitter.

types of response. The time to second breakdown required for the damage model was determined by the most significant voltage drop, as indicated by the arrows on the oscillogram. This drop indicates the complete loss

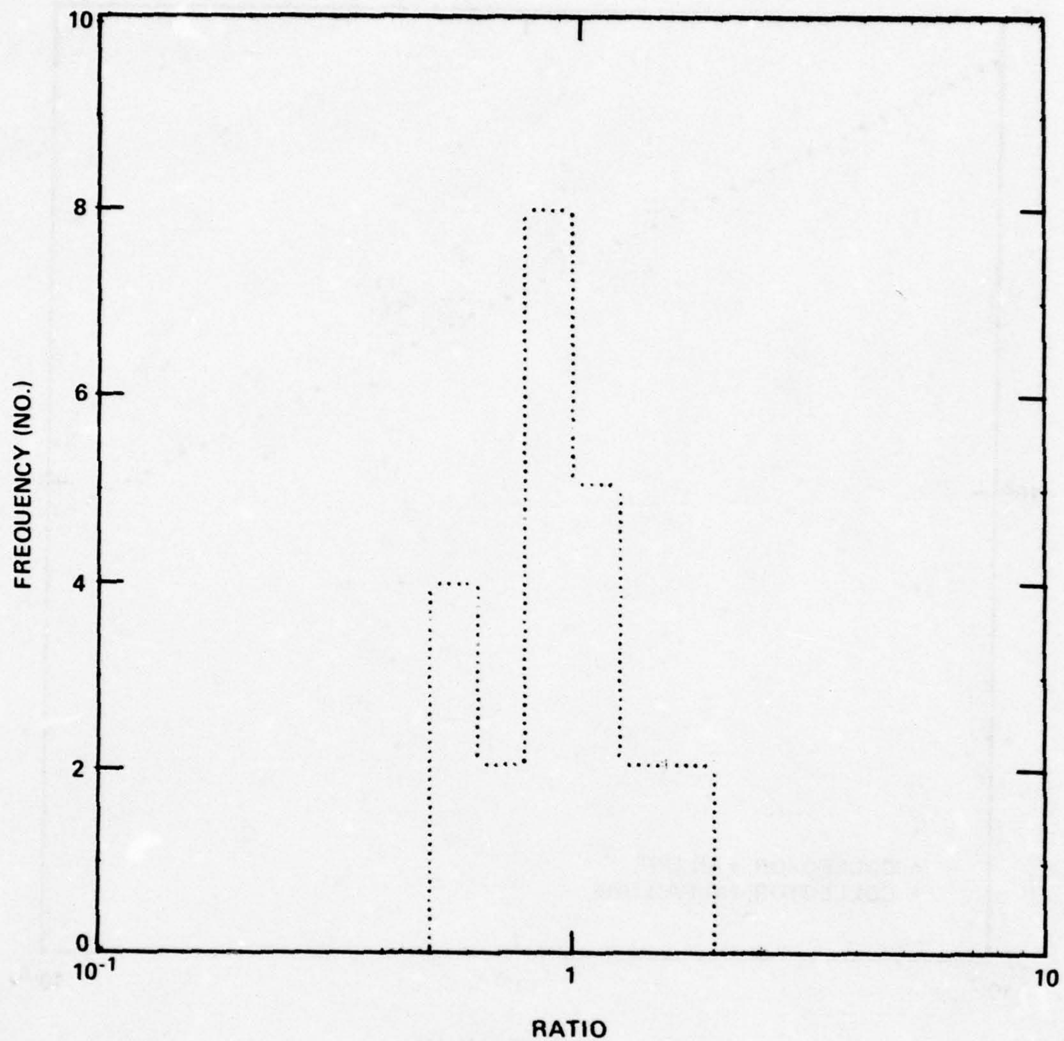

Figure 96. Spread in data points about nominal failure line for Motorola 2N1132 transistor; pulse polarity biased emitter positive with respect to collector.

of rectifying action. Many transistors partially recover from such a pulse. Rarely did a transistor totally recover (based on the pre- and postdamage electrical measurements).

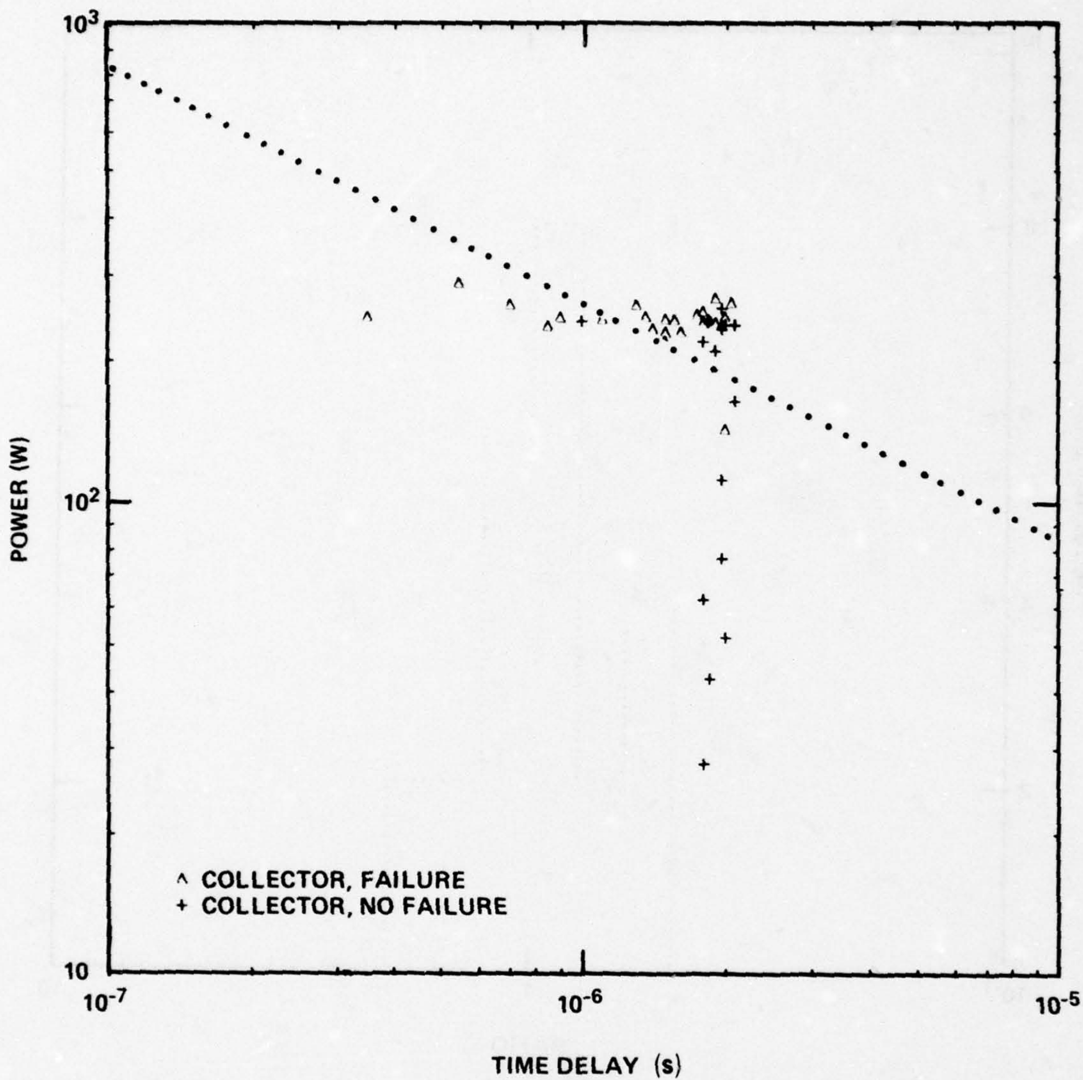

Figure 97. Damage line, power, Texas Instruments 2N1132 transistor pulse tested across collector-emitter terminals with positive pulse applied to collector.

Data reduction from the C(+)-E tests was much more difficult. The typical response of the TI transistor is given in figure 103. The transition region is more prolonged than the clear-cut voltage drops of

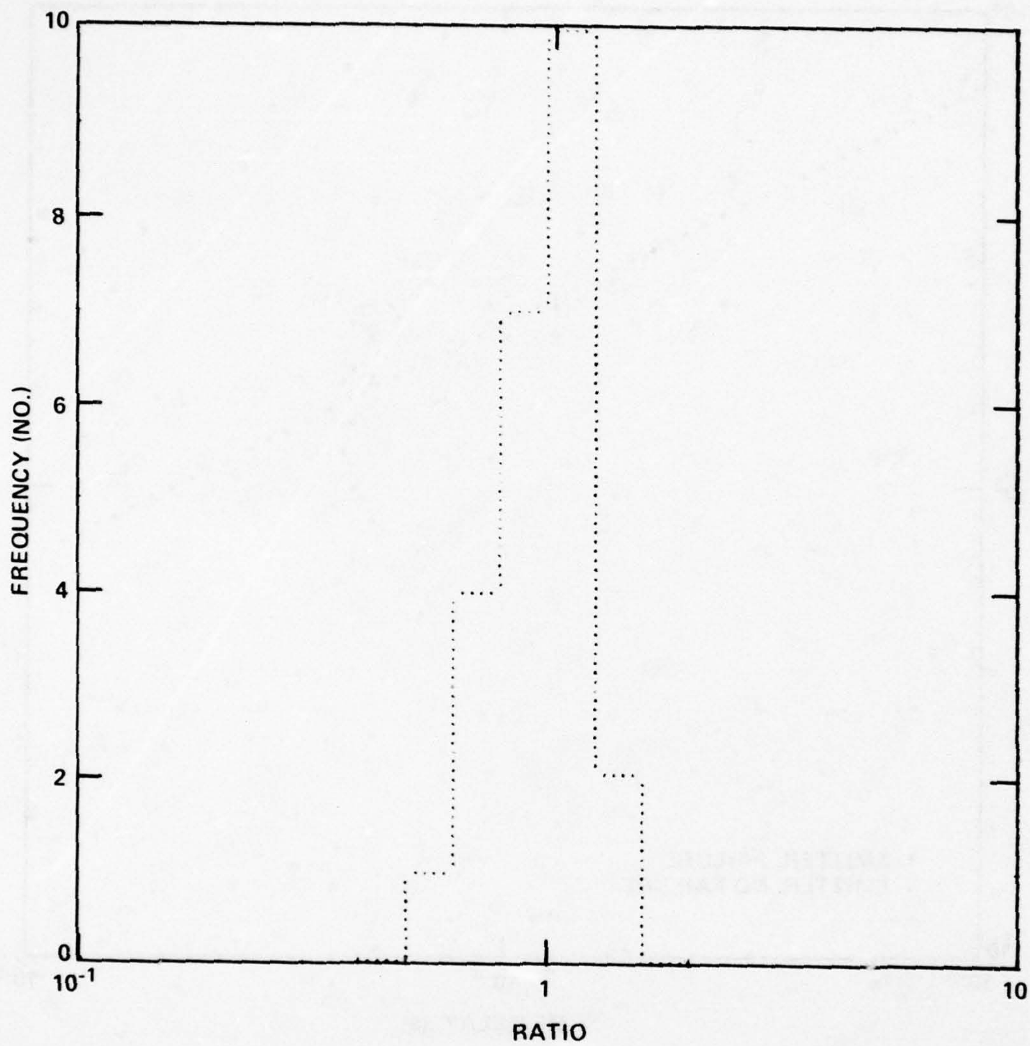

Figure 98. Spread in data points about nominal failure line for Texas Instruments 2N1132 transistor; pulse polarity biased collector positive with respect to emitter.

figures 101 and 102. Further, the relative voltage drop due to the lower breakdown level is smaller and makes it hard in many oscillograms to distinguish a second-breakdown point. The time delay before the

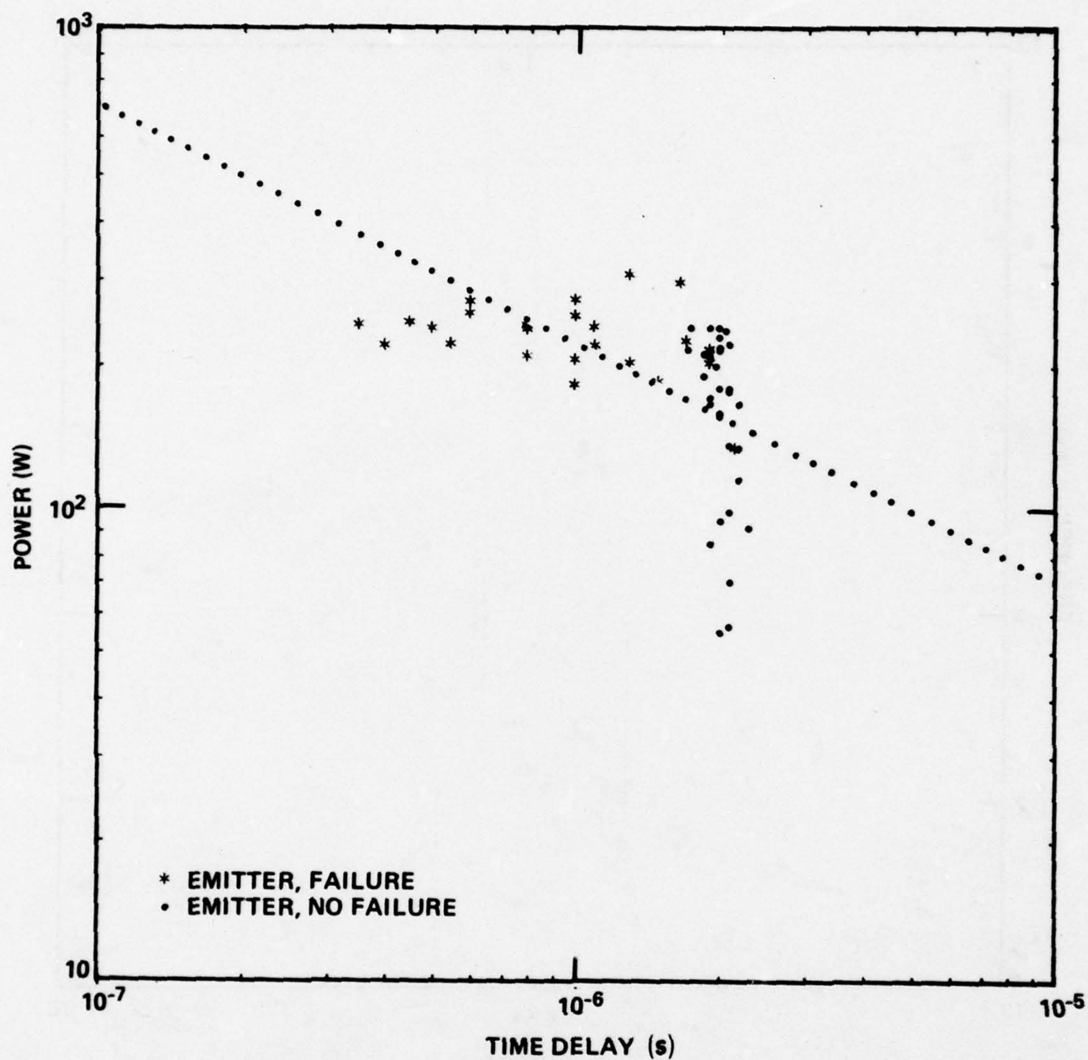

Figure 99. Damage line, power, Texas Instruments 2N1132 transistor pulse tested across collector-emitter terminals with positive pulse applied to emitter.

initiation of second breakdown was chosen at the point on the voltage trace which had the greatest change in slope (arrow, fig. 103).

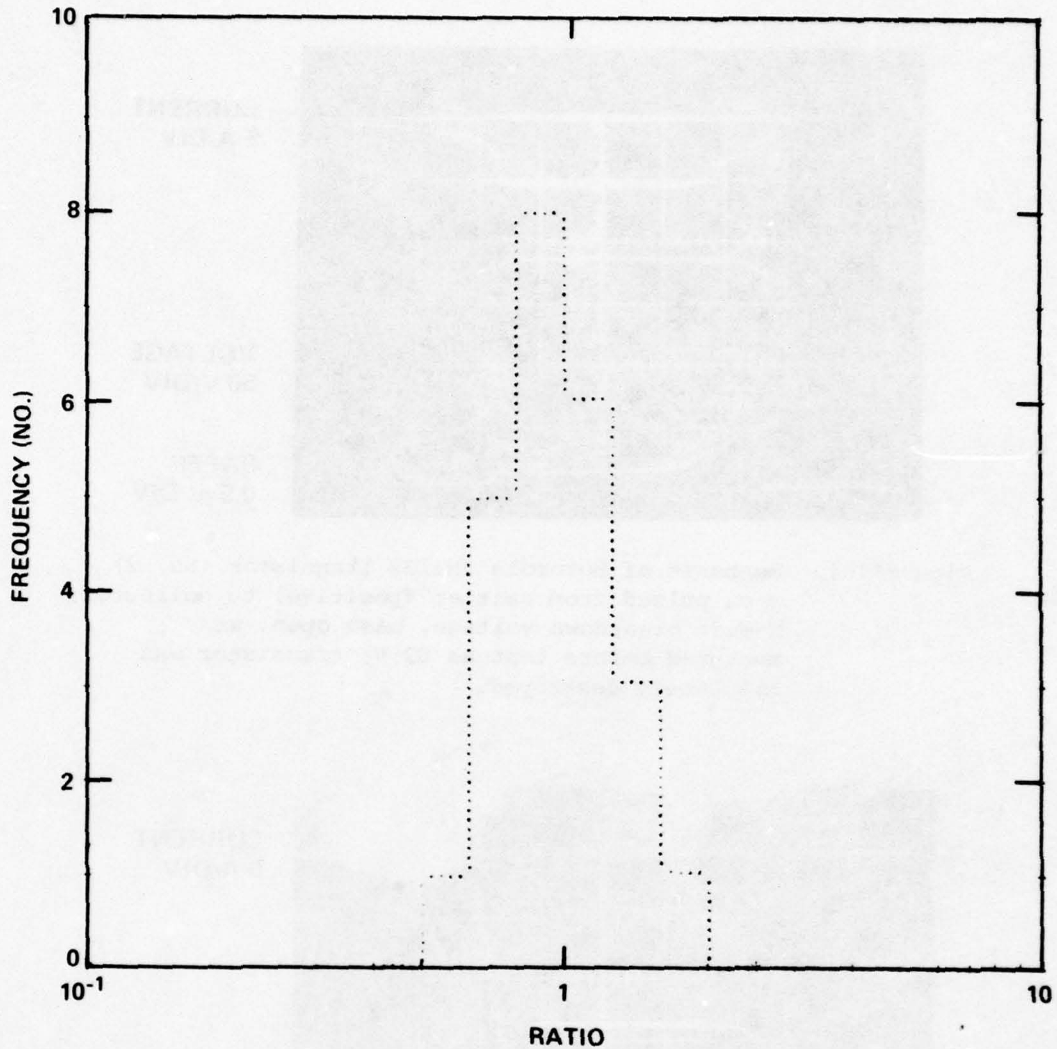

Figure 100. Spread in data points about nominal failure line for Texas Instruments 2N1132 transistor; pulse polarity biased emitter positive with respect to collector.

In comparing the data in figures 89 to 103, although the transistor appears to exhibit failure at the same power and, consequently, energy levels regardless of pulse polarity, it takes

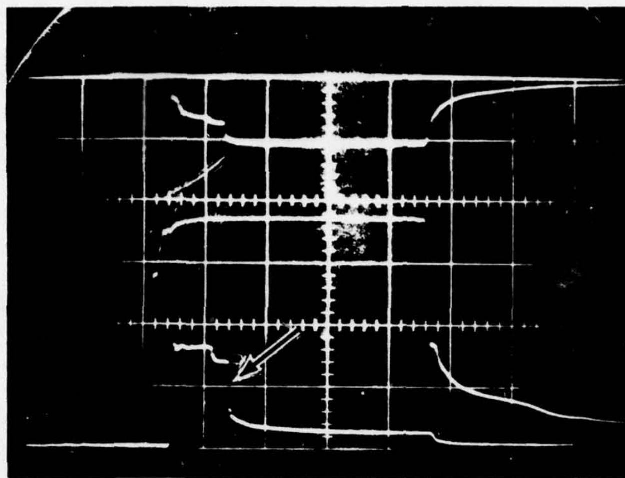

Figure 101. Response of Motorola 2N1132 transistor (No. 2) when pulsed from emitter (positive) to collector; E-C dc breakdown voltage, base open, was measured before test as 82 V; transistor was completely destroyed.

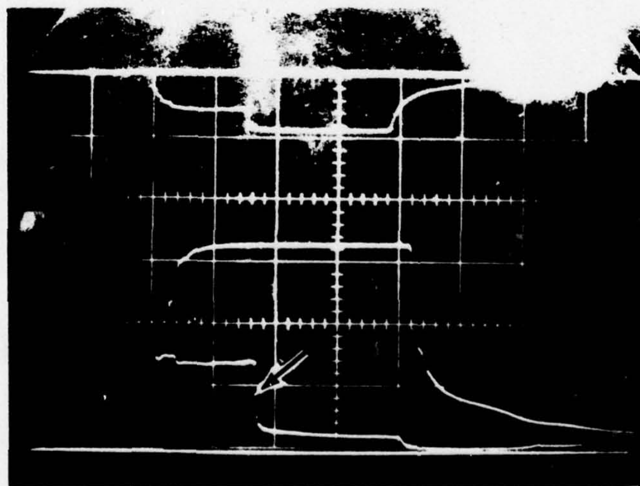

Figure 102. Response of Texas Instruments 2N1132 transistor (No. 9) when pulsed from emitter (positive) to collector; E-C dc breakdown voltage, base open, was measured before test as 73 V; transistor was completely destroyed.

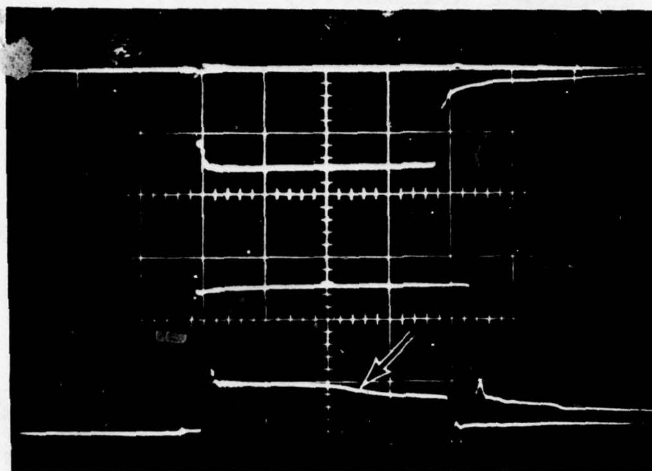

Figure 103. Response of Texas Instruments 2N1132 transistor (No. 48) when pulsed from collector (positive) to emitter; C-E dc breakdown voltage was measured before test as 6.2 V; transistor was completely destroyed.

approximately three times the voltage level to fail the device when the positive pulse is applied to C through 50 ohms. This increase is due to the lower value of transistor breakdown voltage and effective impedance for the C(+) polarity. Table VI summarizes the impedance calculation, as established by the technique described in section 3.2.4.

The second-breakdown initiation levels vary only a small amount among manufacturers and even between the polarities of the applied pulse. The failure points spread normally about the fitted line on the log scale. The figures indicate a few no-failure points at pulses shorter than 2 μs. Since the applied pulse was always 2 μs, these points are obtained from transistors which experienced second breakdown

TABLE VI. BULK SURGE IMPEDANCE, 2N1132 TRANSISTOR, COLLECTOR TO EMITTER

Manufacturer	Polarity	Impedance (ohms)
Motorola, Inc.	E+	2.3
	C+	0.72
Texas Instruments, Inc.	E+	3.9
	C+	0.56
Fairchild, Inc.	E+	2.4
	C+	0.57
Composite	E+	3.1
	C+	0.62

but did not suffer 20-percent degradation, if they were degraded at all.

4.2.2 Combined Data

The data for the MOT, TI, and FSC transistors were combined to produce the plots of figures 104 to 108. Figures 104 and 105 present the combined data for the failure level of the transistor pulsed C(+)-E. Figures 106 and 107 present the failure level for the 2N1132 pulsed E(+)-C. Figure 106 presents the data fitted to the $T_D^{-1/2}$ model, and figure 107 indicates the spread of the data about the fitted line. The points that appear below the fitted line under the 200-W level in figure 104 are, with one exception, from the FSC data set. The exception is one TI transistor failure point. The E failures of figures 106 and 107 exhibit a more consistent spread. Figure 108 displays the spread about the failure lines of figures 104 to 107 with a bin size factor of 0.05 (figures 105-108, pp. 156-159).

The combined bulk surge impedances calculated by the technique described in section 3.2.4 are given in table VI. These values can be used as typical levels. However, the bulk surge impedance as calculated for the E+ polarity has large errors. Because the difference was taken between numbers of approximately the same value, these errors are estimated to be as large as ±100 percent. Some screening of the data was done to arrive at this error estimate. The average should reflect the mean, but with a low confidence level. The C+ impedance measurement calculation also contains similar errors. However, the difference is taken from numbers with a larger difference in value. The confidence in the mean is correspondingly higher for this impedance estimate.

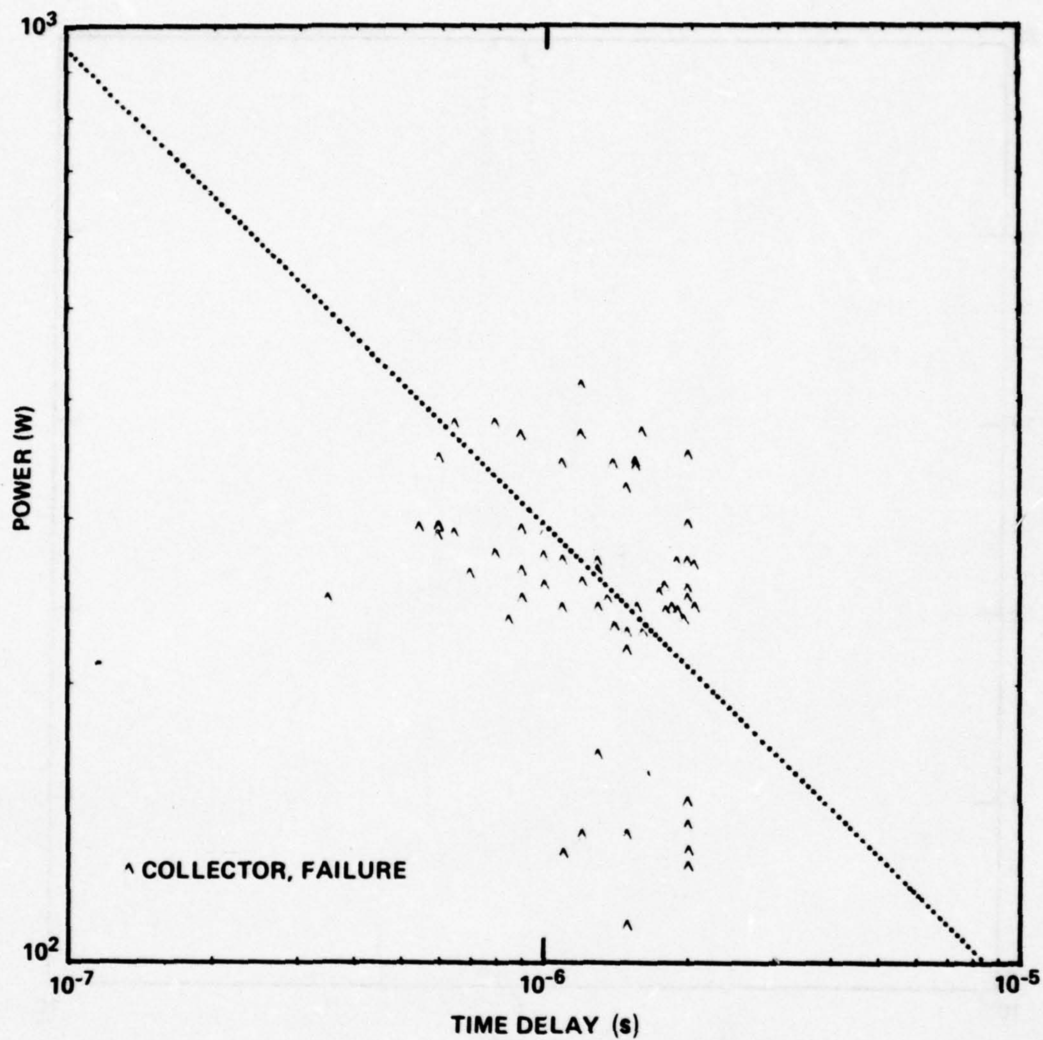

Figure 104. Damage line, power, composite data of Motorola, Texas Instruments, and Fairchild 2N1132 transistors pulse tested across collector-emitter terminals with positive pulse applied to collector.

4.2.3 Failure Analysis

A number of the 2N1132 transistors from each manufacturer were decanned and the surfaces of the chips were viewed under a

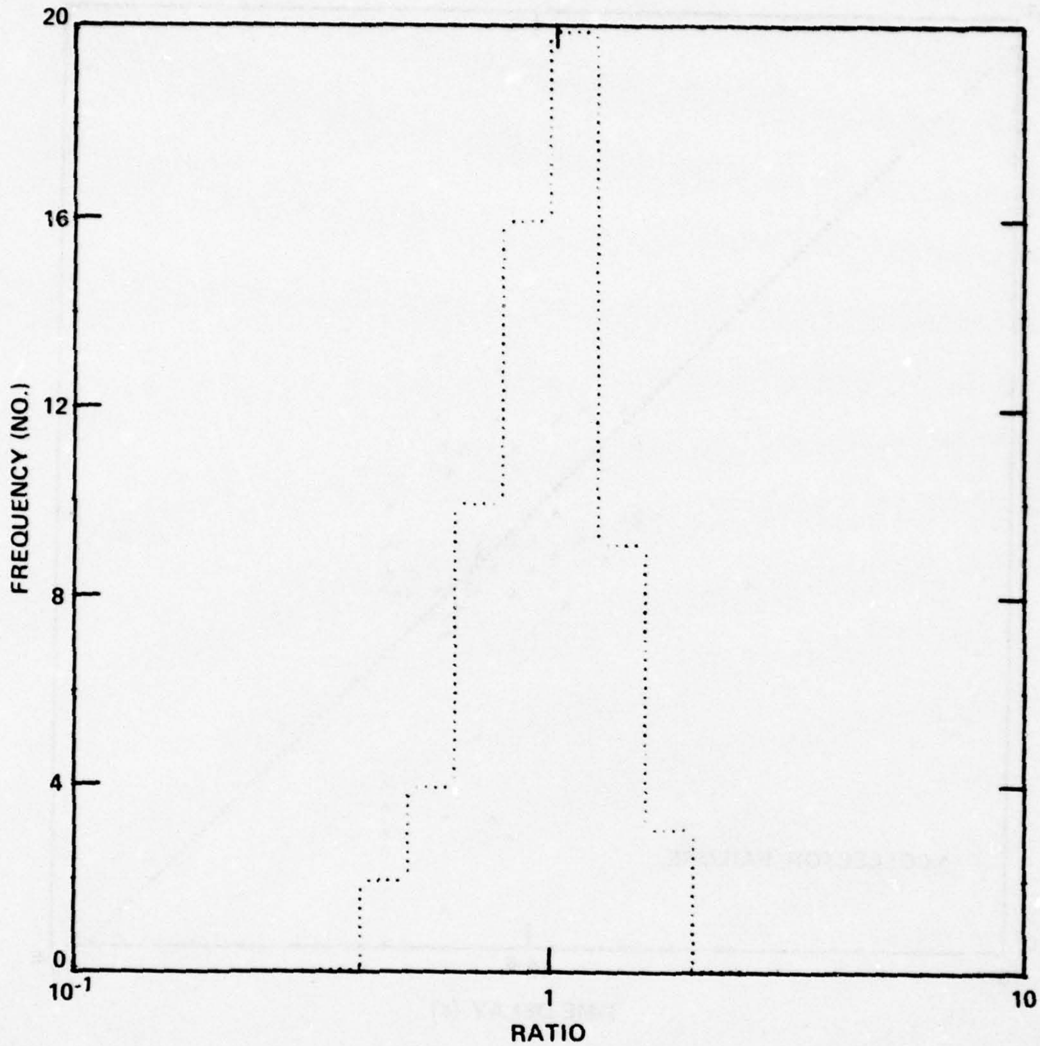

Figure 105. Spread in data points about nominal failure line for composite data of Motorola, Texas Instruments, and Fairchild 2N1132 transistors tested with collector pulse biased positive with respect to emitter; bin size factor: 0.1.

microscope. The purpose of this investigation was twofold. First, an inspection of the chip surface might indicate the nature of the transistor failure. Second, there might be some indication for the

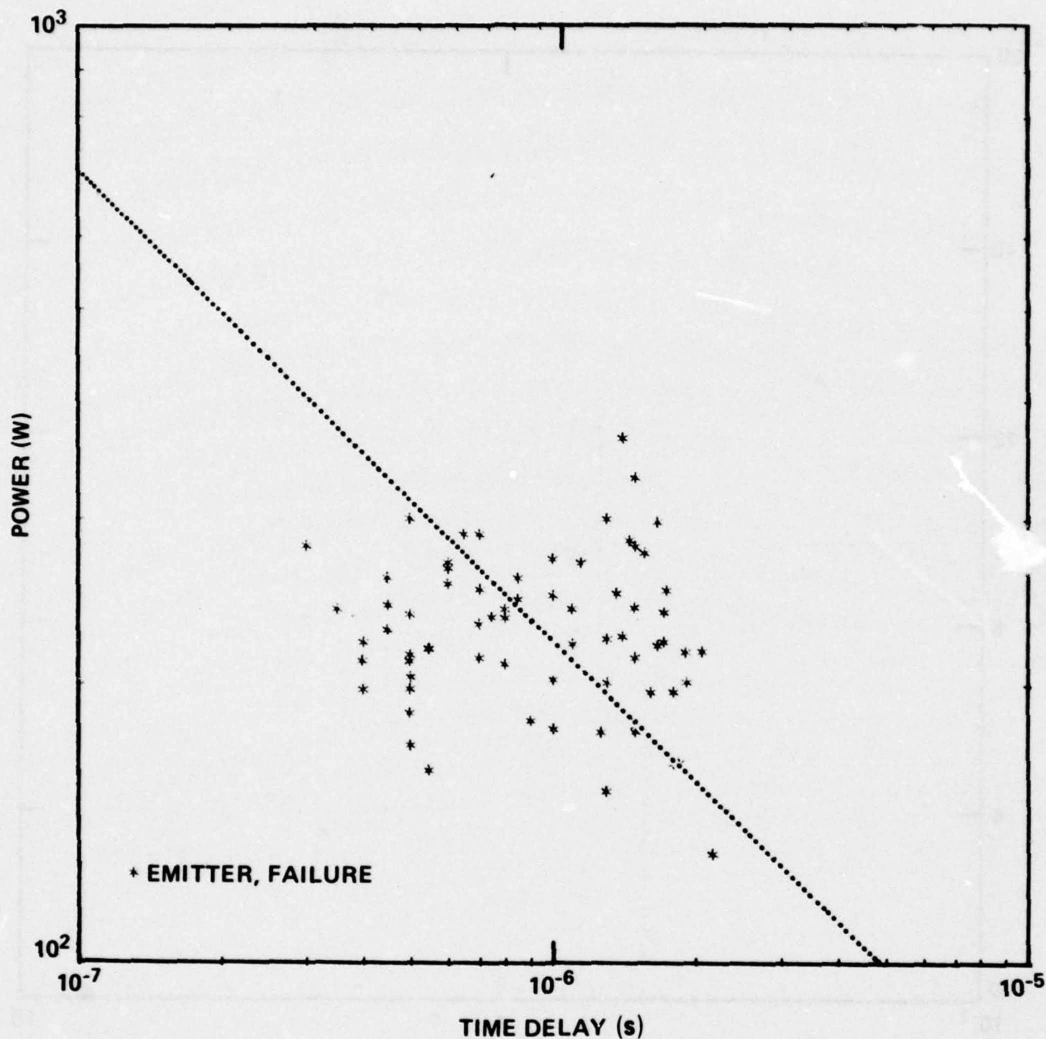

Figure 106. Damage line, power, composite data of Motorola, Texas Instruments, and Fairchild 2N1132 transistors pulse tested across collector-emitter terminals with positive pulse applied to emitter.

spread seen in the failure data. Although tests were conducted across the E-C pins, it was hoped that sufficient evidence would be available on the surface of the chip to identify the possible chain of events that led to failure within the bulk of the transistor. The geometries used

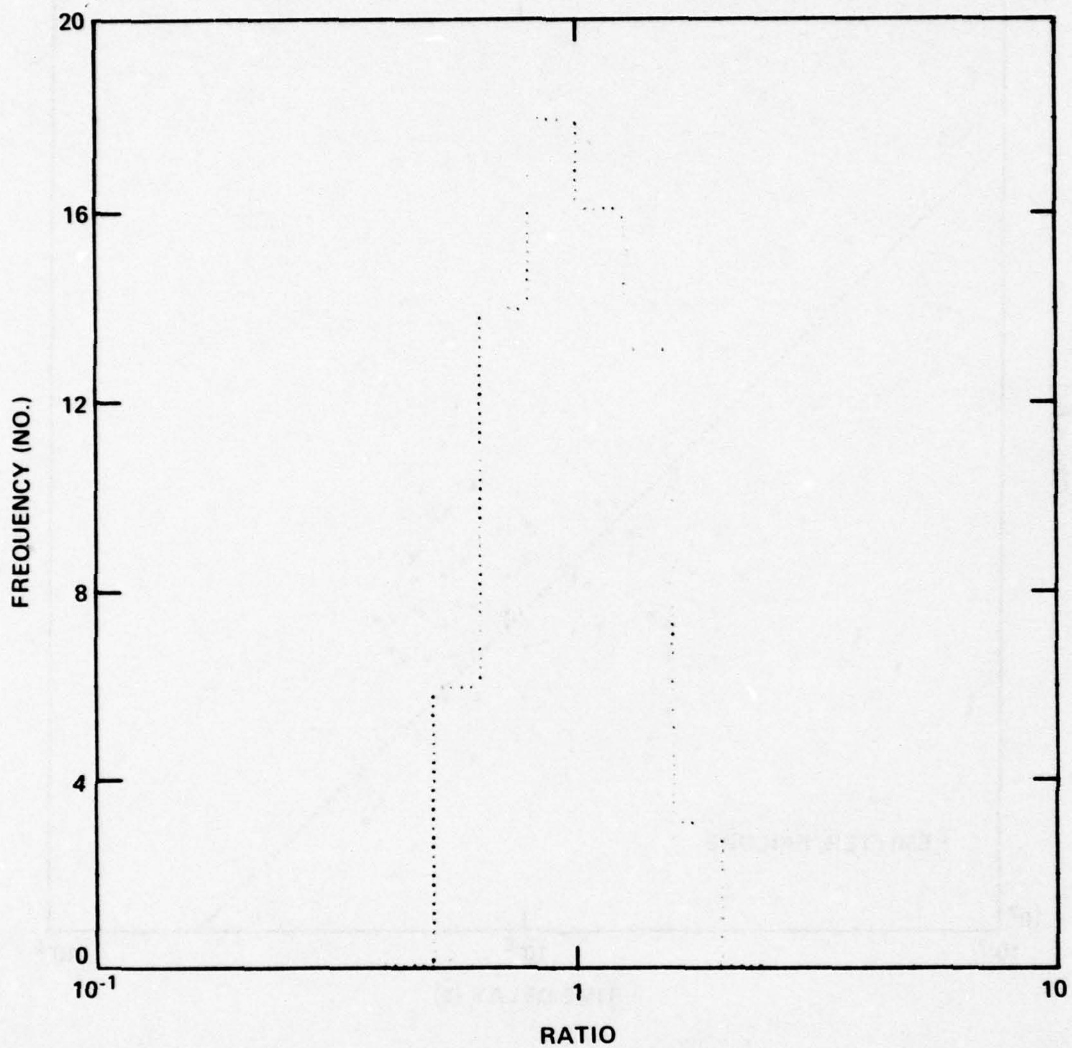

Figure 107. Spread in data points about nominal failure line for composite data of Motorola, Texas Instruments, and Fairchild 2N1132 transistors tested with emitter pulse biased positive with respect to collector; bin size factor: 0.1.

by the manufacturers would be identified, and anomalous transistor failures might be related to defects that were manifested on the transistors' surfaces.

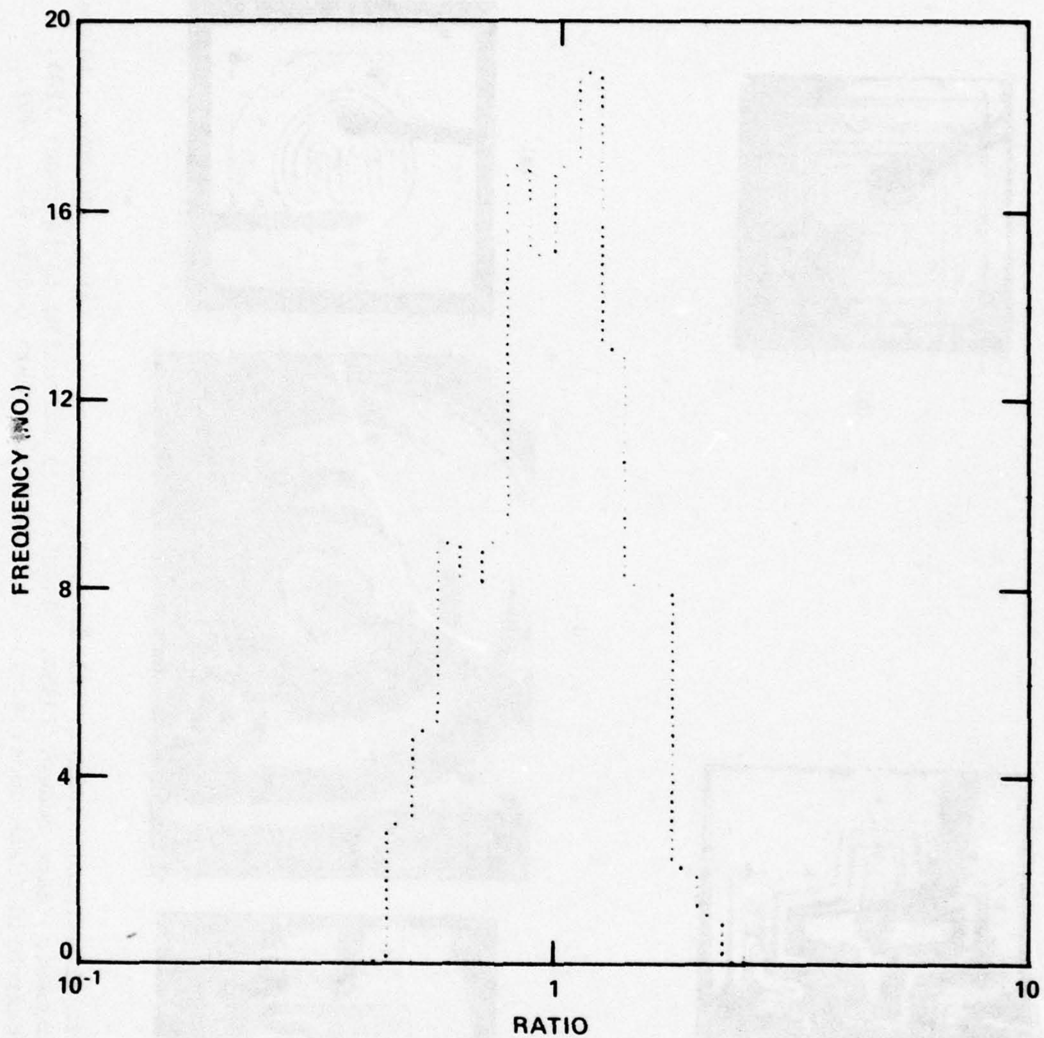

Figure 108. Spread in data points about nominal failure line for composite data of Motorola, Texas Instruments, and Fairchild 2N1132 transistors (independent of pulse polarity); bin size factor: 0.05.

Figure 109 identifies the chip geometries observed microscopically (96X). The MOT and TI transistors each had their own consistent geometry, though transistors of both manufacturers bore two date codes. Test damage data on these transistors showed a consistent, relatively tight distribution about the established failure line. The

(a)

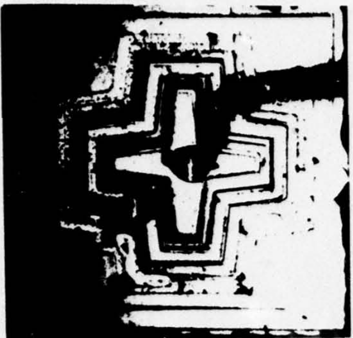

(b)

(c)

(d)

(e)

Figure 109. 2N1132 transistors (96X): (a) Motorola (date codes: 6917L, 6943T); (b) Texas Instruments (date codes: 7035B, 7040B); (c) Fairchild (date code: 124); (d) Fairchild (date code: 425); (e) Fairchild (date codes: 020, 740).

FSC transistors, on the other hand, were not bought to JAN specifications. Three separate geometries were evident when transistors with four different date codes were examined.

Figure 109 gives a good idea of the relative variation in size for the FSC devices. This variation could explain the larger spread about the damage line for the FSC transistors; transistor No. 71, which had the ring-dot geometry of figure 104, failed uniquely. Power levels up to 7.8 kW and current levels up to 50 A were sustained for the 2-μs pulse E(+)-B without transistor failure. Other transistors failed at power levels of ~200 W. This transistor accounts for the train of no-failure points seen in figure 91.

The transistor eventually failed after 18 pulses of increasing power level. The voltage and current oscillogram was not obtained for this 18th pulse; consequently, a failure point for this transistor does not appear in figure 91. This high energy failure level was not consistent to the ring-dot geometry, because other failures in this geometry were at comparable levels to those of the other two geometries. There was no visual indication of why this transistor was able to sustain the high levels impressed.

Surface indication of transistor damage was not prevalent. Figures 110 to 112 indicate the character of some of the visible damage. Figures 110 and 111 show the chip surface of devices which were pulsed biased E-C; the E-B junction therefore was forward biased, and the B-C junction was reverse biased. The effect of subsurface heating is evident. Motorola transistor No. 12 failed on the fourth pulse at 0.4 μs and 366 W after surviving 80-, 225-, and 291-W power during 2-μs pulsing. Texas Instruments transistor No. 1 failed on the third (reverse-biased) pulse at 130 W after sustaining 54 and 84 W on the two previous 2-μs pulses.

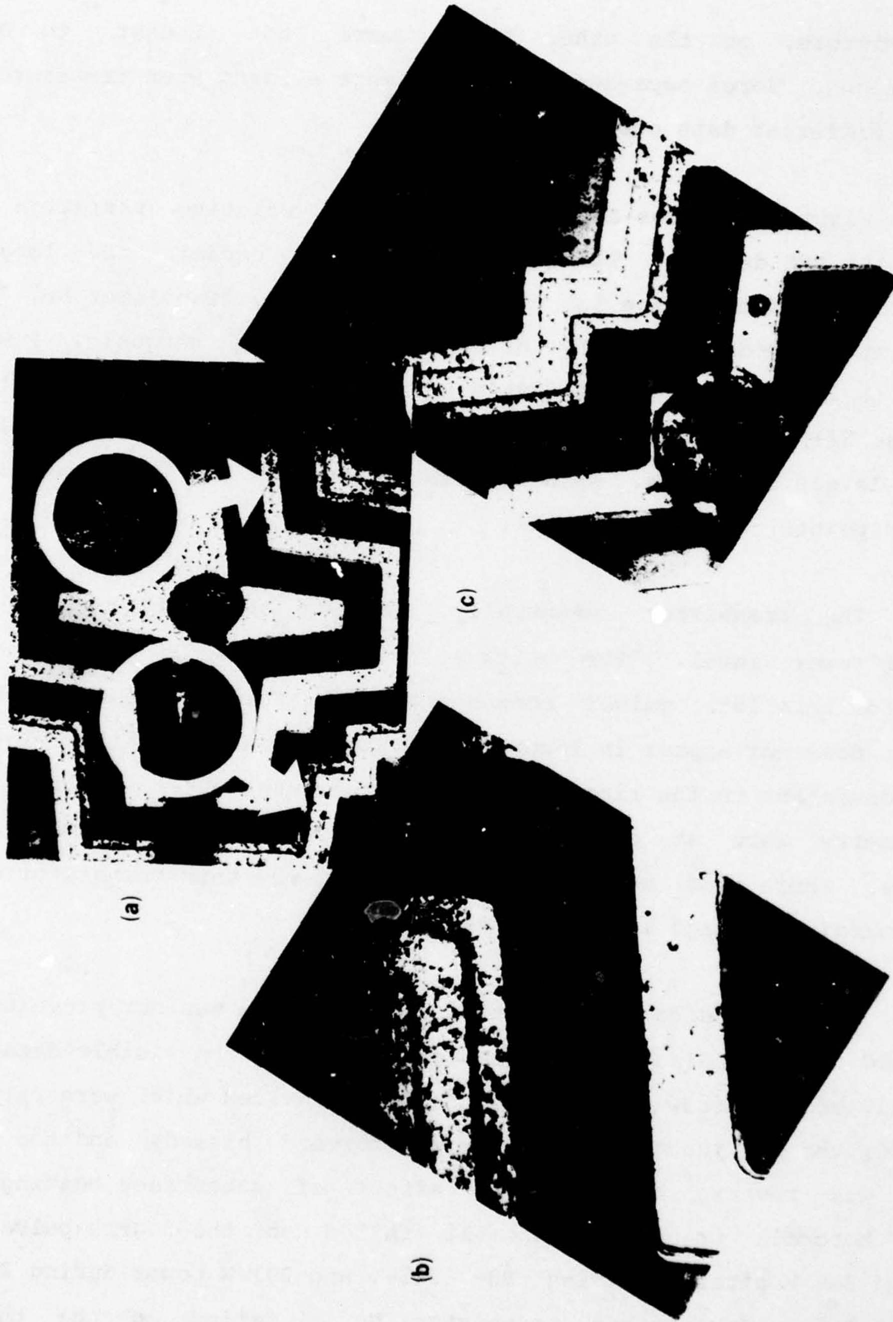

Figure 110. Motorola 2N1132 transistor (No. 12) (date code: 6943T), tested emitter positive to collector: (a) 196X; (b) 770X (emitter-to-base junction); (c) 390X (base lead removed).

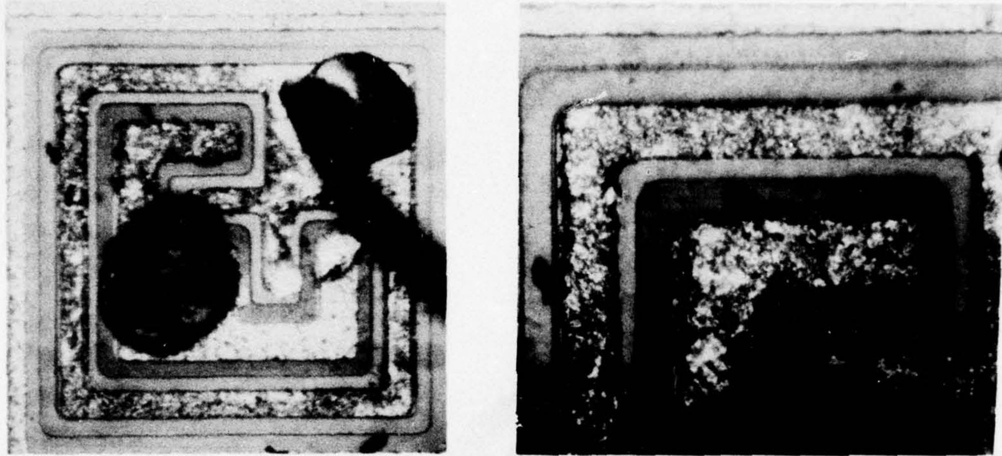

Figure 111. Molten metalization damage on Texas Instruments 2N1132 transistor (No. 1) (date code: 7040B), tested emitter positive to collector: (a) 190X; (b) 390X.

Figure 112 shows more varied surface damage on FSC transistor No. 91. The test pulse polarity forward biased the C-B junction and reverse biased the E-B junction. This transistor failed on the first pulse of 1.2 μs and 270 W. A tunneling at various points around the E metalization periphery was due, presumably, to local melt regions between the E and B metalizations. Damage of this type has been seen in reverse-biased B-E pulse damage tests. In these B-E tests, tunneling was seen partly and sometimes completely to traverse the region between the metalization. Also, the obvious damage occurred in a region which apparently had not passivated due to a misalignment problem during manufacture. This relationship between manufacturing defects and locations of surface damage has been seen in a number of transistors. The insufficient number of data prevents evaluation of the significance of such defects.

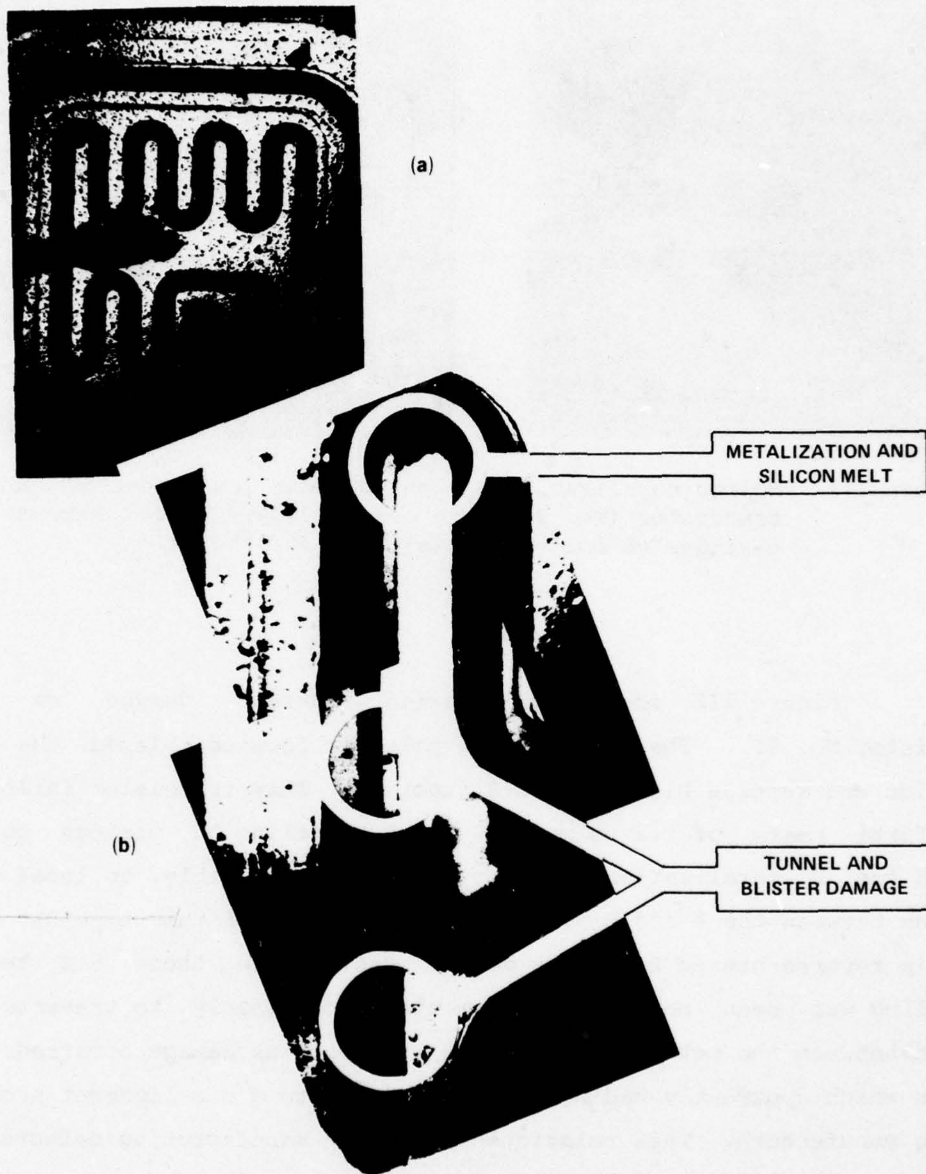

Figure 112. Fairchild 2N1132 transistor (No. 91) (date code: 124), tested collector positive to emitter: (a) 190X; (b)770X.

4.3 Nonsemiconductor and Hardening Device Tests

The following test descriptions have been abstracted from the individual test reports issued for each of the items specified.

4.3.1 SM-C-602932 Surge Arrestor

One SM-C-602932 surge arrestor was tested by using two high-voltage rectangular-pulse generators. The thyratron generator was used at a pulse of 1 μs and at amplitudes ranging from 400 to 2500 V. The pulse rise time was ~30 ns, and the unit output impedance was ~10 ohms. The coaxial high-voltage generator permitted tests at 50-ns pulses at rise times of 2 ns or less. The voltage range was from 1400 to 6000 V. The unit has a nominal 50-ohm output impedance.

The tests with the long-pulse generator indicated that large currents could be sustained, in excess of 600 A, without noticeable degradation of any kind. The surge arrestor appeared to have a breakdown resistance ranging from 1 to 2 ohms as calculated from the voltage across and current through the arrestor during the test. The short-pulse, fast rise-time tests demonstrated that the surge arrestor had a turn-on time much less than could be measured by the instrumentation (less than 5 ns) with no apparent turn-on delay for voltage levels in excess of 1400 V.

4.3.2 SM-C-602933 Filter

Four SM-C-602933 filters were both frequency characterized and pulse tested. The attenuation with frequency was obtained from the input and from the output pins with a load impedance of 20 kilohms. The frequency characterization from 100 kHz to 100 MHz was performed by using a Hewlett-Packard (HP) 8553B spectrum analyzer. Lower-frequency

measurements were obtained by using an HP 651A signal generator and a Tektronix (TEK) 454 oscilloscope. A 20-kilohm load was used. The filter was pulse tested at voltages ranging from 200 to 2500 V, by using the thyratron generator, and to 2000 V at 50-ns pulses, with the coaxial high-voltage generator.

Figure 113 (p. 167) presents the typical attenuation characteristics of the filter loaded as described. The pulse tests indicated that only a very small fraction of energy reached the load, an indication consistent with the characterization of figure 110. There was no apparent degradation of performance to applied voltage levels of 2500 V and a 1-μs pulse. No nonlinear effects appeared such as arcing or saturation.

4.3.3 1N5649A TransZorb Diode

Two 1N5649A TransZorb diodes from General Semiconductor Industries, Inc., were tested under high-voltage transient conditions to evaluate their clamping ability and their ability to survive high-voltage, high-energy pulse transients. TransZorb diodes are two-layer reference diodes designed to carry large currents. Unique bonding to the large-area semiconductor chip permits large power dissipation without thermal expansion fractures. The diode has a reference level ranging from 44.7 to 49.4 V. First, the diodes were pulse tested with a rectangular pulse of ~2 μs and a varying amplitude from 100 to 1000 V on the thyratron generator. Then the diodes were subjected to a high-voltage, short rise-time pulse as generated by the dielectric-gap generator to determine if they had an appreciable device turn-on time which could preclude their use as an EMP terminal protection device.

Both diodes limited the voltage developed across their pins to ~60 V when subjected to an open-circuit generator voltage of 1000 V

(a)

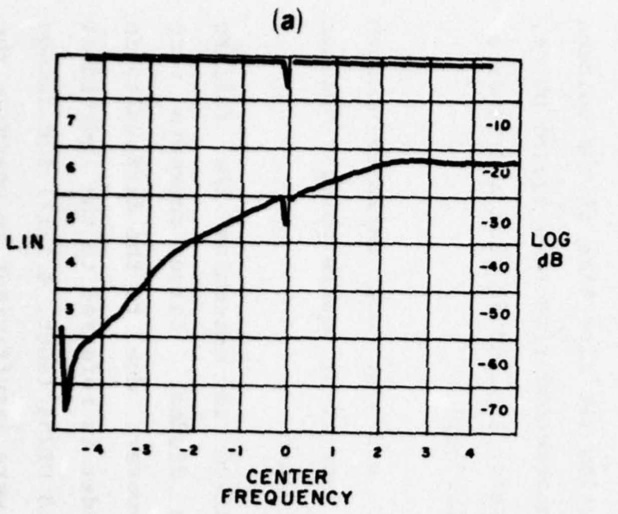

100 kHz 100 MHz

FREQUENCY (kHz)	VOLTAGE IN (V)	VOLTAGE OUT (V)	ATTENUATION (dB)
0.5	1.2	1.2	0
1	1.2	1.2	0
5	1.2	0.90	2.477
10	1.2	0.60	6.021
50	1.2	0.19	16.001
100	1.2	0.08	23.522

(b)

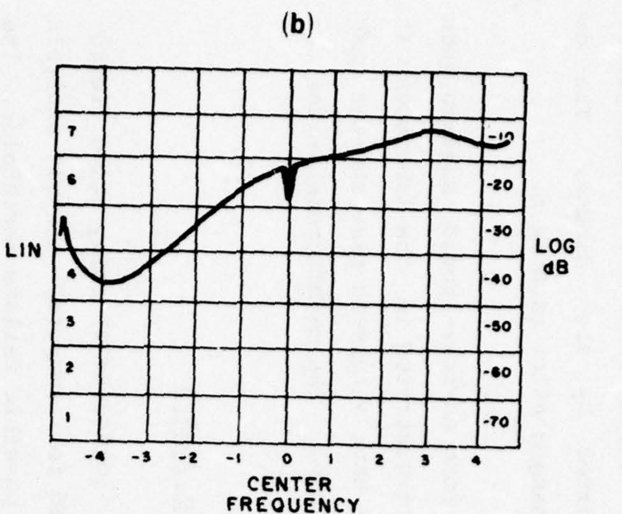

100 kHz 100 MHz

FREQUENCY (kHz)	VOLTAGE IN (V)	VOLTAGE OUT (V)	ATTENUATION (dB)
0.5	1.2	1.2	0
1	1.2	1.2	0
5	1.2	0.90	2.477
10	1.2	0.60	6.021
50	1.2	0.12	20.000
100	1.2	0.05	27.604

Figure 113. Typical attenuation characteristics for SM-C-602933 filter; center frequency (notched), 50 MHz; bandwidth, 100 kHz; load, 20 kilohms: (a) output to input; (b) input to output.

reverse biased. Less than 40 V was developed across the diodes forward biased. A current ≥100 A was supported by the diodes. The dc characteristics of the diodes were unchanged after each test.

It appeared that these TransZorb devices could sustain much higher levels than could conveniently be generated in the laboratory at the time. Also, the diodes appeared to have a turn-on time shorter than the 2- to 3-ns resolution of the generators. The manufacturer rates the turn-on time as less than 1 ps.

4.3.4 10164126(19) and 10158808(19) Relays

One 10164126(19) and one 10158808(19) relay (Ling Temco-Vought, Inc., part numbers) were modeled for computer circuit analysis and then pulse tested to establish possible failure thresholds. The computer models are given in figure 114. The values for the diode, resistor, and inductor were obtained from manufacturer's specifications. The capacitance was determined by measuring the rise time of the voltage developed across the coil from a subnanosecond rise-time square pulse, as generated by a TEK T-109 pulse generator applied in such a manner as to back bias the diode shunting the relay coil.

The possibility of contact arc-over was explored on both relays. Both relay types sustained a 2-kV, 2-μs square pulse. Neither arcing nor significant capacitance was found.

The relay coils were pulsed to determine the failure threshold of the internal shunting diodes. Large currents were sustained without apparent damage. (However, due to the difficulty in making diagnostic measurements, the reader is referred to the individual tests on the 1N647 (sect. 4.1.7) and UT254 (sect. 4.1.17) for damage thresholds.) The 2000-V, 2-μs pulses were insufficient to energize the relay coil and close the relay contacts.

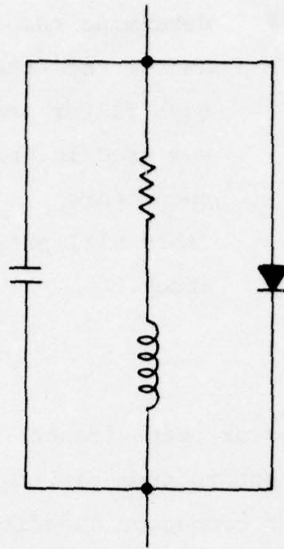

RELAY	10164126 (19)	10158808 (19)
DIODE	UT254	1N457
RESISTANCE	830 Ω ± 10%	200 Ω ± 10%
INDUCTANCE	1.3 H	1.5 H
CAPACITANCE	70 pF	110 pF

Figure 114. Relay characterizations.

4.3.5 Capacitors

Seven polar Cornell-Dubilier Electronics capacitors of two types were tested to high-voltage, 2-μs rectangular pulses of a polarity opposite to the case markings, by using the thyratron generator. Table VII (p. 170) summarizes the tests. There was no observed degradation in any of the samples.

4.3.6 21-900098 and 21-900099 Filter Connectors

Four Bendix (BDX) capacitive filter connectors were evaluated: 21-900098-1, -2, and -3 and 21-900099-1. The filter connectors were subjected to rectangular voltage pulses of 2 to 10 μs and amplitudes up to 2000 V. The objective of the study was to

TABLE VII. CAPACITOR TEST RESULTS

Capacitor No.		Maximum voltage (V)	Pulses* (No.)
CL25BL101TB3 (100 µF, 75 Vdc)	1	2244	13
	2	2244	2
	3	2243	2
	4	2244	2
	5	2244	2
CL25BE401VP3 (400 µF, 15 Vdc)	1	2243	3
	2	2243	2

**The number of pulses of increasing level applied to the capacitor before the specified maximum was attained.*

determine the failure threshold and the nature of the failure mechanisms for each filter connector. The information was used in the evaluation of the filter connectors for EMP hardening. Table VIII presents the results of the study.

The filter-connector capacitance values for the 21-900098-1 and 21-900099-1 filter connectors from pin to case and from pin to pin were such that the filter connector capacitor charged to the value of the open-circuit pulse level within 1 or 2 µs. Consequently, damage thresholds were established for these two filter connectors by step stressing. That is, the thresholds were found by pulsing at increasing amplitudes until damage occurred. The experiments on the remaining filter connectors were conducted with fixed open-voltage pulse generator levels. The filter connector capacitor charged through the entire pulse in those tests. The peak voltage reached was that before an arc is initiated in the filter connector. Figure 115 presents a typical pulse response indicating the presence of an internal arc and the peak voltage reached prior to the arc. Before and after each pulse test, measurements were made by using the HP 8553B spectrum analyzer and Simpson 260 volt-ohmmeter on the pin pairs of interest. Reduced leakage resistance always followed the indication of internal filter connector arcing. However, there appeared to be no degradation of the filter connectors' attenuation characteristics with frequency at the signal levels of the HP 8553B spectrum analyzer. The decrease in leakage resistance was in many tests quite severe, dropping below 20 kilohms. Also, arcing occurred at lower levels in subsequent pulse tests, and leakage resistance continued to drop after each subsequent arc.

TABLE VIII. SUMMARY OF BENDIX FILTER CONNECTOR TESTS*

Filter	Pin pair	Open circuit voltage (V)	Approx bulk source impedance (ohms)	Pulse width (μs)	Peak voltage across pin pair (V)	Comments
21-900098-1 (0.12 μF)	A-case	350	10	2	200	Pin pair was tested at 2000 V, and arcing occurred previously to test data presented.
	A-B	300	10	2	220	Pin pair was tested at 2000 V and arcing occurred previously to test data presented.
	D-case	900	10	2	800	
	D-E	1100	10	2	1000	D-case test conducted first.
	F-case	2000	10	2	2000	No attempt to establish threshold.
	E-F	2000	10	2	2000	No attempt to establish threshold.
	C-case	2000	10	2	1300	No attempt to establish threshold.
21-900098-2 (1 μF)	A-case	1265	50	10	870	
	B-case	770	50	10	170	
	C-case	770	50	10	220	
	D-case	1245	50	10	880	
	E-case	1250	50	10	940	
	F-case	2000	50	10	340	
21-90098-3 (2 μF)	A-case	2000	50	10	400	No failures were observed with open-circuit pulse amplitude of 1250 V; amplitude was immediately raised to 2000-V maximum.
	B-case	2000	50	10	450	
	C-case	2000	50	10	360	
	D-case	2000	50	10	150	
	E-case	2000	50	10	380	
	F-case	2000	50	10	400	
21-900099-1 (0.007 μF)	A-case	900	10	2	900	
	A-B	900	10	2	900	A-case test conducted first.

**The pulse test is given where internal filter arcing was initiated. The pulse test data taken before and after arcing are not summarized.*

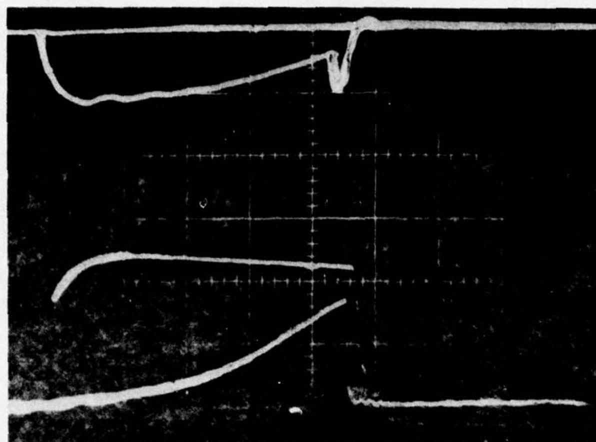

Figure 115. Pulse test of Bendix filter connector 21-900098-2 (1 μF), pin A to case; arcing in filter is indicated by drop in voltage and surge in current near end of pulse (~9.5 μs from start of pulse); peak voltage, 870 V.

4.3.7 Erie 1200 Filter

Tests similar to those described in section 4.3.6 were performed on an Erie 1200 filter. Since the filter had a 2.6-μF capacitance from input to case along with a much higher voltage rating, it was not possible to damage the filter with the pulse instrumentation available and obtain meaningful data. The filter was subjected to an open-circuit voltage of 2000 V. The associated peak impressed voltage was only 30 V for the 2-μs pulse.

5. SUMMARY

For convenience, the data presented in section 4 are condensed in a more usable format in this section. The semiconductor component failure data have been condensed to the parameters of equations (9) and (10) rewritten here:

$$P_D = K_1 T_D^{-1} + K_2 T_D^{-\frac{1}{2}} ,$$

$$E_D = K_1 + K_2 T_D^{\frac{1}{2}} ,$$

where the energy or power required to damage a device is related to the duration of a rectangular pulse transient (T_D) and the parameters K_1 and K_2. For each device type tested, an average bulk surge impedance was estimated from the calculated bulk surge impedances determined from each device test. The general expression defining the bulk surge impedance, after equations (25) and (26), is

$$Z = \frac{V_p - V_z}{I_p} ,$$

where Z is the bulk surge impedance, V_p is the average pulse voltage from the test oscillograms, V_z is the device breakdown voltage (if applicable; zero, if not), and I_p is the average current from the test oscillograms. Since voltage failure (sometimes termed "turn-on failure" in the text) was evidenced for a number of device types, the minimum open-circuit voltage for which failure resulted has been termed "voltage threshold." The parameters K_1, K_2, Z, and voltage threshold for all the semiconductor components of meaningful sample size tested in the program are listed in table IX. All data in the table, unless otherwise indicated, were obtained from reverse-biased tests.

Table X summarizes the main features of tests of the other components. The SM-C-602932 surge arrestor (when subjected to voltages above 1400 V) and the 1N5649A TransZorb showed turn-on times of less than 3 ns. The relays tested did not demonstrate contact arc at the voltages and pulse widths indicated in table X.

TABLE IX. SUMMARY OF SEMICONDUCTOR DEVICE FAILURE PARAMETERS

Device	Terminals*	Manufacturer	K_1 (J)	K_2 (W-s$^{1/2}$)	Impedance[+] (ohms)	Voltage threshold (V)
1N69A[‡]		General Electric Co. (GE)	--	--	4200	200
1N270A		General Instruments Corp. (GIC)	$100(10)^{-6}$	0.23	L≃3400; S≃22; Fwd≃16	--
1N457[‡]		Texas Instruments, Inc. (TI)	--	0.75	Rev≃620; Fwd≃ 0.40	500
1N539		TI	$750(10)^{-6}$	--	L≃810; S≃8.8	--
1N645[‡]		TI	--	7.2	L≃1100; S≃9.7	1600
1N647		TRW Semiconductors, Inc. (TRW)	--	4.2[¶]	S≃17; S Fwd≃5.2	--
1N816		ITT Semiconductors (ITT)	--	5.2[¶]	Rev≃20; Fwd≃10	--
1N914		TI	$22(10)^{-6}$	0.21	40	--
1N956B		TRW	--	1.5	Rev≃2.5; Fwd≃0.37	--
1N965B[‖]		Motorola Semiconductor Products (MOT)	--	--	Rev≃0.15; Fwd≃6.8	--
1N1200[‡]		GE	--	--	Rev≃900; Fwd≃0.05	2100
		MOT	--	--	Rev≃110	600
1N1202[†]		GE	--	40	Rev≃64; Fwd≃0.09	1700
		MOT	--	14	Rev≃65; Fwd≃0.1	700
1N1202A		Bendix (BDX)	--	11.2	Rev≃12; Fwd≃12	--
1N3047B		International Rectifier Corp.	$17,000(10)^{-6}$[§]	--	S≃7.1; L≃1.2; Fwd≃4.2	--
1N3064		Raytheon Co., Semiconductor Div. (RAY)	--	0.8[¶]	5.2	--
1N3666[‡]		ITT	--	0.41	Rev≃7.1; Fwd≃1.8	300
1N4003[‡]		MOT	--	--	Rev≃197	1500
		TRW	--	0.78	Rev≃129	800
1N4005[‡]		MOT	--	--	Rev≃116	1000
UT254		Unitrode	$210(10)^{-6}$	1.2	L Rev≃639; S Rev≃115; Fwd≃0.32	--
2N270	E-B	RCA Corp. (RCA)	$200(10)^{-6}$	0.5	L Rev≃107; L S≃18	--
2N297A	E-B	MOT	--	0.9	L≃188; S≃9.5	--
		BDX	--	1.3[¶]	Rev≃73; Fwd≃12	--
2N328A	E-B	Crystalonics Div., Teledyne, Inc. (CRY)	$16(10)^{-6}$	0.042	S≃16; L≃475	--
2N335	E-B[‖]	TI	--	--	Rev≃11; Fwd≃13	--
2N489A	E-B_2	TI (JAN)	$100(10)^{-6}$	0.16	Rev≃160; Fwd≃190	--
2N526	E-B	MOT	--	1.1[¶]	Rev≃15; Fwd≃5.7	--
2N598	E-B	GIC	--	0.5[¶]	Rev≃160; Fwd≃30	--
2N738	E-B	TI	$53(10)^{-6}$	0.11	L Rev≃18; S Rev≃5.4; L Fwd≃1; S Fwd≃3.6	--

NOTE: See footnotes at end of table.

See footnotes at end of table.

TABLE IX. SUMMARY OF SEMICONDUCTOR DEVICE FAILURE PARAMETERS (Cont'd)

Device	Terminals*	Manufacturer	K_1 (J)	K_2 (W-s$^{1/2}$)	Impedance † (ohms)	Voltage threshold (V)
2N1132**	E-C	MOT (JAN)	--	E+≃0.23 C+≃0.28	E+≃2.3 C+≃0.7	
		TI (JAN)	--	E+≃0.21 C+≃0.26	E+≃3.9 C+≃0.6	
		Fairchild Semiconductor Div. (FSC)	--	E+≃0.21 C+≃0.26	E+≃2.4 C+≃0.6	
2N1132A	E-B	MOT	--	0.21	L Rev≃2.7; S Rev≃18 L Fwd≃1.4	
		FSC	--	0.1		
		RAY	--	0.57[¶,‖]		
		Combined	$50(10)^{-6}$	0.13		
2N1204	E-B	MOT	--	0.01	L Rev≃96; L Fwd≃0.45; S Rev≃50; S Fwd≃3.8	
2N1308	E-B	GIC	$55(10)^{-6}$[§]		L Rev≃46; L Fwd≃10; S Rev≃62	
		TI	$12(10)^{-6}$[§]		L Rev≃550; S Rev≃68; S Fwd≃35	
		Combined	$21(10)^{-6}$			
2N1613	E-B	MOT	--	1	L Rev≃1.4; L Fwd≃0.1 S Rev≃3.7; S Fwd≃3.0	
2N1711	E-B	FSC MOT	--	0.13	Rev≃4.3; Fwd≃1.8	
2N2198	E-B	Electronic Transistors Corp.	--	0.55	Rev≃5; Fwd≃2.9	
2N2297	E-B	RAY FSC	--	1 0.5	Rev≃9.2	
2N2323	G-C	GE	--	0.4	Rev≃3.2	
2N2453	E-B	MOT FSC	-- --	0.06 0.08	Rev≃7.5; Fwd≃1.05	
2N2727	E-B	GE	$1200(10)^{-6}$	2.1	Rev≃1.2; Fwd≃1.0	
2N2801	E-B	FSC MOT	--	0.11 0.22	Rev≃2.9; Fwd≃1.5	
2N3069[‡]	G-D	Solitron Devices	--	--	None	
2N3440[‖]	E-B	RCA	--	--	Rev≃1.7; Fwd≃1.3	
2N3636	E-B	MOT	--	1	1.05	
SM692-1 (2N3801)		MOT	--	0.005	L Rev≃450; L Fwd≃2.5 S Rev≃72; S Fwd≃3.2	
μA709**		FSC	--	--		
2(B)-3(C)		(IC)		0.011	35	
6(F)-4(D)				D+ 0.011 F+ 0.044	21.4 102.5	

*B = base; C = collector or cathode; D = drain; E = emitter; G = gate.

†Fwd = forward bias; L = long pulse width (>100 ns); Rev = reverse bias; S = short pulse width (<100 ns).

‡A voltage threshold failure was observed. Where a value for K_1 or K_2 is given, both voltage and thermal mechanisms were evident. The voltage threshold value shown is the minimum pulse generator voltage (open circuit, 50-ohm internal impedance) for which a failure resulted.

¶The failure constant was computed from data <100-ns pulse width. The constant energy for failure was not apparent from the data obtained.

‖Limited sample size.

§The failure constant was computed from data that extended to 1-μs pulse widths but did not, based on the limited sample numbers, appear to have a T_D^{-1} curve.

**The positive sign indicates the pin or junction receiving the positive pulse bias.

--No data.

TABLE X. SUMMARY OF MISCELLANEOUS TESTS

Device	Description	Open-circuit voltage (V)*	Current (A)	Pulse width (μs)	Power (W)	Failure
1752/17	Burr-Brown operational amplifier					
	Unpowered					
	Pin 1 to pin 2	160	--	2	--	No
	Pin 2 to pin 1	160	--	2	--	No
	Pin 2 to pin 4	160	--	2	--	No
	Pin 4 to pin 2	160	--	2	--	No
	(-) to pin 2	160	--	2	--	No
	Pin 2 to (-)	460	2	2	880	Yes
	Powered					
	Pin 2 to ground	230	--	2	--	Yes
SM-C-602932	Surge arrestor	2500	--	1	--	No
		6000	--	0.05	--	No
SM-C-602933	Filter	2500	--	1	--	No
1N5649A TransZorb	General Semiconductor Industries, Inc.	1000	≥100	2	>6000	No
10164126(19)	LTV relay	2000	--	2	--	No
10158808(19)	LTV relay	2000	--	2	--	No
CL25BL101TB3	Cornell-Dubilier capacitor 100 μF, 75 Vdc, reverse bias	2244	--	--	--	No
CL25BE401VP3	Cornell-Dubilier capacitor 400 μF, 15 Vdc, reverse bias	2243	--	--	--	No
21-900098-1	Bendix 0.12-μF filter connector	~900	--	2	--	Yes
21-900098-2	Bendix 1-μF filter connector	770**	--	10	--	Yes
21-900098-3	Bendix 2-μF filter connector	1250**	--	10	--	No
		2000**		10		Yes
21-900099-1	Bendix 0.007-μF filter connector	900	--	2	--	Yes
1200	Erie 2.6-μF filter	2000	--	2	--	No

The pulse generator impedance was approximately 10 ohms, except.*
***The impedance was 50 ohms.*
(-)Negative terminal.
--No data.

ACKNOWLEDGEMENTS

The author is indebted to Raymond Parsons of HDL and Raymond Richter (formerly of HDL), who made the majority of the measurements and assisted in the data reduction. Other contributors were Oscar Turner, Jim Beck, and Vic Simulia (formerly of Potomac Research, Inc.) and Robert Brown (formerly of HDL).

LITERATURE CITED

(1) Paul P. Budenstein, Duane H. Pontius, and Wallace B. Smith, Second Breakdown and Damage in Semiconductor Junction Devices, Auburn University Report No. RG-TR-72-15, Auburn, AL (April 1972).

(2) Dante M. Tasca and Joseph C. Peden, Feasibility Study of Developing a Nondestructive Screening Procedure for Thermal Second Breakdown, General Electric Co., Philadelphia, PA (July 1971).

(3) J. B. Singletary and D. C. Wunsch, Final Summary Report on Semiconductor Damage Study Phase II, Braddock, Dunn, and McDonald BDM/A-66-70-TR, Albuquerque, NM (June 1970).

(4) M. E. Daniel, Development of Mathematical Models of Semiconductor Devices for Computer Aided Circuit Analysis, Proceedings of IEEE, 55, (November 1967), 1913.

(5) H. A. Schafft, Second Breakdown--A Comprehensive Review, Proceedings of IEEE, 55, (August 1967).

(6) EMP [Electromagnetic Pulse] Handbook, Vol. 2, Defense Nuclear Agency (November 1971).

(7) R. L. Davies and F. E. Gentry, Control of Electric Field at the Surface on PN Junctions, IEEE Trans. Electron Devices, ED-11, (July 1964), 313-323.

(8) D. C. Wunsch and L. Marzitelli, Semiconductor and Nonsemiconductor Damage Study, Final Report, Vol. 1, Braddock, Dunn, and McDonald BDM-376-69-F-0168, Albuquerque, NM (April 1969).

(9) D. M. Tasca and J. C. Peden, Pulsed Power Failure Modes in Semiconductor Devices, U.S. Army Mobility Equipment Research and Development Center, Fort Belvoir, VA (April 1970).

(10) L. R. McMurray and C. T. Kleiner, Adaptation of the P-N Junction Burnout Model to Circuit Analysis Codes, IEEE Annual Conference on Nuclear and Space Radiation Effects, 19, (July 1972), 76.

(11) J. E. Godts, Semiconductor Avalanche Power Failure, Martin Marietta Corp. Technical Note, Orlando, FL (December 1968).

(12) R. Brown, J. D. Holder, and V. W. Ruwe, Statistical Component Damage Study, Component Damage Conference, U.S. Army Mobility Equipment Research and Development Center, Fort Belvoir, VA (April 1970).

(13) LANCE Vulnerability and Hardening Program, Test Plan, Annex A, General Procedures, Harry Diamond Laboratories (3 April 1972).

(14) J. R. Miletta, R. E. Parsons, and M. S. Bostian, Lance Vulnerability and Hardening Test Program Interim Semiconductor Damage Report, Harry Diamond Laboratories (September 1971).

(15) B. Kalab, Analysis of Failure of Electronic Circuits from EMP Induced Signals--Review and Contribution, Harry Diamond Laboratories TR-1615 (August 1973).

SELECTED BIBLIOGRAPHY

Albright, L. A., Braddock, J. V., LePoer, K. T., and Miletta, J. R., Modeling and Simulation Techniques for Damage Prediction and System Assessment, Defense Atomic Support Agency EMP Conference, Fort Belvoir, VA (29-30 January 1969).

Glassbrenner, C. J., and Slack, G. A., Thermal Conductivity of Silicon and Germanium from 3 K to the Melting Point, Phys. Rev., 134, (May 1964), A1058-A1069.

Neuberger, M., et al, Silicon, Hughes Aircraft Co., Culver City, CA (October 1969).

Stadler, P. H., Failure Threshold and Resistance of the Protected and Unprotected 2N2222 Transistor in the Short Pulse Width Regime, Philco-Ford Corp. Report U-4976, Newport Beach, CA (May 1972).

Sze, S. M., Physics of Semiconductor Devices, John Wiley and Sons, Inc., New York (1969).

SYMBOLS

A	Junction area, effective junction area anode, scale factor
B	Base
B_1	Base one
B_2	Base two
C	Collector, cathode
C_p	Specific heat at constant pressure
D	Drain
E	Emitter
E_D	Energy to damage
E_g	Forbidden band or gap energy
G	Gate
I	Current
I_p	Load current
I_s	Junction saturation current
k	Boltzmann's constant
k'	Thermal conductivity
K	Constant, damage constant
K'	Constant
K_1	Damage constant, short-pulse region
K_2	Damage constant, transition region
K_3	Damage constant, long-pulse region
N	Shaping constant
P	Power

SYMBOLS (Cont'd)

P_D	Power to damage
P_f	Power dissipated under forward bias
P_r	Power dissipated under reverse bias
q	Charge on electron
R	Resistance, bulk surge impedance
R_A	Resistance in avalanche region
R_B	Device bulk resistance
R_C	Resistance in second breakdown
R_L	Leakage resistance
S	Short pulse tests (5 to 100 ns)
t	Time
T	Temperature
T_D	Time delay to second breakdown
T_{DOC}	Pulse width
T_i	Initial temperature
T_m	Critical temperature, melt temperature
V	Voltage
V'	Volume, effective volume
V_A	Avalanche voltage level
V_D	Diode junction voltage
V_g	Generator voltage
V_τ	Average value of presecond-breakdown current
V_k	Known-load voltage

SYMBOLS (Cont'd)

V_{oc} Open-circuit voltage

V_p Load voltage

V_t Extrapolated voltage

V_z Impedance voltage

x Distance

Z Bulk surge impedance

Z_g Generator impedance

α $k'/\rho C_p$

δ Skin depth

θ Emission constant, qE_g/kT

μ Permeability

ρ Density

σ Conductivity

ω $2\pi\cdot$frequency

DISTRIBUTION

DEFENSE DOCUMENTATION CENTER
CAMERON STATION, BUILDING 5
ALEXANDRIA, VA 22314
ATTN DDC-TCA (12 COPIES)

COMMANDER
USA RSCH & STD GP (EUR)
BOX 65
FPO NEW YORK 09510
ATTN LTC JAMES M. KENNEDY, JR.
CHIEF, PHYSICS & MATH BRANCH

COMMANDER
US ARMY MATERIEL DEVELOPMENT
& READINESS COMMAND
5001 EISENHOWER AVENUE
ALEXANDRIA, VA 22333
ATTN DRXAM-TL, HQ TECH LIBRARY

COMMANDER
US ARMY ARMAMENT MATERIEL
READINESS COMMAND
ROCK ISLAND ARSENAL
ROCK ISLAND, IL 61201
ATTN DRSAR-ASF, FUZE &
MUNITIONS SPT DIV

COMMANDER
USA MISSILE & MUNITIONS CENTER
& SCHOOL
REDSTONE ARSENAL, AL 35809
ATTN ATSK-CTD-F

DEFENSE COMMUNICATION
ENGINEERING CENTER
1860 WIEHLE AVENUE
RESTON, VA 22090
ATTN CODE R720, C. STANSBERRY
ATTN CODE R410, JAMES W. MCLEAN
ATTN CODE R400
ATTN CODE R124C, TECH LIB

DIRECTOR
DEFENSE NUCLEAR AGENCY
WASHINGTON, DC 20305
ATTN RATN
ATTN DDST
ATTN RAEV
ATTN STTL, TECH LIB
ATTN STSI, ARCHIVES
ATTN STVL

COMMANDER
FIELD COMMAND
DEFENSE NUCLEAR AGENCY
KIRTLAND AFB, NM 87115
ATTN FCPR

COMMANDER
US ARMY MISSILE MATERIEL
READINESS COMMAND
REDSTONE ARSENAL, AL 35809
ATTN DASMI-RGP, DAVE MATTHEWS
ATTN DRSMI, RGD, VICTOR RUWE
ATTN TECHNICAL LIBRARY

COMMANDER
NAVAL SURFACE WEAPONS CENTER
WHITE OAK, MD 20910
ATTN CODE 730, TECH LIB
ATTN CODE 431, EDWIN B. DEAN
ATTN CODE 1224, NAVY NUC PROGMS OFF
ATTN CODE 431, EDWIN R. RATHBURN
ATTN CODE 431, JOHN H. MALLOY

BOEING COMPANY, THE
P.O. BOX 3707
SEATTLE, WA 98124
ATTN DONALD W. EGELKROUT, MS 2R-00

GENERAL ELECTRIC COMPANY
SPACE DIVISION
VALLEY FORGE SPACE CENTER
P.O. BOX 8555
PHILADELPHIA, PA 19101
ATTN DANTE M. TASCA
ATTN JOSEPH C. PEDEN, CCP 8301

NORTHROP CORPORATION
NORTHROP RESEARCH AND
TECHNOLOGY CENTER
3401 WEST BROADWAY
HAWTHORNE, CA 92050.
ATTN LIBRARY
ATTN JAMES RAYMOND

R&D ASSOCIATES
P.O. BOX 3580
SANTA MONICA, CA 90403
ATTN TECHNICAL LIBRARY

DISTRIBUTION (Cont'd)

HARRY DIAMOND LABORATORIES
ATTN DANIEL, CHARLES D., JR., MG,
COMMANDING GENERAL (ERADCOM)
ATTN RAMSDEN, JOHN J., LTC, COMMANDER/
FLYER, I.N./LANDIS, P.E./
SOMMER, H./OSWALD, R. B.
ATTN CARTER, W.W., DR., TECHNICAL
DIRECTOR/MARCUS, S.M.
ATTN KIMMEL, S., PAO
ATTN CHIEF, 0021
ATTN CHIEF, 0022
ATTN CHIEF, LAB 100
ATTN CHIEF, LAB 200
ATTN CHIEF, LAB 300
ATTN CHIEF, LAB 400
ATTN CHIEF, LAB 500
ATTN CHIEF, LAB 600
ATTN CHIEF, DIV 700
ATTN CHIEF, DIV 800
ATTN CHIEF, LAB 900
ATTN CHIEF, LAB 1000
ATTN RECORD COPY, BR 041
ATTN HDL LIBRARY (5 COPIES)
ATTN CHAIRMAN, EDITORIAL COMMITTEE
ATTN CHIEF, 047
ATTN TECH REPORTS, 013
ATTN PATENT LAW BRANCH, 071
ATTN GIDEP OFFICE, 741
ATTN LANHAM, C., 0021
ATTN MILETTA, J. R., (25 COPIES)
ATTN WIMENITZ, F. N., 0024
ATTN KALAB, B., 1040
ATTN CORRIGAN, J., 0024